DEVELOPMENT OF NEW MULTI-DISCIPLINARY TECHNIQUES FOR MINERAL EXPLORATION IN SEVERAL AREAS OF THE WESTERN IBERIAN PENINSULA

VOL. I

EEC Contract MA1M-0032-C (A)

FINAL REPORT

Alburquerque-La Codosera Area (Extremadura-Spain)

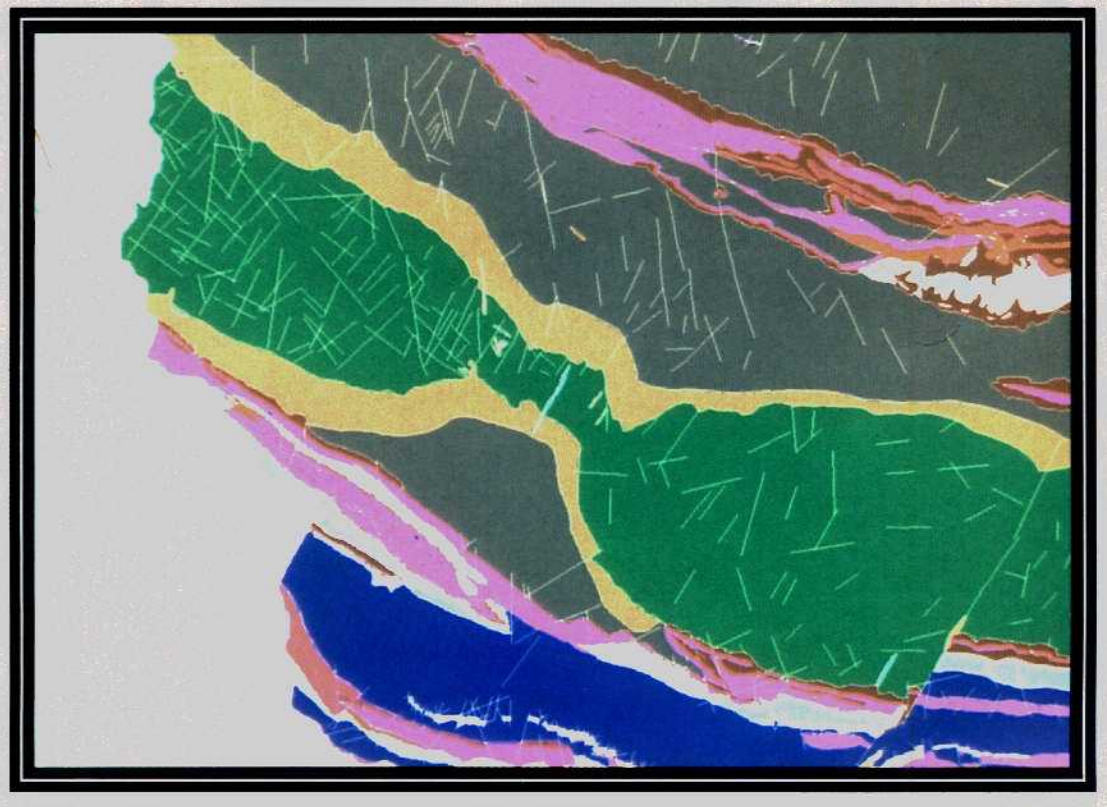

Instituto Tecnológico GeoMinero de España (SPAIN)

University of Southampton (U.K.)

1990,

DEVELOPMENT OF NEW MULTI-DISCIPLINARY TECHNIQUES FOR MINERAL EXPLORATION IN SEVERAL AREAS OF THE WESTERN IBERIAN PENINSULA

(Contract MA1M-0032-C(A))

ALBURQUERQUE - LA CODOSERA AREA (EXTREMADURA - SPAIN)

(VOL.1)

FINAL REPORT

Edited by

P. Gumiel, C. Antón-Pacheco, R. Campos and F.Pérez-Cerdán.

ITGE, Madrid (Spain).

R. W. Nesbitt, S. Roberts, and D. J. Sanderson.

University of Southampton. (U.K.)

1990 - June

CONTENTS This report has been elaborated by the following authors:

* ITGE, Madrid, Spain.
** Southampton University, U.K.

CONTENTS

INTRODUCTION.

This report outlines the findings of an EEC funded joint research and development programme; contract Nº MA1M-0032-C; involving the ITGE (Spain), ENUSA (Spain), ENU (Portugal), Salamanca University (Spain) and Southampton University (U.K). The fundamental aim of the programme is to develop new mineral exploration strategies applicable within the Iberian Peninsula for a variety of elements, as designated by the EEC, including Sn, W, Nb, Ta, Li, Sb, Au and U.

It is ambitious in that it involved government, industry and university groups for three nationalities, with a wide variety of techniques and expertise, attempting to tackle several areas of considerable mineral potential. The logistical support of ITGE has been particulary important in the coordination of these participating institutions.

Finally, the most important aspect of this venture has been the final report. The intention was to produce a common report in which an attempt has been made to integrate the data and provide a summary of relevant results. This particular report (Vol.1) presents the results of the collaboration between ITGE, Spain and the University of Southampton, U.K. which focused on an area of gold mineralisation, the La Codosera area, within the Extremadura region of SW Spain.

The present investigation commenced in the Autumn of 1987 and utilised the initial work of the ITGE who have contributed significantly to the current knowledge of the area throught several mineral exploration projects in the "State Reserva of La Codosera". Extensive fieldwork periods were undertaken in the initial stages to establish a "Geological Framework" within which the more sophisticated geochemical and remotely sensed data could be interpreted.

Ten chapters are presented outlining the results of the various techniques employed (structural geology, geochemistry, remote sensing, gravity, etc.) and which clearly reflect the multidisciplinary nature of the programme. Most importantly, the key findings of each contribution are then draw together in the final chapter to provide new exploration targets within the region and relevant to future exploration in the Community.

CHAPTER - 1 - GEOLOGICAL BACKGROUND.

P.Gumiel & M. Gallego.

1.1 - STRATIGRAPHIC OUTLINE.

The Hercynian crust of the Iberian Peninsula can be subdivided into a number of tectonic zones or terranes, the boundaries between which are often highly deformed. In this section we describe the geology (stratigraphy) from the La Codosera area in western Spain, which lies at the southern margin of the Central Iberian Zone and is separated from the Ossa-Morena Zone, to the south, by the Badajoz-Cordoba Shear Zone (Fig. 1.1), a complex structural lineament along which movements were focused during the Hercynian orogeny (Arthaud & Matte, 1975; Le Fort & Ribeiro, 1980; Burg et al., 1981).

An outline of the geology of the La Codosera area, which can be subdivided into a number of tectono-stratigraphical units: is showed in Fig.1.2.

1.1.1- PRE-CAMBRIAN SEQUENCE (01 CEG/02 F.Urra-seeFig.1.4 (1))

Locally known as the Complejo Esquisto-Grauvquico (CEG- Carrington da Costa, 1952), it comprises a monotonous sequence of slates and greywackes which crop out mainly to the north of the La Codosera Syncline. These rocks are of presumed late Proterozoic age; elsewhere they are overlain unconformably by more varied lithologies, including dolostones and limestones, variously attributed to the Vendian or even Cambrian (Bouyx, 1970). Most of the outcrops to the north of La Codosera can be equated with a lower series within the CEG, but highly deformed microconglomerates or "porphyroids" (Urra Formation) to the south of the Southern Ridge may represent an upper unit (Vendian?).

1.1.2 - PALAEOZOIC SEQUENCE (See Fig. 1.4 (1)).

Lower Palaeozoic quartzites and slates unconformably overlie the CEG and occupy three WNW-ESE trending ridges (Fig.1.2 and 1.3*).

(1)- Northern (San Pedro) Ridge.

(2)- Central Ridge, (Jola-Alcorneo).

(3)- Southern Ridge, which also includes highly sheared PreCambrian to Devonian sediments.

---

(1) - The numbers refer to Figure 1.4.

* Fig 1.3 - Outside of text.

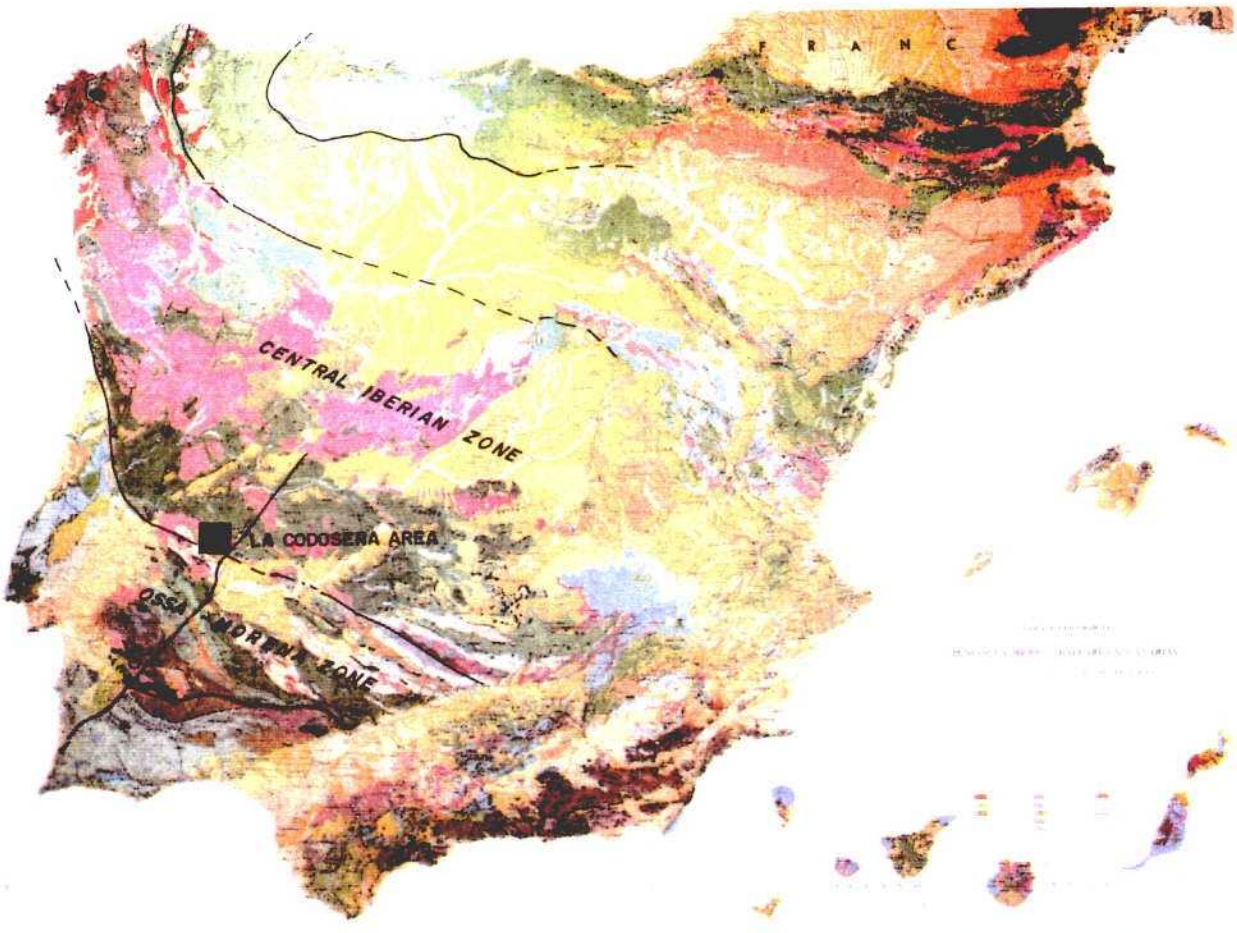

FIG. 1.1 - LOCATION OF THE LA CODOSERA AREA IN RELATION TO MAJOR HERCYNIAN ZONES.

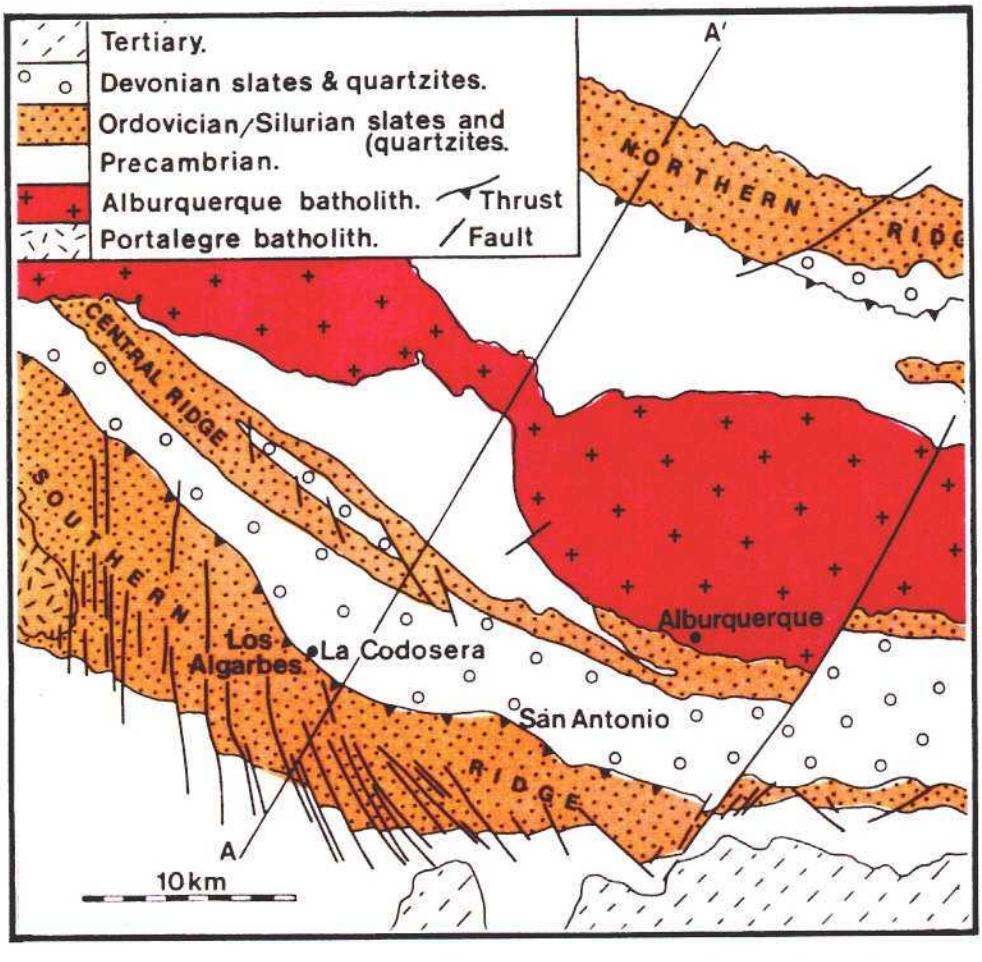

FIG. 1.2 - OUTLINE GEOLOGY OF THE LA CODOSERA AREA.

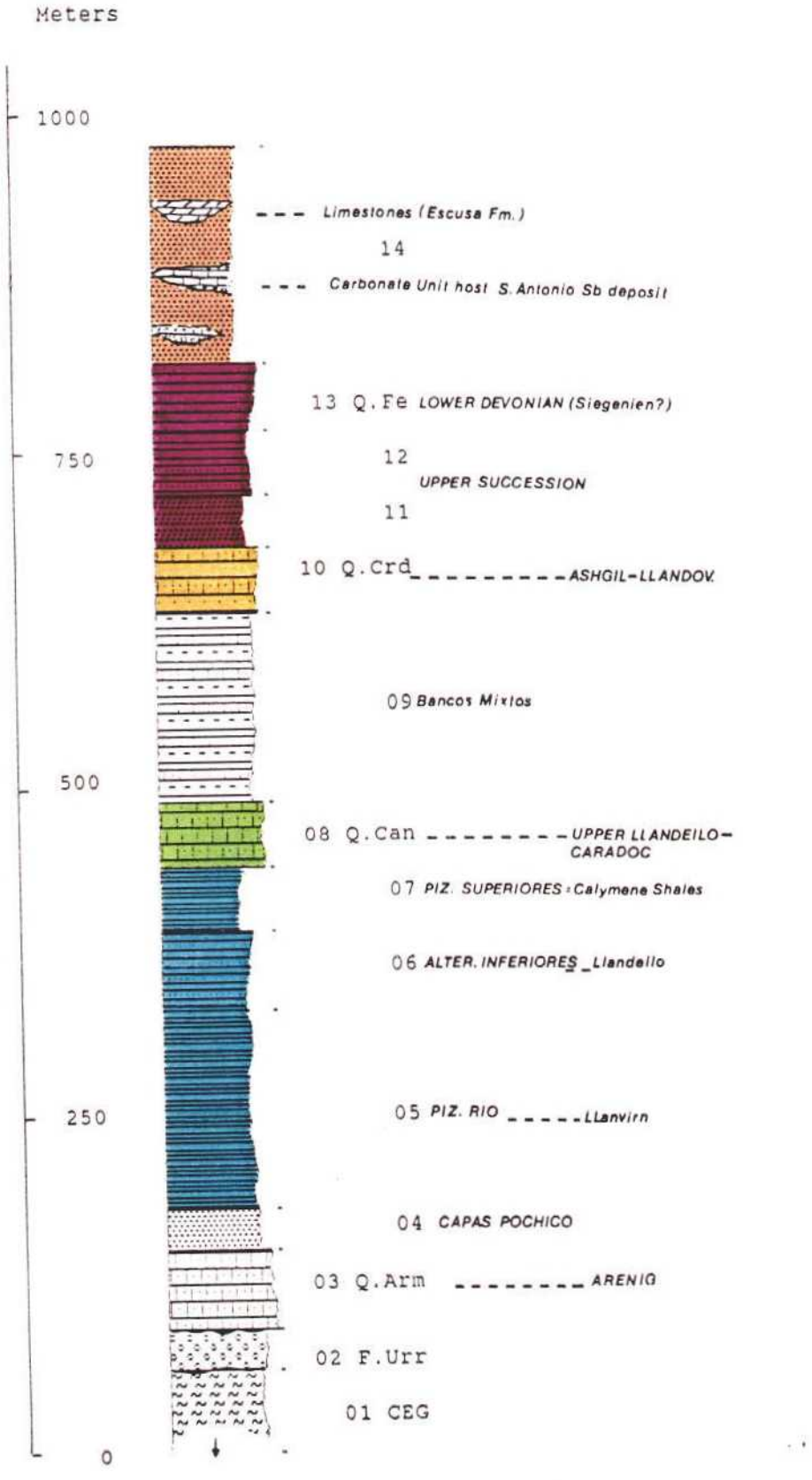

FIG. 1.4 - GENERALIZED STRATIGRAPHICAL SERIE OF THE LA CODOSERA AREA.

The La Codosera Syncline lies between the Central and Southern ridges and is cored by red and grey Devonian slates, with some thin sandstone and limestone units. The Albuquerque Granite is a late Hercynian batholith mainly intruded into CEG, but which farther west in Portugal cross cuts the La Codosera Syncline.

Armorican Quartzite (0.3 Q.Arm-Arenig)

Near the base of the lower Palaeozoic rocks a prominent quartzite unit, generally termed the Armorican Quartzite, forms a good mappable horizon of Arenig age. Sporadically, underlying this unit a reddish slate, sandstone and micro-conglomerates sequence appears which corresponds to the "Lie de Vin" series (Tamain, 1972) of Tremadoc age.

The Armorican Quartzite comprises white recrystallised quartzites interbeded with silicic sandstones with quartz veining evident. The recrystallised nature of the rocks makes the recognition of sedimentary structures difficult, however ripple marks and cruzianas are observed. The thickness is about 50 m.

Alternations of slates and quartzites (04).

The Armorican Quartzite is overlain by a fining upwards succession of dark grey shales (slates), thin sandstones and quartzites. This formation has been correlated with the "Capas Pochico" of the Valle de Alcudia (Tamain, 1972). The thickness is about 30m and the total sequence is condensed compared to the equivalent sequences of Eastern Sierra Morena and Almaden. The Palaeozoic succession of the La Codosera Syncline has been subdivided on the basis of correlation of several better studied successions in the Alcudia Valley (Tamain, 1972) and Almaden (Ortega, 1988).

The Capas Pochico is overlain by 150 m of black slates (05) similar to the "Pizarras Rio" of Llanvirn age and a sequence (06) made up of sandstones, quartzites and slates, 60 m. thickness, and correlated with the "Alternancias Inferiores" of Llandeilo age. Overlying this formation are 50m of black slates named "Pizarras Superiores" (07) which can be correlated with the "Pizarras Botella" or "Esquistos con Calymene" (Calymene Shales) of the Almaden area (Llanvirn-Llandeilo).

Cantera Quartzite (08.Q.Can.)

The Cantera Quartzite (Upper Llandeilo-Caradoc) separates the underlying Calymene Shales from overlying upper Ordovician shales. The sequence coarsens and thickens upwards with alternations of recrystallised quartzites and grey sandstones, varying between 30 and 50m in thickness. It is utilized as a distinctive mappable horizon and correlated to the same unit in the Almaden area.

Intermediate Series (09.Caradoc-Ashgill)

Conformably overlying the Cantera Quartzite are a series of alternations of pyritic black shales (slates), sandstones and white quartzites with sporadic iron nodules and limolites. This formation has been correlated with the "Bancos Mixtos" of the Eastern Sierra Morena (Tamain et al., 1971, Tamain, 1972) These upper Ordovician slates, in turn, are separated from Silurian shales by the Criadero Quartzite.

Criadero Quartzite (10. Q.Crd. Ashgill-Llandovery)

This formation is a well bedded sequence of quartzites with sedimentary structures (trough cross-bedding, channels etc). Sporadically two quartzites horizons can by distinguished separated by a thin level of lutites. Quartz veining is widespread and iron oxides are frequently observed. The total thickness of this unit varies between 40 and 50 m.

Upper Succession (11 and 12, Llandovery-Lower Devonian).

Conformably overlying the Criadero Quartzite there is a unit of pyritic black shales (11), a sandstone sequence demonstrating flaser bedding, with Monograptus sp and brachiopods. This alternance is correlated with the "Pizarras con Monograptidos" (Llandovery) of Eastern Sierra Morena. Overlying this succession is another sandstone, quartzite, limolite sequence (12), which is 100m thick.

Lower Devonian Quartzite (13.Q.Fe, Sigenien?).

This iron-rich quartzite, sandstone sequence with sedimentary structures (cross-bedding and ripples) varies between 40 and 50m thickness. Overlying the Lower Devonian Quartzite there is an iron rich shales (black and red slates), sandstone and quartzite succession which made up the core of the La Codosera Syncline. Quartz-veining is widespread and this formation hosted some of the auriferous quartz veins of the area. Two carbonate units are remarkable. The first, located in the Southern Ridge of the La Codosera Syncline, is made up by black silicic limestones, deformed intraformational breccias with chert, quartz, limestones and slate pebbles in a carbonaceous matrix which is the host-rock of the Sb-W mineralisation of San Antonio (Gumiel et al., 1976; Gumiel, 1982). Upper Coblecien- Eifelien age has been attributed to this carbonaceous unit by Santos & Casas, (1979) and the thickness varies between 60 and 150 m, pinching towards west of La Codosera. The other carbonate unit (Escusa Fm.), made up by dolomitic limestones and graphitic slates outcropping in the Central Ridge shows characteristics of reef environments, and has been dated of Couvinian age (Correia Perdigao & Peinador Fernandes 1976).

Interbedded within the Lower Devonian sequence there are basic rocks which form a volcano-sedimentary succession. These rocks, mainly diabases, gabbros and tuffs exhibit hydrothermal alteration processes which in turn were utilized to attribute an hydrothermal-exhalative origin to the Sb-W mineralisation of San Antonio (Gumiel, 1982) probably related to late events (hot spring) of this intradevonian volcanism.

CHAPTER - 2 - STRUCTURAL SETTING OF THE LA CODOSERA AREA.

D.J. Sanderson, S. Roberts, P. Gumiel & J. McGowan.

2.1 - INTRODUCTION

Having presented the stratigraphic background to the area this chapter now presents the structural evolution as perceived from a regional scale. Thus, following the first two chapters the structural and geological background of the area will be in place enabling a better insight into the setting of the mineralisation of the study area.

2.2 - STRUCTURES WITHIN THE CEG.

The structure within the CEG has been examined in several traverses through the northern part of the area and in a well exposed river section in the Rio Salor, to the NE of Aliseda (Fig. 2.1). Sedimentary structures (ripples, load and flute casts, grading, etc) are reasonably well developed, allowing younging and facing to be determined at most outcrops. The rocks display a series of tight upright folds and a strong cleavage. Cleavage often cuts across (or transects) both horizontal and steeply- plunging folds and in places early quartz veins are clearly folded around tight folds. These features indicate that many of the folds and some of the faults and veins within the CEG initiated prior to cleavage development, but have subsequently been modified by the intense nature of the superposed Hercynian deformation.

The association of variably oriented folds, faults and veins, with the absence of an associated cleavage is taken to indicate epirogenic deformation prior to the Hercynian. Much of this deformation could involve tilting and faulting associated with the regional unconformities within the CEG and at the base of the Ordovician. That this deformation was of regional extent is supported by the variable nature of the bedding/cleavage intersections (often steep) and facing directions within the CEG, compared to the gently inclined upward-facing nature of these lineations within the Palaeozoic strata.

Pre-Ordovician deformation in the Central Iberian Zone may be linked to the Sardic discontinuity, but suggestions of folding generally rely on indirect evidence, such as the absence of Cambrian strata. Recently Roda Querol, (1986) has recognised NE- SW trending, pre-Ordovician folds overprinted by NW-SE Hercynian cleavage in an area immediately to the north of the present study area. Our data support these observations and suggest that this pre-Hercynian deformation may have been widespread in the CEG, but, in the absence of strain data it is not possible to determine the precise pre-cleavage geometry of these structures.

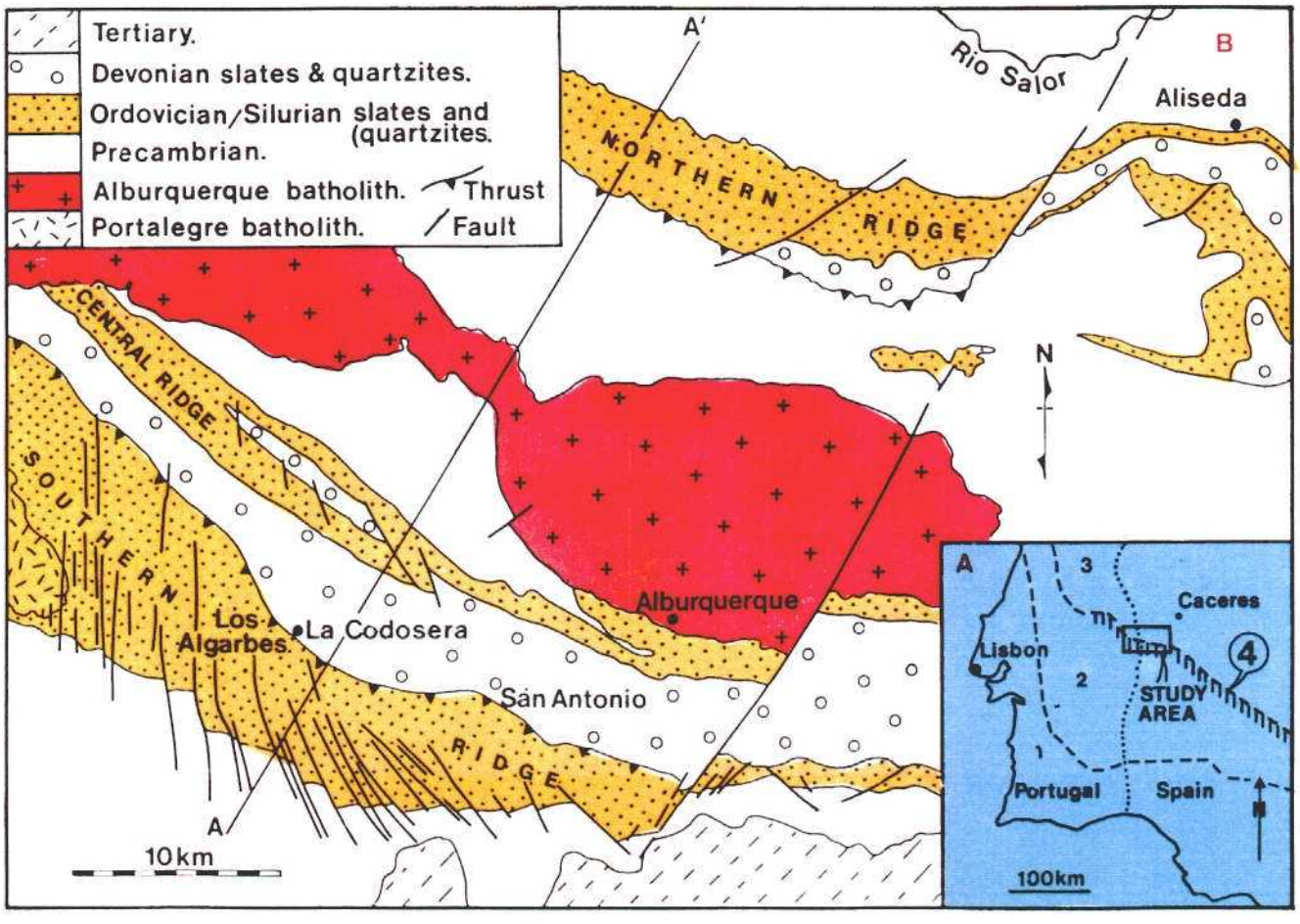

FIG 2.1 - A) LOCATION MAP OF THE LA CODOSERA/ BADAJOZ SHEAR ZONE.
1 - SOUTH PORTUGUESE ZONE, 2 - OSSA MORENA ZONE,
3 - CENTRAL IBERIAN ZONE, 4 - BADAJOZ SHEAR ZONE.

B) OUTLINE GEOLOGICAL MAP OF THE LA CODOSERA AREA.

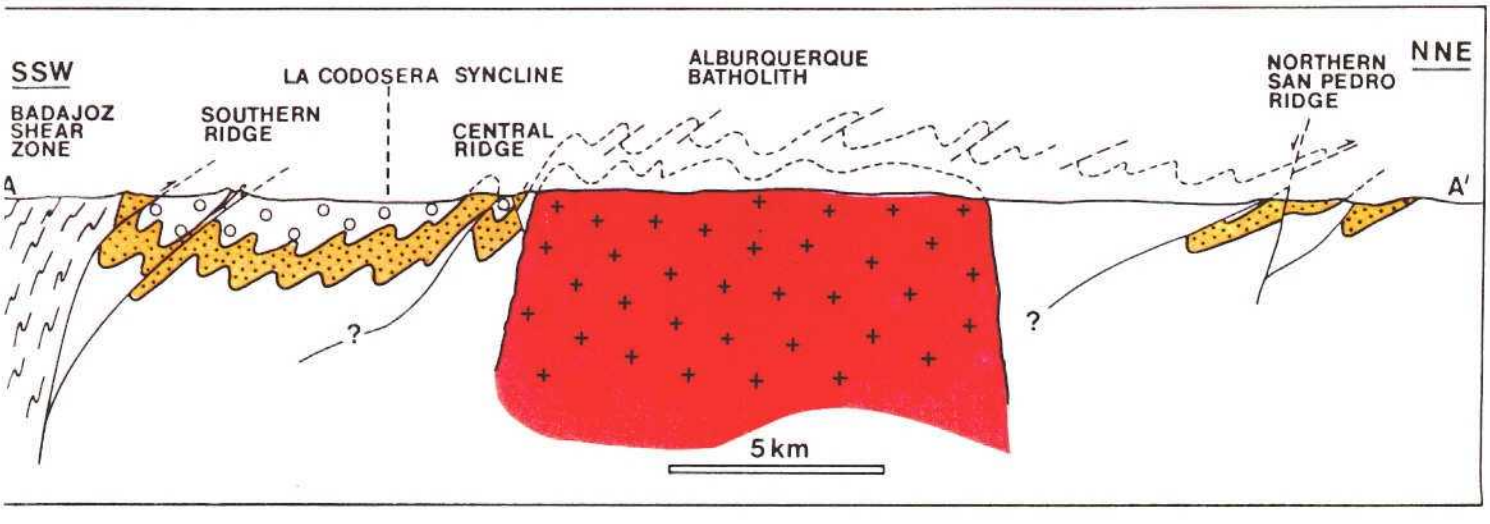

FIG 2.2 - SIMPLIFIED CROSS-SECTION ACROSS THE LA CODOSERA AREA;
LINE OF SECTION A - A' SHOWN IN FIG. 2.1.

2.3 - STRUCTURES WITHIN THE PALAEOZOIC ROCKS

Hercynian deformation affects the Palaeozoic strata and the underlying CEG producing: a) D1 - early, steeply inclined, sub- horizontal folds, with a steep slaty cleavage; b) D2 - steeply inclined, gently to moderately plunging asymmetric folds with a crenulation cleavage; c) extensive late fracturing and faulting. The youngest rocks affected by this deformation in the La Codosera area are of Devonian age, but farther east, towards Caceres, the Hercynian deformation affects Carboniferous strata. The early folds and cleavage are cut by the Alburquerque Granite, which contains only late and post- Hercynian fractures. We will describe the progressive change in the structures based on a north-south cross-section (Fig. 2.2), highlighting the structural style of the three main ridges of Palaeozoic rocks (ie. the Northern, Central and Southern ridges).

2.3.1 - Northern (or San Pedro) Ridge.

This consists of gently to steeply dipping strata, which are folded and thrust. The overall structure is that of a complex footwall syncline (the San Pedro Syncline). The northern limb of the structure is formed by a steeply-dipping, southward-younging, conformable sequence of Armorican Quartzite to Devonian quartzites and slates, which rests unconformably on the CEG. At Aliseda the sequence extends up into Lower Carboniferous limestones, but towards the west the higher strata are progressively cut out by a thrust which brings up CEG within the ridge.

The southern margin of the ridge is formed from CEG thrust northward over Devonian quartzites. From the attitude of the quartzite the thrust is constrained to dip at some 30°S. Within the centre of the ridge the dips are generally shallow to moderate and the strata are cut by various high-angle faults, often with oblique movements.

2.3.2 - Central Ridge.

The Central Ridge consists of tightly folded, generally steeply-dipping Palaeozoic rocks, lying unconformably on CEG. Several faults have been mapped, which strike parallel to the folds but cut across their limbs. Many of these faults have reverse stratigraphic separation in cross-section (ie. appear as thrusts), but have important strike-slip components. Large grooves and slickenfibres pitching gently within the fault planes indicate at least a late stage of movement with an important left- lateral component. Overall the 'thrusts' appear to accommodate the folding, rather than the folds having initiated on thrust ramps. Essentially the Central Ridge is a large north-verging fold pair, cut by steeply-dipping faults, on the northern limb of the La Codosera Syncline; it resembles an asymmetrical flower structure (Fig. 2.2).

2.3.3 - The La Codosera Syncline.

The Devonian slates between the Central and Southern ridges form the core of the La Codosera Syncline. They exhibit upright folds and a steeply-dipping cleavage. The syncline is asymmetric with a more gently dipping fold envelope on its northern limb and steeply inclined, more strongly deformed rocks to the south (Fig. 2.2)

Several sets of later crenulation cleavages and kink bands are developed in the Devonian slates, but these produce little significant refolding of the slaty cleavage. Steep NNE trending kink bands are similar to those observed within the CEG and represent a widespread, late, regional deformation event. The other cleavages have not been correlated throughout the area and may represent local deformation, some in response to faulting within the syncline.

2.3.4 - Southern (or Border) Ridge.

This is comprised of steeply-dipping and overturned Ordovician to Devonian quartzites and slates, which form the highly deformed, southern limb of the La Codosera Syncline. Two generations of steeply inclined folds and cleavage are developed, with variably oriented fold axes. Intense left-lateral shearing on the southern limb of the La Codosera Syncline produced augen, shear bands, sub-horizontal stretching lineation and boudinage.

To the west of La Codosera, the Southern ridge strikes NW-SE (Fig. 2.3a) into Portugal. Detailed mapping, around the gold prospects of Los Algarbes, has revealed quartzite units repeated by faulting, usually with a northerly directed reverse separation. These faults clearly cross-cut the early folds and slaty cleavage and have been reactivated in association with a second phase of folding and crenulation cleavage. Minor F2 folds have sinistral or northerly vergence, consistent with the fault offsets and slickenfibres on fault surfaces indicative of at least late phases of oblique thrust/left-lateral movement.

To the southeast of La Codosera the ridge swings to strike almost E-W (Fig. 2.3b) and the rocks become highly sheared, with a pronounced sub-horizontal stretching lineation, boudinage and left-lateral shear bands. Deformed lower Devonian breccias at San Antonio antimony mine (Arribas & Gumiel, 1984) show sub-horizontal stretching lineations and approximately plane strains with $X/Z > 4$. The beds steepen towards the southern part of the ridge and the left-lateral shearing intensifies. These changes represent a transition into the Badajoz Shear Zone.

2.3.5 - Summary of cross-section.

The cross-section (Fig.2.2) indicates the changing structural style from folding and thrusting in the Central Iberian Zone to strong strike-slip deformation in the Badajoz Shear Zone. The following changes occur progressively towards the south:

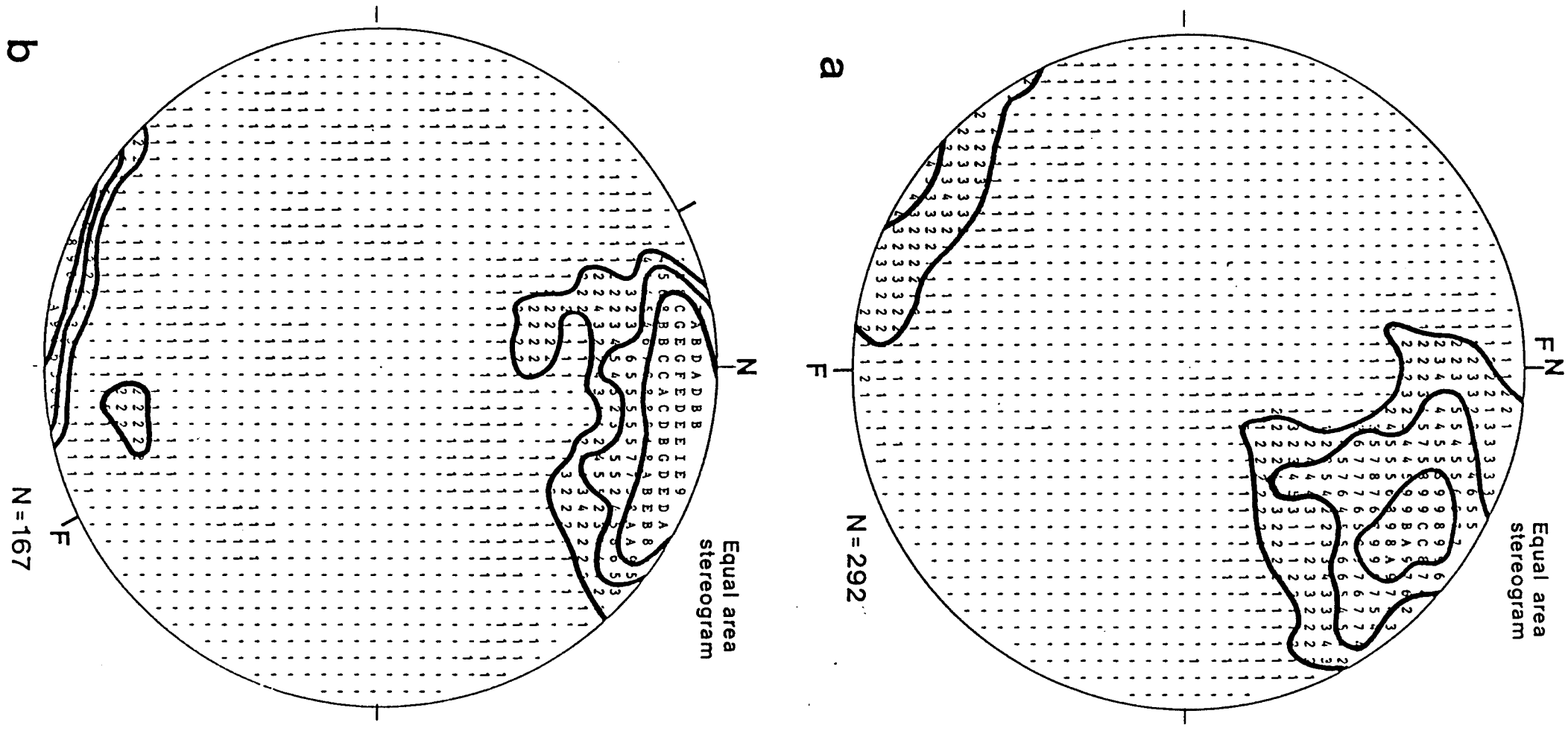

FIG 2.3 - EQUAL-AREA STEREOGRAPHIC PROJECTIONS OF POLES TO CLEAVAGE (S1), A) UNROTATED FAULT BLOCKS, B) ROTATED FAULT BLOCKS TO SE OF LA CODOSERA, F - TREND OF FAULTS. CONTOURS AT 2%, 4% AND 8%

1) "thrusts" steepen and show increasing evidence of oblique or strike-slip movement,

2) deformation increases and folds tighten,

3) a strong sub-horizontal stretching lineation develops,

4) left-lateral shear bands become common (these together with the cleavage form a strong S-C fabric),

5) the strike of bedding and cleavage swings from NW-SE to E-W (Figs. 2.1 and 2.3),

6) F2 folding intensifies,

7) cross-faulting becomes common, with large right-lateral off- sets on NW-SE trending faults (Fig. 2.1 and see below). We interpret these changes as resulting form an increasing strike- slip component within a transpressive regime developed at the Southern margin of the Central Iberian Zone.

2.4 - THE BADAJOZ SHEAR ZONE - TRANSPRESSIVE TECTONICS.

We have already commented on the progressive change from fold-thrust to strike-slip tectonics towards the Badajoz Shear Zone, ie. towards the major left-lateral shear zone separating the Central Iberian and Ossa Morena zones (Burg et al., 1981; Le Fort & Ribeiro, 1980). Although the effects of strike-slip shearing, in the form of sub-horizontal stretching, boudinage, shear bands and other shear criteria, are most clear within the Southern Ridge and in the Urra Formation immediately to the south, we consider that the whole area was subject to prolonged transpression (Sanderson & Marchini, 1984), with increasing shear components towards the south.

There is a consistent obliquity between the strike of the faults and folds within the ridges and that of the main Hercynian cleavage (S1), the latter being slightly clockwise suggesting sinistral shear (Sanderson et al., 1980; Soper et al., 1987). The D2 folds are markedly asymmetrical, with sheared and extended short limbs, and show a consistent sinistral vergence. These features can be attributed to an increasing left-lateral component accompanying shortening (ie. transpression) towards the shear zone. Whilst both the S1 and S2 cleavages progressively swing in strike from NW-SE in the north and west to more E-W in the south (Fig. 2.3), as would be predicted for a left-lateral shear zone, this is mainly due to late domino faulting (see below) and the restored trace of the Southern Ridge curves only slightly.

2.4.1 - Domino faulting.

In addition to this early ductile deformation there is evidence for continued left-lateral strike-slip during the late Hercynian. A set of N-S to NW-SE trending faults with extensional and right lateral offsets, are antithetic to the main shear zone and form a "domino" or "bookshelf" type of geometry (Mandl, 1987).

These faults post-date the Alburquerque batholith. Where the faults have a N-S trend they show little lateral off-set of the steeply dipping bedding, but as they rotate towards the NW-SE the right-lateral displacement increases markedly and the bedding within the fault blocks is rotated into an E-W trend (Fig. 2.4).

This "domino" or "bookshelf" faulting has been studied by several workers in connection with extensional (Wernicke & Burchfiel, 1982) and strike-slip (McKenzie & Jackson, 1983, 1986; Ron et al., 1984; Garfunkel & Ron, 1986) tectonics. Those models, involving rigid fault blocks, imply that as the blocks rotate the displacement/thickness ratio increases and a stretch develops along the zone boundary or decollement (Fig. 2.5a). Since this stretch occurs only within the shear zone there would be a strain incompatibility between the rotated and unrotated parts of the zone, with local gaps and/or overlaps necessary at the zone boundaries. Although some decollement is possible along the northern margin of the Southern Ridge, this is not sufficient to accommodate the stretch produced by the rotating blocks.

McKenzie & Jackson (1986) suggested that for an extending (transtensional) zone one could consider the blocks to be attached across the boundary and allow gaps to develop between them (these could be accommodated by extension and thinning within the blocks). Where rotation would produce overlapping of blocks, as is the case in the La Codosera area (Fig. 2.5b), this must be accommodated by deformation within the block. If the blocks are allowed to lengthen parallel to the faults and thin across them, then it is possible to maintain simple shear boundary conditions and continuity with the unrotated areas. Alternatively, the blocks may thicken vertically to accommodate a reduction in width producing a bulk transpressive deformation, with an overall reduction in the horizontal area of the zone (Fig. 2.5c). This style of deformation essentially involves partitioning of deformation with slip and rotation on the bounding faults and internal horizontal shortening and vertical thickening within the blocks. The internal deformation may have been accommodated by minor reverse/oblique faults and by late NNE-trending kink bands.

2.4.2 - Localization of antithetic faulting.

On a regional scale the Badajoz-Cordoba Shear Zone is characterized by intense ductile deformation with kinematic indicators demonstrating an important component of left-lateral shear (Burg et al., 1981, Abalos, 1989). Continued movement produced antithetic (right-lateral) faults at a high angle to the zone in the La Codosera area, in contrast to E-W trending, synthetic, strike-slip faults which are

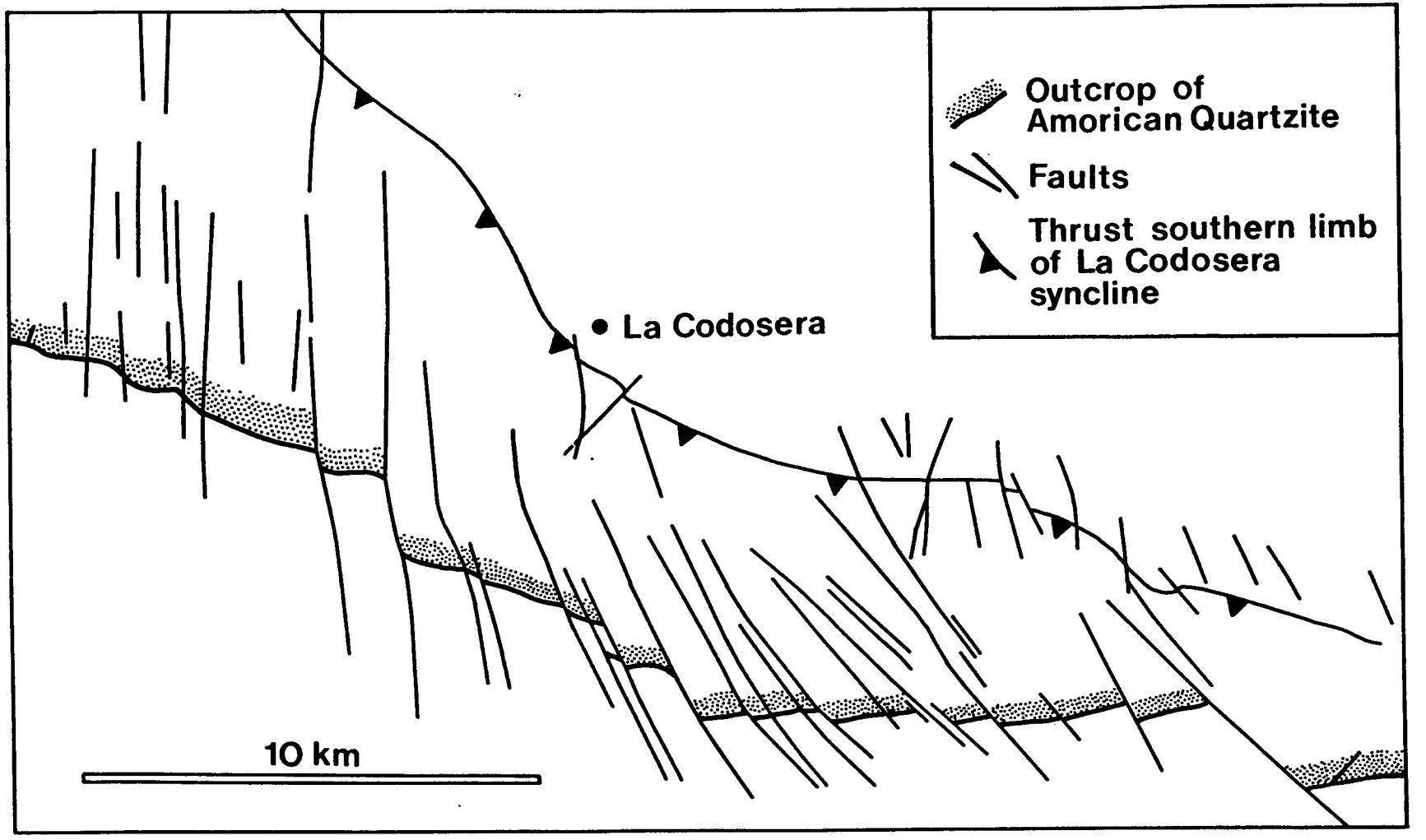

FIG 2.4 - SIMPLIFIED MAP OF FAULTING IN SOUTHERN RIDGE, SHOWING PROGRESSIVE ROTATION OF FAULTS TO SOUTH AND EAST OF LA CODOSERA (BASED ON PUBLISHED MAPS OF THE GEOLOGICAL SURVEYS OF SPAIN AND PORTUGAL).

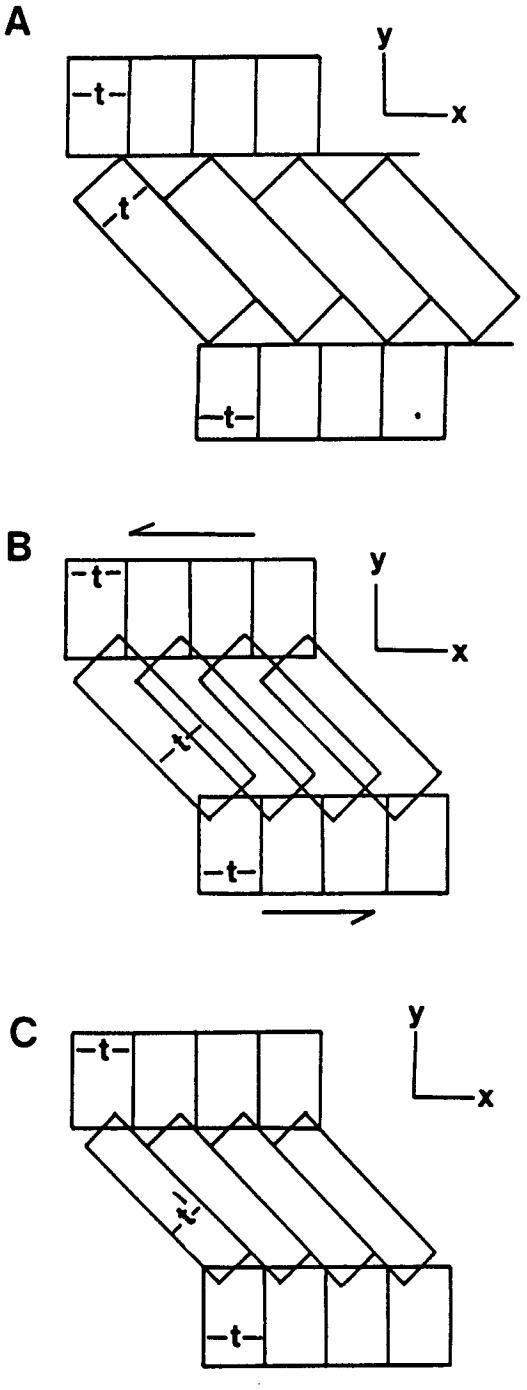

FIG 2.5 - MODELS OF DOMINO OR BOOKSHELF FAULTING.

A) SIMPLE RIGID BLOCK ROTATION PRODUCING EXTENSION ALONG THE ZONE AND DISPLACEMENTS AT ZONE MARGINS.

B) MODEL WITH ROTATING BLOCKS PINNED TO ZONE MARGINS, WHICH REMOVES ALONG ZONE EXTENSION BUT REQUIRES BLOCK OVERLAP.

C) TRANSPRESSION MODEL WITH NO ALONG ZONE EXTENSION BUT WITH LATERAL THINNING OF BLOCKS (t'), ACCOMMODATED BY VERTICAL THICKENING.

more typical of the late stage structures along most of the length of the zone (see for example Abalos, 1989 and the ITGE 1:50,000 geological maps). In this regional setting how can the localisation of antithetic bookshelf-type faulting in the La Codosera area be explained?

An interesting analogy exists with other strike-slip systems, notably the San Andreas system in Southern California. It is important to remember that the San Andreas is a right-lateral system, whereas the Badajoz-Cordoba Shear Zone is left-lateral, thus in the following discussion we will refer to faulting as synthetic and antithetic to allow easier interchange of concepts. Along most of its length, the San Andreas system is characterized by synthetic faulting, but locally zones of anthithetic (left- lateral) faults occur. The two most notable of these areas are in the San Gabriel Mountains (Dibblee, 1977) and the Easternmost Transverse Ranges, to the east of the Salton Trough (Williams et al., 1990). Both are located near major bends in the San Andreas system and are separated by an area of compression in the San Bernardino Mountains. To compare the settings of these regions of antithetic faulting in the San Andreas and Badajoz-Cordoba strike- slip systems, we have taken a sketch map of the San Gabriel example from Dibblee, (1977) and rotated and reflected the fault pattern to conform to that of the left-lateral movement on the Badajoz Shear Zone (Fig. 2.6b).

It is clear that the northern boundary of Badajoz Shear Zone is not straight, but consists of a series of releasing and restraining bends (Crowell, 1974). We have used this observation as the starting point to model the development of the structures on this part of the shear zone (Fig. 2.6a). We consider that the northern boundary of the shear zone was formerly located in the current position of the Alburquerque Batholith and at a releasing bend. Left-lateral shear produced dilation allowing emplacement of the batholith along this part of the margin. On consolidation the granite effectively sealed this branch of the shear zone and displacement was transferred southward to the Southern Ridge. The post-granite, antithetic "bookshelf" faults developed in response to renewed movement on the shear zone allowing both the continued counter-clockwise rotation of the blocks forming the Southern Ridge and their extension around the bend by fracturing and rotating.

2.5- CONCLUSIONS

The geometry of the structures in the La Codosera area, and their spatial and temporal variations, suggest a tectonic model for the boundary between the Ossa Morena and Central Iberian zones. We confirm the importance of left-lateral components of movement throughout much of the Hercynian deformation. The boundary between the two zones suffered left-lateral transpression, with the greatest strike-slip component localized within the Badajoz-Cordoba Shear Zone. Thus early folding and thrusting, in response to NE-SW shortening within the Central Iberian zone, became increasingly transpressive towards the southern margin, producing a progressive change from thrust to strike-slip tectonics across the La Codosera area. The early, penetrative, D1 deformation, became more localized during D2 folding, but maintained a left-lateral component. Late Hercynian fracturing was

characterized by a domino-style rotation of fault blocks, induced by continued left-lateral transpression.

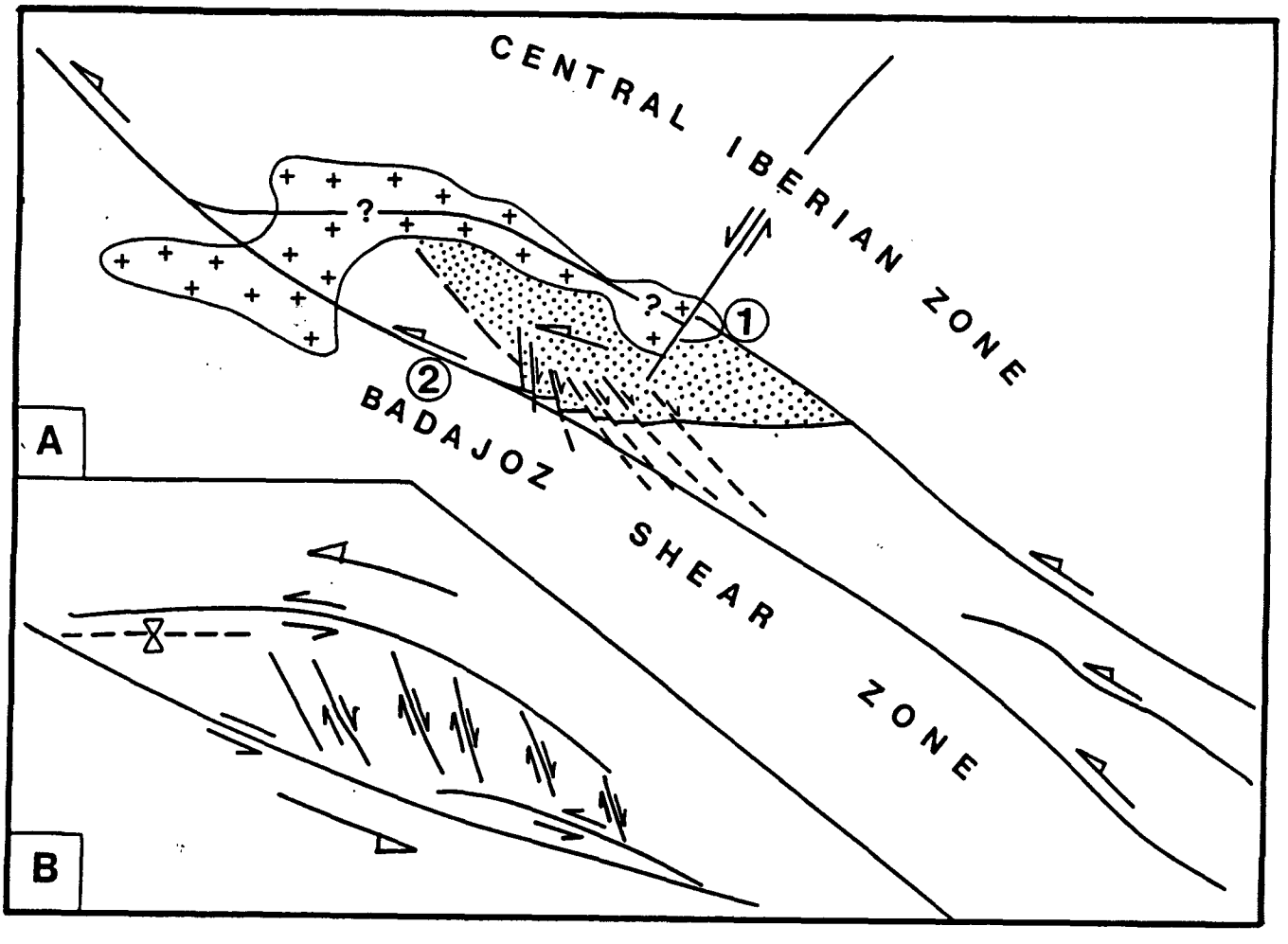

FIG 2.6 - A) SCHEMATIC MODEL FOR THE GENERATION OF THE LATE STAGE STRUCTURES IN THE LA CODOSERA AREA. THE ALBURQUERQUE BATHOLITH (CROSS ORNAMENT) WAS INTRUDED INTO A RELEASING BEND ON FAULT 1, EFFECTIVELY LOCKING IT. MOVEMENT WAS TRANSFERRED TO FAULT 2 AND EXTENSION AROUND THE FAULT BEND PRODUCED THE DOMINO FAULTING.

B) REFLECTED AND ROTATED SKETCH OF THE RIDGE BASIN/SAN GABRIEL MOUNTAINS AREA, CALIFORNIA (AFTER DIBBLEE 1977, FIG. 2-10) TO ILLUSTRATE SIMILARITY TO LA CODOSERA AREA.

CHAPTER - 3 - GEOCHEMICAL SURVEYS.

P. Gumiel & C.G.S.

3.1 - THE GOLD EXPLORATION PROJECT AT LA CODOSERA, BADAJOZ.

ITGE's Gold Exploration Programme at La Codosera, Badajoz has involved geological mapping at various scales, panning (heavy mineral concentrates), soil and stream sediment sampling as well as lithogeochemistry of specific formations*. In the anomalous gold zones, ITGE has reopened old workings, trenched and diamond drilled specific targets. The programme began in 1985, and involved the following stages:

3.1.1 - Strategic geochemical survey.

In the preliminary stage 60 heavy mineral concentrates were collected on a 300x400m grid within the La Codosera area. Six anomalous gold zones were defined by the survey and a stream sediment sampling exercise covered the zone of interest. (Fig. 3.1, Unpub. report ITGE, 1987).

A second heavy concentrate survey involved an extension of the initial area to include the CEG and the Palaeozoic sediments outcropping to the north of La Codosera. 300 heavy mineral concentrates were taken. In this latter survey, 113 (37.6%) concentrates gold nuggets appear (anomaly threshold 164 mg/m3), and several main gold-anomaly areas were delimited (Fig. 3.2). In these anomalous zones a lithogeochemical survey was undertaken. 610 rock samples were collected along sample profiles in the varying lithologies of the CEG and the Palaeozoic rocks (Unpub. report ITGE, 1987). Specific black shales horizons in both sequences show several samples with more than 0.045 ppm of gold, which can be considered as another exploration target in the area.

3.1.2 - Tactical geochemical survey.

In Los Algarbes - Portilla, one of the most interesting areas of gold-potential, more detailed work was carried out. This involved mapping on a 1:5.000 scale, soil geochemistry and trenching and drilling to assist the research. 1400 soil samples were collected on a 500x25 meters grid (Fig. 3.3). The results of the soil sampling indicated three major anomalies: La Portilla, Breña, and Matasiete (Fig.3.4) with gold values higher than 0.1 ppm of gold (Unpub. report ITGE, 1987).

---

*Samples were taken by C.G.S. (ITGE consult).

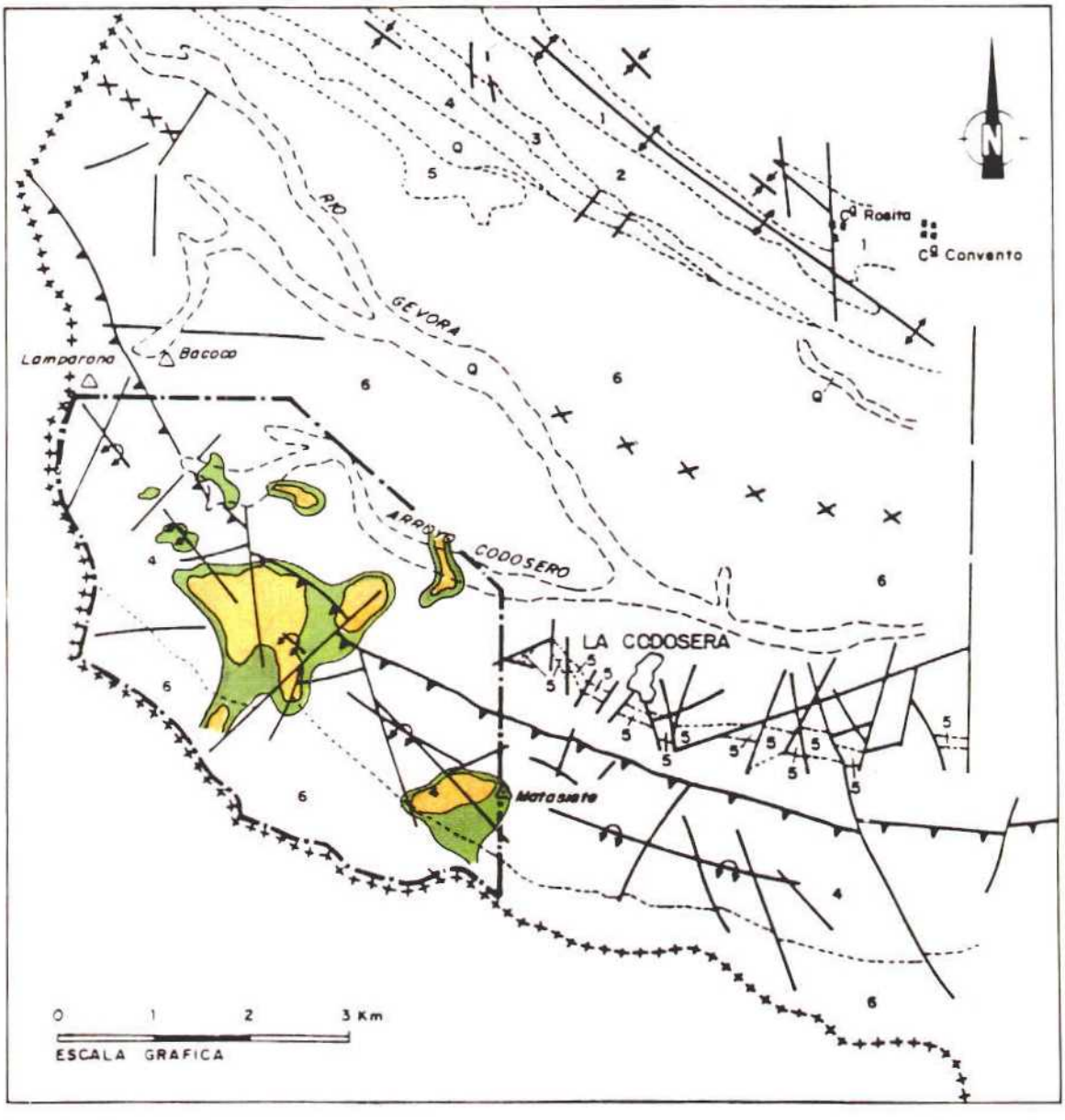

Q CUATERNARIO
Aluviales

6 DEVONICO MEDIO
Filitas

5 EIFELIENSE
Calizas dolomíticas, calcoesquistos y liditas.

4 COBLECIENSE
Cuarcitas y filitas.

3 SIEGENIENSE
Filitas y areniscas ferruginosas.

2 SILURICO SUPERIOR - GEDINIENSE
Cuarcitas, areniscas y filitas.

1 ORDOVICICO SILURICO
Filitas ampelíticas.

100 mg/m³ Au

240 mg/m³ Au

Selected gold potential area

FIG. 3.1 - SELECTED GOLD POTENTIAL AREAS WEST OF LA CODOSERA.

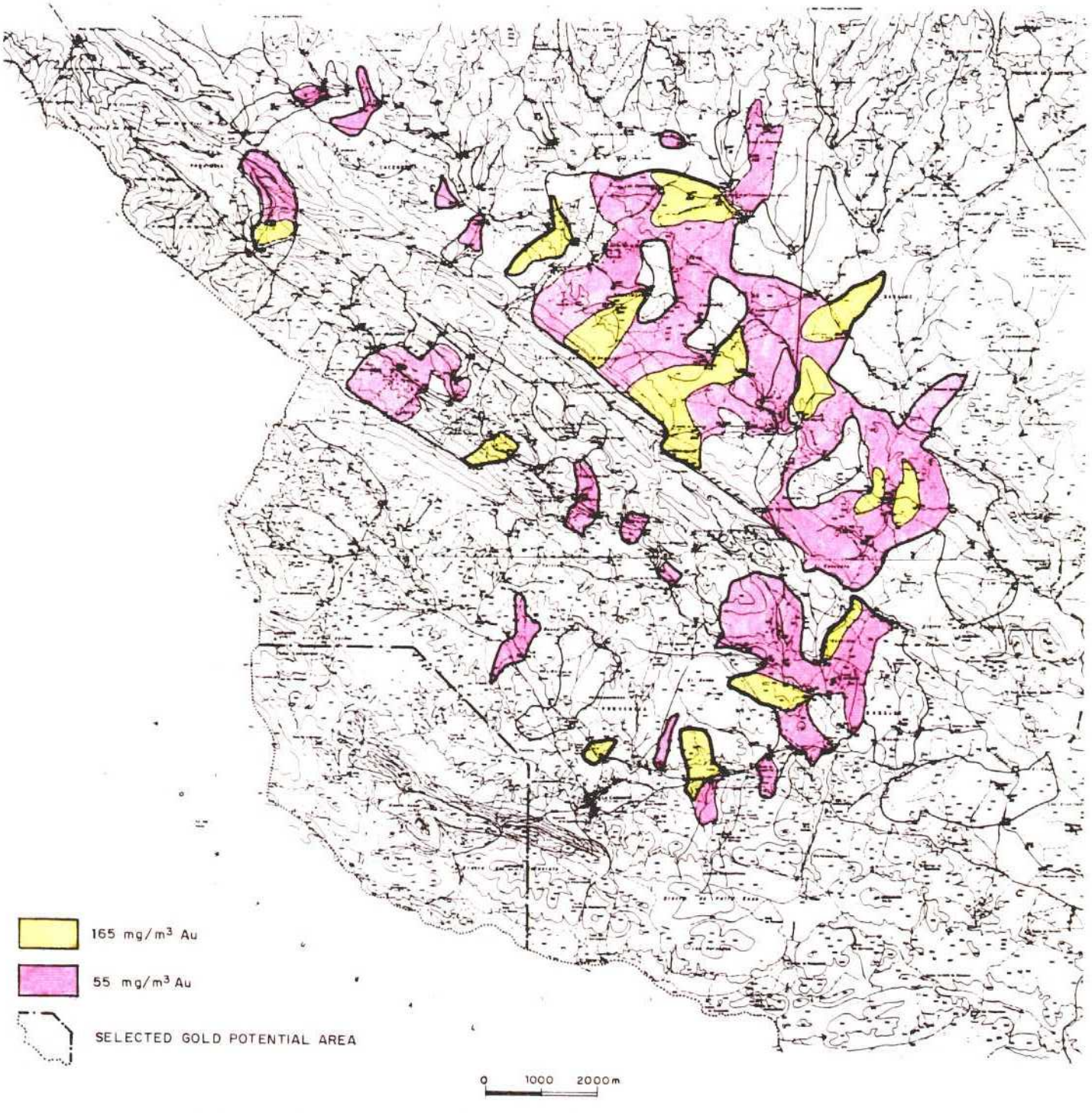

FIG. 3.2 - STRATEGICAL GEOCHEMICAL SURVEY OF THE STUDY AREA (PANNING).

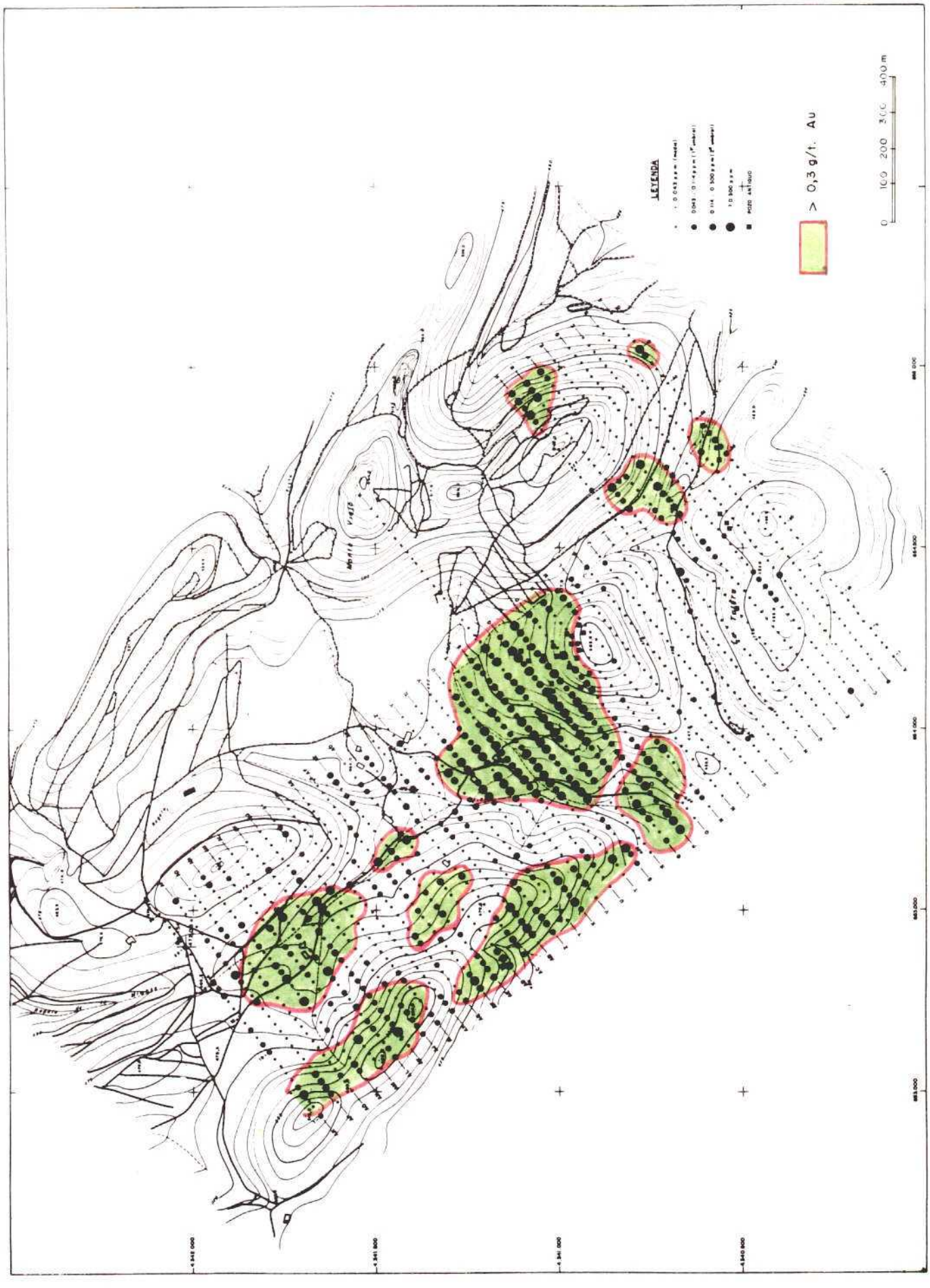

FIG. 3.3 - TACTICAL SOIL GEOCHEMICAL SURVEY IN THE SOUTHERN RIDGE (ALGARBES - LA PORTILLA AREA).

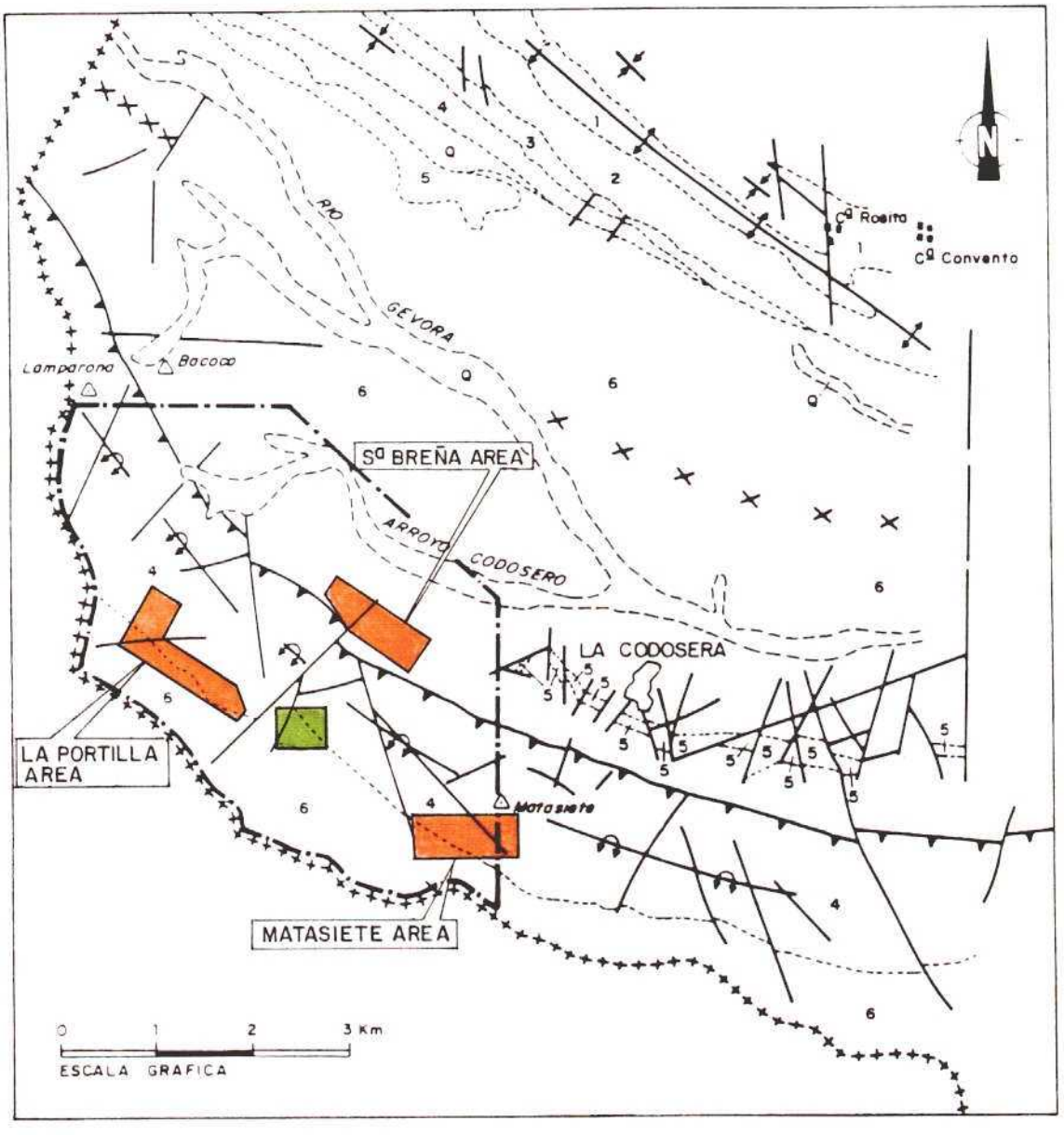

Q	CUATERNARIO Aluviales
6	DEVONICO MEDIO Filitas
5	EIFELIENSE Calizas dolomiticas, calcoesquistos y liditas.
4	COBLECIENSE Cuarcitas y filitas
3	SIEGENIENSE Filitas y areniscas ferruginosas.
2	SILURICO SUPERIOR - GEDINIENSE Cuarcitas, areniscas y filitas.
1	ORDOVICICO SILURICO Filitas ampelíticas

Detail soil geochemical survey in selected areas

Algarbes gold prospect

Selected gold potential area

FIG. 3.4 - LOCATION OF DETAILED SOIL GEOCHEMICAL SURVEY IN SELECTED GOLD POTENTIAL AREAS.

3.1.3 - Detailed soil geochemical survey.

A detailed soil geochemical survey in these three selected areas (Fig. 3.4) was carried out by ITGE (Unpub. report 1989) and the samples were taken from the B-C soil horizon.

The data were imput to the SURFER programme and then X,Y,Z files were generated. An interpolation method of adjusting by kreaging was used to define the 200 and 100x50 m. grids from which contour lines were obtained with a contour interval of 0.005 ppm Au.

At the Sierra de La Breña area 300 samples were taken along 22 profiles (Fig.3.5). The background value was 0.015 ppm Au and six anomalies were present. The most prominent trend is N40°-50°E and N120°E. The first Au-bearing anomaly trend is coincident with the gold-bearing veins at La Perla de Anibal prospect (see Fig. 4.4). Smaller anomalies are open to the southwest and to the east.

In La Portilla area 117 samples were collected along 17 profiles (Fig. 3.6). 67 had gold values higher than the regional background and seven anomalies were present trending approximately N70°E-80°E, N40°-50°E and N110°E. Other, smaller anomalies are open to the west and to the northeast towards the mineralised area of the Algarbes.

At la Portilla, in an anomalous area covering 700x100m several trenches have been dug by ITGE (Fig. 3.7). The lithogeochemical sampling shows Au values ranging from 3.7 g/t Au/1m in CATO III, 5.2 g/t Au/1m in CATO VI, through 8 g/t/2m in CATO IV, to 16 g/t/2m in CATO I, with an average ore-grade between 0.4-0.5 ppm Au. The gold mineralisation appears to be in fractures and veinlets and as impregnations in iron quartzites, microconglomerates and sandstones. The old-workings are located in NE-SW extensional strike-slip fractures where the gold is concentrated in dilation zones in these structures.

At the Matasiete area, 90 samples were taken along 7 profiles (Fig. 3.8). 29 showed gold content higher than the regional background (0.015 ppm) defining three anomalies. Two of them are aligned trending N50°E approximately coincident with the gold bearing veins of the Matasiete prospect and can be traced for over 400 m. along strike. The other anomaly trending E-W can be traced for over 200 m. along strike.

Following the strategic geochemical survey funded by the ITGE and the associated studies within the EEC contract, ITGE has promoted a new self financed programme to follow up on the mining potential of the area.

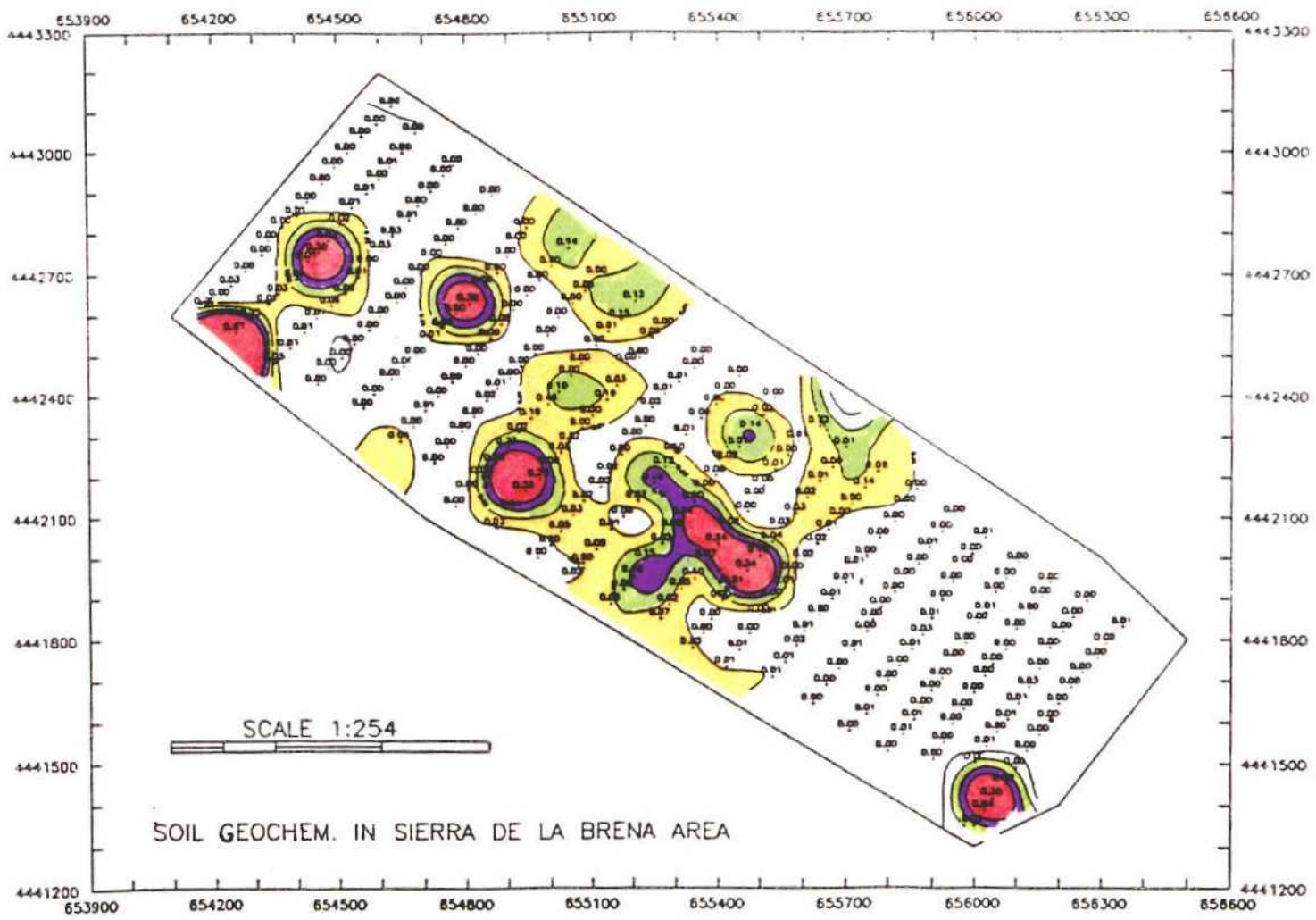

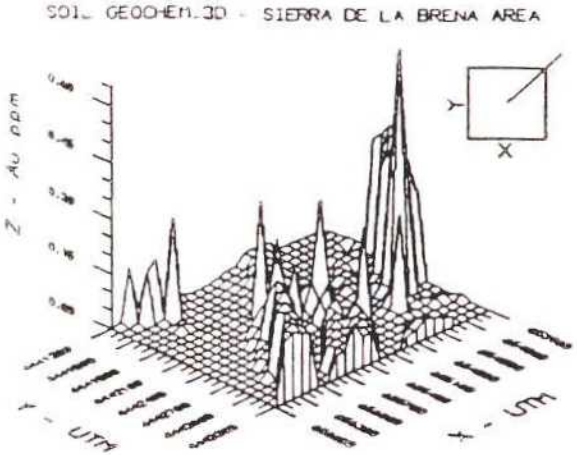

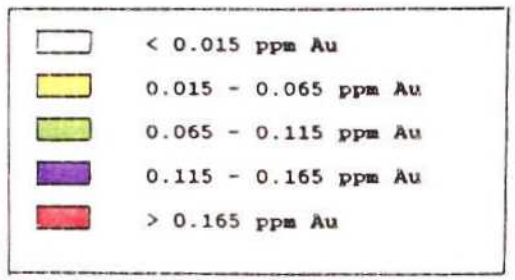

FIG. 3.5 - SOIL GEOCHEMISTRY IN SIERRA DE LA BRENA AREA.

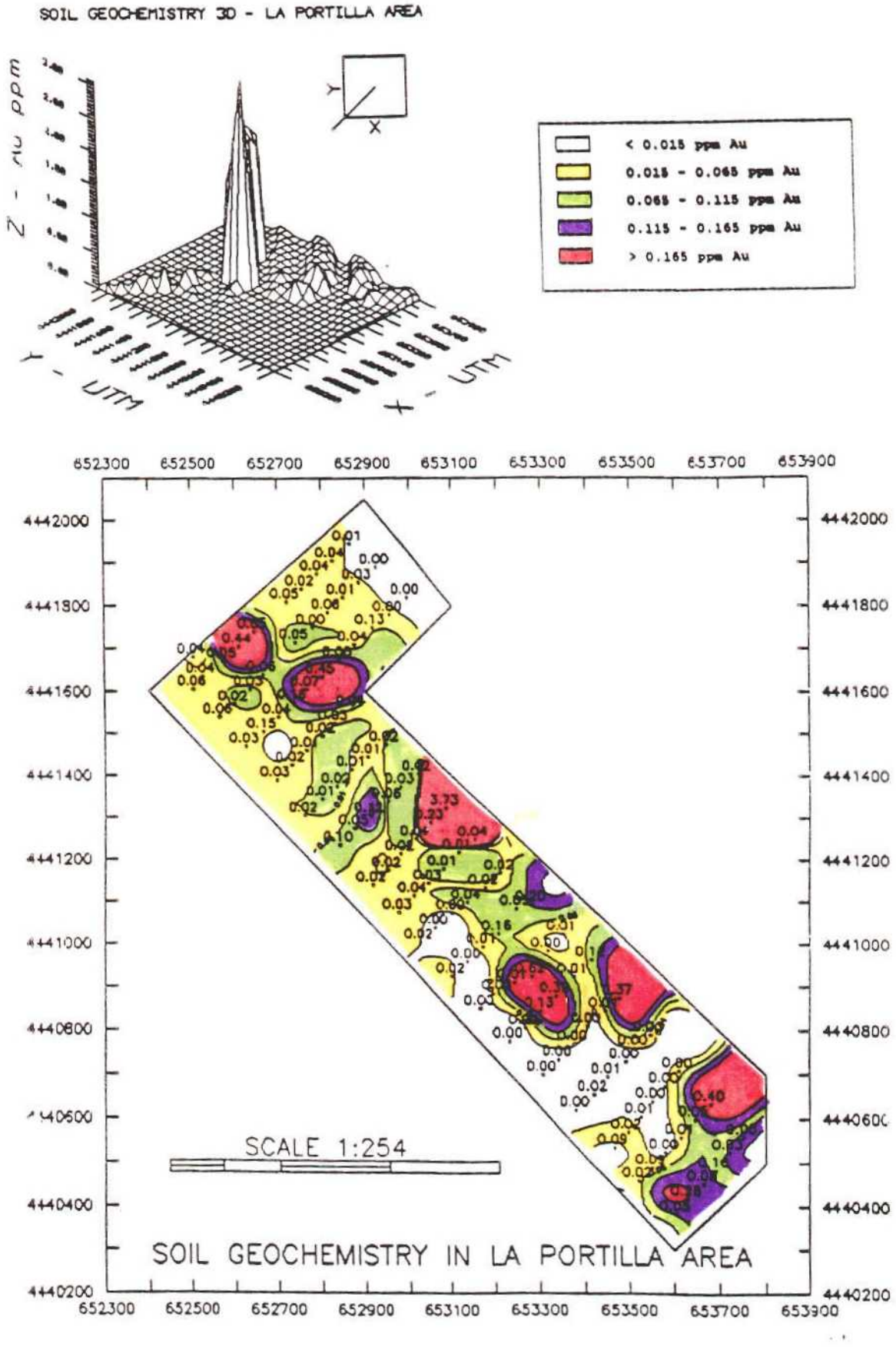

FIG. 3.6 - SOIL GEOCHEMISTRY IN LA PORTILLA AREA.

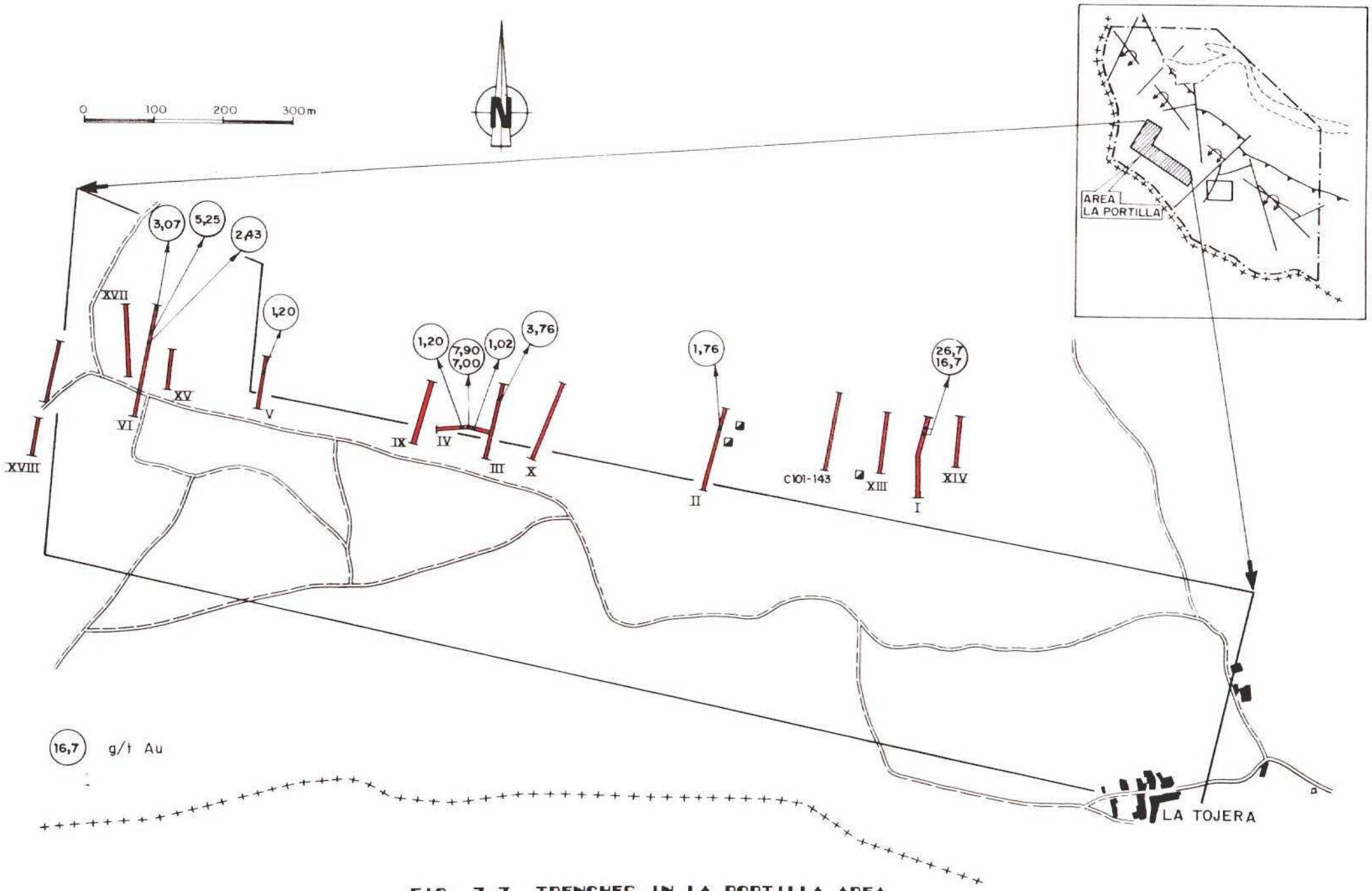

FIG. 3.7 -TRENCHES IN LA PORTILLA AREA.

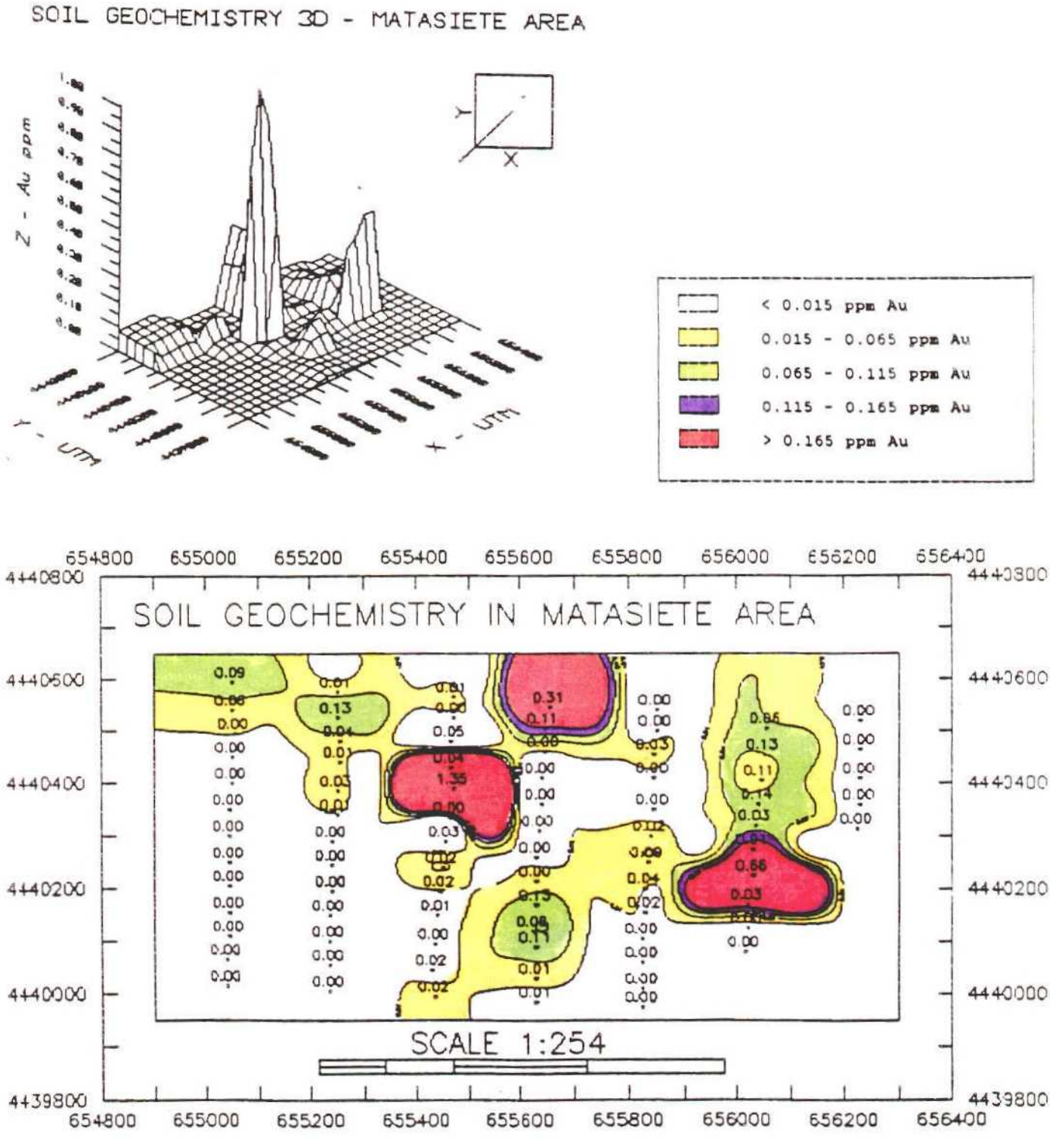

FIG. 3.8 - SOIL GEOCHEMISTRY IN MATASIETE AREA.

CHAPTER - 4 - GOLD PROSPECTS.

S. Roberts, S. Dee & P. Gumiel.

The previous chapter described a series of tactical geochemical surveys, completed by the ITGE, which delimited areas of known and potential gold mineralisation. Many of these prospects represent former Roman workings for gold and are located within the Central and Southern ridges of the La Codosera area. Despite these old workings little previous literature on the gold mineralisation of this region exists save for an obscure reference by Brown, (1864), presented in a private internal report for "The Peninsula Gold Mining and Washing Company". In this report, old mines were attributed to the Romans and the La Codosera area was considered "one of the main places where the Romans Governors removed the almost fabulous wealth acquired during the Spain's Occupation", obviously an erroneous observation given the huge Roman workings recognised from the NW Iberian peninsula (Hewerel & Reading, 1980). The author found several granite millstones and dump material. According to Brown (op.cit.) the gold was associated with quartz veins accompanied by pyrite and Fe and Cu oxides. The main prospects were: Chirriato, Algarbes, Perla de Anibal, Matasiete, Manzana de Oro and Borranchones.

This chapter now describes the geology of the prospects of the Central and Southern Ridges paying particular attention to their different tectonic settings and matallogenic characteristics.

4.1 - STRUCTURE AND MINERALIZATION OF THE CENTRAL RIDGE.

The Central Ridge consists of tightly folded, generally steeply-dipping Palaeozoic rocks, lying unconformably on CEG (Fig.4.1). Several faults have been mapped, which strike parallel to the folds but cut across their limbs. Many of these faults have reverse stratigraphic separation in cross-section (i.e. appear as thrusts), but have important strike-slip components. Large grooves and slickenfibres pitching gently within the fault planes indicating at least a late stage of movement with a left- lateral component. Overall the 'thrusts' appear to accommodate the folding, rather than the folds having initiated on thrust ramps. Essentially the Central Ridge is a large north-verging fold pair, cut by steeply-dipping faults, on the northern limb of the La Codosera Syncline; it resembles an asymmetrical flower structure (Fig. 2.2). All the lithologies of the area show abundant quartz veining, both mineralised and barren.

4.1.1 - E-W trending auriferous veins.

A series of E-W trending auriferous quartz veins are well developed towards the core of the anticline, in particular within the Ordovician slates (Fig 4.1, Table 4.1). The veins show variable thickness < 0.1 - 1.5 m cross-cut the prevailing S1 fabric and can be traced for over 100m along strike. In the field the veins show no discernable alteration halo, a common observation for veins in black schist enviroments (Bottrell et al., 1988).

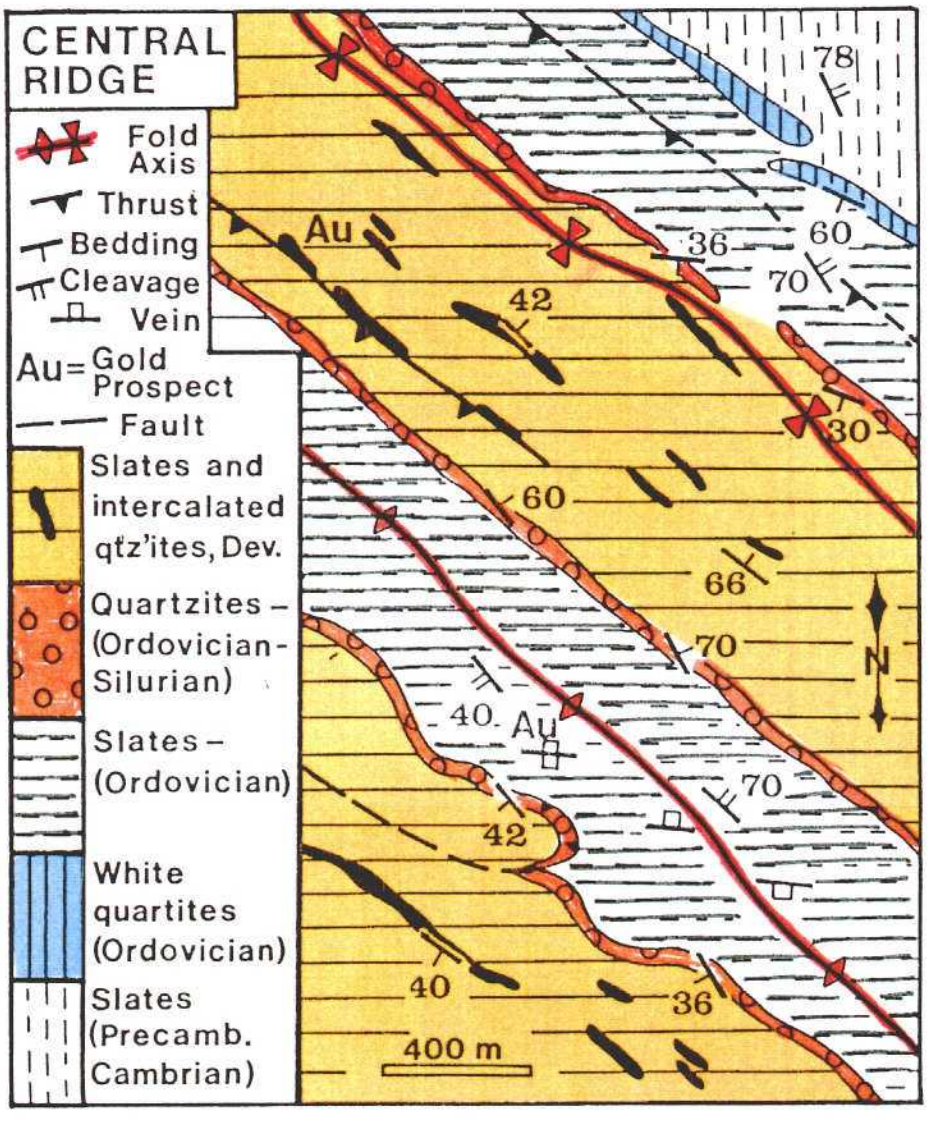

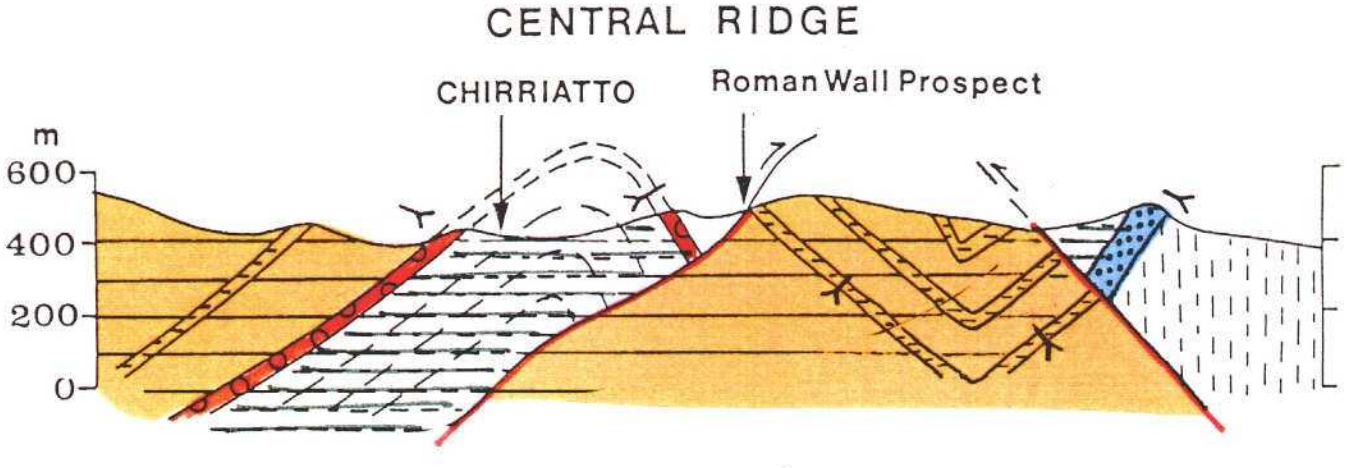

FIG 4.1 - MAP AND CROSS-SECTION OF THE CENTRAL RIDGE.

TABLE 4.1 - INFORMATION ON THE GOLD PROSPECTS OF THE CENTRAL RIDGE.

Locality	Vein Structure	Tectonic Setting	Host Lithology	Wallrock Alteration	Primary Mineralisation	Secondary Mineralisation	Paragenesis	Reported Au values
Chirriato (090/86N) (1)	Composite east west quartz vein post dating 060 composit vein. White quartz. c. 1m wide	Vein oblique to F1 fold axis. Cross cuts So.S1 fabric. Small normal displacement on vein.	Black slates Pyrite rich Ord - Sil	Py - Aspy observed as cubic or rhombic cavities. c.4m zone	Py - Aspy Primary texture not well preserved. Mineral aggregates up to 1cm.	Scorodite. Fe oxide Aspy replaced by scorodite has close spatial relationship with pseudomorphed pyrite.	Qtz Py + Aspy Scorodite Goethite + Limonite	.96-5.1ppm
100m E-W Vein (090/82N) (2)	Composite east west quartz vein White quartz with slate wallrock inclusions common c.1m wide	Vein oblique to F1 fold axis. Cross cuts fabric with normal displacement.	Grey Slates Quartite Ord - Sil	Bleached slates. Quartzite rich in pyrite	Py - Aspy 1mm isolated Aspy rhombohedra. 2cm clusters of Aspy +Py Small Py < 1mm rim aggregates.	Little scorodite or Fe oxides present	Qtz Py + Aspy Py Scorodite Fe oxides	
Penon (140/40SW) (3)	Composit quartz vein strike parallel White quartz. Sulphides occur adjacent to the fwall. 50cm wide	Vein parallel to oblique slip "thrust" with cataclastite Several generations of movement on fault surface	Quartzite Sil	Minor Py + Aspy	Py + Aspy Isolated 1mm Py Aspy + Py along 0.5mm Fractures 20 micron inclusions of Aspy in Py.	Scorodite. Fe oxide Partial or complete replacement of Aspy Pseudomorphs of isolated Py	Qtz Py Py + Aspy Scorodite Fe oxides	1.15ppm
Mina Marianella (130/60SW) (4)	Thin quartz vein strike parallel cross cuts 060 veins. White quartz Main c.10cm 060 c.2.5cm	Vein parallel to F1 fold axis. Cross cuts fabric.	Black Slate Ord - Sil	Extensive Py. Zone c. 1m.	Py 5mm subhedral Py in main vein. 1mm Py fractures parallel to 060. Euhedral Py c.5mm in wallrocks	Goethite Partial or complete pseudomorphs of Py	Qtz Py Geothite	0.015-0.420ppm
Loc 101 (Jola Rd.) (5)	Thin white veins c.1cm cross cut 7cm concretions	Synclinal limb Stockwork of thin extension veins.	Quartzite Sil - Dev	None	Subhedral 1mm Py in veins. Anhedral Py rims euhedral Py + rutile in qtzite. Chpy +Pyrr inclusions.	Goethite Partial alteration of Py.	Py Chpy Pyrr Qtz Py Goethite	0.009-.013ppm

Within the veins drusy quartz grains show pressure solution along compromise grain boundaries and undulatory extinction. Often, the predominant dusty, fluid inclusion rich, quartz grains give way to bands of relatively clear quartz. The sulphide assemblage within the veins is arsenopyrite and pyrite, which may be locally enclosed within drusy quartz grains, or occur as aggregates, >1.5cm in longest dimension, of predominantly arsenopyrite with minor pyrite. Chlorite is locally present within some sections and secondary oxides are common. Pyrite is replaced by goethite and lepidocrocite as cubic pseudomorphs or concentric and nested boxworks, controlled by (100) symmetry planes (Andrew, 1980). Arsenopyrite is replaced sequentially by scorodite and Fe- oxides with pseudomorphs of lozenge shaped crystals or diffuse boxworks, controlled by (110) symmetry planes (Ramdohr, 1969). No visible gold has yet been recorded from the veins, although assays from several of the 080^{o}-110^{o} trending quartz veins show Au contents between 0.960 and 5.10 ppm Au (ITGE Unpub. Report, 1987).

Notably, from an exploration viewpoint, the major E-W trending veins occupy topographic lows within the core of the anticline. This enables their position to be predicted through a combination of geological, topographic and aerial photo-interpretation.

4.1.2 - The Peñon Prospect.

Within the central part of the ridge, just to the north of the anticline, a major quartzite scarp trends 140/48SW across the hillside, for over 300m along strike. This feature resulted from the removal of a 30cm thick quartz vein during Roman exploitation of the area. Structures preserved on the quartzite surface include sub-horizontal slickensides and gutter structures (Hancock & Barka, 1987) which indicate that, latterly at least, strike-slip movement occurred on this surface. The hangingwall to the quartz vein is an imbricated quartzite. This imbrication is in some instances very intense and results in the formation of "fish-eye" rock (see Fig. 4.2).

The quartz vein comprises drusy quartz grains which are cut by bands of recrystallised quartz. Arsenopyrite and minor pyrite occur within both the drusy and recrystallised quartz bands. In places pelitic clasts are enclosed within the vein. No visible gold has yet been reported, although a Au value of 1.15ppm, is presented in a unpublished ITGE report (1987).

4.1.3 - Barren quartz veins.

A series of barren milky quartz veins are observed, trending 020-060, cross-cutting the strike of the bedding within the ridge ($\sim$140), (Fig. 4.1). The veins are particularly well developed within the quartzites and vary between 100 and 300mm in thickness and show no apparent mineralisation (with the exception of one 060^{o} trending vein). Displacement at vein intersections, pinnate veins and the development of slickensides on associated fracture sets, (especially those trending

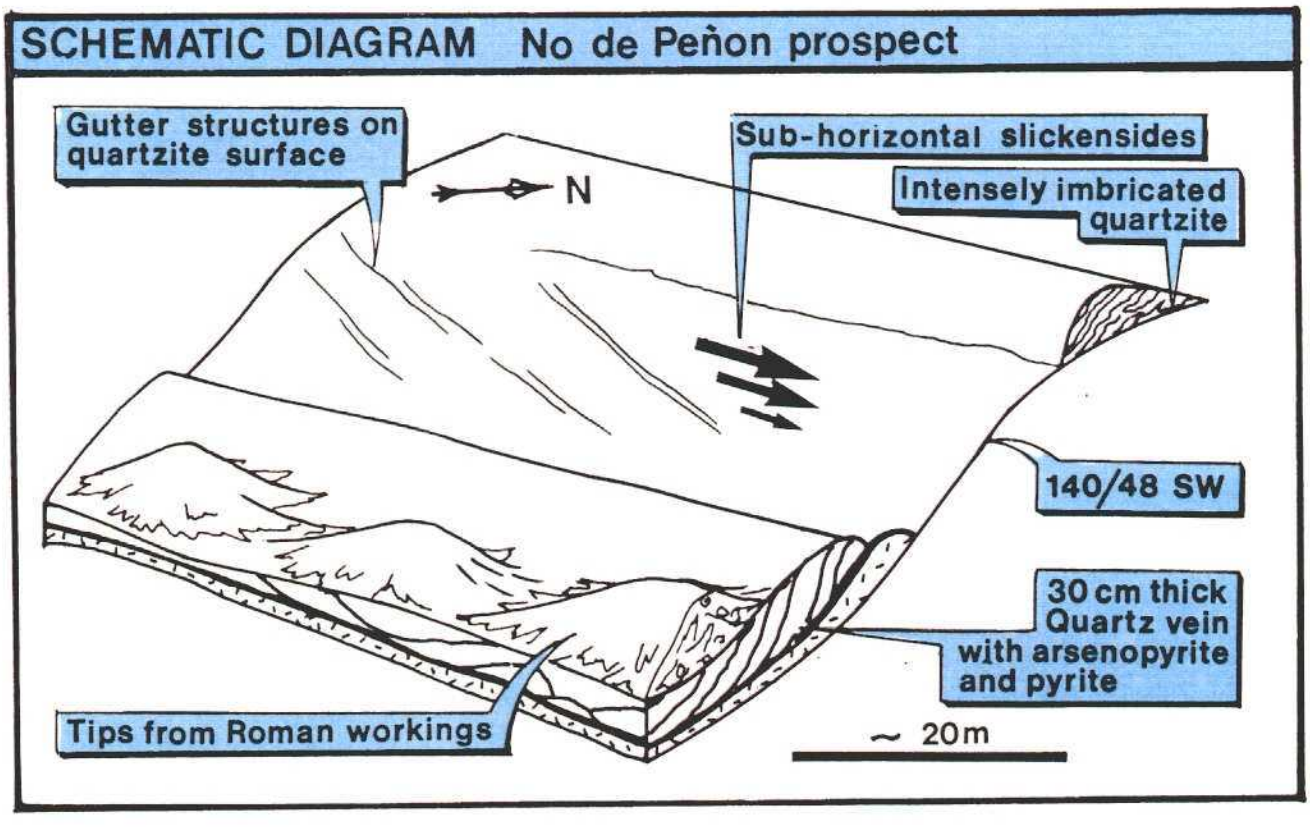

FIG 4.2 - SCHEMATIC DIAGRAM OF THE PEÑON PROSPECT (CENTRAL RIDGE).

020°-040°), indicate that the veins developed with a component of shear. En echelon arrays and rhombic pull-apart structures develop in shear zones associated with pressure solution seams. The veins commonly develop a fibrous internal structure, an indication of crack-seal phenomenon. In thin section there is evidence of continued post- depositional shear in the form of sigmoidal drusy quartz grains and undulatory extinction.

In summary the prospects of the Central ridge comprise a series of syn/post kinematic quartz veins, varying between 10 and 100cm thickness containing a sulphide assemblage of arsenopyrite within sub-ordinate pyrite, with little visible gold. No discernable alteration halos and gold grades varying between 1 and 5 ppm Au.

4.2 - SOUTHERN (OR BORDER) RIDGE

Steeply-dipping and overturned Ordovician to Devonian quartzites and slates, form the highly deformed, southern limb of the La Codosera Syncline. To the west of La Codosera, the Southern ridge strikes NW-SE into Portugal. Detailed mapping around the gold prospects of Los Algarbes, has revealed quartzite units repeated by faulting, usually with a northerly directed reverse separation (Fig. 4.3). They clearly cross-cut the early folds and slaty cleavage and have been reactivated in association with a second phase of folding and crenulation cleavage. Minor F2 folds have sinistral or northerly vergence, consistent with the fault offsets and slickensides on fault surfaces indicative of at least late phases of oblique thrust/left-lateral movement.

The area , in particular the quartz rich lithologies, shows pervasive veining. However, it is on a series of veins restricted to the Devonian black slates that a series of prospects/former Roman workings are present. These can broadly be divided into two main geometrical categories:

4.2.1 - Strike-fault related Prospects.

Within the Devonian sediments of the ridge a series of small quartz veins (5-15cm thick) are observed, commonly situated on minor detachment surfaces (strike parallel, trending 120, shallow-dipping towards the SW) which commonly show reverse separation (thrusts). Reactivation of these structures is indicated by the presence of multiple generations of vein quartz and the development of slickensides which often indicate oblique movement. They all show a late-stage Fe-brecciation event. The size, and lack of strike continuity of these prospects explain why extensive workings are rarely developed.

4.2.2 - High-angle Veins.

In contrast to the above are a series of auriferous quartz veins, which crop out throughout the area and are particularly well developed within the Devonian slates

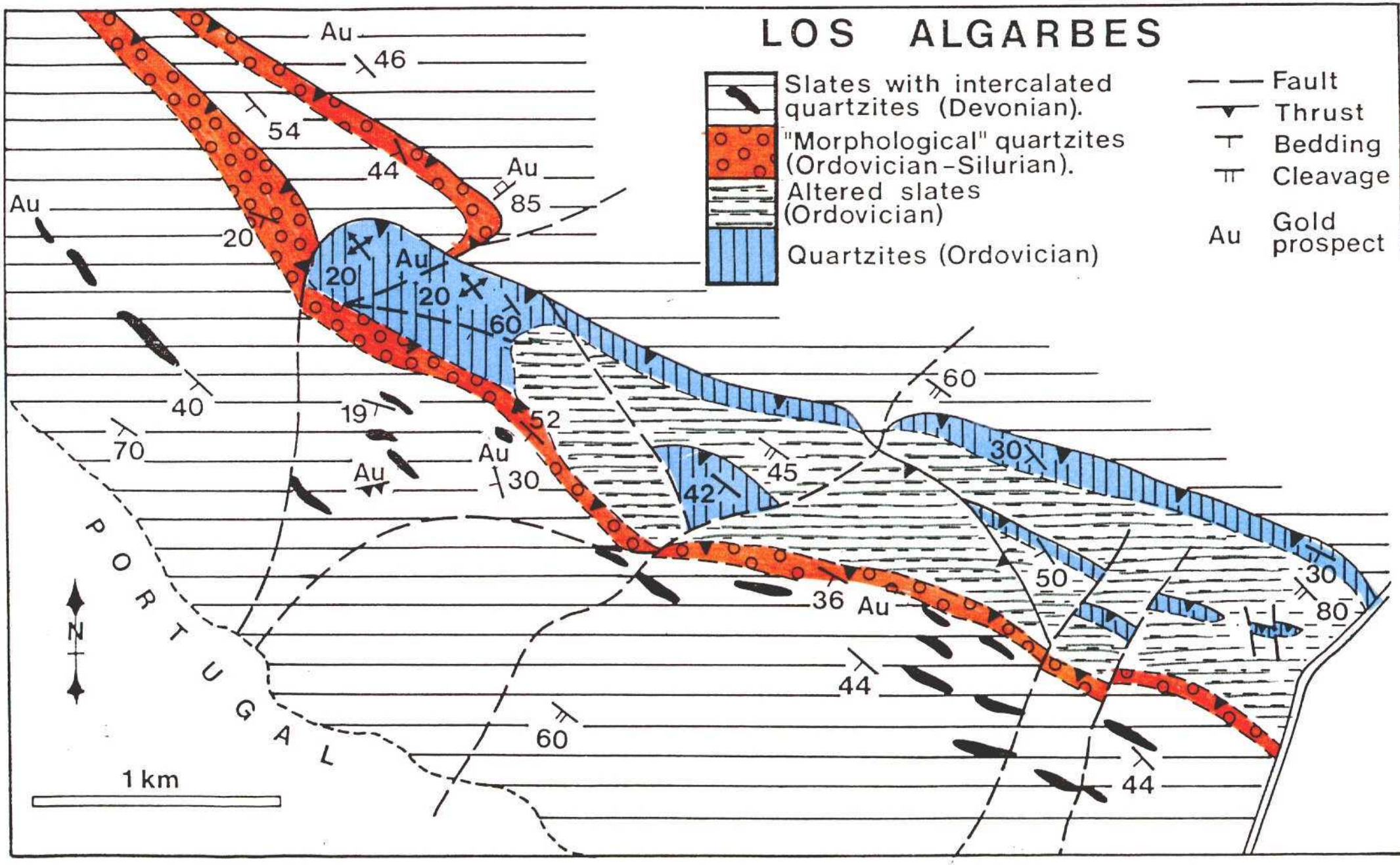

FIG 4.3 - MAP OF THE LOS ALGARBES AREA.

of the Southern part of the ridge and those within the syncline directly to the north of the main thrust (Fig 4.4 and Table 4.2). They trend around 040°, show a high angle to the prevailing structure, and dip steeply to the NW and SE. These veins show little alteration within the syncline, however an area of supergene alteration is associated within the sediments to the southern part of the ridge. These veins show significantly higher grades than the detachment prospects, with reported values of between 2 and 10 ppm Au.

Within both settings the sulphide assemblage is a relatively straightforward one of pyrite and arsenopyrite often with a late goethitic brecciation. Visible gold is rarely observed.

In summary the mineralised veins of the La Codosera area trend 040°, reach a maximum thickness of 1.5 m. and are generally restricted to the Devonian, black slate, lithologies of the area. Their orientation and relationship to the prevailing S1 fabric suggests the veins post-date the main deformation. The veins show little visible wall rock alteration in the field and conform to the commonly described "gold only" veins with a restricted mineralogy of pyrite and arsenopyrite.

4.3 - DRILLING PROGRAMME IN THE ALGARBES AREA (SOUTHERN RIDGE).

On the basis of these observations and following up the tactical geochemical survey ITGE initiated a drilling programme over the area. The initial findings of this survey are outlined below. A three-dimensional model of the Algarbes prospect has been established (Fig 4.5). The structural model is similar to the model of La Perla de Anibal prospect (see Fig. 4.4). The major structure is a N60°-70°E trending extensional fault, with sinistral strike-slip movement, developing dilation zones and N20°-25°E trending pinnate quartz veins. These structures provide sites for the formation and preservation of gold mineralisation and the old-workings appear to be aligned with these pinnate structures. Structural control is therefore of major importance.

The three-dimensional model has been compiled from detailed logging, which involves the plotting of the most relevant structural data, intersections of different sets of veins, faults, bedding and cleavage. The highest gold values(*) ranging from 3.41 g/t over 0.90m, 3.71 g/t over 2.30m in CODO 5, 2.235 g/t over 0.40m at 190m depth in CODO 10, 2.145 g/t over 0.60m in CODO 12, to 0.5 and 1.5 g/t Au in the associated pinnate veins.

(*) Nb) High core loss when intersecting gold adits and fault.

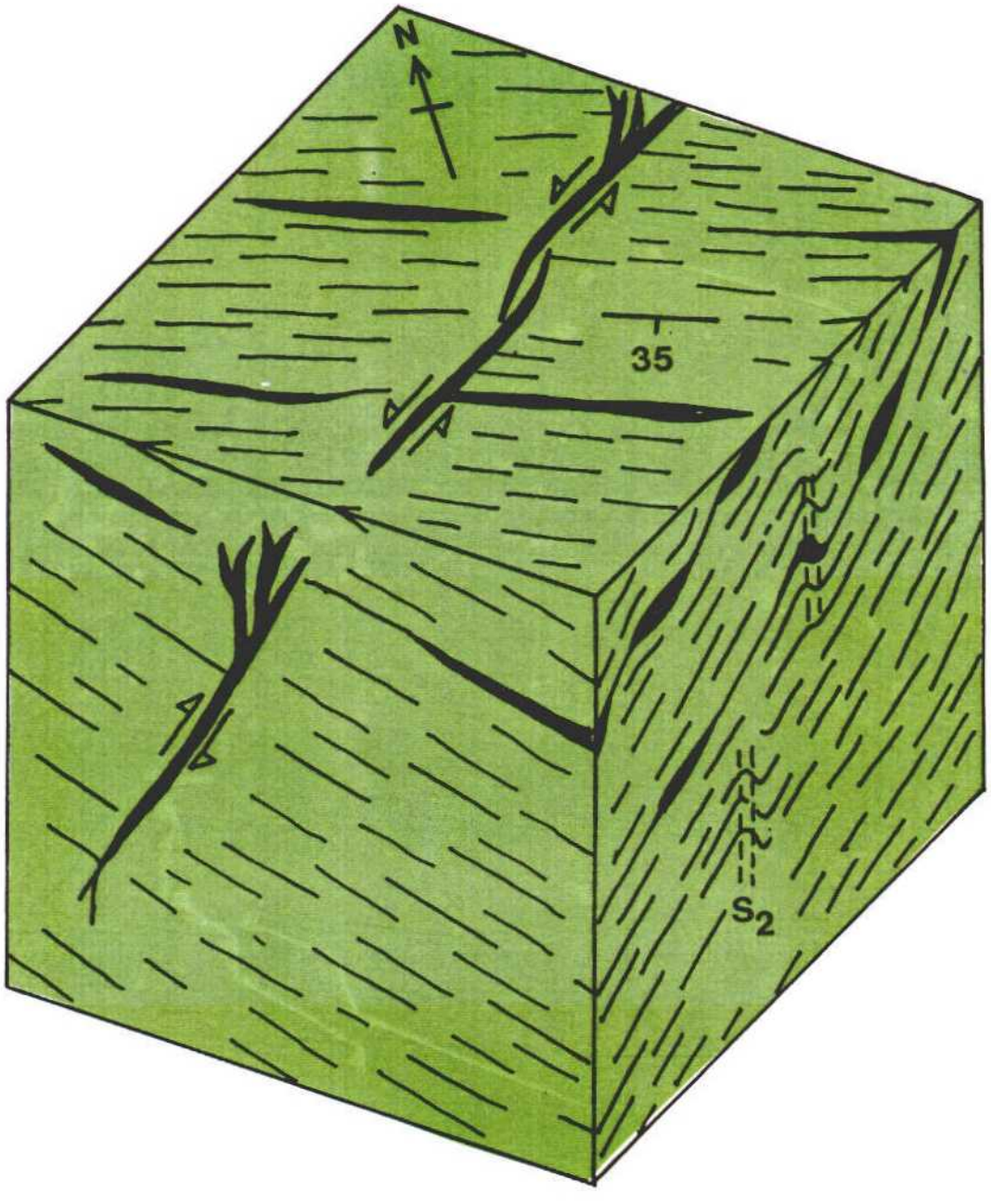

FIG 4.4 - SCHEMATIC BLOCK DIAGRAM OF THE PERLA DE ANIBAL PROSPECT. A HIGH ANGLE MINERALISED VEIN WITHIN DEVONIAN BLACK SLATES.

TABLE 4.2 - INFORMATION ON THE GOLD PROSPECTS OF THE LOS ALGARBES AREA.

Locality	Vein Structure	Tectonic Setting	Host Lithology	Wallrock Alteration	Primary Mineralisation	Secondary Mineralisation	Paragenesis	Reported Au Values
Matasiete (080/72S) (1)	Composit quartz vein strike parallel White quartz with few wallrock inclusions c. 10 - 30cm	Vein parallel to strike in thrust? related seting	Quartzite Slate Dev.	Py - Aspy Chlorite Variable	Py - Aspy Sporadic aggregates c2mm of Py + Aspy	Fe Oxides Extensive matted geothite + limonite +0.1mm remnant Py Replacement of Aspy by Scorodite.	Qtz Py + Aspy Scorodite Goethite Limonite.	
Los Algarbes (080/40S & 030/86NW) (2)	Composit quartz vein strike parallel White quartz with few wallrock inclusions. c.20 - 100cm	Veins related to detachment surfaces and high angle veins cross-cutting fabrics	Quartzite Slate Dev.	Py - Aspy in slate	Py - Aspy Sporadic aggregates c2mm of Py + Aspy Py in thin extension veins.	Fe Oxides Extensive brecciated qtz + matted Fe oxides +0.1mm remnant Py Replacement of Aspy by Scorodite.	Qtz Py Py + Aspy Scorodite Fe oxides	.11-3.7ppm
Perla de Anibal (050/85NW) (3)	30cm thick qtz vein	High angle to So.S1.	Black Slate Dev.	Py	Py-Aspy			.15-7.2ppm
La Portilla Arriba (040/62SE & 140/50S) (4)	Discrete white qtz veins. Abundant minor veining in slates	Discete veins at high angle to So.S1. Minor veining subparallel So.	Altered Dev slates.	Py	Py-Aspy			Veins 1.2-26.7ppm Zones of minor veining .05-7.6ppm
La Portilla Larga (020/78NW) (5)	Milky qtz vein.	High angle So.S1	Qtzite Dev.	Py				.09-22.8ppm

GEOLOGICAL MAP OF "LOS ALGARBES" GOLD PROSPECT
(FROM FIELD WORK AND DRILL-HOLES DATA)

SCALE = 1 5000

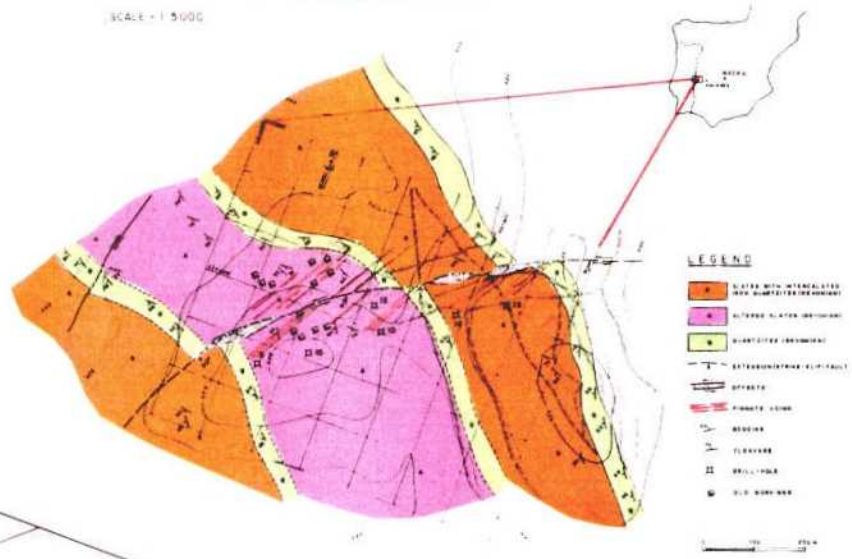

THREE-DIMENSIONAL MODEL OF "LOS ALGARBES" - GOLD DEPOSIT
FROM DRILL-HOLES DATA LA CODOSERA, BADAJOZ (SPAIN)

SCALE = 1 2 000

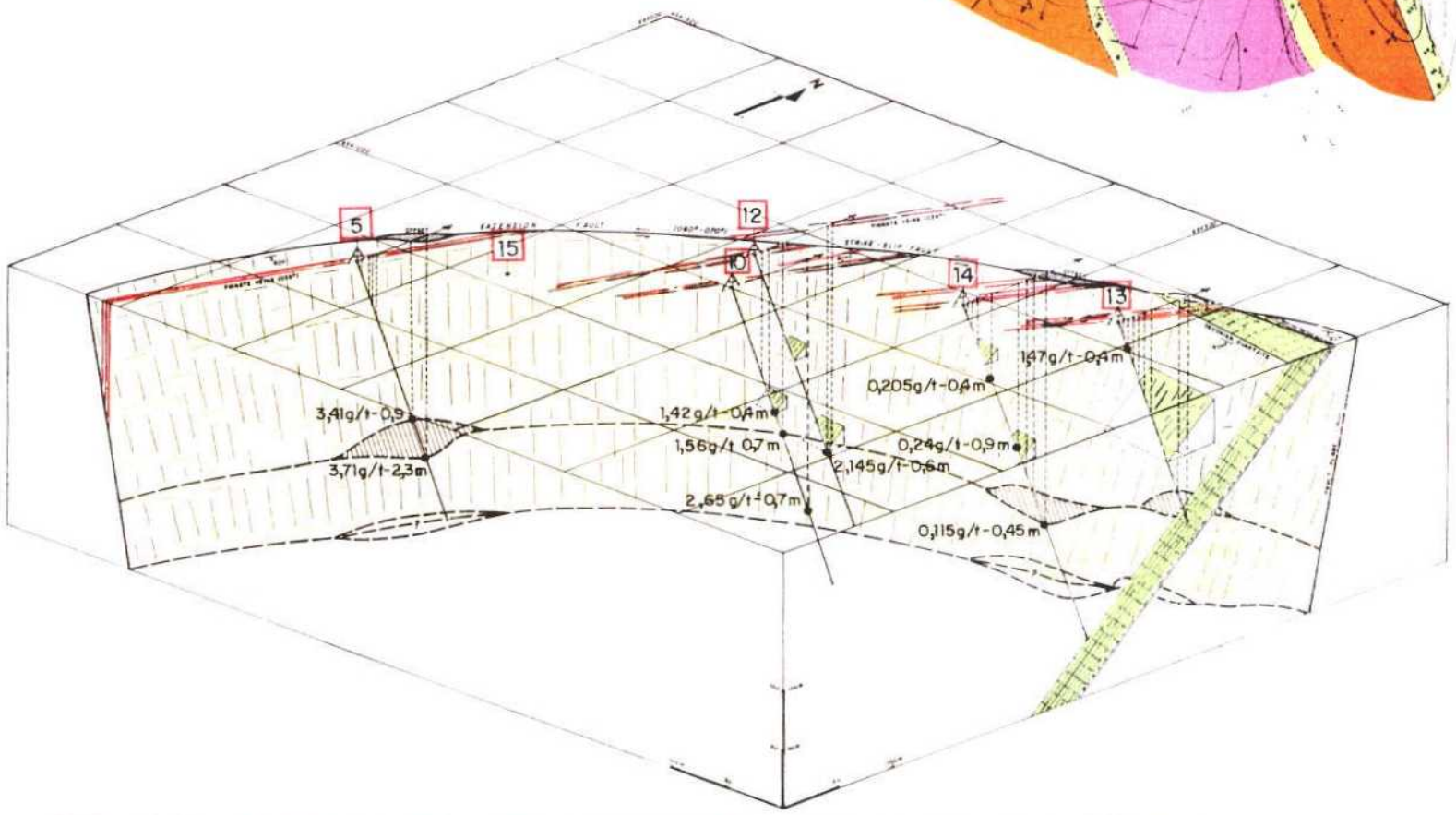

FIG. 4.5 - THREE-DIMENSIONAL MODEL OF LOS ALGARBES GOLD PROSPECT FROM DRILL-HOLES DATA.

This structural model, established from ground observations and drilling data, can provide an explanation for the location of other gold occurrences in the study area (Matasiete, Portilla, Borranchones).

A complementary lithogeochemical drill-core sampling has been carried out to check if any specific host-lithology (Table 4.3) had enough gold-content, which could be considered as "gold- bearing lithology". This lithogeochemical study has been done in unmineralised rock samples aimed to prove if any specific target had higher "gold-bearing stock" and thus the remobilisation processes towards fractures could play an important role in the genesis and gold concentration.

TABLE - 4.3 - Gold Lithogeochemistry.
(Gold content in different lithologies from drill cores)

Litholog.	codo13	codo14	codo12	codo10	codo5	Average Composition
Quartzites	(1) -0.005	- -0.005	(1) -0.005	(2) -0.005	(2) -0.05	(6) -0.05
Quartzites with veining	-	-	(1) +0.530	(3) +0.480	-	(4) +0.4925
Black shales with py	(2) -0.005	(3) +0.005	-	(1) -0.005	(3) -0.005	(9) +0.005
Black shales with veining	(4) +0.005	(3) +0.015	(2) +0.110	(8) +0.153	(1) +0.025	(18) +0.085
Iron sandsto-nes	(3) +0.005	(3) +0.026	-	(4) +0.0125	(1) +0.010	(11) +0.0139

CHAPTER - 5 - GEOCHEMISTRY.

S. Roberts & S. Dee.

This chapter presents the results of a series of geochemical analyses aimed at complimenting the geology of the mineralised terrain established so far.

First, a study of the P-T-X systematics of both mineralised and barren vein sets provides information on the nature of the mineralising fluid and the temperature and pressure prevalent during entrapment. When combined with other geological information these data will contribute significantly to the overall exploration model.

The results of the fluid inclusion investigation are then followed by three short sections outlining:

a) Arsenopyrite geothermometry of the sulphide assemblage

b) A thermoluminescence study of the Vein sets.

c) A beta-autoradiographic study of the mineralisation

Other geochemical data acquired within the auspices of the study, e.g. major, trace, REE and Rb/Sr isochron analyses of the Albuquerque Batholith and whole rock analyses of the host lithologies are excluded for the sake of brevity but are available on request.

5.1 - FLUID INCLUSIONS.

Fluid inclusion analyses have been completed on a series of auriferous and barren veins from the La Codosera area.

5.1.1 - Analytical Technique.

Unmounted, doubly polished 100-200 m thick wafers of vein quartz were analysed using a LINKAM THM600 heating/freezing stage. The stage was attached to a LIETZ DIAPLAN microscope using a NIKON PLAN 40 objective; for operating procedure see Shepherd (1981). Accuracy is calibration dependent and is estimated at $\pm 0.5^{\circ}C$ between -100° and -20°C, $\pm 0.2^{\circ}C$ between -20° and 30°C, $\pm 1^{\circ}C$ between 30° and 200°C and $\pm 5^{\circ}C$ between 200° and 500°C. As demanded in modern thermometric analysis measurements of phase transitions were reproducible to $\pm 0.2^{\circ}C$. Thus, analytical errors are insignificant with regard to any geological interpretation.

Two distinct inclusion populations were recognised throughout the study of both auriferous and barren veins and are described below.

5.1.2 - Type 1 Inclusions.

These inclusions are characteristically large (5-25 μm) three phase L(aq) + L(CO_2) + V, classical "bubble in bubble" inclusions, which tend to occur as clusters sporadically distributed throughout individual samples. The inclusions show flattened and negative crystal shapes and are generally discrete, although they can occur as large inclusions within trails of smaller $<5\mu$m ones. No daughter minerals have been observed.

Type 1 inclusions show a typical degree of fill around 0.5 (F = volume fraction of the aqueous phase), although a second peak can be discerned around 0.7. During the freezing/warming cycle melting of solid CO_2 ($TmCO_2$) showed a range of values from -57.0° to -66.2°C (See Fig. 5.1a/b). These data show that the melting point of solid CO_2 has been significantly depressed indicating the presence of an additional volatile phase to CO_2. Moreover, close examination of the data (Fig 5.1a, b) reveals that, whereas all veins show relatively pure CO_2-rich inclusions (-56.6° to - 58°C) it is the auriferous veins which contain the more depressed inclusion population (-57° to -67°C). If we attribute the depression of $TmCO_2$ values to the most likely volatile component CH_4, following Heyen et al. (1982), amounts in excess of 20 mole % CH_4 appear to be present within some of the mineralised samples.

In these CO_2-rich Type 1 inclusions ice melting was not established with any confidence and so the next reported phase transition is clathrate melting in the range 8.2°C to 11.6°C. Using the experimental data of Collins (1979) a salinity of <4 wt% equiv. NaCl for all inclusions is indicated. The preponderance of clathrate values >10°C confirms the presence of additional volatile phases and signals that the estimated salinity values should be viewed with caution (Burruss, 1981).

The homogenisation of CO_2(CO_2(L + V)---> CO_2(L)) ranges from 12 to 26.9°C and shows two discrete modes around 14 and 24°C. From the available thermometric data (F, and $ThCO_2$) the Type 1 inclusions, with $TmCO_2$ in the range -56.6° to -58°C, contain approximately 40 wt% CO_2, (Mole fraction ~.21). A plot of $TmCO_2$ v $ThCO_2$, (Fig. 5.2), suggests that the lower $ThCO_2$ corresponds to a general increase in additional volatiles (CH_4), as indicated by the depression of the melting point of CO_2 and predicted from phase equilibria in the system CO_2-CH_4 (Hollister & Burruss, 1976). Thus on the basis of $TmCO_2$ v $ThCO_2$ a broad subdivision of Type 1 inclusions may be attempted. On returning to the samples it is observed that the more volatile rich, Type 1(b) inclusions are more prevalent in proximity to sulphide grains within the sample (Raman analyses have subsequently confirmed these additional volatiles as methane with an notable amount of Nitrogen)

Total homogenisation (Th(TOT)) in Type 1 inclusions is rarely observed due to the decrepitation of the inclusion prior to homogenisation. Where observed the mode of change is either critical or from L + V--> V with values ranging from 287.3°C to 372°C with a mode around 300°C for both "mineralized" and barren fluids.

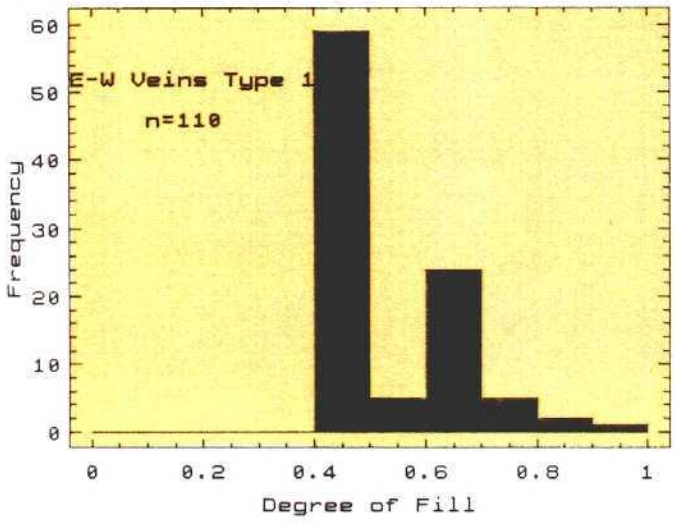

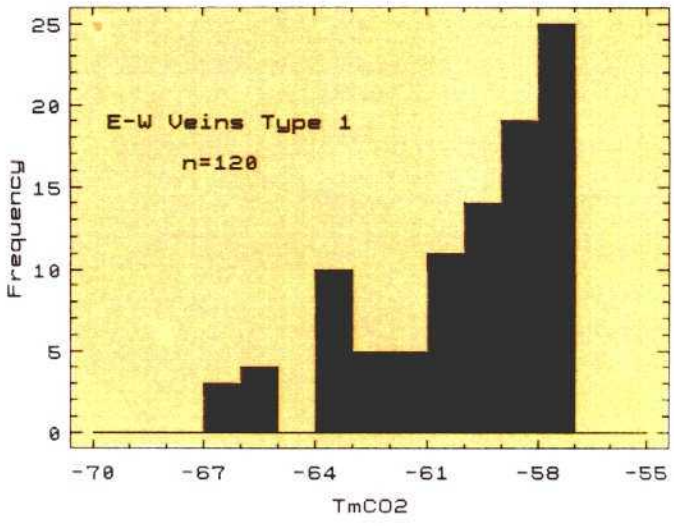

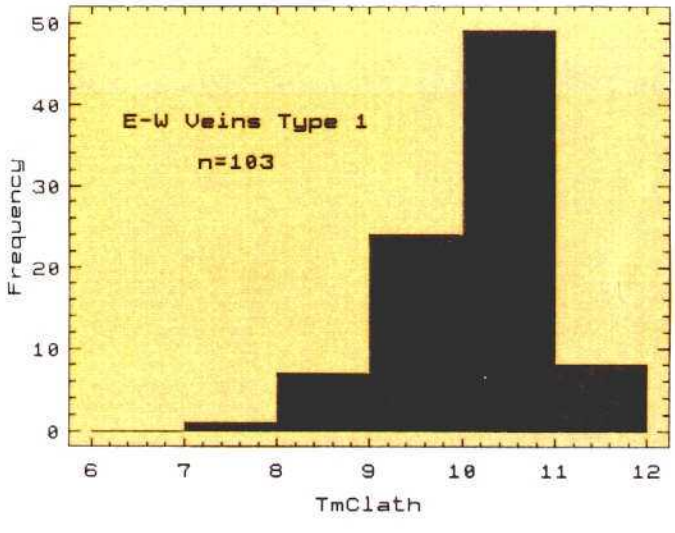

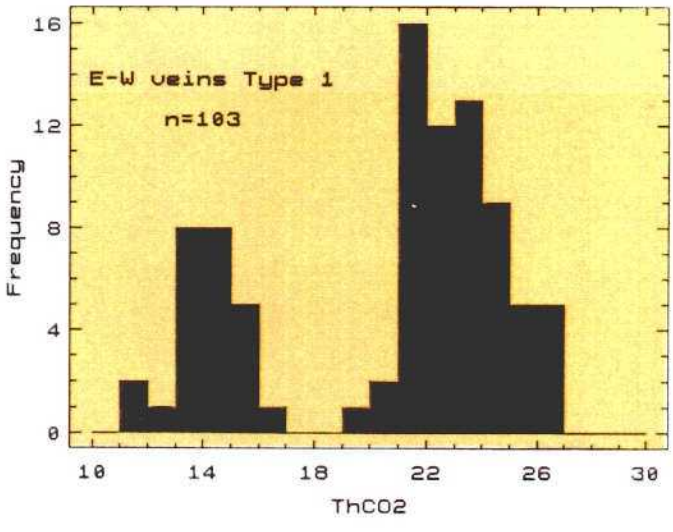

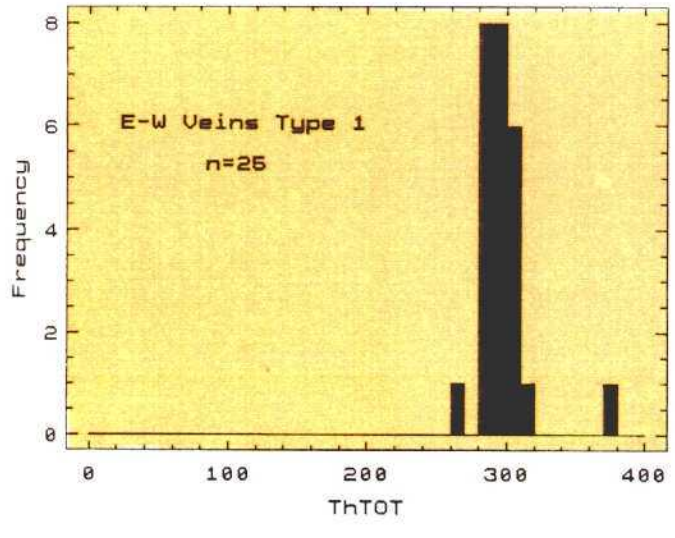

CENTRAL RIDGE E-W VEINS
(MINERALISED)

TYPE 1 INCLUSIONS

FIG 5.1a - FREQUENCY HISTOGRAMS OF FLUID INCLUSION DATA FOR TYPE 1 INCLUSIONS FROM MINERALISED VEINS OF THE CENTRAL RIDGE.

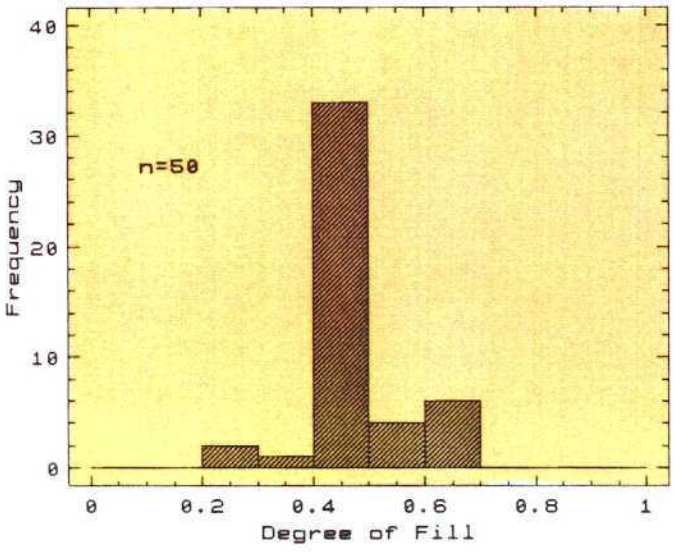

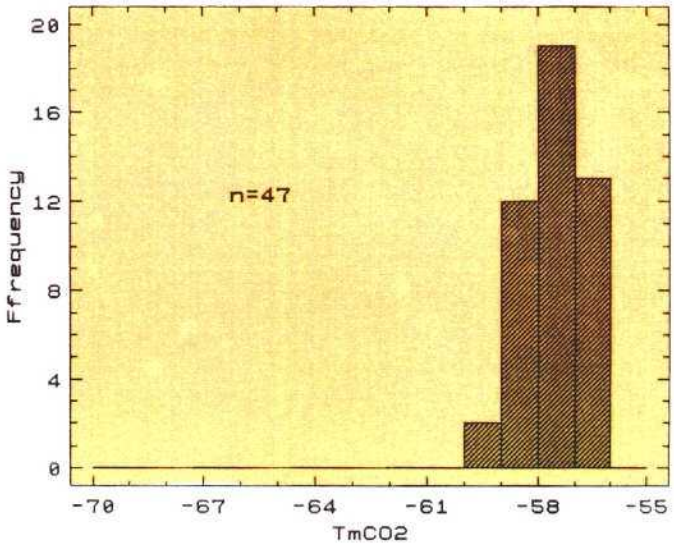

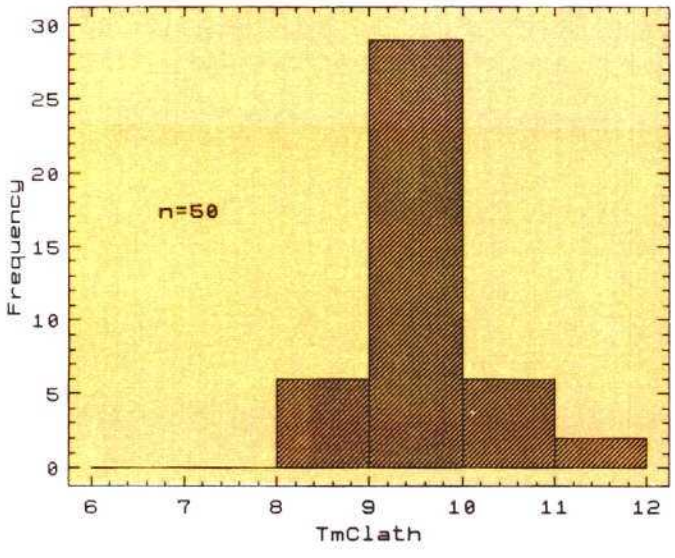

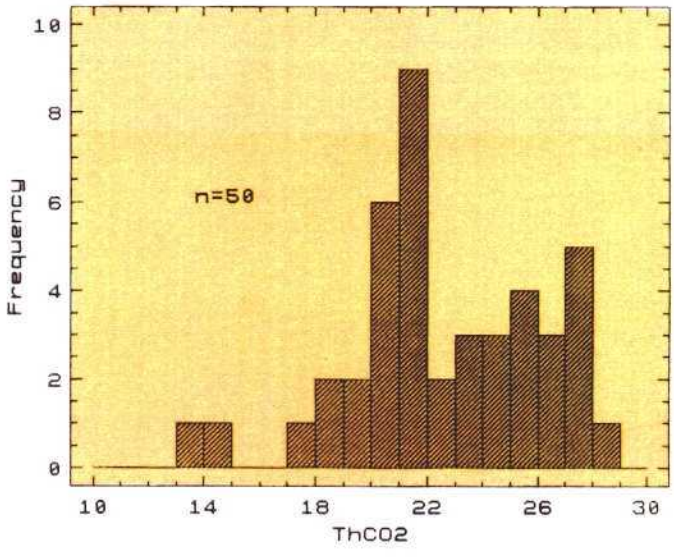

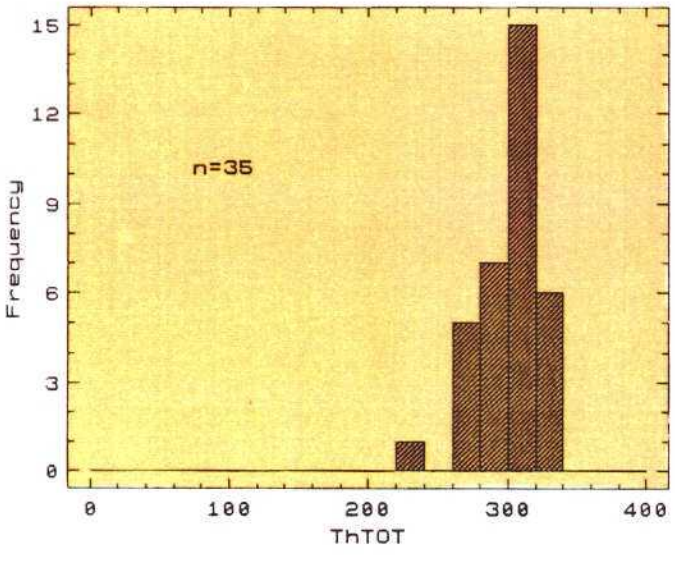

CENTRAL RIDGE OTHER VEINS

TYPE 1 INCLUSIONS

FIG 5.1b - FREQUENCY HISTOGRAMS OF FLUID INCLUSION DATA FOR TYPE 1 INCLUSIONS FROM BARREN VEINS OF THE CENTRAL RIDGE.

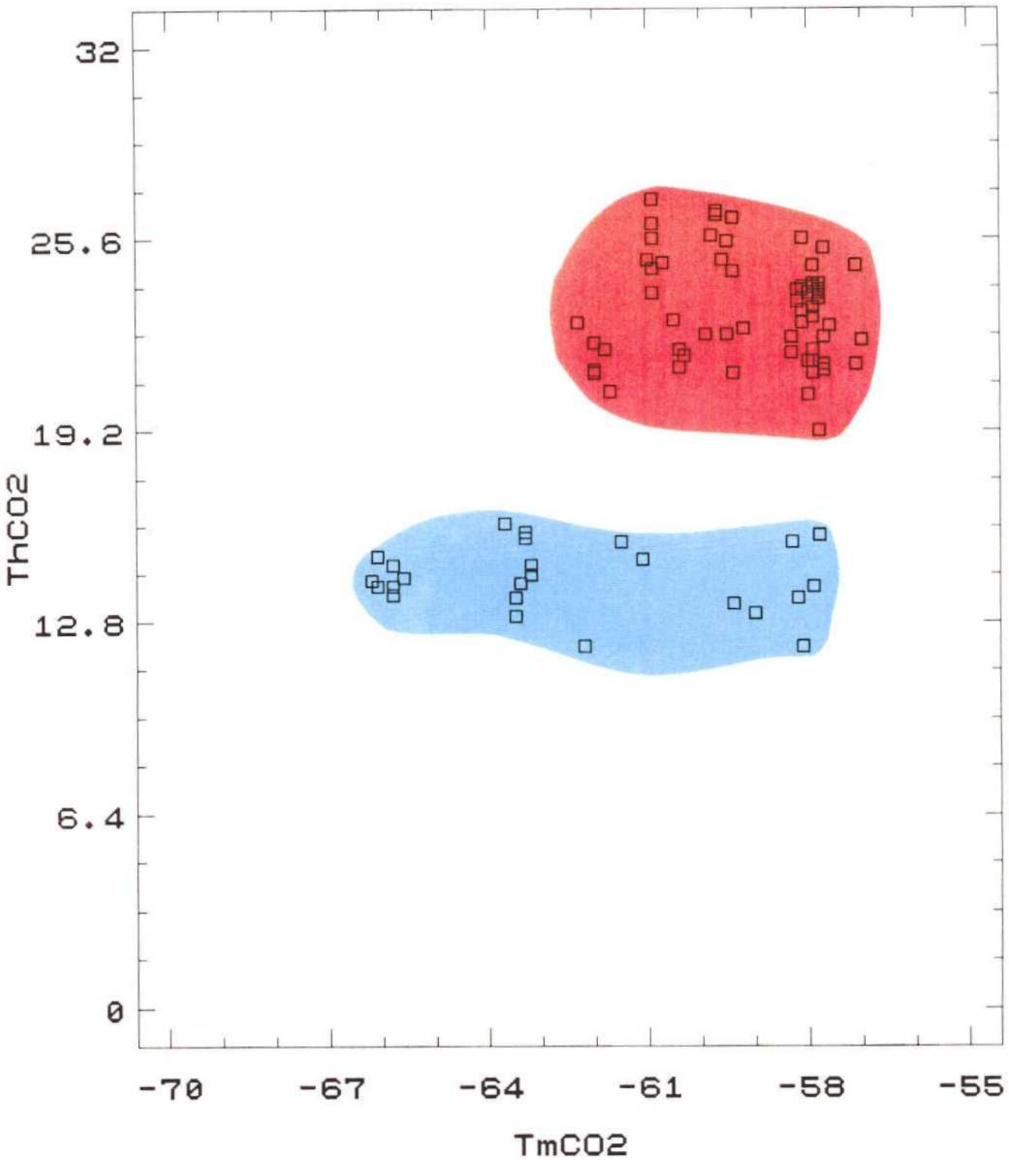

FIG 5.2 - Tm CO2 v Th CO2 FOR MINERALISED VEINS FROM THE CENTRAL RIDGE.

5.1.3 - Type 2 Inclusions.

Type 2 inclusions are the most abundant and are typically two phase L(aq) + V (F ~ .9) (Fig. 5.3a/b). Generally they are small (< 5 μm) and form trails within inclusion - rich quartz. Although, they can often be discrete and in close proximity to Type 1 inclusions. The Type 2 inclusions are aqueous rich (F = .9). A slight deformation of the vapour bubble and restoration -57.7°---> 61.3°C is interpreted to indicate the presence of a thin film of CO_2 around the vapour bubble which is barely visible optically. Similarly clathrate melting (+9--> 10.8°C) is also observable in many inclusions suggesting the presence of CO_2. Type 2 inclusions are aqueous-rich, and ice melting can be observed from -3.7 to -2.6°C, indicating < 5 wt% equivalent of NaCl, (Potter et al., 1978). On heating total homogenisation occurs between 215---> 331.5°C with a mode around 240°C.

5.2 - DISCUSSION OF FLUID INCLUSION DATA.

5.2.1 - P & T of Vein Formation.

The presence of two inclusion populations, one CO_2-rich (Th(TOT) L + V---> V) the other aqueous-rich (Th(TOT) L + V---> L) initially suggests an unmixing population from which a direct estimate of the P and T of vein formation could be made. However, the abundance of Type 2 inclusions in annealed fracture planes and their lower Th(TOT) ~250°C tend to support a "later" formation. Given the absence of an "unmixing population" P-T estimation from fluid inclusion studies alone requires a cautious evaluation (Roedder & Bodnar,1980). However, by combining inclusion data with other available geological information e.g. the sulphide assemblage and its geochemistry/geothermometry, and metamorphic grade, by petrography and vitrinite reflectance data, the P-T conditions prevalent at vein formation can be estimated.

The Th(TOT) for the "primary" Type 1 CO_2-rich inclusion assemblage provides a minimum trapping temperature for the system of 300°C. Furthermore, the relatively straightforward nature of the type 1a inclusions i.e. their low salinity, lack of an additional volatile content and their ubiquitous presence makes them ideal candidates upon which to base an estimate of the P-T of the system. Using a variety of published equations of state an isochore for the type 1 inclusions can be calculated within P-T space. Various published equations were applied but these resulted in little variation in the nature of the isochores in the area of interest. To more closely define our formation T and P. Three lines of additional geological information are now include on Figure 5.4. The coexisting assemblage of pyrite and arsenopyrite provides an upper limit to vein formation of 500°C Furthermore, arsenopyrite geothermometry completed on the sulphides of the mineralised veins analysed (see section 5.3 for details) infer a formation temperature of T = 400°C. In turn vitrinite reflectance data for the host rock and available petrographic observations indicate a lower greenschist metamorphic environment and temperatures of 300-350°C.

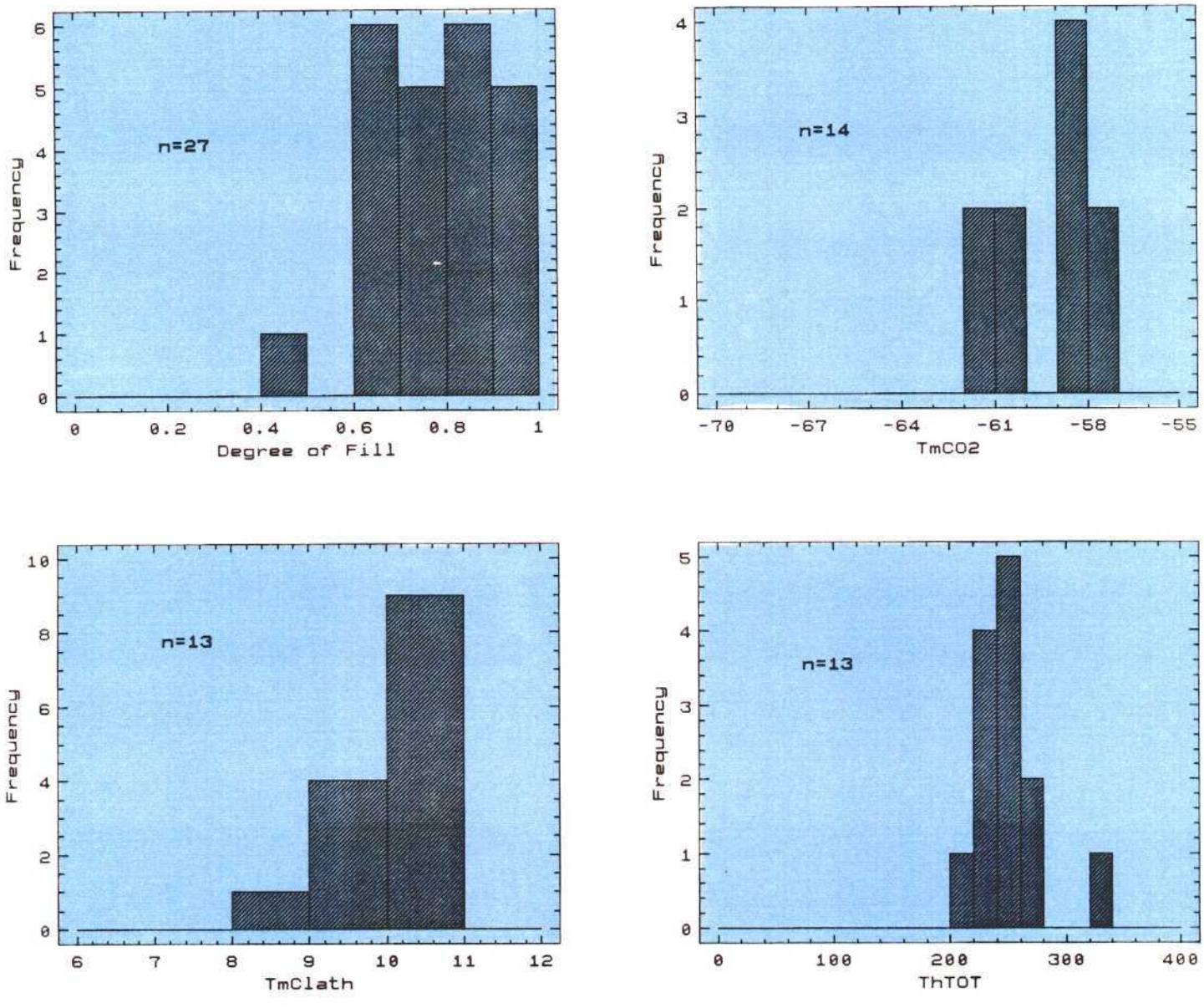

CENTRAL RIDGE E-W VEINS
(MINERALISED)

TYPE 2 INCLUSIONS

FIG 5.3a - FREQUENCY HISTOGRAMS OF FLUID INCLUSION DATA FOR TYPE 2 INCLUSIONS FROM MINERALISED VEINS OF THE CENTRAL RIDGE.

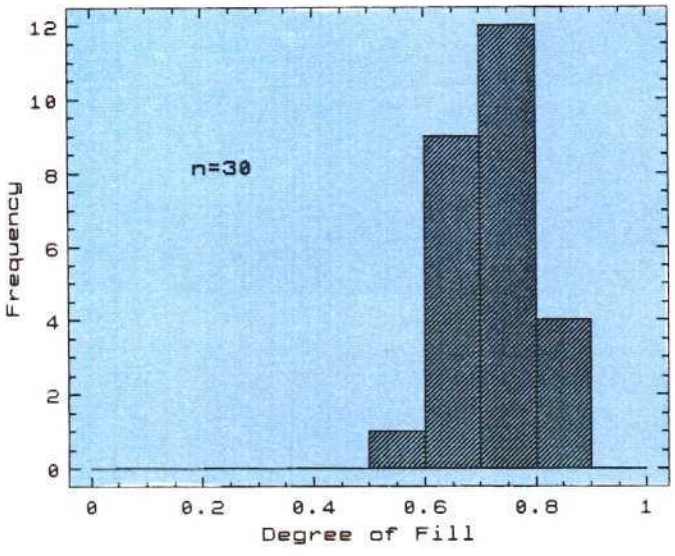

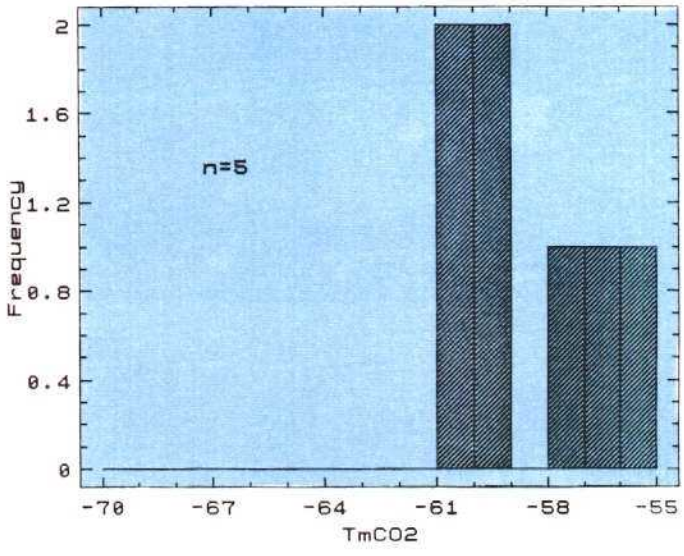

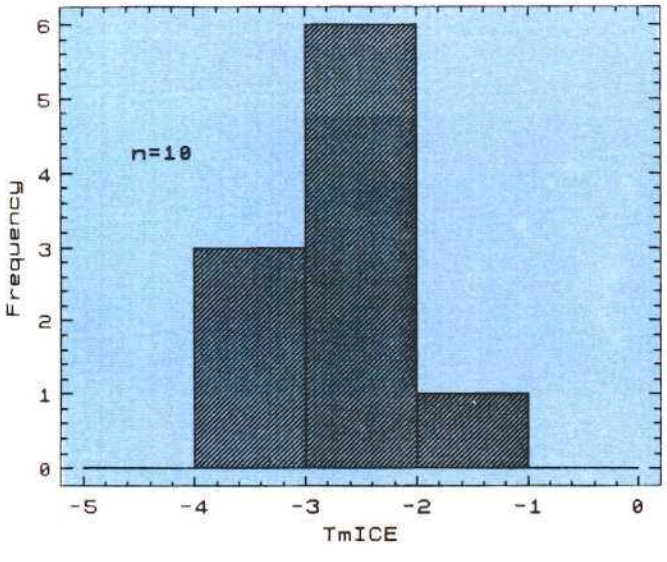

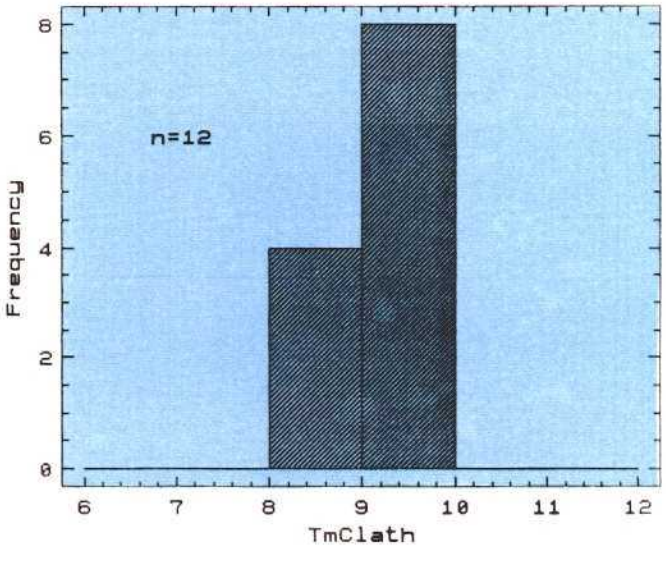

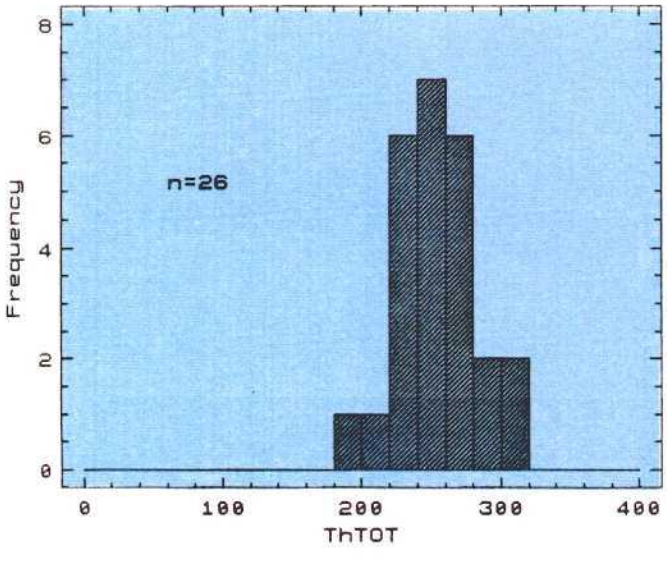

CENTRAL RIDGE OTHER VEINS

TYPE 2 INCLUSIONS

FIG 5.3b - FREQUENCY HISTOGRAMS OF FLUID INCLUSION DATA FOR TYPE 2 INCLUSIONS FROM BARREN VEINS OF THE CENTRAL RIDGE.

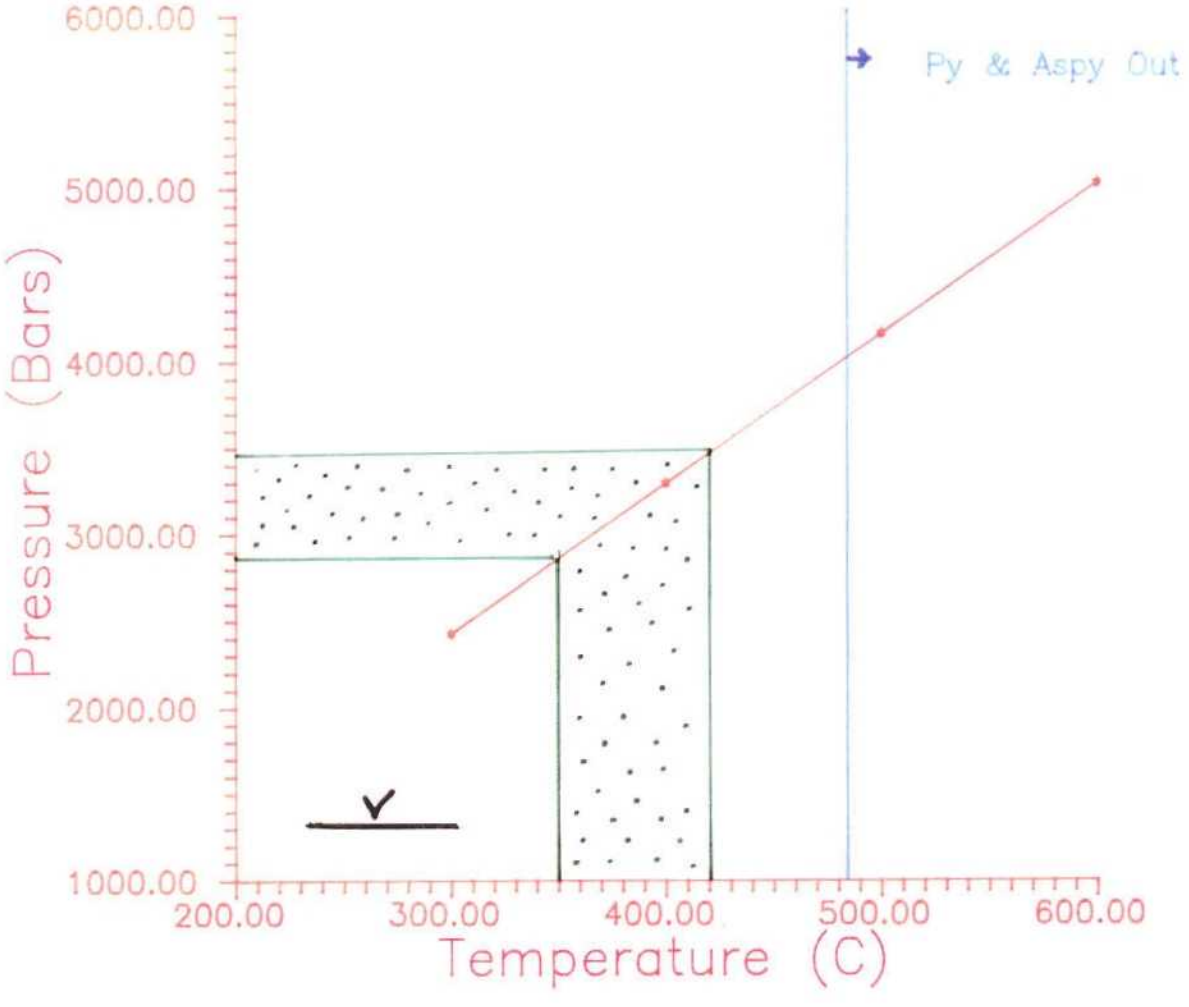

FIG 5.4 - P-T DIAGRAM FOR MINERALISED VEINS. V INDICATES THE TEMPERATURE RANGE OF VITRINITE REFLECTANCE DATA FOR THE AREA. SLOPING LINE REPRESENTS THE MEAN ISOCHORE FOR THE CO2-RICH TYPE 1 INCLUSIONS. STIPPLED AREA REPRESENTS THE RANGE OF TEMPERATURE, AND CORRESPONDING PRESSURES ESTIMATES FROM THE SULPHIDE GEOTHERMOMETER.

A combination of these data suggests that vein formation took place at temperatures between 350°C and 400°C between 2.85 and 3.5 kbs which assuming lithostatic pressure indicates a formation depth of 10-13km beneath the surface.

That the mineralised veins present higher temperatures than predicted by the host vitrinite is in keeping with the observation that the mineralised veins cross-cut the S1 fabric and are derived from an "external" heat source.

5.2.2 - CO_2-CH_4 & Auriferous Veins

The type 1 inclusions described conform to the increasingly documented association of dilute CO_2 - rich inclusions and lode Au mineralisation in shear zone environments (Smith et al., 1984; Colvine et al., 1988). In this instance the correlation between the mineralisation and elevated CH_4 values is particularly pronounced. Such a relationship has been quantitatively demonstrated for auriferous veins of the Dolgellau Gold Belt, N Wales where CH_4 was directly correlated with Au-grade (Bottrell et al. 1988). More recently Naden & Shepherd (1989) demonstrated that in black shale environments the reaction of a fluid with graphitic wall-rocks ($C+2H_2O \rightleftarrows CH_4 + 2(O)$ to produce CH_4 promotes the onset of an unmixing assemblage during which H_2S is preferentially partitioned into the volatile phase promoting gold precipitation.

The data presented above are in keeping with these hypotheses. In particular the restriction of the methane - rich inclusions to the mineralised veins, and more specifically their close proximity to the sulphide assemblage. The lack of an unmixing assemblage may explain the paucity of "bonanza" grades observed for much of the region.

5.2.3 - Fluid Source

In the construction of "robust" exploration model an indication of fluid source provides crucial information on potential fluid pathways and thus aids in the definition of exploration targets. Having outlined the P-T-X systematics of the veins a tentative estimation of the most likely fluid source can be made. Intriguingly, the area provides two obvious potential sources of heat and fluid, the Badajoz Shear Zone and the Albuquerque Batholith. Vein data indicates that the fluid is "externally derived" in so much as the veins cross cut the S1 fabric and the homogenisation temperatures of the fluid are in excess of those temperatures derived from a vitrinite study of the wall-rocks. The fluid may be considered typical of "auriferous fluids" from mesothermal systems i.e low salinity, CO_2-rich. Such fluids are often ascribed a metamorphic origin (Colvine et al., 1988). Given the connectivity of the mineralised structures to the shear zone and the metamorphic nature of the observed fluids a shear zone origin for the auriferous fluid is suggested.

5.3 - SULPHIDE GEOTHERMOMETRY.

Experiments on the stability of arsenopyrite in the system Fe-As-S have led to the use of arsenopyrite compositions as a geothermometer (Clarke, 1960, Kretschmar & Scott, 1976, Sharp et al., 1985). Given the common sulphide assemblage of arsenopyrite and pyrite within the auriferous veins of the La Codosera area these relations may provide information of the temperature of formation of the sulphide minerals.

The experimental work of Kretschmar & Scott (1976) outlined a pseudobinary P-X section (Fig. 5.5) relating atomic % arsenic to temperature. Their data and a subsequent re-evaluation of the data by Sharp et al. (1985) show that providing arsenopyrite compositions lie on the true FeS_2-$FeAs_2$ binary join, its composition will be fixed when buffered either by pyrite or loellingite at constant pressure and temperature. Slight deviations from the stoichiometric ratio Fe/(As + S) = 1/2 will displace arsenopyrite from the binary join and into the three phase field Fe-As-S. Thus given stoichiometric analyses of arsenopyrite grains, a temperature can be estimated directly from the pseudobinary diagram.

Table 5.1 outlines the results of a microprobe study of arsenopyrite grains from the La Codosera area completed at the Open University (U.K) on a Geoscan Mk9 Microprobe. Twenty five analyses of arsenopyrite grains in contact with pyrite, were analysed from a number of prospects. The data for atomic % As varies between 29.9 and 32.1%, with a mean value of 31.2 atomic %. No significant core/rim variation is observed and the minor elements e.g Co,Cu,Ni and Bi have a combined total of <0.1 wt%. Encouragingly, the data does not depart markedly from the stoichiometric ratio Fe/(As+S) +1/2 and direct application of the data to the pseudobinary T-X section of Kretschmar & Scott, 1976 indicates palaeotemperatures of $400^{\circ}C \pm 30^{\circ}C$ for the formation of the arsenopyrite. (Note, marginally lower T's are obtained following the "re-evaluation" of Sharp et al. (1985) of around $385^{\circ}C$). These data combine with the inclusion data to provide a good estimate of the T-P conditions during the formation of the auriferous veins of the La Codosera area.

Furthermore, having established the geochemical systematics of the arsenopyrites an estimation of the sulphur activity prevailing during precipitation of the sulphide minerals can be made (Kretschmar & Scott, 1976): utilising a S(act) v Temperature diagram. A value of S(act) log -7 is recorded.

5.4 - THERMOLUMINESCENCE.

5.4.1 - Introduction.

Thermoluminescence refers to the property of crystals and non-conductive materials to emit light when they are heated, provided they have previously been submitted to an irradiation whether natural or artificial. By heating common minerals, for example quartz, and measuring the light intensity against the

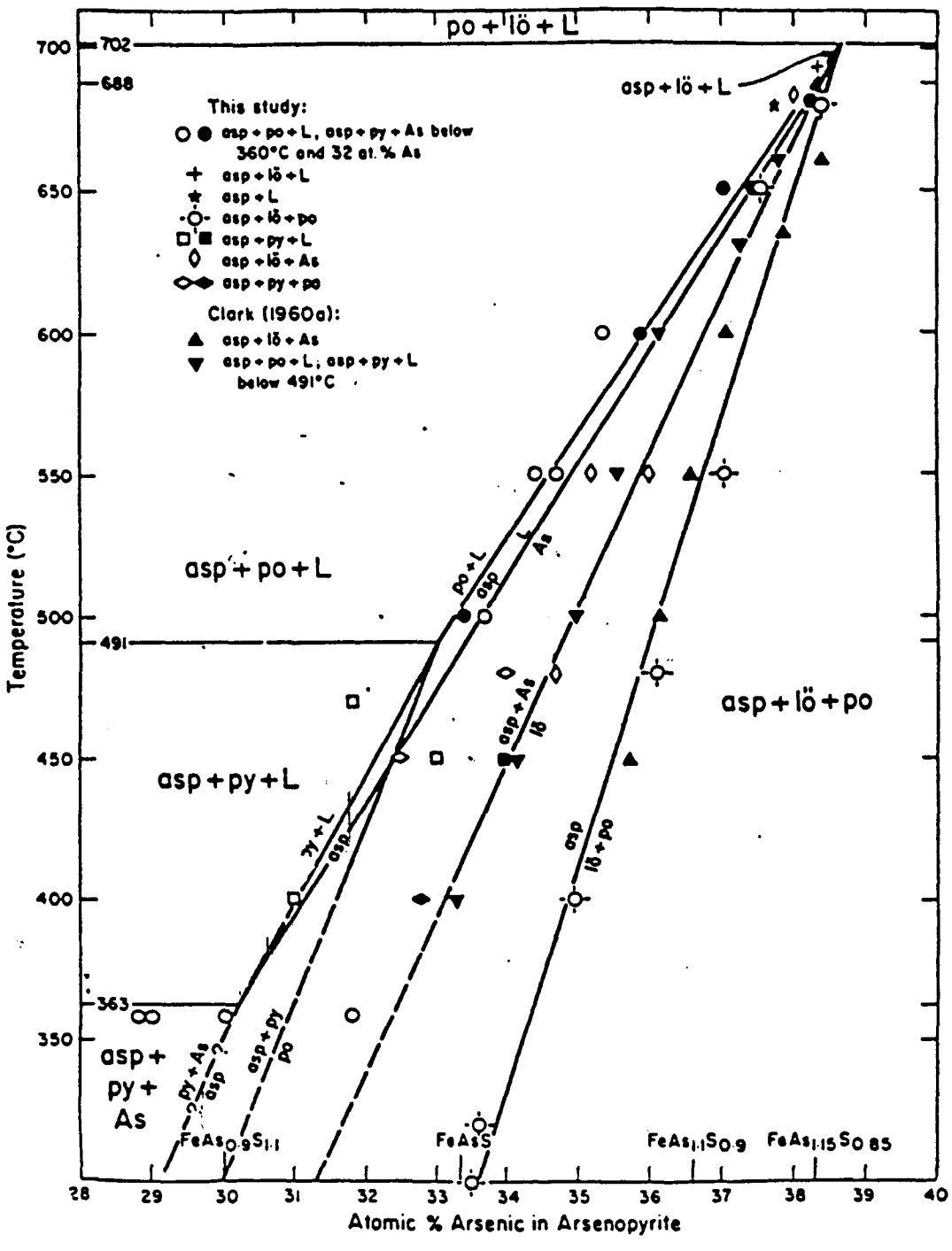

FIG 5.5 - PSEUDO-BINARY CONDENSED T-X SECTION ALONG THE PYRITE-LOLLINGITE JOIN OF THE Fe-As-S SYSTEM (FROM KRETSCHMAR & SCOTT, 1976).

Locality	Sample No	Grain	S	Fe	As	ToT	Anal.
100m Vein	1072	rim	37.2	32.9	29.9	100	a
		core	37.1	32.8	30.1	101.7	b
		core	37	32.9	30.2	101.4	c
		rim	35.9	33.1	30.9	100.6	d
		rim	35.8	33.2	30.1	99.9	e
		core	35.6	32.8	31.5	100.9	f
		core	35.4	32.8	31.8	101.1	g
		rim	35.5	33	31.4	100.9	h
Matasiete	211a	core	35.8	33.1	31	99.9	i
		rim	34.7	33	32.1	101.2	j
		core	34	33.7	32.3	99.6	ba
		rim	34.6	33.5	31.7	99.8	bb
		rim	34.9	33.4	31.5	100	bc
Penon	1080a	whole	36.6	33.2	30.2	100.4	m
		whole	35.6	32.9	31.5	99.3	n
	1080b	whole	34.9	33	32	99.1	v
Chirriato	1076b	core	35.1	32.8	32.1	100.5	q
		core	35.9	33.1	31	100.5	r
		core	35.4	33	31.5	99.9	s
		rim	35.4	33	31.5	100.6	t
		rim	36.5	33	30.5	100.3	u
		rim	35.6	33.2	31.1	99.6	w
	1076a	core	36.4	33.5	30.2	100.2	x
		core	35.9	33.4	30.5	99.9	y
		rim	35.1	33.5	31.3	99.9	z
		AVE	35.7	33.1	31.1		

TABLE 5.1 - MICROPROBE ANALYSES OF ARSENOPYRITES FROM AURIFEROUS VEINS OF THE LA CODOSERA REGION.

temperature a "glow curve" can be obtained. The light measured represents the liberation of electrons from crystal defects previously disassociated from their parent nuclei by the action of radionuclides.

5.4.2 - Sample Rationale and Analytical Technique.

In order to evaluate the potential of the technique in the La Codosera area a subset of 12 vein samples were analysed which included both mineralised and barren samples from the Central Ridge, Los Algarbes and the Albuquerque Batholith. The samples were forwarded to Prof. Charlet at the Faculte Polytechnique de Mons (Belgium). Prior to analyses the samples were subject to a physical and chemical treatment including, moderate crushing of the samples, sieving to 100-125 microns, washing, treatment by heavy liquids, recovering the underflow (density <2.83) and finally HF attack in order to clean the grains.

5.4.3 - Results.

Glow curves are presented for all sample analyses in Fig. 5.6 and are grouped according to their geographic location i.e, Central Ridge, Los Algarbes, Albuquerque Batholith.

Los Algarbes.

The Los Algarbes samples show three intensity peaks 100°, 280° and 340°C. Both mineralised and barren veins show essentially similar patterns. Interestingly the two high temperature peaks correspond to the predicted decrepitation temperatures for the two inclusion described in Section 5.1. This suggests that the crystal defects housing the electrons similarly hold the fluid inclusions.

Central Ridge.

The majority of the Central Ridge samples show similar patterns, and a distinction between mineralised and barren veins in the syncline is not possible. In comparison to the Los Algarbes data set the Central Ridge samples tend to show less obvious intensity peaks at 280° and 340°C and show a lower total intensity. One sample from the Central Ridge stands apart, this represents a mineralised sample from the Penon prospect. Three strong intensity peaks are observed at 100°, 210° and 280°C. This sample shows a curve more in keeping with the within granite veins presented in the following section.

Alburquerque Batholith.

Two samples were analyze of vein quartz located at the margin of the batholith. They show distinctive, although not exactly similar patterns, with three peaks with intensities well in excess of those recorded from the Central Ridge and Algarbes

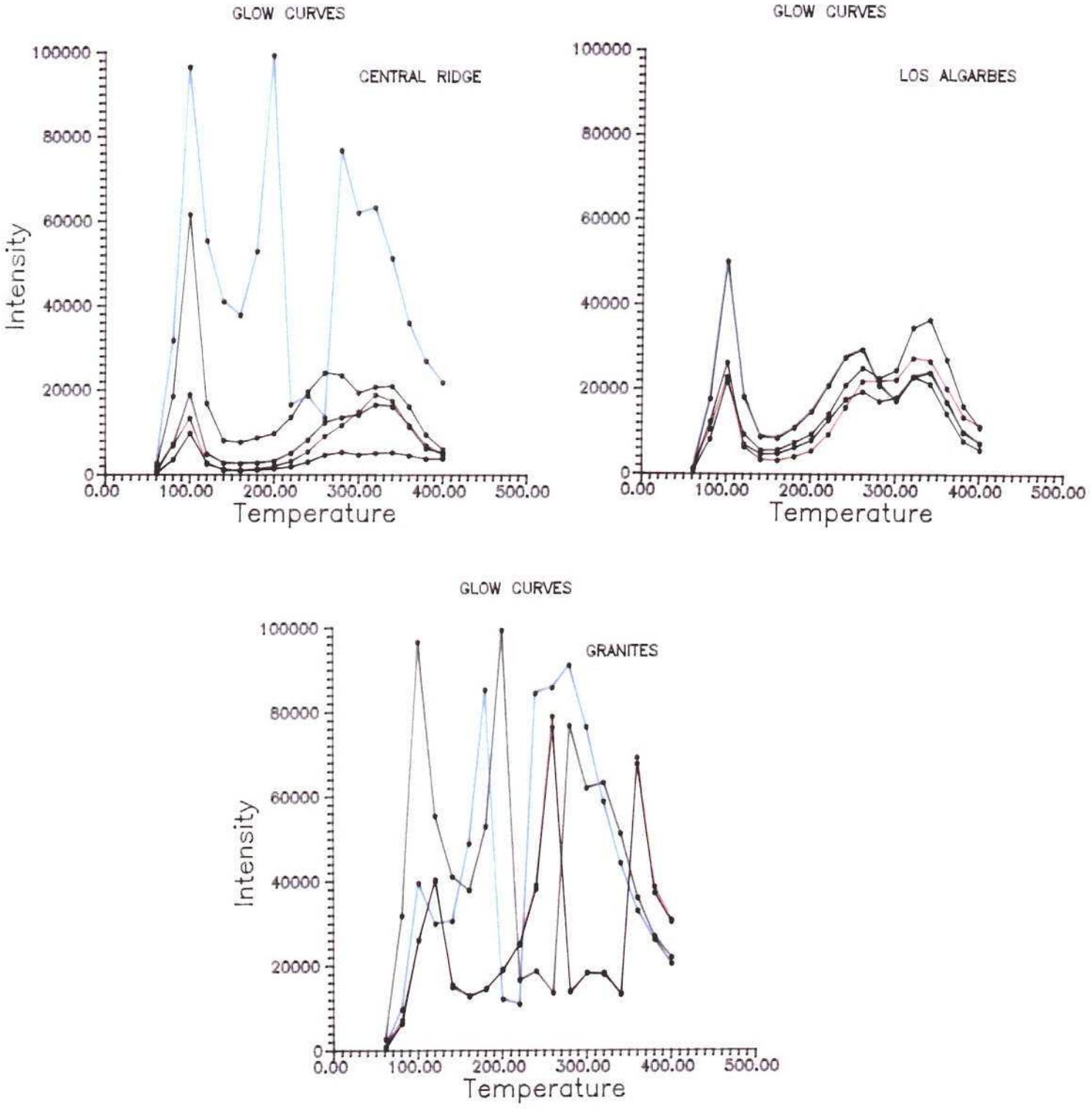

FIG 5.6 - GLOW CURVES FROM QUARTZ VEINS FROM THE LA CODOSERA AREA (SEE TEXT FOR DETAILS)

zones, with the exception of the Peñon prospect. The granite samples are thus distinct, though given the "theory" outlined in the introduction they would clearly be subjected to a high radionuclide flux being located in close proximity to the granite and thus a high intensity would be predicted.

5.4.4 - Discussion.

The technique offers some interesting insights into the region. In terms of a simplistic mineralised v barren approach the technique provides no working discriminant. Although a negative result suggests that the vein source /conditions of mineralisation are not markedly different. This is in keeping with observations concerning the relative timing and orientation of both the mineralised and barren veins presented earlier.

The distinctive Peñon sample is puzzling, although structurally, (orientation and kinematic data), and petrographically, (quartz textures), Peñon represents an atypical prospect within the Central Ridge.

Finally the increased total intensity of the Algarbes samples compared to the Central Ridge offers the intriguing possibility of a radionuclide source i.e. granite in close proximity to the Los Algarbes zone.

5.5 - BETA-AUTORADIOGRAPHY.

Despite the preparation of more than 50 polished thin sections from auriferous veins no visible gold was recorded. In all cases a simple pyrite arsenopyrite sulphide assemblage was observed. In an attempt to discern the position of the gold a beta-autoradiography study was attempted on a series of sections.

The theory of neutron activation induced beta-autoradiography is well documented (e.g. Potts, 1984). The technique essentially records the beta-emission of elements, using a sensitive emulsion. It is important to note that unlike other autoradiographic techniques, because high energy beta particles from any beta emitting nuclide are detected, the technique is not element specific. To this end samples were further subjected to neutron activation analyses to confirm the presence of Au in the section and to guide in the interpretation of data.

As arsenopyrite is the main sulphide, in order to optimize the detection of Au over As the first exposure was taken after 12 days, as this exceeds 10 half lives for As). Qualitative gamma spectra from the samples studied indicated the presence of gold.

However relatively few "spots" recording beta-emissions were observed on the emulsions and following further investigation with the scanning electric microprobe, these do not to correspond to any discrete Au grains. Thus whilst the presence of

gold can be confirmed within the sulphide bearing a asemblage its exact location appears to be as a lattice bound constituent of the sulphide grains and not as discrete free Au grains.

5.6 - SUMMARY.

The geochemical analyses of this chapter indicate that the auriferous veins of the La Codosera resulted from the passage of a dilute 350°C, CO_2-rich fluids at between 10-13km depth in the crust. The fluid contains appreciable amounts of methane, up to 20 mole % and given the common association of the veins in black slate environments suggest a close relationship between reaction of the fluid with the carbonaceous wall-rock and gold precipitation. The dilute nature of the fluid in association with the connectivity of fractures to the shear zone promotes a shear zone origin for the fluid. Beta-autoradiography indicates the gold is most likely lattice bound within the arsenopyrite structure.

CHAPTER - 6 - OTHER PROSPECTS.

P. Gumiel & M. Gallego

Having presented the geological framework to the area this chapter now is dealing with the other mineral occurrences within which, the San Antonio antimony mine represents the largest deposit in the Iberian Peninsula, in order to get a better insight of the mineral potential of the region.

6.1 - ANTIMONY

The largest antimony deposit in the Iberian Peninsula is the San Antonio mine (Fig. 6.1 and Fig. 6.2) which is located in the Southern Ridge of the La Codosera Syncline. This mine was worked until 1986 and the deposit was first studied in detail by Gumiel et al. (1976), Gumiel (1982) and Arribas & Gumiel (1984). The mineralisation of San Antonio occurs in a carbonaceous horizon made up of black limestones, intraformational breccias, and calcareous shales, as well as some siliceous layers of Devonian age.

The San Antonio ore body is a stratabound mineralisation under strict lithostratigraphic and structural control, located in the normal limb of a northely overturned and thrusted fold within the Southern Ridge of the La Codosera Sinclyne.

The intrasedimentary and deformed breccia, whether it is mineralised or not, keeps a constant thickness from 1.8 to 2.2 m. both in depth and along the strike. Within the breccia, the mineralised bodies are channel-like in shape and average 30 to 35 m. in length and 600 m. in depth (Fig. 6.2). The stibnite shows a fine grained or tabular habit and surrounds the quartz, limestone and chert fragments are stretched along bedding planes. The ore decreases gradually into the unmineralised breccias along an interfingering contact. Nodules of scheelite, ranging from 5 to 7 cm. in diameter, are frequently found within the stibnite aggregates.

The main ore minerals present at the San Antonio deposit are stibnite, scheelite, berthierite and pyrite; arsenopyrite and antimony are the main accesories; stibiconite, cervantite and goethite are the most important secondary minerals, whereas very scarce quartz and calcite are the sole constituents of the gangue. This mineral assemblage belongs to the Sb-W-Hg association as defined by Maucher (1965). The breccia could be generated in an outer continental shelf sedimentary environment, at the shelf break or the inner continental slope. This geological setting became the site for intraformational breccias resulting from the tectonic activity to which such a zone would be prone, given the active fault system that created the Devonian shelf itself. Along these faults, submarine hydrothermal processes related to the pre-orogenic intra-Devonian mafic volcanism gave place to Sb-W (Hg) mineralisation.

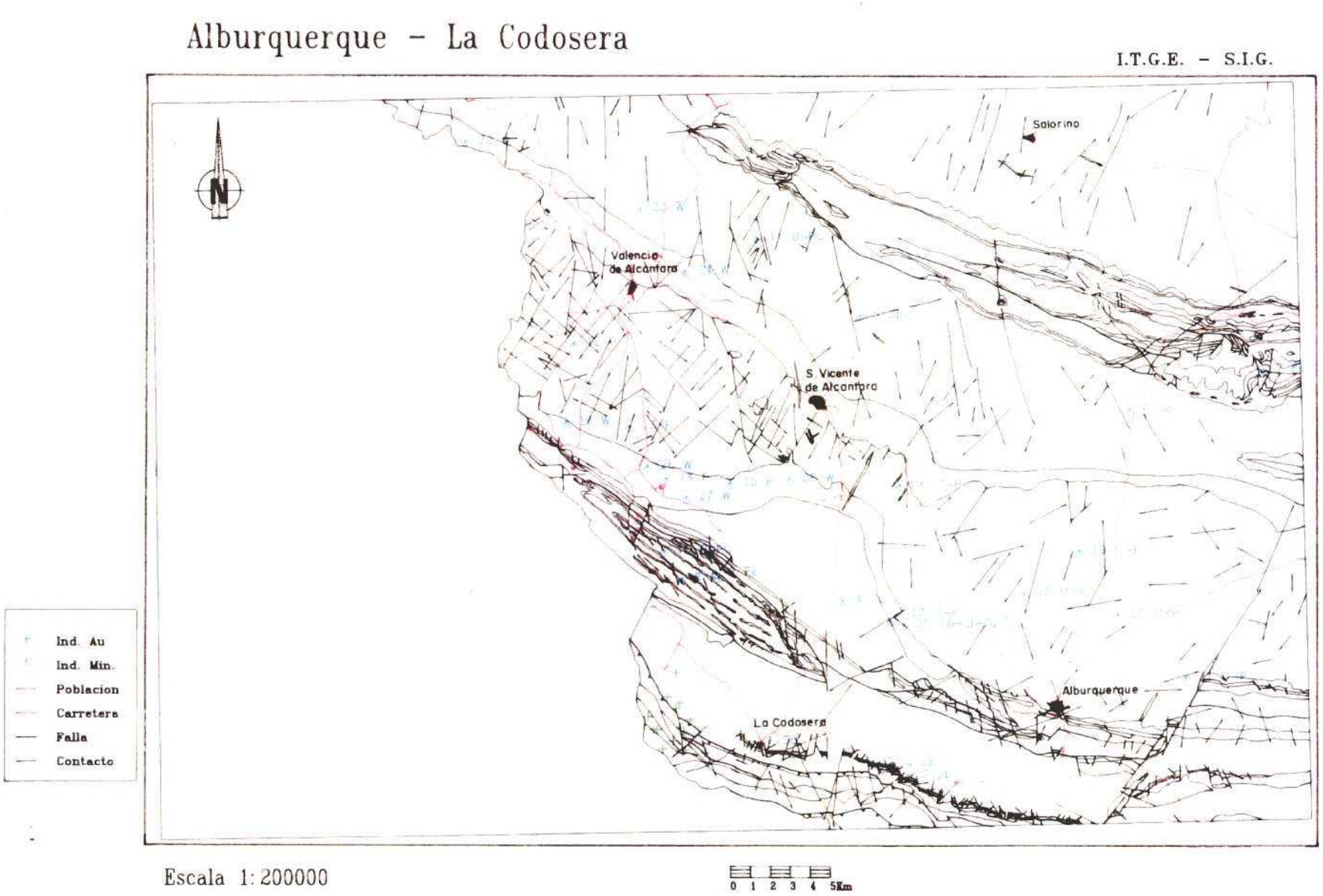

FIG. 6.1 - MINERAL OCCURRENCES MAP OF THE ALBURQUERQUE-LA CODOSERA AREA.

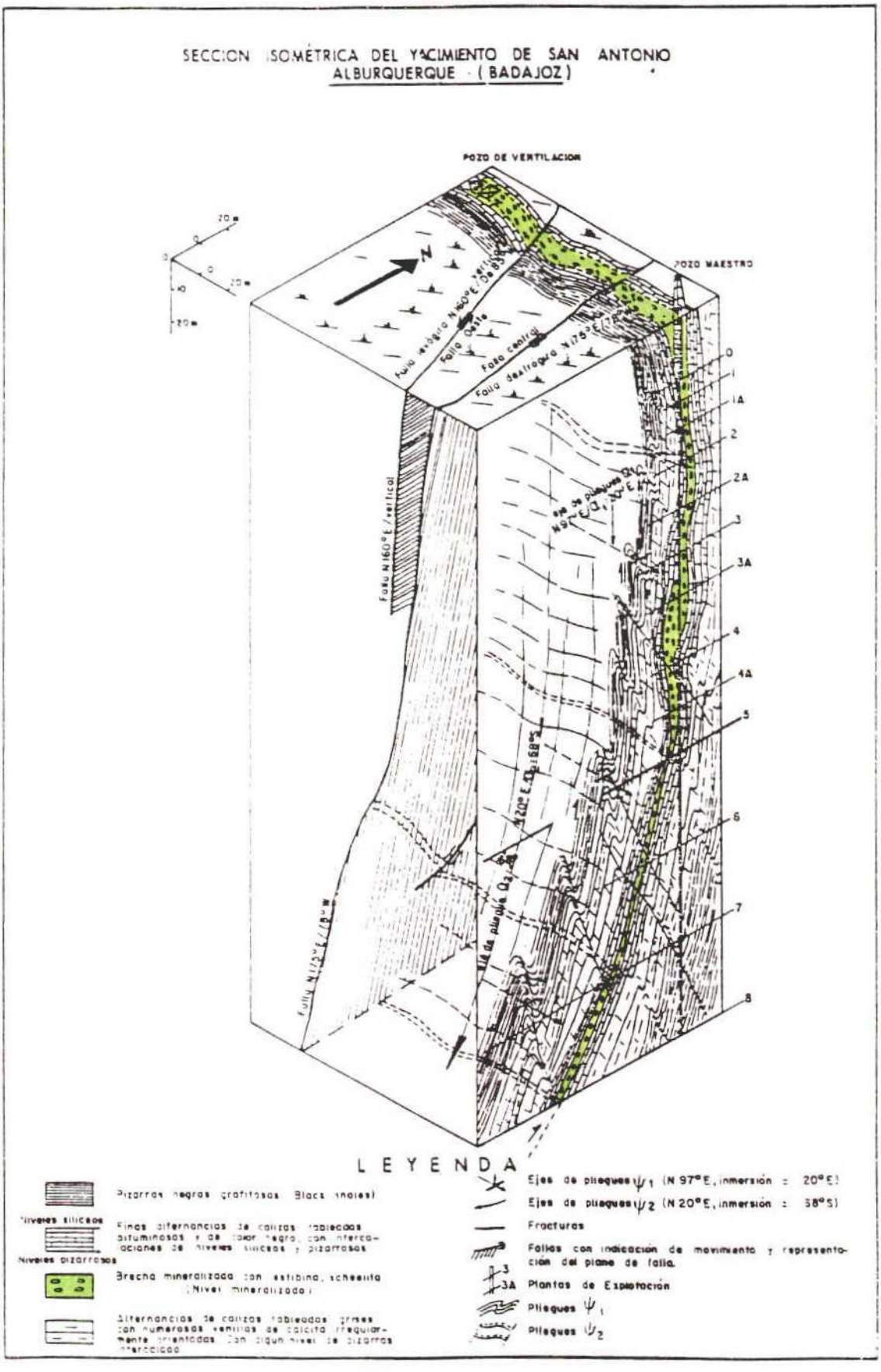

FIG. 6.2 - THREE-DIMENSIONAL MODEL OF SAN ANTONIO ANTIMONY DEPOSIT (After GUMIEL, 1982).

Other probably alternative hypothesis could be that the antimony as well as the gold mineralisations would be spatially and genetically related to the Main Badajoz-Cordoba shear zone. The mineralisation could be emplaced, following the antithetic NW trending fractures to the main shear zone acting as channelways, and the mineral deposition occurred in dilation zones within second order structures shear zone related, in specific carbonaceous lithologies, as deformed breccias, within the Southern Ridge of the La Codosera Syncline.

6.1.1 - Antimony-gold prospects.

The quartz-stibnite-gold mineral association has been defined in the Mari Rosa mine (Fig. 6.3) near Valencia de Alcantara (Caceres) by Gumiel (1982) and Gumiel & Arribas (1987). The paragenesis is made up by stibnite, arsenopyrite, pyrite and native gold. The mineralisation appears in veins hosted in black shales within CEG. Sedimentary structures (ripples, load and flute cast, grading etc.) are reasonably well developed in these rocks, which display a series of tight upright folds, strong cleavage and subvertical stretching lineation.

Three different quartz vein sets can be recognised, from pre-cleavage metamorphic segregation veinlets (V1), through syn- cleavage veining and segregations in boudin necks (V2), to late fractures which cross-cut the Hercynian cleavage (V3). Gold mineralisation and minor antimony appear to be concentrated in N110°-130°E trending V2 fractures, dipping 60°-75° to the south. Antimony mineralisation and minor gold are predominantly located in post-cleavage V3 fractures trending N-S to N 30°E and dipping 30° towards the east, pockets of stibnite are developed in dilation zones and pinnate veins which opened due to right lateral movements (Fig. 6.3). The stibnite contain up 3.4 ppm Au. Other prospects in the area belonging to this type correspond to Sta. Aurelia mine (4), Mari Pepa (5) and La Cobacha (6) near San Vicente de Alcantara (Badajoz) (Fig. 6.1 and Table 6.1).

6.2 - LITHIUM.

The "Tres Arroyos" mine (Fig. 6.4 and Table 6.1), the only Li mine in the area, is located in the SW margin of the Alburquerque Batholith, in the contact between the granite and the CEG.

In this area, the batholith is made up of a two-mica granite and an albitite sheet with tourmaline, muscovite and garnet intrudes in the CEG. This albitite sheet strikes 140° and dips gently towards NE. Its emplacement can be related to an important fracture observed in the TM image (Fig. 6.5), crosscutting both the granite and the CEG materials, which can also be responsible of the stretching of the Alburquerque batholith (see Chap.7).

From a petrological viewpoint this sheet represents a transition between the two-mica granite and the Li-pegmatites s.s, through intermediate stages such as

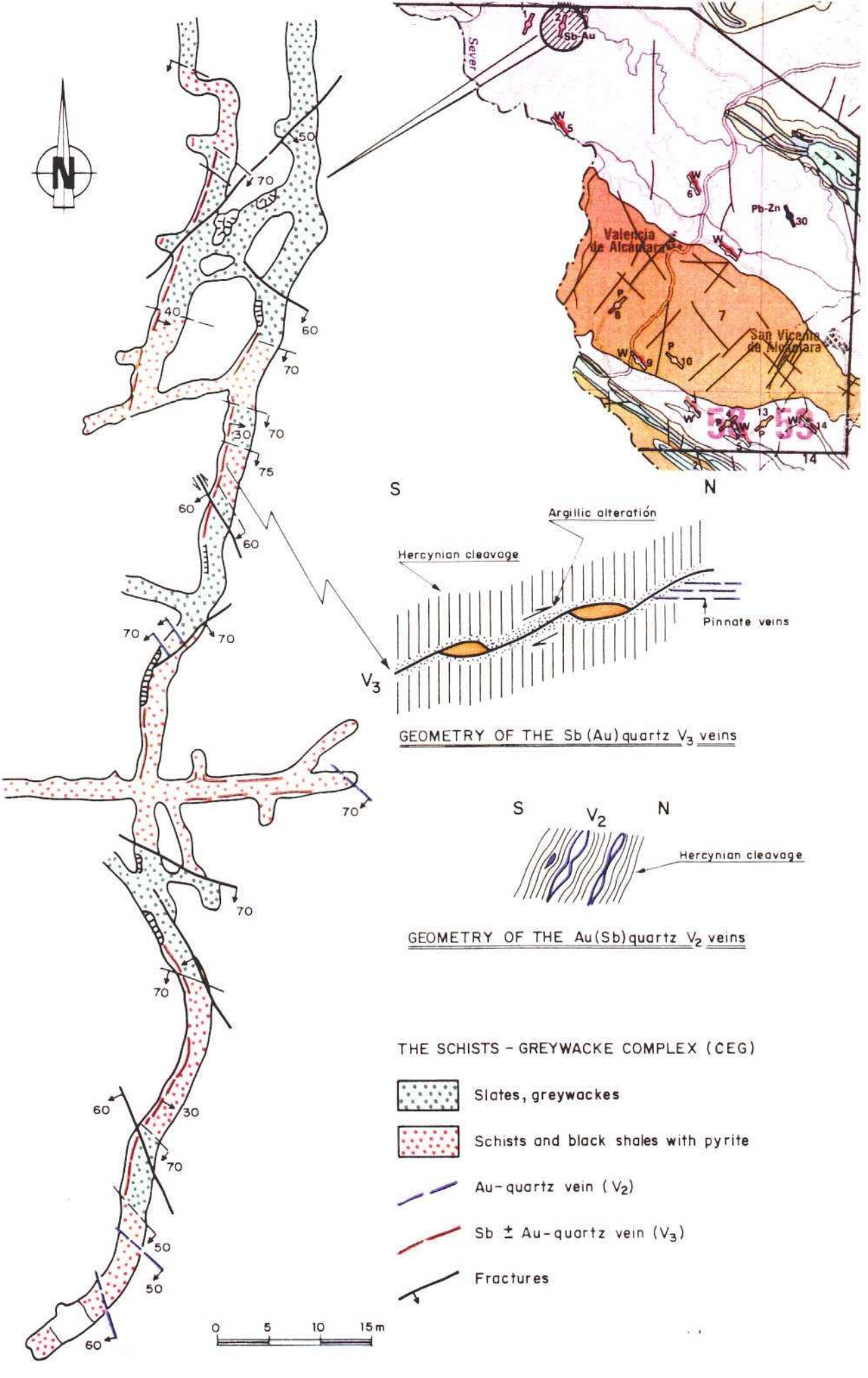

FIG. 6.3 - GOLOGICAL SCHEME OF THE MARI ROSA Sb-Au PROSPECT.

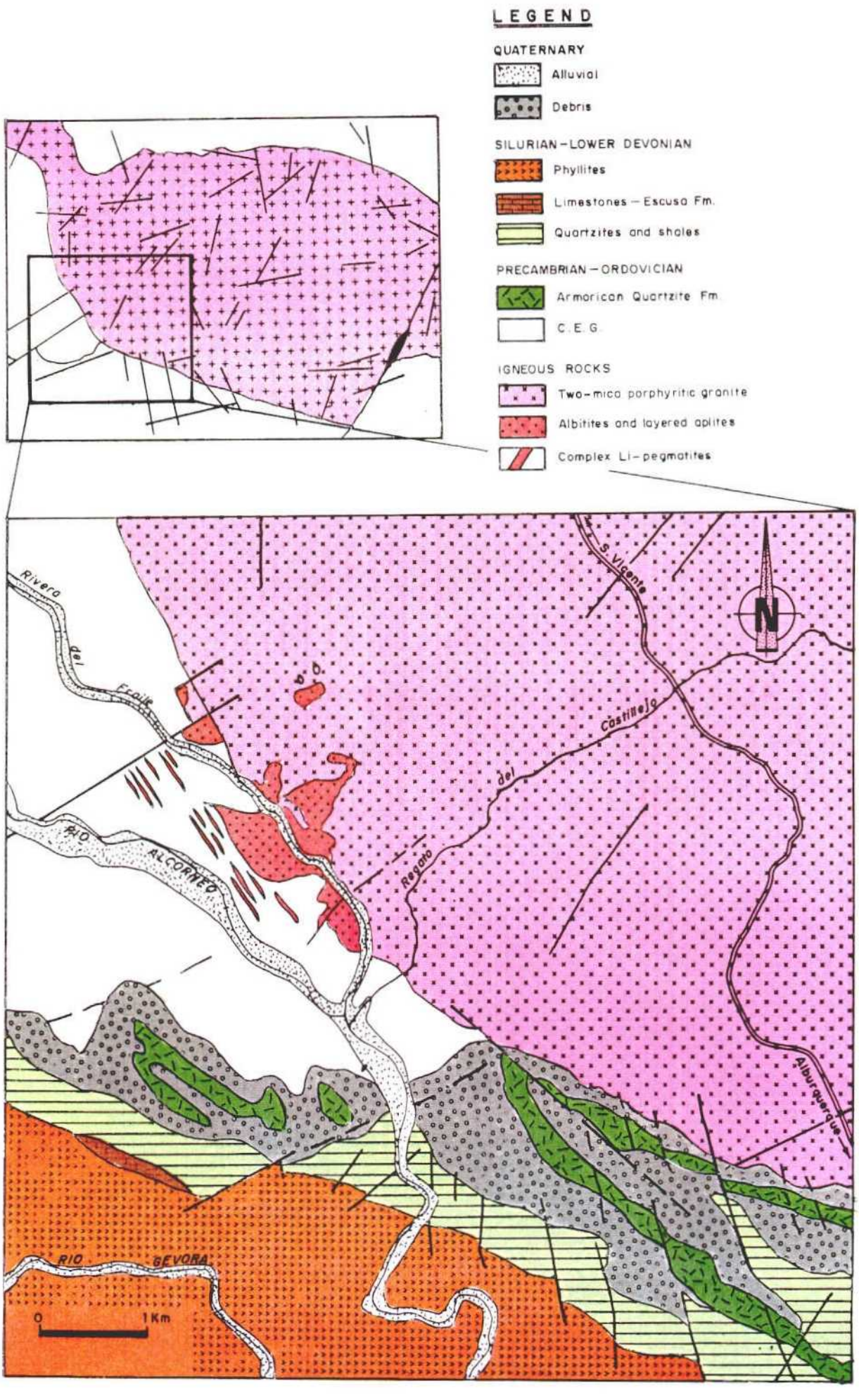

FIG. 6.4 - GEOLOGICAL SCHEME OF THE TRES ARROYOS LI PROSPECT.

FIG. 6.5 - STRUCTURAL CONTROL OF THE STRECTCHING OF THE ALBURQUERQUE BATHOLITH.

muscovite - albitites with garnet and tourmaline schlieren, and layered aplites with quartz - albite - muscovite pegmatitic zones. These pegmatitic zones are progressively more abundant towards the Li-pegmatites (i.e. SW.), and generate tourmaline halos in the layered aplites. The CEG consists mainly in lutites affected by contact metamorphism that develops andalucite, cordierite and biotite porphyroblasts. In this zone, there are abundant lenticular hornfels, with scarce lateral continuity.

The Li mineralization appears in a complex pegmatite dyke swarm striking between 120° and 150°E. and dipping 10°NE., spatially connected with the albitite sheet. Texturally and compositionally, four internal zones can be recognized, following the criteria given by Cameron et al. (1949):

a)Border zone

It is made up by a quartz-albite-muscovite assemblage with minor apatite and tourmaline, forming an outer aplitic discontinuous shell several centimeters wide. The accesory minerals are cassiterite, Nb-tantalite, zircon and rutile.

b)Wall zone

It consists on the same mineral assemblage that the previous zone, but texturally is coarser-grained. It is relatively continuous and forms the most of the pegmatite contacts.

c)Intermediate zone

This occupies the central parts of the pegmatite dykes and consists of an spodumene-quartz-albite-amblygonite assemblage. This is very difficult to recognize because the original mineral association has been replaced by a lepidolite-quartz-albite assemblage due to a pervasive sodic-lithiun metasomatism. Accesory minerals are cassiterite, Nb-tantalite, zircon and complex Li-Fe-Mn secondary phosphates.

d)Core zone

It is confined to the central parts of the pegmatites and were mined for cassiterite, Nb-tantalite and accesory base-metals sulphides. Sometimes, they have been developped within a fracturing period in the later stages of pegmatite emplacement and appear as "fracture fillings" crosscutting all the external zones and even the metamorphic host-rocks.

From a geochemical viewpoint, the pegmatites correspond to granites s.s. and alkaline granites with normative corundum and phosphates, low contents of Fe, Ca, Ba, Sr and high values of K/Na ratios due to pervasive Na-Li metasomatism, with

high contents of Rb, Ga, Cr, Nb, Ta and Sn. The large amounts of lepidolite, apatite and other phosphates suggets that the original magma was highly enriched in hyperfusible compounds such as P, F, and B (although there is not a significant amount of tourmaline in the dykes, a considerable B-rich volatil phase has been expeled to the host-rocks forming a tourmalinite metasomatic halo several centimeters wide around the pegmatites).

Finally, due to the absence of characteristic wide alteration patterns, we consider that the best prospecting tool would be the integrated use of both petrologic and structural data. In this sense, the existence of highly differentiated igneous rocks (albitite facies), also with coexisting fracture zones favourable for the pegmatitic-dykes emplacement provides a useful target for Li-Sn ore-deposits exploration in this area.

6.3 - TUNGSTEN (Table 6.1 and Fig. 6.1).

The tungsten prospects of the study area show the following features in common:

1. The mineralisation appears generally in N110E-trending extension veins and as stockworks surrounding the Alburquerque Batholith. Thickness of the veins ranges from a centimeter to one meter.

2. The mineral assemblage in most of the prospects is made up by high temperature minerals (wolframite, and accessory scheelite), with an intermediate temperature sulphide stage deposited in two phases: a) with arsenopyrite, and b), the final stage, with pyrite and traces of chalcopyrite. Quartz is formed continuously during the whole deposition sequence. This metallogenic sequence has been observed in most of the occurrences in this zone.

6.4 - URANIUM. (Table 6.1 and Fig. 6.1).

The uranium prospects are vein-like and occupy NE-trending extensional fractures and are located mainly within the Alburquerque Batholith.

The mineral association quartz-pitchblende-Fe sulphides, which characterises the intragranitic deposits, consists almost exclusively of pitchblende, coffinite, pyrite, marcasite and melnikovite in a gangue of quartz and jasper, usually hematitic, with traces of calcite (Arribas, 1975, 1978). The secondary U minerals are very abundant in all the orebodies.

6.5 - PHOSPHATES. (Table 6.1 and Fig. 6.1).

This peculiar and widespread type of deposits occurs in granites of the southern Central Iberian Zone (Extremadura) where they are called "fosforites". The NE-trending veins are up to 1Km long, 1 to 3 m wide and up to 100 m deep. They consist almost exclusively of quartz and apatite (mainly the radial-fibrous variety dahllite) (Arribas, 1978; Aizpurua et al., 1982).

The phosphate veins are also frequently uranium-bearing and are hosted within the Alburquerque Batholith or in the surrounding metamorphic rocks (CEG).

TABLE 6.1 - MINERAL OCCURRENCES IN THE STUDY AREA (GOLD EXCLUDED. MINERAL OCCURRENCE NUMBERS REFER TO FIG. 6.1).

NUM.	SUBSTANCE	LOCALITY	NAME	X UTM	Y UTM	MORPHOLOGY	HOST ROCK	ALTERATION	MINERAL ASSOCIATION
1	Sb	La Codosera	Codosera	659.60	4341.00	Stratabound	Lower Devonian limestones.	Hematizat. Silicificat.	Stibnite, carbonates, pyrite, chalcopyrite, Sb, Fe and Mn-oxides
2	Sb	Alburquerque	Quinola	665.80	4339.65	Stratabound	Carbonaceous deformed breccias of Lower Devonian	Silicification	Quarz, stibnite, berthierite, pyrite, Sb-oxides
3	Sb	La Codosera	San Antonio	665.45	4339.65	Stratabound	Limestones,intraform. deformed breccias. Lower Devonian	Silicification	Quartz, stibnite, scheelite, berthierite, pyrite, Sb-oxides.
4	Sb	San Vicente	Santa Aurelia	661.70	4348.45	N120E q.vein	Slates of C.E.G. (Upper Precambrian)	Hematizat. Chloritizat.	Quartz, stibnite, native Sb, pyrite, berthierite, Sb-Oxides
5	Sb	San Vicente	Mari Pepa	662.90	4361.85	N120E q.vein	Slates and greywackes (C.E.G. Upper Precambrian)	Chloritization	Quartz, stibnite, berthierite, Sb-Oxides
6	Sb	San Vicente	La Cobacha	675.70	4358.00	N30E q.veins	C.E.G. Slates and greywackes (Upper Precambrian)	Chloritization	Quartz, stibnite, berthierite, Sb-Oxides
7	Fe	San Vicente	La Ahumada	682.90	4360.20	Stratiform	Medium Devonian quartzites		Goethite, secundary Fe and Mn-Oxides
8	Fe	Valencia de A.	Unnamed	653.90	4349.65	Stratiform	Fe-rich sandstones with Fe-nodules (Ordovician-Silurian).	Hematization	Goethite, china-clay, native S.
9	Fe	Valencia de A.	Unnamed	655.95	4349.75	Stratiform	Fe-rich quartzites (Ordovician-Silurian).		Goethite, secondary Fe and Mn-oxides.

TABLE 6.1 - CONT. *MINERAL OCCURRENCES IN THE STUDY AREA (GOLD EXCLUDED)*

NUM.	SUBSTANCE	LOCALITY	NAME	X UTM	Y UTM	MORPHOLOGY	HOST ROCK	ALTERATION	MINERAL ASSOCIATION
10	BPGC	Valencia de A.	Jola mine	653.50	4350.65	060E q.veins	Quartzites and slates (Lower Palaeozoic)	Chloritization	Quartz, galene, pyrite and accesory sphalerite.
11	BPGC	Valencia de A.	Zamorano	657.65	4366.95	Quartz-vein	C.E.G. shales and greywackes.	assist	Quartz, galene, pyrite, accesory chalcopyrite.
12	P	Valencia de A.	El Prado	647.95	4360.90	050E q.veins	Muscovitic aplitic granite	Sericitizat.Muscovitizat.	Aplitic granite.
13	P	Valencia de A.	La Lanchuela	651.20	4357.90	050E q.veins	Granite and spotted slates of C.E.G.	Sericitization	Quartz, dahllite, sericite.
14	P	Valencia de A.	Unnamed	654.45	4354.30	050E q.veins	Hornfels C.E.G. (Upper Precambrian)	Sericitizat. Chloritizat.	Quartz, dahllite, sericite.
15	P	Valencia de A.	Unnamed	656.40	4354.55	045 q.veins	Hornfels C.E.G. (Upper Precambrian)	Sericitizat. Chloritizat.	Quartz, dahllite, sericite
16	U-P	San Vicente	C. Valdehuelo	664.75	4354.00	030 q.veins	Two-micas granite.	Sericitizat. Chloritizat.	Quartz, apatite, phosphorite, gummite and other U-oxides.
17	U-P	Alburquerque	El Sabio	666.25	4347.25	030E q.veins	Tourmalinic two-micas granite	Muscovitizat. Hematizat.	Pitchblende, coffinite, quartz, pyrite, limonite, muscovite, autunite, torbernite.
18	U-P	Alburquerque	Valderrascón	671.25	4349.00	040E q.veins	Two-micas monzogranite.	Tourmal.Chloritiz.Hematiz	Quartz, apatite, spherulitic and massive pitchblende, coffinite, pyrite, marcasite, phosphorite, fluorite, jasperoidal quartz, autunite, torbernite, hematites, saleite.

TABLE 6.1 - CONT. *MINERAL OCCURRENCES IN THE STUDY AREA (GOLD EXCLUDED)*

NUM.	SUBSTANCE	LOCALITY	NAME	X UTM	Y UTM	MORPHOLOGY	HOST ROCK	ALTERATION	MINERAL ASSOCIATION
19	U-P	Alburquerque	Calderilla	673.40	4351.90	040E q.veins	Two-micas monzogranite.	Tourmaliniz. Chloritiz.	Quartz, pitchblende, coffinite, pyrite, marcasite, melnikovite, autunite, torbernite, hematites.
20	U-P	Alburquerque	Pedro Negro	675.80	4347.95	035E q.veins	Two-micas monzogranite.	Tourmaliniz. Chloritiz.	Quartz, pitchblende, marcasite, apatite, pyrite, melnikovite, jasperoidal quartz,U-black oxides, autunite, torbernite, gummite and limonite.
21	U-P	Alburquerque	Engorda	679.10	4344.70	NE q.veins	Two-micas monzogranite.	Tourmaliniz.Chloritiz.	Quartz, pitchblende, jaspe, phosphouranilite, gummite and autunite.
22	W	Val. Alcantara	El Carrascal	649.95	4371.30	N130 q.veins	spotted slates and hornfels (CEG).	Tourmalinization	Quartz, wolframite, arsenopyrite, pyrite, Fe-oxides
23	W	Valencia de A.	Los Barreros	652.15	3268.10	NW-SE q.vein	Spotted slates and hornfels of the C.E.G.(Upper Precambrian).	Tourmalinization	Quartz, wolframite, arsenopyrite, pyrite.
24	W	Valencia de A.	Sotomayor mine	654.50	4364.15	NW-SE q.vein	Spotted slates and hornfels of the C.E.G. (Upper Precambrian).	Tourmalinization	Quartz, wolframite, pyrite, arsenopyrite, tourmaline, Fe-oxides.
25	W	Valencia de A.	Las Huertas	648.85	4357.55	NW-SE q.vein	Spotted slates and hornfels of the C.E.G. (Upper Precambrian).	Tourmalinization	Quartz, wolframite, pyrite, arsenopyrite, tourmaline, Fe-oxides.

TABLE 6.1 - CONT. *MINERAL OCCURRENCES IN THE STUDY AREA (GOLD EXCLUDED)*

NUM.	SUBSTANCE	LOCALITY	NAME	X UTM	Y UTM	MORPHOLOGY	HOST ROCK	ALTERATION	MINERAL ASSOCIATION
26	W	Valencia de A.	El Asiento	652.15	4354.90	NW-SE q.vein	Hornfels of C.E.G. (Upper Precambrian).	Tourmalinization	Quartz, wolframite, arsenopyrite, Fe and Mn-oxides.
27	W	Valencia de A.	Aceña mine	654.80	4354.05	NW-SE q.vein	Hornfels and spotted slates of the C.E.G. (Upper Precambrian).	Tourmalinization	Quartz, wolframite, pyrite, arsenopyrite, Fe and Mn-oxides.
28	W	Valencia de A.	Unnamed	659.35	4354.40	NE q.veins	Hornfels of C.E.G. (Upper Precambrian).	Tourmalinization	Quartz, wolframite, pyrite, arsenopyrite, sericite.
29	Sn-Li-Ta	Alburquerque	La Mantecona	664.60	4347.75	Dyke swarm	Hornfels and spotted slates of C.E.G. (Upper Precambrian)	Tourmaliniz. Hematizat.	Quartz, albite, cassiterite, Nb-tantalite and lepidolite.
30	Sn-Li-Ta	Alburquerque	Tres Arroyos	665.70	4346.80	Dyke swarm	Hornfels and spotted slates of C.E.G. Layered muscovite, garnets and tourmaline-bearing albitites.	Tourmaliniz. Hematizat.	Quartz, albite, spodumene, lepidolite, adularia, muscovite, Li-Fe-Mn phosphates.

CHAPTER - 7 - GRAVITY SURVEY.

R. Campos & J.L.Plata.

Having presented the geological and metallogenical framework to the study area, the next two chapters (Gravity and Multispectral analysis of Landsat TM) show the other multi- disciplinary techniques utilized in this project. The integrated information was sophisticatelly processed using the Geographical Information System (GIS - Chapter 9) available at ITGE, in order to provide new exploration targets within the region.

7.1 - INTRODUCTION.

One of the techniques utilized in this project was a gravity survey carried out by ITGE, initial results of which have been published (Campos & Gumiel, 1990). This technique combined with remote sensing data and field structural geology has been integrated in a common geological framework.

The study area (Fig. 7.1) is located in the southwestern part of Spain (Extremadura region), between Caceres and Badajoz provinces. The select area extends 32Km x 97Km delimited by the following UTM coordinates:

A- X = 656000; Y = 4370000 B- X = 657000; Y = 4339000

C- X = 753000; Y = 4371000 D- X = 738000; Y = 4339000

The area partially covers the following 1:50,000 topographic sheets of M.T.N (Mapa Topografico Nacional): 702, 703, 704, 705, 727, 728, 729, 730, 750 and 751 (Fig 7.1).

The aim of this work was to study:

1) the geometry (shape and extension in depth) of the main intrusive bodies (the Alburquerque Batholith and the Albala Pluton);

2) the relationship between the granites and the metamorphic rocks;

3) the support of the structural work, and finally

4) to utilize the gravity modelling as a guide to the mineral exploration of the area.

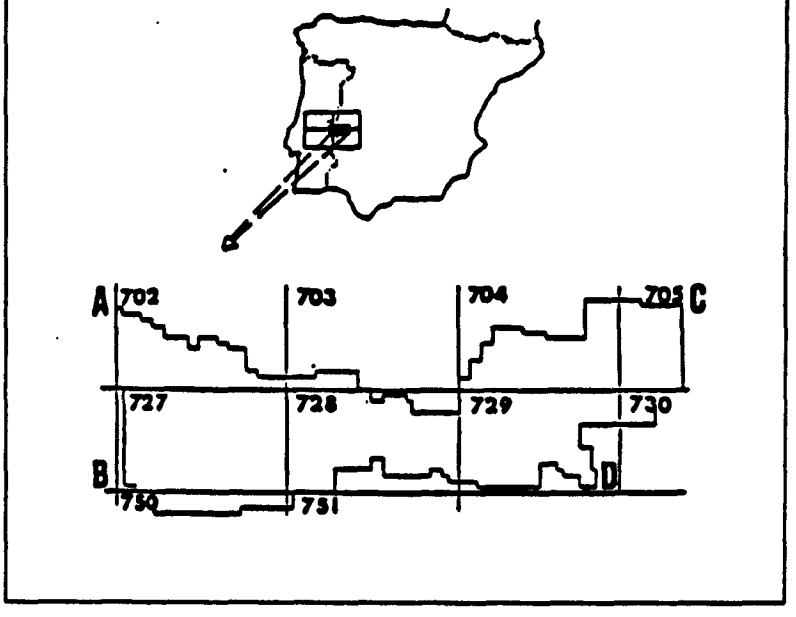

FIG. 7.1 - LOCATION OF THE GRAVITY STUDY AREA.

7.2 - MEASUREMENTS AND DATA TREATMENT.

The Bouguer gravity anomaly map was the starting point of this study accompanied by a topographical support to provide the X, Y, Z coordinates of each point. 1543 gravity field measurements were taken in a grid of 1 point/Km^2.

In order to work with absolute values of gravity, four gravity bases were established, which were linked to the International Gravity Standardization Net (ISGN-1971): BF-16 (Caceres) and BF-11 (Badajoz). (Internal Report ITGE, 1989).

In order to produce the Bouguer anomaly map the standard UNE rules (22-611-1985) relating to gravity studies were adopted providing a normalized calculation system, units etc. The following corrections and calculations have been included:

- Earth-Tide corrections, with 0.005 mGal of appreciation.

- Drift correction with an average drift value determined during the whole field work of 0.004 mGal/Hour.

- Calculation of the theoretical gravity based on the International Formula of 1967:
$g67 = 978031.85 (1 + 0.0053024 \sin^2\Phi - 0.0000059 \sin^2 2\Phi)$

- Calculation of density reduction based on the method described by Plata (1983).

- Terrain corrections for gravity measurements using the method of Hammer (1939) for the near and medium correction and the interpolation method (Neuman, 1963) for the topographic far correction.

The gravimeter was checked repeatedly during the field work. The following controls were carried out by ITGE to improve the quality of the measurements:

- secular drift control;
- gravimeter checking involving 8% repetition of the field measurements;
- topographic correction with about 5% of the field measurements repeated.

7.3 - DETERMINATION OF DENSITIES.

The standard density (2.67 gm cm^{-3}) established by Daly (1933) has been utilized in the reduction to produce the Bouguer anomaly. A rock density study was also carried out in order to determine the average density of the different rocks that made up the area.

This study covered the main lithologies of the complete area and also involved collecting samples from drill-cores at different depths. Rock density was determined for each sample and the results treated statistically (Table 7.1, Fig. 7.2).

TABLE 7.1 (*) - Rock Density.

	Lithology	Average Density gm/cc
Granitica Facies	Granites	2.64
	Granodiorites	2.72
C.E.G	Slates And Greywakes	2.72
Palaeozoic	Quartzites	2.64
	Basic Rocks	2.78
	Other Facies	2.72

(*) - Analysis made in ITGE.

Thus, it has been possible to establish a precise density contrasts of the local rocks, which increases the accuracy of the quantitative interpretation and modelling of the Bouguer anomaly profiles.

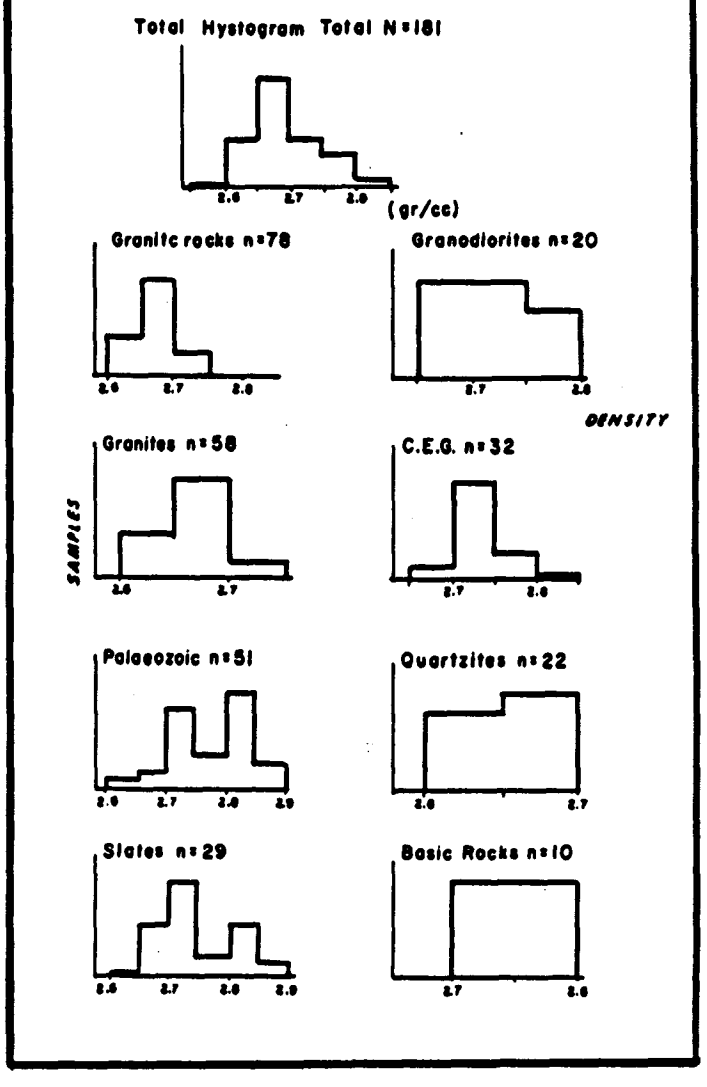

FIG. 7.2 - DENSITY HISTOGRAMS.
(n: number of samples).

7.4 - BOUGUER GRAVITY ANOMALY MAP.

The Bouguer gravity anomaly map (Fig. 7.3a and b) has been produced using a Bouguer reduction density of 2.67 gm cm^{-3} and shows the main geological features of the study area. Two distinct anomalous areas are present in the Bouguer anomaly map (Fig. 7.3a); 1) Albala area (to the East) and 2) La Codosera- Alburquerque area (to the West). The boundary between the two areas is defined by a pronounced N130-140E trending gradient (A anomaly, Fig.7.3a). This anomaly with a very strong gradient, corresponds to the Palaeozoic rocks that make up the Sierra de San Pedro Syncline (easternly prolongation of the Northern Ridge).

The Albala zone shows a very large negative gravity anomaly of -30 mGal (Fig. 7.3a, B anomaly) corresponding to the Albala Batholith. This area also exhibits other minor anomalies, among them, prominent minima at C and D, which represent the southern prolongation of the Cabeza de Araya Batholith, which is probably unconnected with the Albala Batholith, and the positive gravity anomaly (E) related to metamorphic rocks of the CEG.

The La Codosera-Alburquerque area has been the main study area and shows several gravity anomalies. The most prominent is the negative anomaly (Fig. 7.3a, anomaly F) produced by the Alburquerque Batholith. The differences between the gradients of this anomaly can be interpreted as different dips of the contact of the intrusive body, which forms an asymmetrical shape (elliptical) which is also observed towards the east.

Anomaly G, located towards the west corner of the map, is characterized by negative gravity values (-11 mGal) and corresponds to the western prolongation of the Alburquerque Batholith. The two anomalies (F and G) are linked via anomaly H. The regional trend in this area is NE-SW ($N20^{o}$-$30^{o}E$), but a subsidiary lineation is noted, trending NW-SE. The NE-SW trending lines correspond to extensional fractures parallel to the Alentejo-Plasencia Fault, and the NNW-SSE trend to a set of NW- SE trending faults, which has good correlation with ground observations and have been interpreted as antithetic to the main sinistral shear zone and form a "domino" or "bookshelf" type of geometry (Sanderson et al., 1990) (Fig. 7.4 - see Chap. 2 - Fig. 2.4).

The negative gravity anomaly (Fig. 7.3a,anomaly I) is the start of an interesting anomaly located to the west of La Codosera. This anomaly lies at the edge of the survey area and is currently being checked by further data since it lies close to the Los Algarbes gold prospects and hence may be of major importance (see section 7.6).

Other positive anomalies located towards the north and south in the Bouguer gravity map correspond to the Palaeozoic rocks that make up, respectively, the Sierra de San Pedro (Northern Ridge) and the La Codosera Syncline (Southern Ridge).

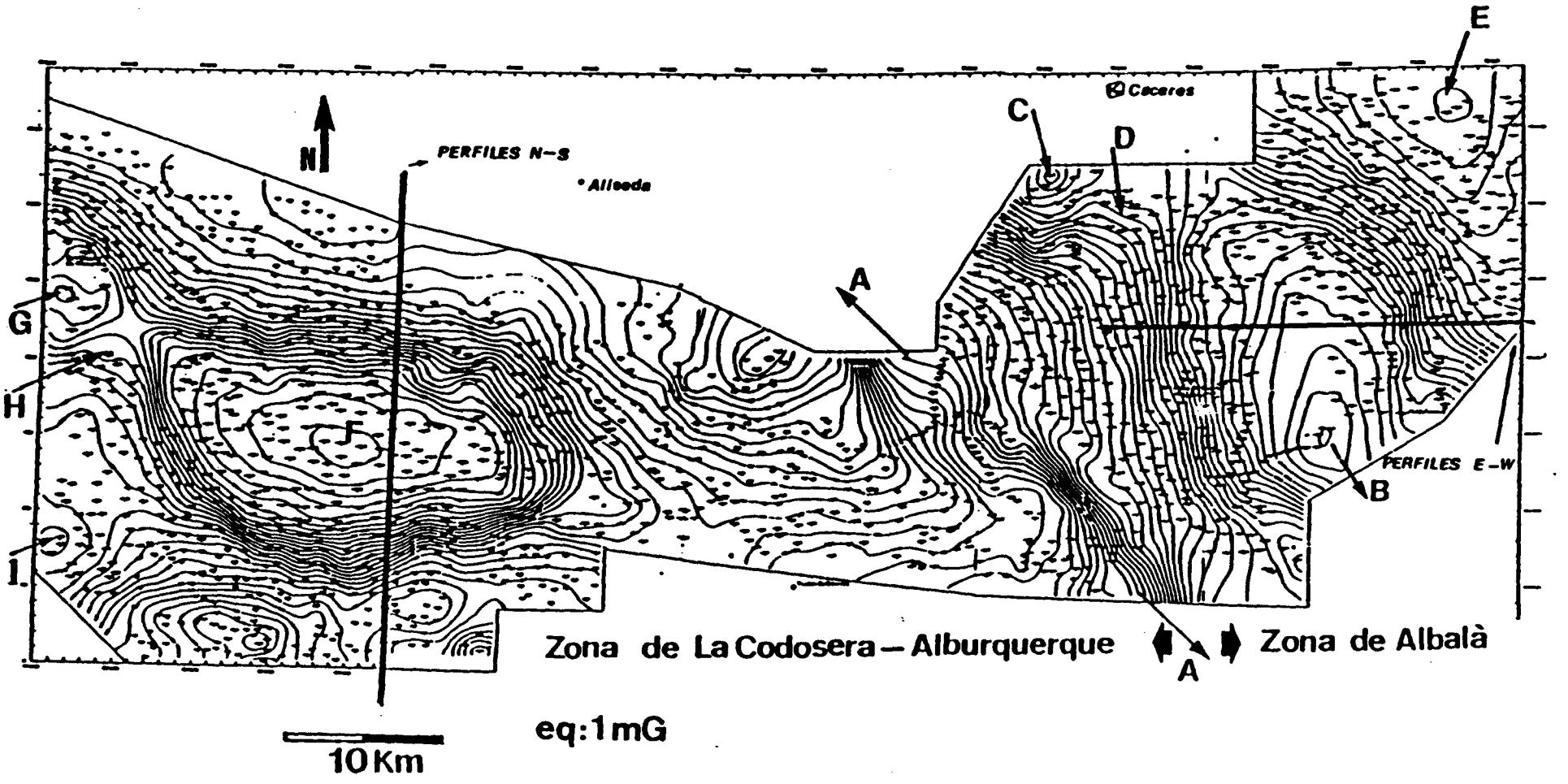

FIG. 7.3a - BOUGUER GRAVITY ANOMALY MAP. (Contour interval is 0.1 mGal).

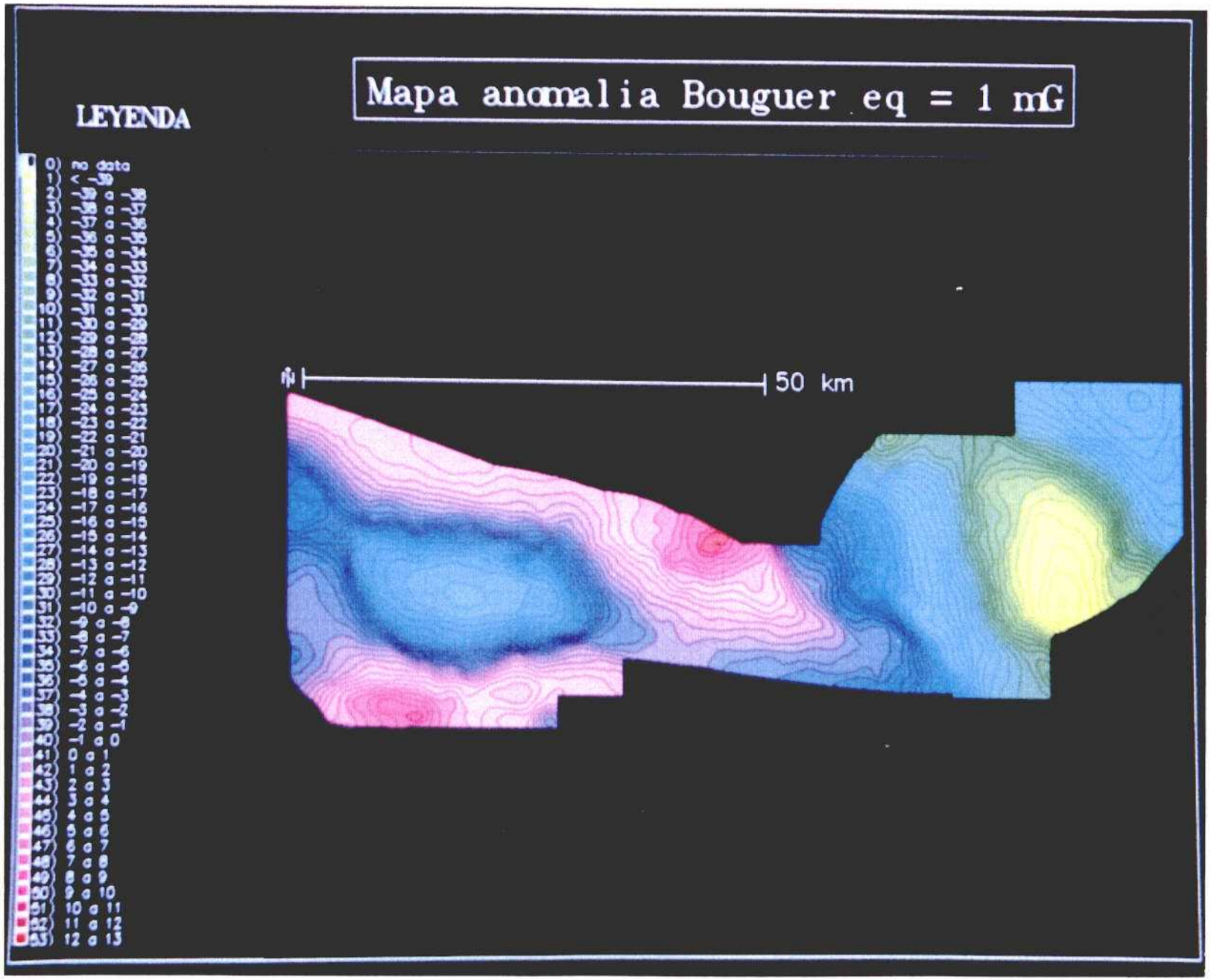

FIG. 7.3b - INTEGRATED BOUGUER ANOMALY MAP.

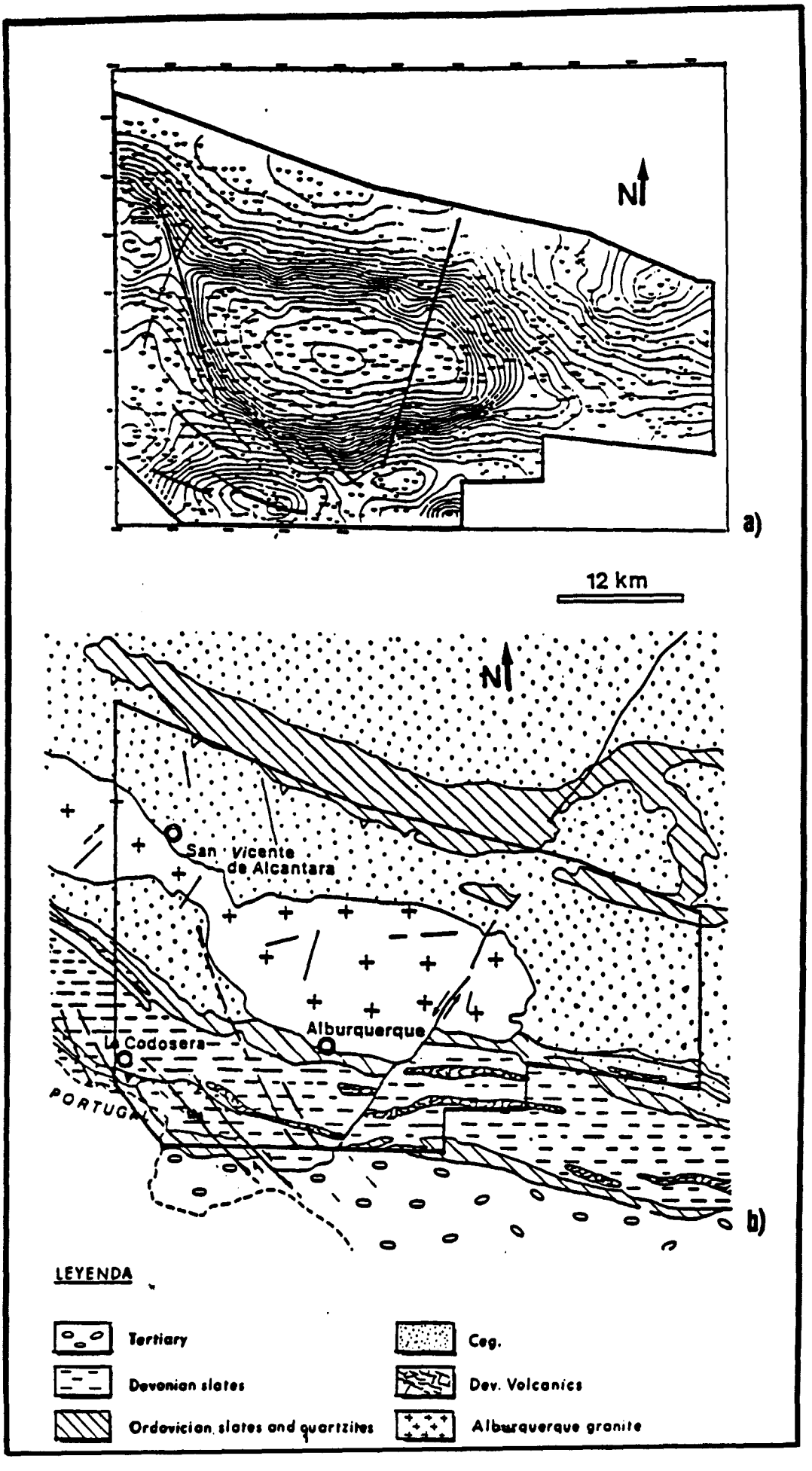

FIG. 7.4 - CORRELATION MAP BETWEEN GEOLOGY AND GRAVITY.

7.5 - GRAVITY MODELLING.

Gravity models of selected anomalies have been calculated in order to investigate the geometry and extension in depth of the plutonic bodies. The quantitative interpretation is based on the 2-D method of Talwani et al. (1959) and has been generated using the MAGIX programme (Golden, CO.USA).

7.5.1 - Albala area.

The interpretation of the Albala area has been made using six E-W trending gravity profiles (Fig. 7.5), which show a very large negative gravity anomaly (-30 mGal - B anomaly) corresponding to the Albala Stock. Taking into account that this intrusion cross-cuts the CEG and studying the characteristics of this gravity low, the negative gravity anomaly is due to the low density of the granitic rocks that make up the Albala intrusive.

The subsurface interpretation of the pluton (Fig. 7.5) is of a "balloon"-shaped body, which shows a vertical extent (depth) of between 9 and 10 Km and thickens upwards. More than 60% of the plutonic mass is located above 5 km depth. This characteristic fits well with the post-kinematic granites which extend to depths of about 10 Km and are probably emplaced by diapirism and/or forceful injection.

For some of the gravity profiles (Fig. 7.5 a, b and c), the gravity anomaly suggests another granitic body, which would correspond to the Montanchez granitic stock. This body, with the same density contrast (-0.1 gm /cm^3), crops out along the Y4350R and Y4352R profiles and is non-outcropping in the Y4354R profile (Fig. 7.5a/b & c). Its average depth is difficult to establish because it is located towards the edge of the study area, but its dimensions decrease to the north giving it up an elliptical shape, trending N-S and pinching out to the north.

The relationship between these two granitic masses is difficult to establish. From the gravity profiles there appears to exist a discontinuity between them. The two granitic bodies are compositionally quite similar, but both exhibit important structural differences. The Montanchez granite shows a strong C-S fabric due to shearing effects (Castro, 1984), whilst the Albala granite does not. Both granites may be separated by a shear zone corresponding to the discontinuity observed in the profiles.

7.5.2 - Alburquerque - La Codosera area.

The quantitative interpretation of the La Codosera- Alburquerque area has involved modelling, based on geological interpretations of six N-S trending gravity profiles (Fig. 7.3a).

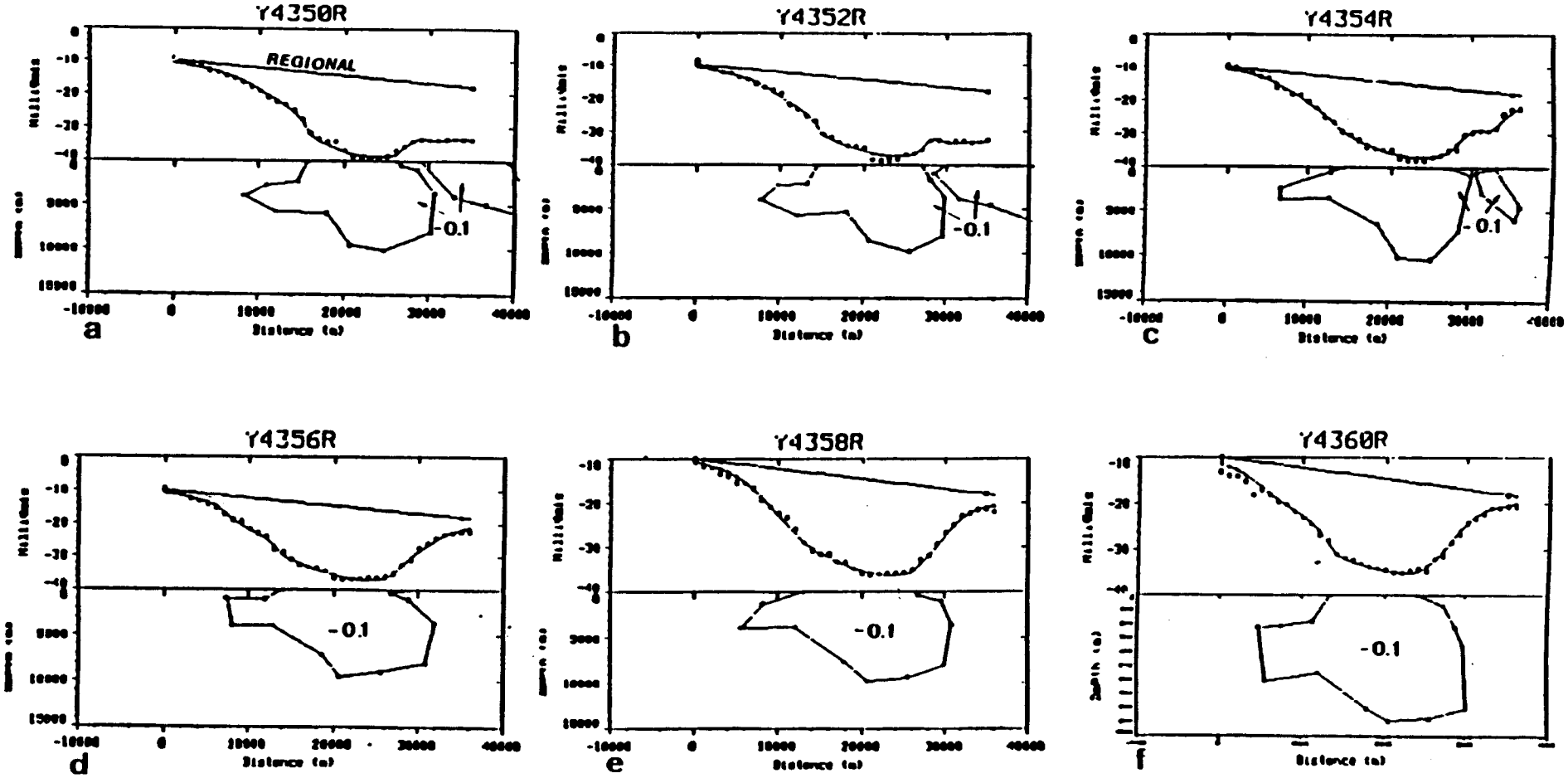

FIG. 7.5 - PROFILES E-W (ALBALA ZONE) RESULT OF 2.5 D MODELLING.

The modelling (Fig. 7.6) has also been made using a density contrast between the granitic rocks and the CEG of -0.1 gm cm^{-3} and between the Palaeozoic rocks and the CEG of +0.05 gm cm^{-3}.

All the profiles display a negative gravity anomaly corresponding to the Alburquerque Batholith. This gravity low in part is counteracted by positive anomalies towards the north and south of the profiles generated by the Palaeozoic rocks of the Sierra de San Pedro and Codosera synclines respectively. Based on the results of these models, it is assumed that the granitic rocks that make up the Alburquerque Batholith reach a maximum depth of between 10 and 11 Km. The average thickness is 12 Km and 60% of the granitic mass is above 5 Km depth. The geometry is a "balloon" - shaped body with a reduction of mass in depth.

The prism of positive density contrast to the south of the granite corresponds to the La Codosera Syncline. The profile X660R, located to the west in the thinnest part of the batholith, shows special characteristics (Fig. 7.7). It exhibits two gravity lows (A and B). A) could be attributed to the mass deficiency generated by the granitic rocks and B) to the superimposition of the negative effect generated by the extension of the granite towards the south and the positive effect of the Palaeozoic rocks of the La Codosera Syncline. We consider that these two negative gravity anomalies are probably generated by only one irregular shape granitic body which would extend towards the south below the La Codosera Syncline. Side A), correlated with the Alburquerque Batholith, reaches out to a maximum depth of 7000 m. We estimate that the extension of this body towards the south (B, Fig. 7.7) would be located around 1700 m below the Palaeozoic rocks of the La Codosera Syncline.

The geological interpretation of this profile is of major importance. Without forcing the geometry, it turns out tempting to suppose that this irregular-shaped granitic body could be separated from the main Alburquerque Batholith (A) by an extension fault, which has been picked up in TM imagery (Fig. 6.5, Chap.6) and in geological field mapping towards the thinning of the batholith. The throw of this fault towards south could be about 1000 m, but is difficult to establish definitively.

7.6 - EXTENSION OF THE GRAVITY SURVEY - LA CODOSERA AREA.

Introduction.

The original Bouguer Anomaly Map did not accurately define anomaly I (Fig. 7.3a). This anomaly is of special interest for two principal reasons: firstly, because of its spatial coincidence with other anomalous data sets such as contact metamorphic soils in the TM imagery, the high-medium $K_{(e)}$ aero-radiometric values (see Chapters 8 and 9), and secondly because of the abundance of the gold prospects existing to the west of La Codosera. For this reason an extension of the gravity survey was carried out by ITGE in order to confirm the form of the gravity minimum more accurately.

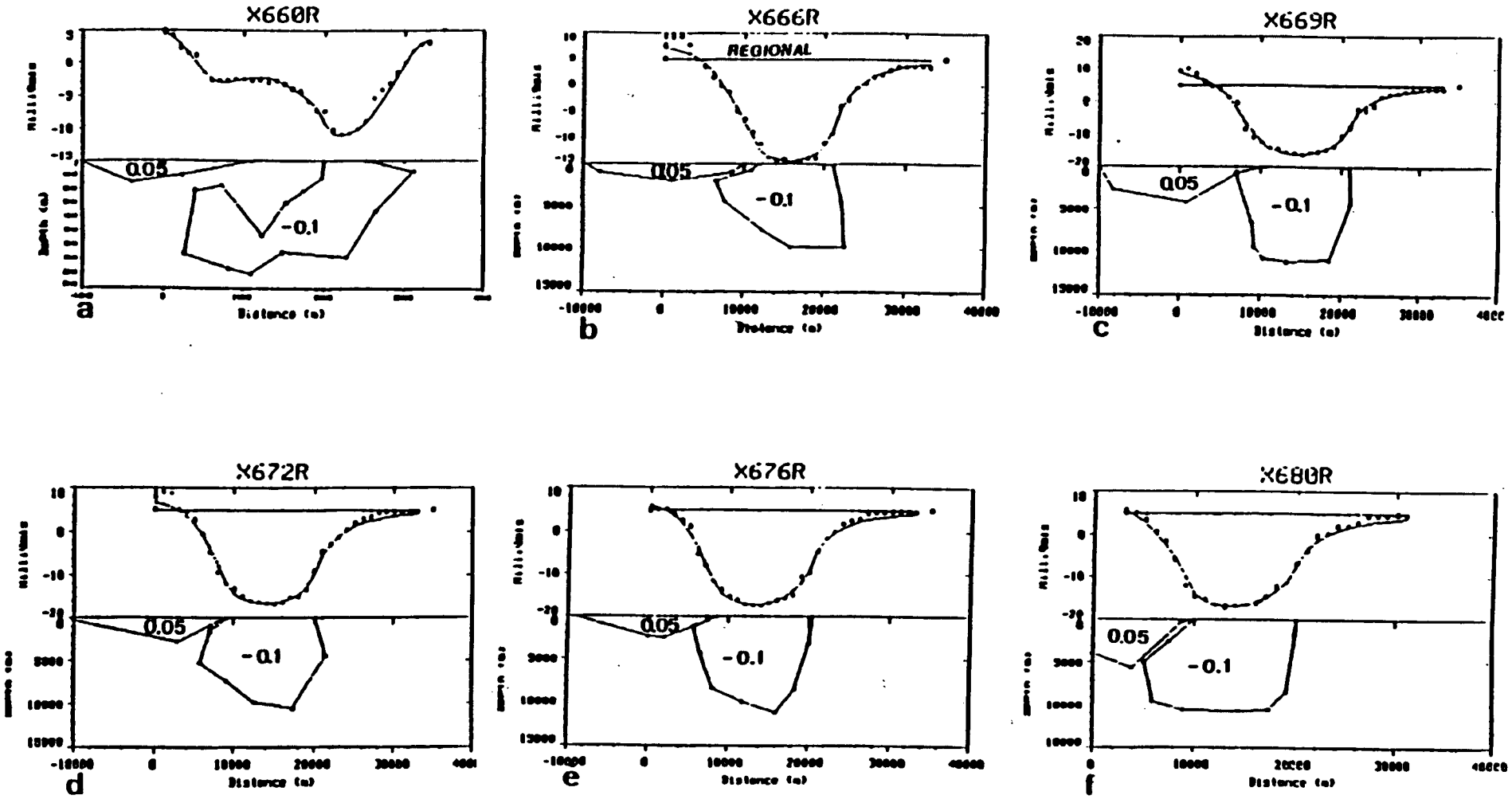

FIG. 7.6 - PROFILES N-S (LA CODOSERA - ALBURQUERQUE ZONE) RESULT OF 2.5 D MODELLING).

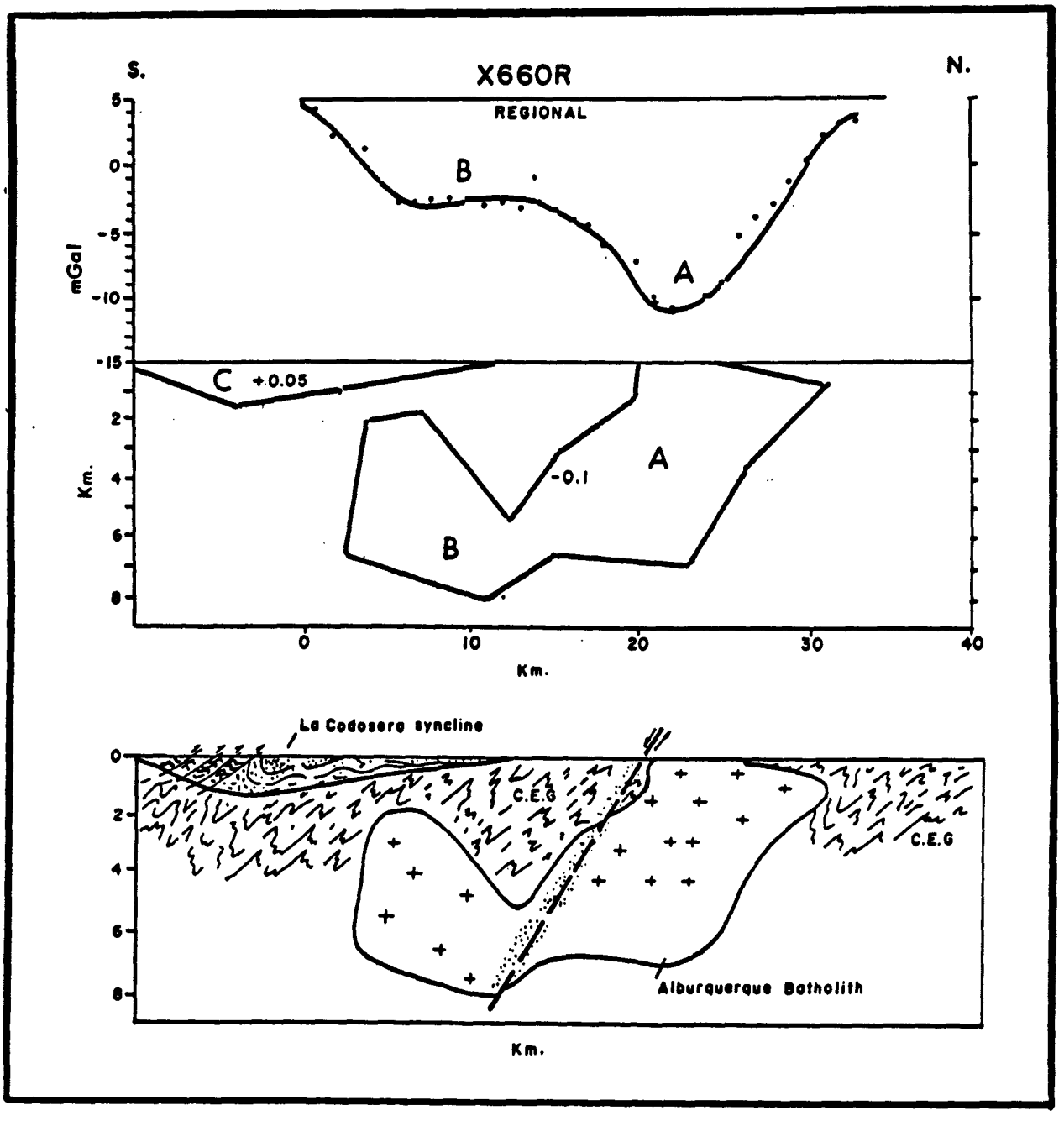

FIG. 7.7 - PROFILE X660R (N-S) SHOWS IN SECTION THE RESULTS OF 2.5 D MODELLING.

Location.

The extended study area is located western of La Codosera and is delimited by the following UTM coordinates:

X east = 651000; X west = 657000

Y south = 4339000; Y north = 4349000.

The new grid was made up from 130 gravity measurements approximately every 700 m. using the same topographic support as in the previous gravity work, in order to get the precision and accuracy required in this detailed second stage of the gravity survey.

The gravity measurements have been linked up with the International Gravity Standardization Net (ISGN - 1971) through the Alburquerque Base (B2 = 980006.38 mGal) which was utilized in the previous gravity work. The corrections and calculations have been made using the same criteria established in the preceding gravity work (see Section 7.2).

7.7 - EXTENSION OF THE BOUGUER GRAVITY ANOMALY MAP.

This map (Fig. 7.8 a/b and c) shows clearly the negative gravity anomaly (I) which is located western of La Codosera. The minimum value is -7.5 mGal and, although the anomaly seems to be opened towards west because no gravity measurements have been taken in Portugal, it is possible to consider this anomaly almost symmetrical being delimited by similar gradients.

It is difficult to establish a correlation of this negative anomaly (I anomaly, Fig. 7.8a/b and c) with the positives that exist over the La Codosera Syncline, which are generated by the Palaeozoic rocks, that have a density higher than the CEG rocks. Moreover, the spatial coincidence of this gravity minimum with the high-medium $K_{(e)}$ aero-radiometric values and with the TM contact metamorphic soils suggests the existence of a lower density body at depth, which could be correlated with a buried granite, similar to the Alburquerque Batholith (Fig 7.8a). Traces of contact metamorphism in the Lower Devonian slates hosting the Perla de Anibal gold prospect, located in the surrounding area support the existence of this granitic body in depth (see section 8.8).

7.8 - MODELLING AND DISCUSSION.

Due to the sub-circular shape of anomaly I, 2D or 2.5D modelling can not been applied in this case. Therefore, we have attempted to model the anomaly as a low density spherical body whose dimensions and depth have been calculated as follows:

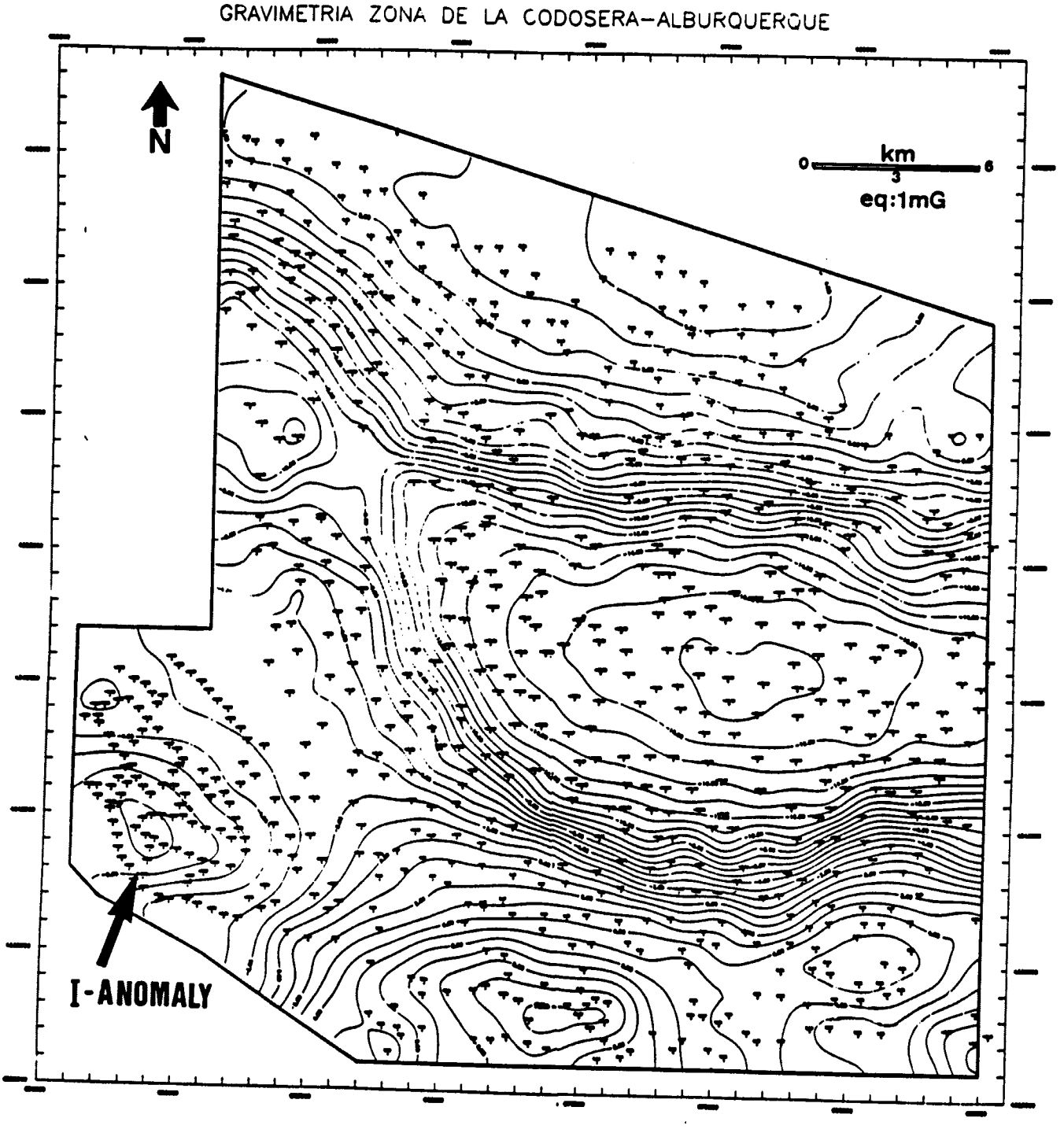

FIG. 7.8a - EXTENSION OF THE BOUGUER GRAVITY ANOMALY MAP.

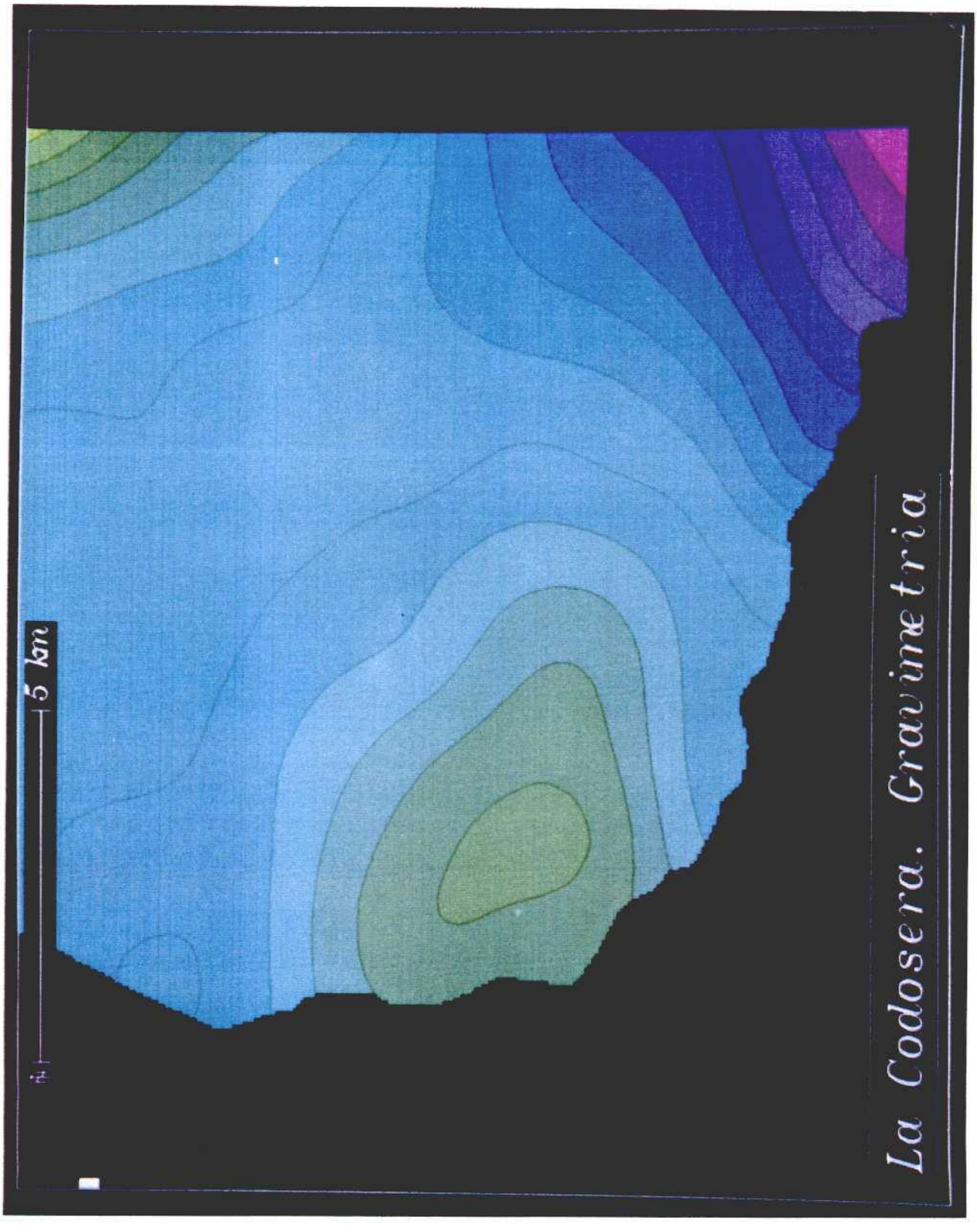

FIG. 7.8b - I-ANOMALY (MINIMUM) IN THE BOUGUER GRAVITY MAP WEST OF LA CODOSERA (GENERATED FROM G.I.S).

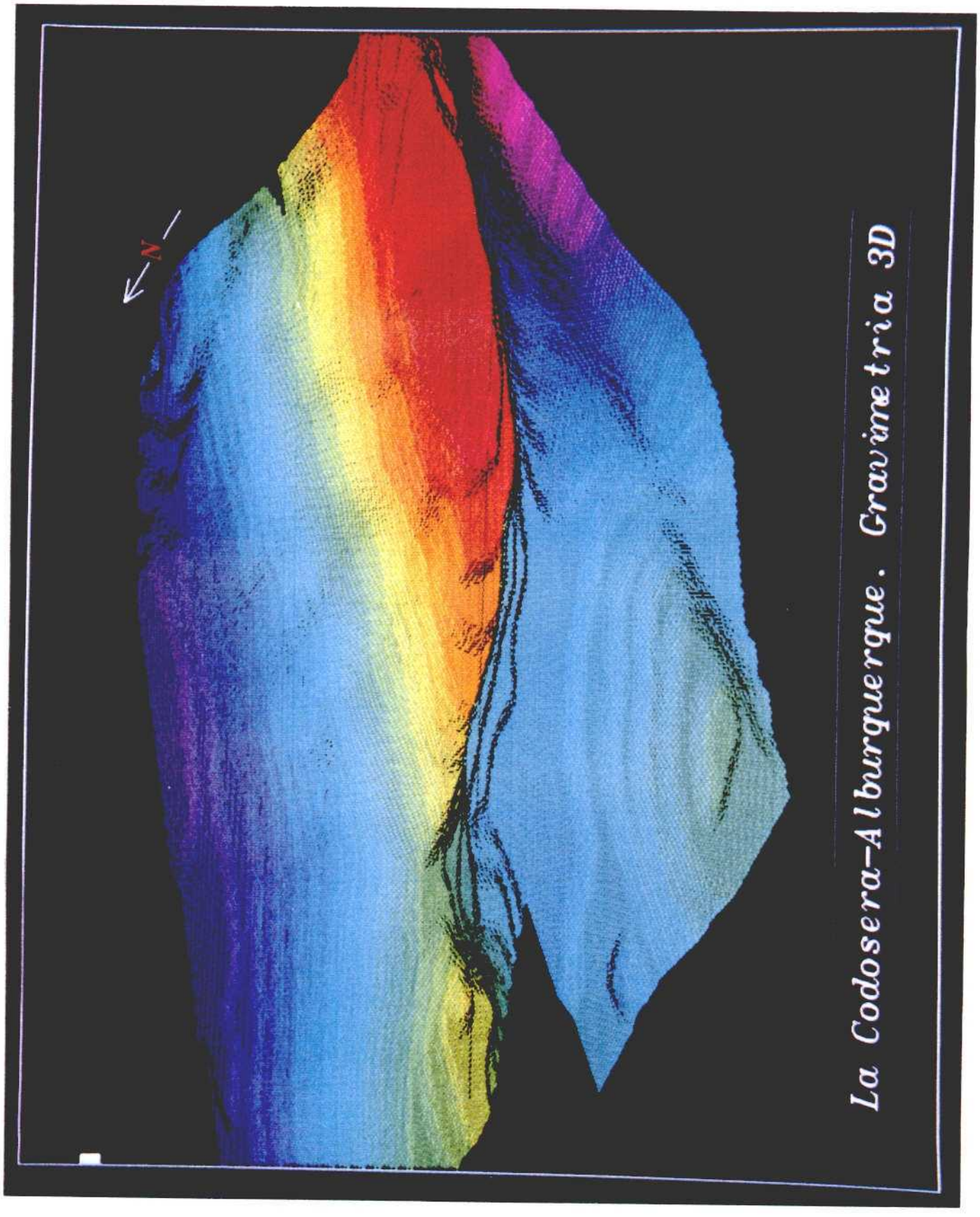

FIG. 7.8c - THREE-DIMENSIONAL MODEL OF THE BOUGUER GRAVITY ANOMALY MAP IN THE LA CODOSERA-ALBURQUERQUE AREA.

The approach is following the equation:

$gmax. = (4\pi K D R^3) / 3) \ (Z / (X^2 + Z^2)^{3/2})$

$gmax. = 6.5$ mGal

$X(1/2) = 3.4$ Km

$Z = 1.3 \ X(1/2) = 4.42$ Km

$D = -0.1$ gm cm^3

$gmax. = 27.94 (D R^3/Z^2)$

$R^3 = (gmax. Z^2) / (27.94 \ D) = 45.4$ Km

$R = 3.5$ Km

The results indicate a spherical granitic body of 3.5 Km radius, with a negative density contrast (-0.1 gm cm^{-3}) which would be located approximately at 1 Km depth. This interpretation is supported by the modelling of the X660R gravity profile (Fig. 7.7).

CHAPTER - 8 - MULTISPECTRAL ANALYSIS AND DIGITAL CLASSIFICATION OF LANDSAT THEMATIC MAPPER DATA.

C. Antón-Pacheco & J.C. Gumiel

8.1 - INTRODUCTION.

Landsat TM multispectral data provide a valuable tool to determine spectral differences in soils and rocks, based on their mineralogical constituents. The adequate radiometric and spatial resolution of the Landsat TM data allows discrimination of the subtle spectral manifestations associated to alterations and lithologies that often characterise the host-setting of metal deposits.

Traditionally TM Landsat data have been used to delineate and discriminate areas of hydrothermal alteration and limonitic materials. The slopes of the spectral reflectance curves as well as the positions of the absorption features, which are diagnostic of the hydroxyl-bearing and the iron-bearing minerals in the near infrared and visible region, characterise the spectral response of the rocks containing these minerals.

A wide range of image processing techniques have been employed to assess clay mineral alteration and iron-staining. The most common are ratio composites which emphasize the differences in the spectral response of the surface materials (Rowan et al.,1974; Abrams et al.,1983). Digital classification techniques have not generally been employed in geological studies as contacts between lithological units are often gradational and surface morphology plays an important role in the interpretation. However, this technique has proved to be most valuable in areas where the materials show good exposures and a moderate topography.

This report evaluates a digital classification technique of Landsat TM data, first developed in the Caceres area where late Hercynian granites extensively outcrop. They produce wide contact metamorphic aureoles in the intruded Precambrian and Palaeozoic metasediments. The spectral characteristics of the contact metamorphic rocks and associated soils in this area permit to distinguish them from the equivalent rocks affected only by the regional metamorphism (Rowan et al., 1987; Antón-Pacheco et al., 1988).

In the Alburquerque-La Codosera area, digital classification of Landsat Thematic Mapper data allows discrimination of two spectrally different types of soils within the contact aureole caused by the Alburquerque pluton. Soils derived from hornfels present a lower radiance response in all TM bands than soils developed on spotted slates. Soils derived from slates of the country rock, only affected by the low-grade regional metamorphism, show a higher TM response than the two former types of soils.

Laboratory reflectance spectra of these three groups of soils present similar differences to the TM spectra derived from the digital number (DN) values of the six visible and near infrared TM channels. X-Ray mineralogy of the soils and petrographical studies of the underlying rocks confirm these differences.

The extent of the digital classification of Landsat TM data over the whole study area has located an area, west of La Codosera, where the soil derived from black Devonian slates presents the same spectral characteristics as the soils within the contact aureole produced by the Alburquerque granite. Another group of soils with high iron content has also been discriminated on the basis of their spectral characteristics.

8.2 - GEOLOGICAL SETTING.

The materials outcropping in the Alburquerque-La Codosera area (Fig.8.1) are very similar to those in the Caceres area, both being included within the Central Iberian Zone of the Hercynian Massif. The lithology of the rocks are described elsewhere in this volume (see Chapters 1 and 2).

The Alburquerque Batholith intrudes the central part of the area, cutting across the Hercynian structures and causing a variably sized aureole in the metasedimentary rocks. The mineral paragenesis of the contact metamorphic rocks is made up by cordierite-andalusite-muscovite-quartz (hornfels facies) and muscovite-biotite-quartz (spotted slate facies).

Several types of mineralization occur related to the granite. U-P mineralisation in intragranitic quartz veins and Sn- W-Li mineralisation mainly in extrabatholitic quartz veins and pegmatites (see Chapter 6).

8.3 - VEGETATION AND LAND USE.

The area has a Mediterranean climate with cool, wet winters and hot, dry summers. Average annual rainfall is 70 cm. The elevation is relatively moderate, ranging from 300 m to 700 m. Main elevations are controlled by the Armorican quartzite ridges. The Precambrian materials (CEG) give rise to a low topography, showing few outcrops and being cultivated for cereal crops, mainly in the area north of San Vicente and Valencia de Alcantara. The Alburquerque granite presents a higher relief than the CEG materials and a typical "roquedo" morphology, with good exposures. The drainage network is strongly controlled by the joint pattern, which affects the granite. This terrain is mainly used for pasture with native oak trees (dehesas). The vegetation cover associated to the Palaeozoic materials is more important: cistus, pine trees and reforested eucalyptus cover most of the quartzite ridges.

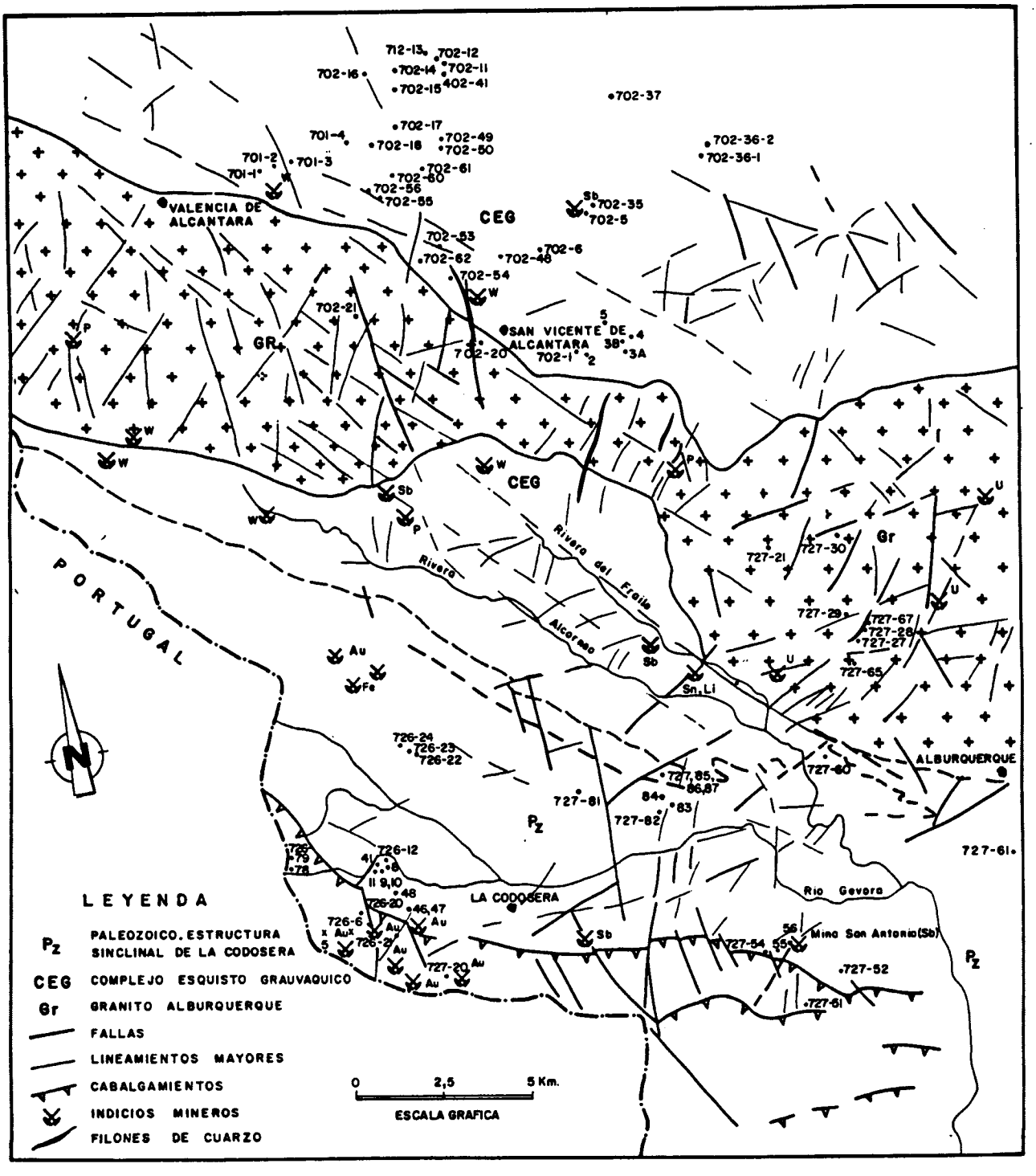

FIG. 8.1 - GEOLOGICAL SKETCH OF THE ALBURQUERQUE-LA CODOSERA AREA WITH LOCATION OF SOIL AND ROCK SAMPLES.

8.4 - IMAGE ANALYSIS.

A Landsat Thematic Mapper (TM) image, registered in August 3, 1985, (203-33, Q2), has been selected to analyze the spectral response differences among the main lithological units in the Alburquerque-La Codosera area. Late - summer Landsat TM images are very adequate to obtain the maximum radiance information from the soil in cultivated areas (Anton-Pacheco et al., 1988).

Standard image processing techniques were used to produce different types of colour composites. The analysis of the images involved the generation of several false colour composites, ratio composites and principal component composites.

In the colour composite TM 745 (BRG) (Fig. 8.2), the main geological features are very distinct. The Alburquerque granite presents a characteristic geomorphological expression and vegetation cover. The north-western sector, in dark blue, shows good exposures and a well expressed fracture pattern while the eastern margin presents a softer texture, indicating a more important soil cover. Lichen and moss cover most granitic outcrops and mask the spectral characteristics of the granite (Ager & Milton, 1987).

Cereal fields in the CEG, north of the granite contact, between San Vicente and Valencia de Alcantara, display a characteristic pattern with different colours given by stubble fields and by bare soils exposed in tilled fields. The latter present different colours depending on their location with respect to the granite. Bare fields near the granite exhibit a dark magenta colour, whereas bare fields far from the pluton are white. These colours are related to the different spectral response of the soils in tilled fields (Rowan et al., 1987). Stubble fields appear in orange to light yellow colours, and fallow fields and pasture are displayed in light blue to greenish, depending on the density of the vegetation cover.

The Lower Palaeozoic materials outcropping in both limbs of the La Codosera syncline, give linear ridges which are densely covered by pine trees and cistus undergrowth and appear in red and black in the image. The middle Devonian pelitic and carbonate materials outcrop in the core of the La Codosera Syncline, giving a softer topography. They are partially cultivated and reforested with eucalyptus trees.

Band ratioing provides further information on the mineral composition of rock and soil by increasing the spectral contrast in the data and decreasing at the same time the effects of illumination due to the topography. TM5/7 is used to detect spectral absorption features originated by hydroxyl and carbonate- bearing minerals. TM4/5 and TM4/3 are used to distinguish bare rock and soil from vegetation. TM3/1 gives high values for rock and soils containing iron-bearing minerals. The combination of the three ratios TM4/5, 5/7, 3/1 (BRG) is depicted in Fig. 8.3. Bare soils in the CEG near the granite appear in blue, indicating high TM4/5 values relatively to TM5/7 and TM3/1. Soils far from the granite exhibit a green colour.

FIG. 8.2 - FALSE COLOR COMPOSITE TM 745 (BRG) OF THE ALBURQUERQUE-LA CODOSERA AREA. SYMBOLS: CEG: SCHIST-GRAYWACKEE COMPLEX; PZ: PALAEOZOIC; GR: ALBURQUERQUE GRANITE; 1: VALENCIA DE ALCANTARA; 2: SAN VICENTE DE ALCANTARA; 3: ALBURQUERQUE; 4: LA CODOSERA.

The green vegetation presents a magenta colour because of relatively high values of TM4/5 and TM5/7.

The ratio TM4/3 (Fig.8.4) emphasizes vegetation which presents light colours corresponding to high ratio values due to the sharp increase of the vegation reflectance in TM4 relatively to TM3. Bare soils exposed in tilled fields present low ratio values and appear in black.

The principal component (PC) transformation is another powerful image-enhancement technique. The bands of the original Landsat TM data set are usually highly correlated. The PC transformation effectively decorrelates the data and displays them more efficiently. The information content of the six visible and near-infrared TM bands are reduced to five principal components of which the three first contain more than 90% of the variance of the original data.

In terms of surface characteristics, the first PC seems to relate to the variation in the overall spectral reflectance and brightness information associated with the topography and the albedo of the scene. The second, third and fourth PCs contain information about more subtle variations in the reflectance among surface materials. The PC colour composites are very colourful but it is not possible to derive relative spectral reflectance signatures related to the surface units. These images are very valuable to outline the contacts between different units. The colour composite PC423 (BRG) in Fig. 8.5. provides a good discrimination of the different materials and minimizes the influence of shadows and other albedo variations. The contacts between the granite and the CEG materials are very sharp in this image as well as the delineation of the Armorican Quartzite ridges of the La Codosera syncline. The fourth component contains information relative to tilled fields which are shown in light blue, very distinctive from the stubble fields which appear in green.

Within the general study area of Alburquerque-La Codosera, a small area was selected in order to carry out a detailed study to analyze the different spectral responses exhibited by the soils exposed in tilled fields. This test area is located within the CEG materials, north of the granite, between San Vicente and Valencia de Alcantara villages (Fig.8.2). In this area, cultivated fields are big enough to be clearly identified in the TM745 image, the lithology is reasonably uniform and the topography moderately low. Hence, the radiance variance of the tilled fields should be mainly controlled by the soil nature.

8.5 - MINERALOGICAL STUDIES.

The granite, particularly in the eastern sector, is very weathered, giving rise to sandy soils, light in colour. The coarse texture of granite derived soil results from the dominant mineral being quartz. There are lesser amounts of feldspars and muscovite, and few kaolinite. Quartz, feldspars and muscovite are primary minerals, whereas kaolinite is a secondary product of the weathering of feldspars.

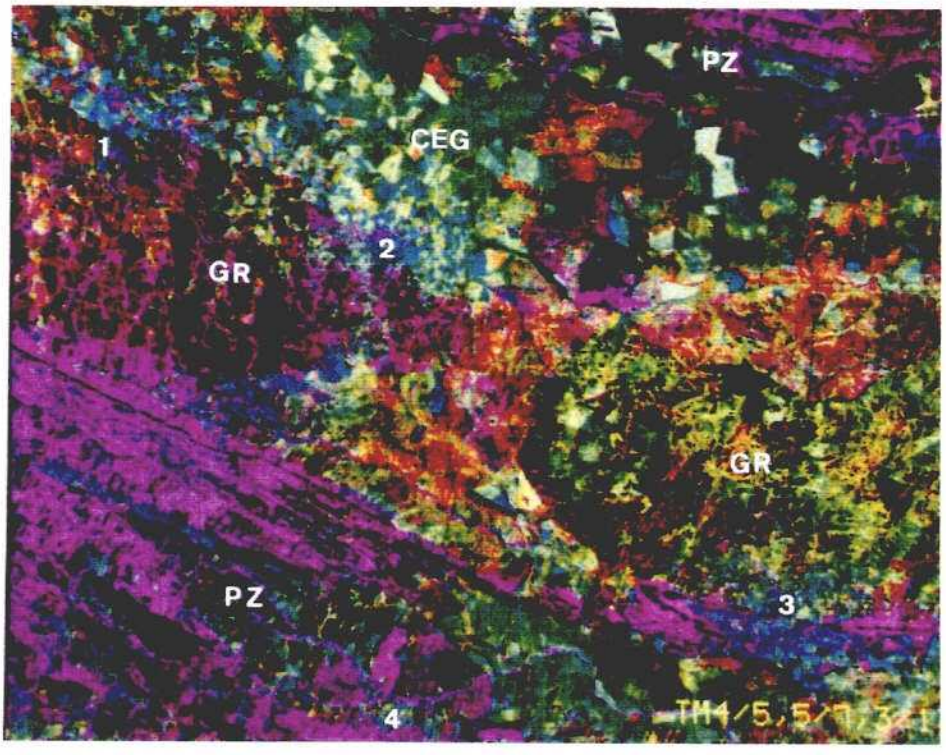

FIG. 8.3 - RATIO COMPOSITE TM 4/5, 5/7, 3/1 (BRG) OF THE ALBURQUERQUE-LA CODOSERA AREA. SYMBOLS AS IN FIG. 8.2.

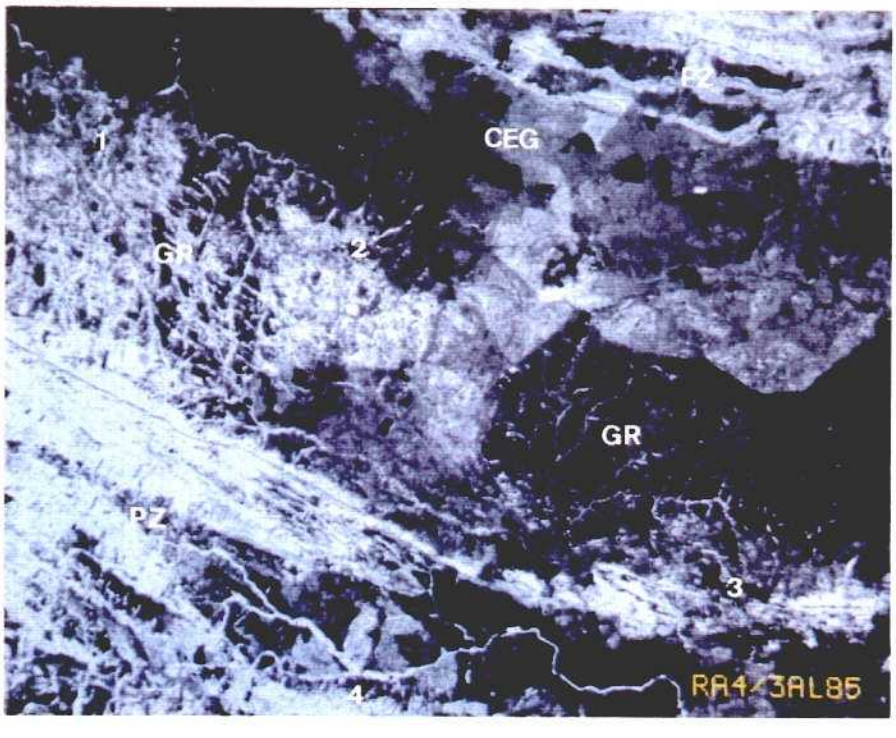

FIG.8.4 - TM 4/3 (B/W) OF THE ALBURQUERQUE-LA CODOSERA AREA. SYMBOLS AS IN FIG.8.2.

FIG.8.5 - PRINCIPAL COMPONENT COMPOSITE PC423 (BRG) OF THE ALBURQUERQUE-LA CODOSERA AREA. SYMBOLS AS IN FIG.8.2.

Soil derived from the CEG rocks has a finer texture and is more silty. This soil contains a considerably amount of quartz and feldspar, the plagioclase being more abundant than the K- feldspar, but with a much higher content of clay size minerals like illite/muscovite and chlorite/vermiculite.

Soils and rocks samples were taken along cross sections within the CEG from the contact with the granite near San Vicente de Alcantara, to the contact with the Ordovician Quartzite of the Aliseda Syncline (Fig. 8.1). Samples of soils were collected, in tilled fields, identified in the Landsat TM 745 colour composite image and in the TM4/3 ratio image.

The mineralogy of soils was determined by visually identifying X-Ray diffraction peaks for both <2 μm and >2 μm size fractions of the samples (Table 8.1). Illite, muscovite, chlorite, vermiculite and kaolinite are the minerals present in the clay-size fraction. Illite and muscovite represent approximately 20% of the minerals in the soils derived from hornfels and spotted slates and constitute a slightly lower proportion (16%) of the soil derived from the regional slates. Chlorite and vermiculite very scarcely appear in soils derived from hornfels, forming approximately 8% of spotted slate and regional slate derived soils. Kaolinite appear exclusively in the hornfels and spotted slate derived soils.

Petrographic studies of the underlying rocks have also been carried out in order to determine the grade of contact metamorphism. Two zones have been distinguished within the contact aureole based on mineral assemblages. The sequence in order of increasing metamorphism is: unaltered slates ---> spotted slate zone ---> hornfels zone. The spotted slate zone is characterised by the presence of small porphyroblast of chloritized biotite in the matrix, the cleavage being still present. In some of the samples the biotites are so small that cannot be recognised in the hand-specimen. In the hornfels zone, the porphyroblasts are identified as andalusite and cordierite. The grain size is coarser, and in the inner hornfels zone the rocks become massive although the cleavage can still be recognised.

8.6 - SPECTRAL REFLECTANCE STUDIES.

Spectral reflectance measurements of soils and rocks were carried out in the laboratory, using a Perkin-Elmer Lambda 9 spectrophotometer, with an integrating sphere and a Barium sulphate standard. Readings were made at 0.5 nm intervals from 400 to 900 nm and at 2 nm intervals from 900 to 2300 nm.

Laboratory reflectance spectra for soils derived from hornfels, spotted slates and regional slates are shown in Fig. 8.6.A. Laboratory spectra for pure muscovite, illite, vermiculite, chlorite and kaolinite are show in Fig. 8.6.B. The spectra have been interpreted according to their absorption features and mean reflectance to 1.6 μm. Three different groups have been differentiated:

		BULK MINERALOGY			CLAY MINERALOGY			
Sample	Type of bedrock	Quartz %	K felspar %	Plagioclase %	Illite/ muscovite %	kaolinite %	Vermiculite chlorite %	Dolomite %
701-3	C	62	-	15	22	traces	traces	-
702-1	C	73	-	13	8	6	traces	-
702-2	C	51	-	15	26	8	-	-
702-52	C	61	17	7	15	traces	traces	-
702-53	C	63	-	10	22	-	5	-
702-54	C	53	19	6	12	6	4	-
702-55	C	62	-	11	27	traces	-	-
702-56	C	70	-	9	17	4	-	-
701-4	PM	62	-	12	15	-	11	-
702-3	PM	58	-	11	23	8	-	-
702-4	PM	61	-	17	13	-	9	-
702-6	PM	60	-	14	15	-	9	-
702-17	PM	60	-	11	28	-	11	-
702-50	PM	70	-	11	14 (K) trac.	-	5	-
702-61	PM	62	-	10	17	-	11	-
702-5	P	62	-	10	18	-	10	-
702-10	P	71	-	8	14	-	7	-
702-11	P	69	3	11	12	-	5	-
702-13	P	58	-	11	20	-	11	-
702-36	P	62	2	6	23	-	7	-
702-40	P	68	-	9	18	-	5	-
702-49	P	62	-	19	11	-	8	-
727-21	GR	46	25	24	5	-	-	-
727-29	GR	42	31	16	8	3	-	-
727-30	GR	70	12	8	6	-	4	-
702-21A	GR	69	17	6	5	3	-	-
702-21B	GR	61	25	4	5	5	-	-
726-22	CR	30	-	-	28	20	traces V	22
726-23	CR	11	-	2	5	traces	-	82
727-51	QP	60	5	6	20	9	-	-
727-20	Q	73	6	3	9	6	3	-
726-5	Q	77	2	6	8	7	-	-

TABLE 8.1 - SEMICUANTITATIVE MINERALOGICAL ANALYSIS BY XRD FOR SOILS SAMPLES LOCATED IN FIG.8.1 AND FIG.8.6. C: HORNFELS SOIL; PM: SPOTTED SLATE SOIL; P: REGIONAL SLATE SOIL; GR: GRANITE SOIL; CR: CARBONATE SOIL; Q: QUARTZITE SOIL.

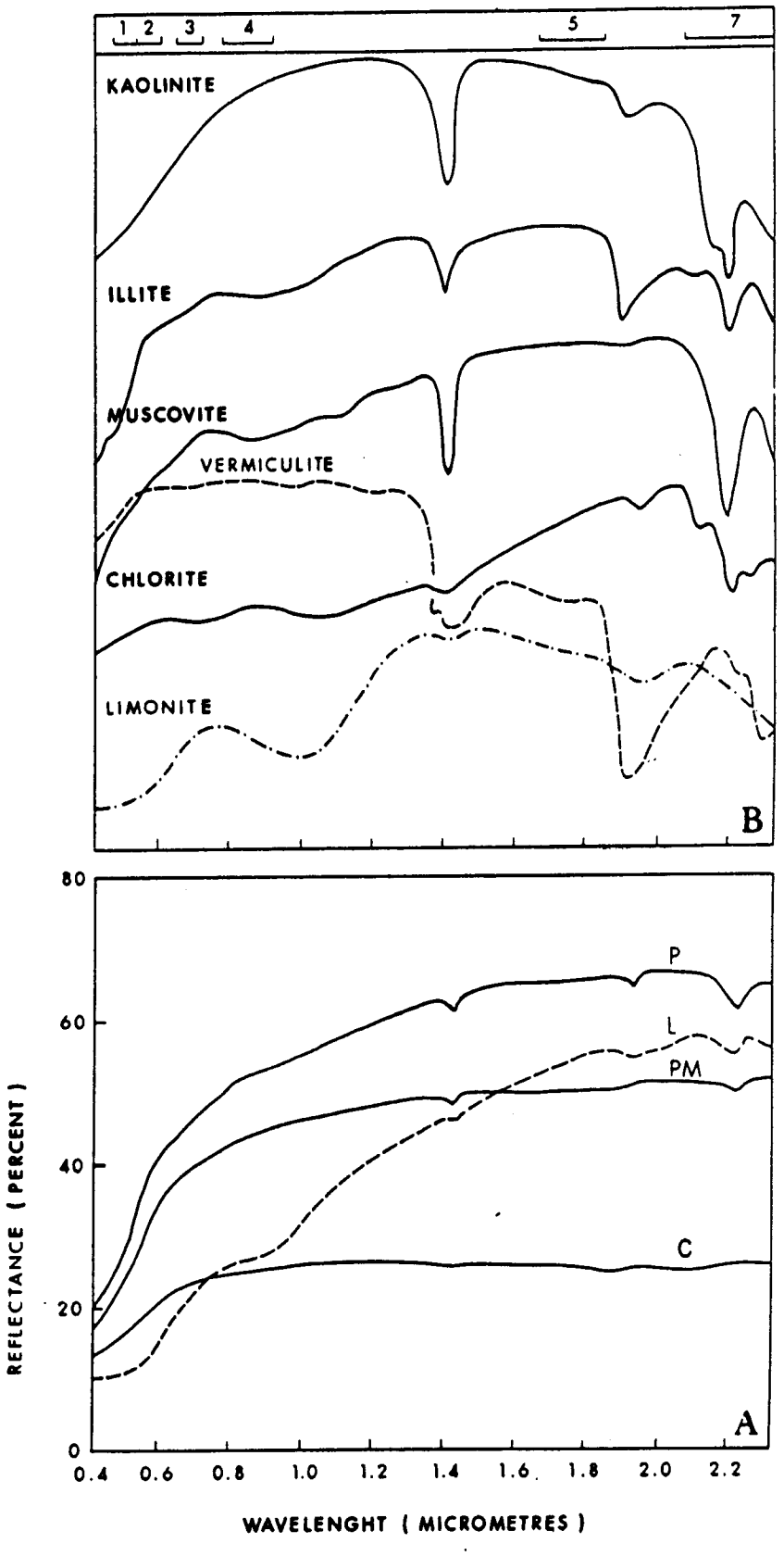

FIG. 8.6A- AVERAGE LABORATORY REFLECTANCE SPECTRA FOR SLATE SOIL, SPOTTED SLATE SOIL (PM), HORNFELS SOIL (C) AND LIMONITIC SOIL (L) LOCATED IN FIG. 8.1 AND FIG. 8.7 AND LISTED IN TABLE 8.1.

B- LABORATORY REFLECTANCE SPECTRA FOR PURE MINERALS PRESENT IN THE SOILS (TABLE 8.1). SPECTRA ARE OFFSET FOR CLARITY.

- The regional slate spectra (P) exhibit a moderately intense absorption feature at 2.20 μm that can be due to Al-OH absorption in muscovite and illite (Hunt & Salisbury, 1976). The absorption peak near 1.4 μm is related to OH^- absorption in these minerals. The absorption at 1.9 μm is produced by molecular water present in illite and vermiculite. The overall reflectance varies between 50-60 percent at 1.6 m, falling sharply to 20 percent in the visible wavelengths.

- The spotted slate soil spectrum (PM) shows similar absorption features than do the spectra of slate soil, although less intense, specially the feature at 2.20 m. The overall reflectance is lower: 40 percent at 1.6 m and also decreasing in the visible wavelengths.

- The hornfels soil spectrum (C) shows much less intense absorption features and the reflectance is 20 percent in the near infrared wavelengths, falling not so abruptly from 0.8 to 0.4 μm. As in previous spectral studies carried out near Caceres (Rowan et al., 1987.), these spectral differences do not seem to be caused by a different mineralogy in the three groups of soils. The main mineralogical difference is that the hornfels soil has kaolinite and the presence of chlorite/ vermiculite is very scarce. However, the typical absorption band related to kaolinite at 2.20μm is not shown in the spectra of the hornfels soil.

Recent studies have demonstrated the relationship between VNIR reflectance and the thermal alteration of the organic matter due to differential heating of carbonaceous pelitic rocks (Rowan et al., in press). In this study, it is not possible to corroborate this as vitrinite reflectance measurements have not been properly performed.

8.7 - DIGITAL CLASSIFICATION.

A digital classification method using a Bayesian maximum likelihood classifier was performed on the six non-thermal TM bands to more objectively separate soils exhibiting different spectral responses.

Training areas within the San Vicente-Valencia de Alcantara sector were selected, using a colour composite TM745 subscene (Fig. 8.7). The previous information gathered from the field and the petrographical studies performed on the collected samples, assured a good knowledge of the bedrock geology. An unsupervised classification of this image window was carried out with the establishment of the class statistics.

The examination of eighteen classes obtained using a maximum likelihood classifier allowed to select three soil classes corresponding to bare soils. The supervised assignation of classes corresponding to bare soils was performed by comparison of the resulting classes to geologically well know test-areas.

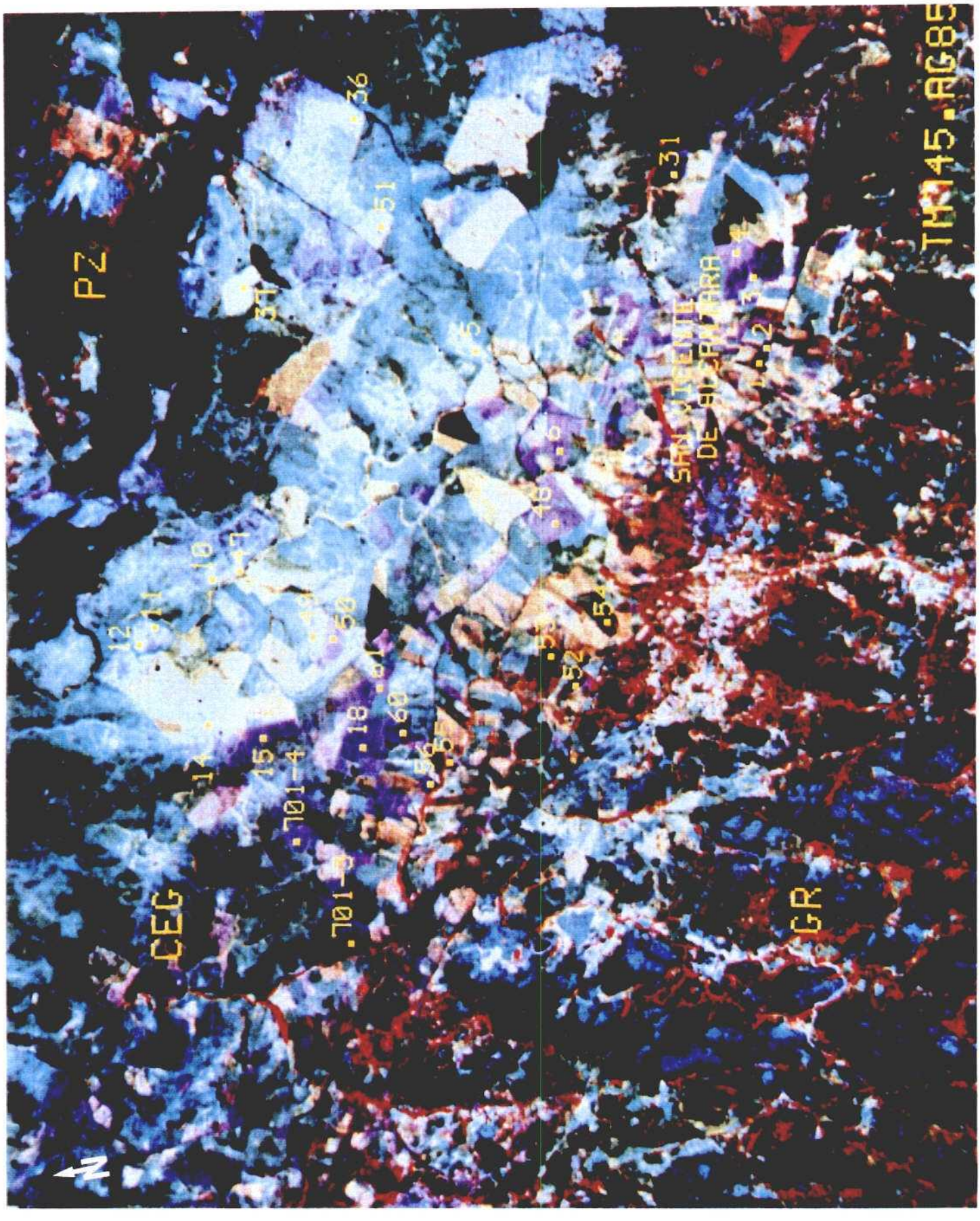

FIG. 8.7 - FALSE COLOR COMPOSITE TM 745 (BRG) OF THE SAN VICENTE DE ALCANTARA AREA WITH LOCATION OF SAMPLES. SYMBOLS: CEG: SCHIST-GRAYWACKEE COMPLEX; PZ: PALAEOZOIC; GR: ALBUQUERQUE GRANITE.

Class centres determined by the classification are given in Table 8.2. Fig. 8.8 shows the classified image where only the classes representing bare soils are colour code. The red colour corresponds to bare soils developed on hornfels which are located along a narrow band close to the granite contact that wides out towards the northwest. The orange colour is ascribed to soil derived from spotted slate and lies beyond the hornfels soil. The yellow colour corresponds to soil derived from the regional slate which situates in more external areas.

The mean digital numbers and ± 1 standard deviation values of the six visible and near-infrared TM channels for these three soil classes (Fig. 8.9), show a good correspondance with the laboratory reflectance spectra (Fig. 8.6.A). The main differences in the visible wavelengths is due to the influences of the solar spectrum and atmospheric absortion and scattering in the uncalibrated TM channels. The TM spectra show that the digital number difference is larger in channel 5.

Finally, a similar classification was performed for the whole study area, merging the hornfels soil class and the spotted slate soil class to obtain a unique "contact metamorphic soil" class. The Landsat TM imagery and the classification have been geo-referenced into an UTM grid in order to superimpose these data to other data sets (Chapter 9). A mask has been applied to the classified image in order to only use the "contact metamorphic class", which has been displayed in red, over the TM5 (B/W) channel where the classified areas are more easily identified (Fig. 8.10). The green colour corresponds to a bare soil class which represents high iron-bearing soils- "limonitic soil class" -mainly developed on iron-rich Devonian quartzites, sandstones and carbonates. The average laboratory reflectance spectrum of these soils (L in Fig. 8.6.A) exhibits a broad absorption band centred at about 0.87μm and a sharp fall-off in reflectance short of 0.7 μm which are attributed to the ferric iron present in limonite (Hunt et al., 1971). The absorption feature at 2.20 μm can be related to Al-OH absorption in muscovite and illite. The mean TM digital numbers (DN) for the limonitic soil class (L in Fig. 8.9) show relatively low values in TM2, TM3 and TM4, related to the absorptions produced by the iron oxides in these wavelengths.

8.8 - INTERPRETATION.

The classified contact soil (Fig. 8.10) which appear north of the Alburquerque granite outline well the northern contact aureole within the CEG materials. However, this class extends out in the northwestern sector, north of Valencia de Alcantara, beyond the contact of the thermal aureole as it appears in the existing geological map. Thin section studies of the underlying rocks have shown that the contact aureole effectively widens out, probably suggesting a more shallow dipping contact of the granite in this sector. The inner zone of the contact aureole close to the granite is only partially shown by the contact soil class, as the most massive hornfels are only partially used for cereals crops and present a more dense natural oak an fruit tree cover. Hence, only a few areas present bare soil exposures which are susceptible of been digitally classified.

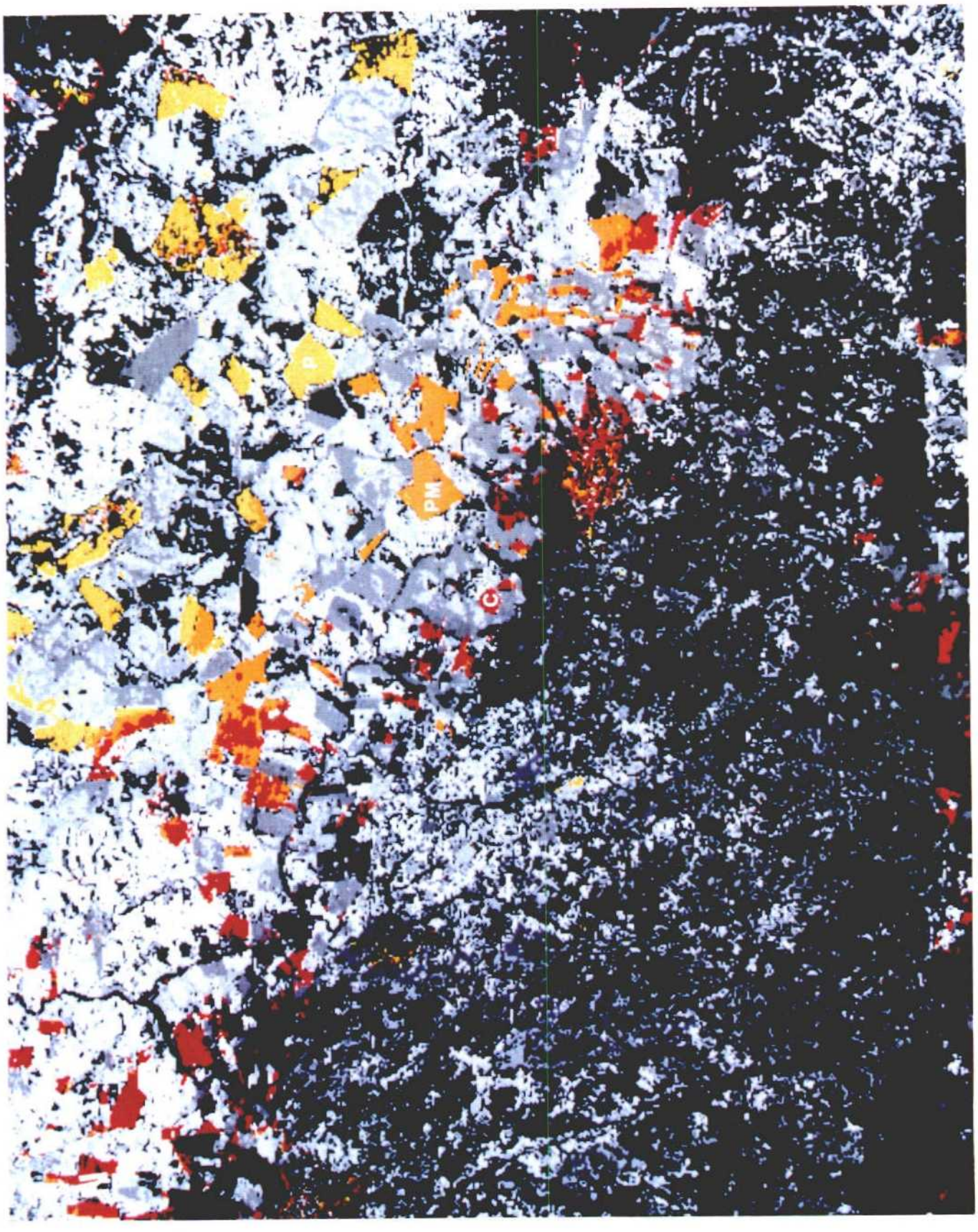

FIG. 8.8 - BAYESIAN CLASSIFICATION OF THE SIX VNIR TM BANDS OF THE SAN VICENTE DE ALCANTARA AREA. RED (C): CLASSIFIED AREAS UNDERLAIN BY HORNFELS; ORANGE (PM): CLASSIFIED AREAS UNDERLAIN BY SPOTTED SLATE; YELLOW (P): CLASSIFIED AREAS UNDERLAIN BY REGIONAL SLATE.

CLASS		TM1	TM2	TM3	TM4	TM5	TM7	PTS
HORNFEL SOIL	MEAN	110.09	58.46	75.46	70.20	120.01	70.25	2.700
	STD.DEV.	5.42	3.00	5.06	6.76	7.56	5.06	
SPOTTED SLATE SOIL	MEAN	120.56	67.56	86.06	76.66	167.26	62.46	2.176
	STD.DEV.	6.56	4.06	4.76	6.64	7.16	4.76	
REGIONAL SLATE SOIL	MEAN	126.16	66.26	80.62	66.66	166.60	100.07	11.256
	STD.DEV.	6.62	4.61	5.62	4.06	12.26	7.66	
LIMONITIC SOIL	MEAN	86.07	41.66	56.12	62.66	121.16	76.66	1.666
	STD.DEV.	2.66	1.40	2.07	2.17	4.46	3.66	

TABLE 8.2 - STATISTICS FOR BARE SOIL CLASSES USING A MAXIMUM LIKELIHOOD CLASSIFIER ON THE SIX VNIR TM BANDS.

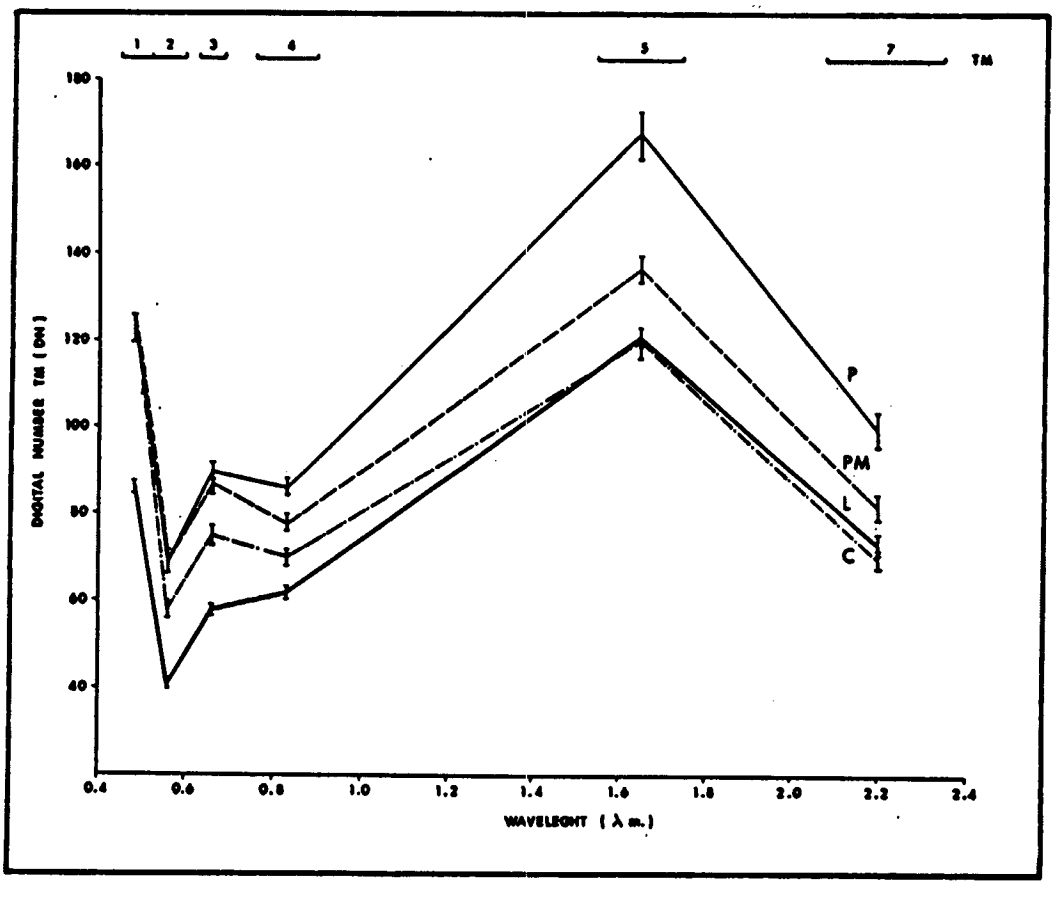

FIG.8.9 - MEAN DIGITAL NUMBERS AND ± 1 STANDARD DEVIATION IN SIX TM BANDS FOR FOUR BARE SOIL CLASSES. P: REGIONAL SLATE SOIL; PM: SPOTTED SLATE SOIL; C: HORNFELS SOIL; L: LIMONITIC SOIL.

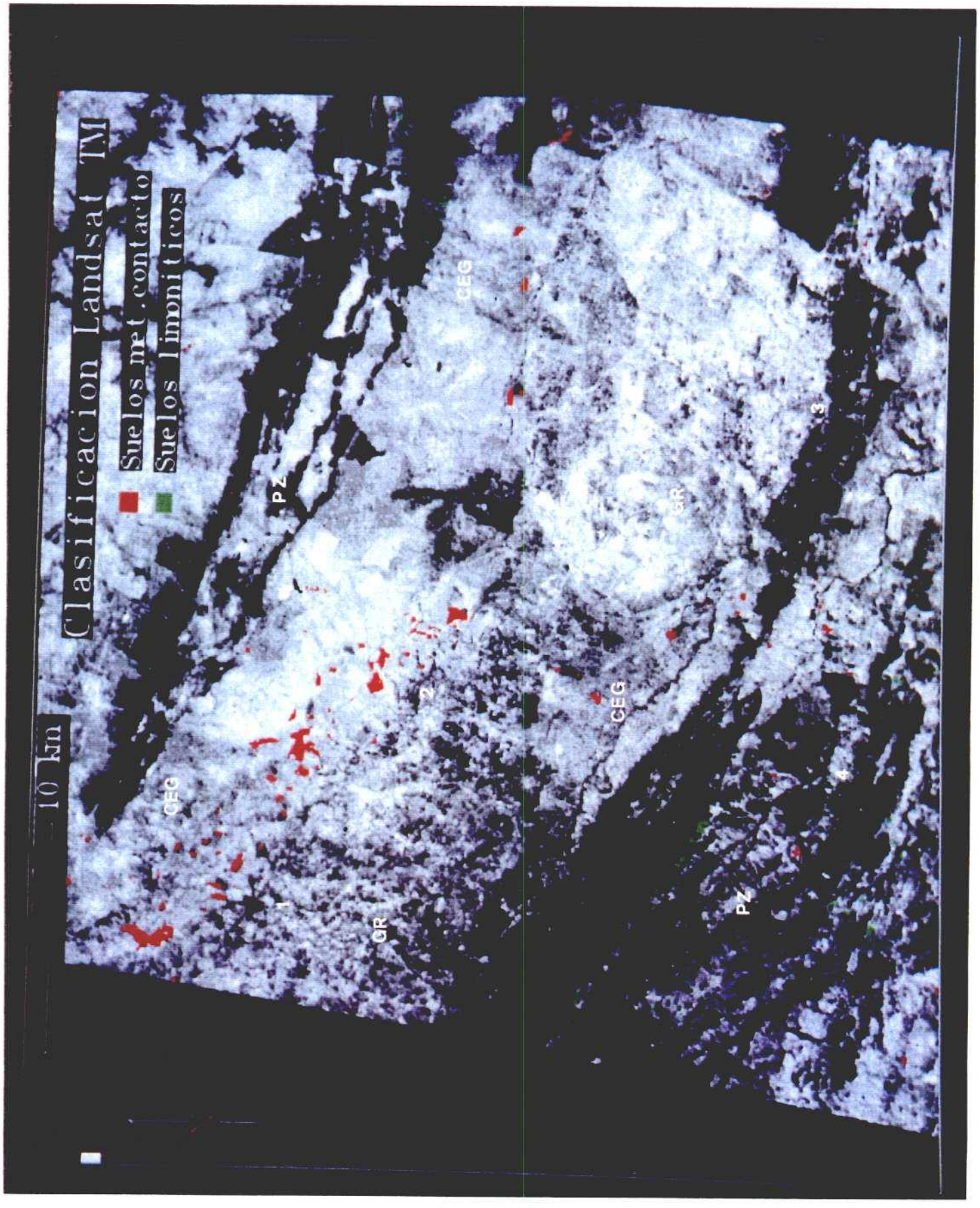

FIG. 8.10 - GEORREFERENCED TM5 (B/W) WITH OVERLAYED CONTACT SOIL AND LIMONITIC SOIL CLASSES OF THE ALBURQUERQUE-LA CODOSERA AREA. SYMBOLS AS IN FIG.8.2.

The contact aureole south of the granite is very much masked by the vegetation cover and few fields are classified as contact metamorphic soil. However, an area, located within the black slates of the Lower Devonian west of La Codosera, and 12 Kms south from the granite contact, close to the Perla de Anibal gold prospect, classifies as "contact metamorphic" soil. Thin section of the bedrock show the presence of pseudomorphed and sericitized cordierite porphyroblasts cross-cutting the crenulation cleavage (S2) which points out that the rocks have been affected by contact metamorphism although it is difficult to asses this effect due to the widespread hydrothermal alteration (mainly sericitization).

The coincidence of high-medium $K_{(e)}$ aeroradiometric values and a negative gravity anomaly in this area (Chapters 7 and 9) points out to the possible existence of an intrusive body in depth.

Bare soil classified as limonitic soil mainly locate in two areas. In the area of La Portilla de los Bastos, southwest of La Codosera, they correspond to iron-rich soils developed on lower Devonian iron quartzites and sandstones to which important Au geochemical anomalies associate (see Chap. 3). The other area is located in La Calera, where the limonitic soil derives from middle Devonian iron-rich carbonates. Not known Au anomalies appear in this sector, which potentially could be investigated.

CHAPTER - 9 - INTEGRATION OF DATA USING A GEOGRAPHIC INFORMATION SYSTEM.

F. Pérez Cerdán; P. García de Santiago ; C. Antón-Pacheco & J.C. Gumiel.

9.1 - GIS DATA BASE.

The existing geologic and aeroradiometric data as well as the information generated by ITGE within this project as gravity and Landsat TM classification were analyzed using the GRASS geographic information system (GIS) software, which is interfaced with the digital image processing system, ELAS, available at ITGE.

Four main types of information have been used to generate the GIS data base.

- **Geology**. Four 1:50000 geological maps (701, 702, 729, 730), which cover the study area, have been digitized independently and then merged to obtain the geologic digital data base. Two main types of maps can by derived from this information: vector-type maps of such features as geological contacts and faults, and raster-type maps of lithology and synthetical geological maps.

- **Aeroradiometric data**. Original raw data in magnetic tape were obtained from a broader aeromagnetic and aeroradiometric survey carried out for ENUSA. Data was taken along N33° E flight lines, with a 1 km separation between lines and 50 m interval between sample points. Duplicities in the original data were eliminated and then xyz files were generated. An interpolation method of adjusting by distance-weighting was used to define a 500 x 500 m grid from which contour lines were obtained.

- **Gravity data**. The interpolated Bouguer gravity information obtained by ITGE (Chapter 7) within the framework of this project were used as another map layer within the GIS.

- **Landsat TM data**. Georeferenced linear-stretched individual TM bands and digital classifications (Chapter 8) were transferred into the GIS.

9.2 - ANALYSIS AND INTERPRETATION

Different types of derived maps have been generated from the GIS data base.

A synthetical geologic map was created reclassifying the different lithological units existing on the original geological map (Fig. 9.1). This synthetical geological map forms the base map to which other data sets have been referenced and interpreted.

FIG. 9.1 - SYNTHETICAL GEOLOGICAL MAP OF THE ALBURQUERQUE-LA CODOSERA AREA.

Aeroradiometric anomaly maps were derived from original radiometric values of $U_{(e)}$, $Th_{(e)}$ and $K_{(e)}$. Anomalous areas were defined where $U_{(e)}$ exceeds 4000 ppb, $Th_{(e)}$ exceeds 12000 ppb, and $K_{(e)}$ exceeds 0.175 %. The geological interpretation has been carried out according to the spatial coincidences of the different data sets.

The aeroradiometric $U_{(e)}$ values (Fig. 9.2) shows a good correlation with the Alburquerque batholith which is very well delineated by the high and medium $U_{(e)}$ values. The metasedimentary rocks show a wider range of radiation values, therefore there is not any lithostratigraphic control on the distribution of uranium within the country rocks. Only in the western area of the Central Ridge and in the core of the La Codosera Syncline is there a minor E-W trending anomaly made up by moderate $U_{(e)}$ values.

There is a very good correlation between $K_{(e)}$ radiometric values and the outcrop of the Alburquerque granite (Fig. 9.3). The $K_{(e)}$ radiation shows high values for the granite, with the highest values in the southeastern sector of the pluton. The CEG rocks have moderate $K_{(e)}$ values, whilst the Lower Palaeozoics correspond to the lowest $K_{(e)}$ values. The Devonian rocks show medium values along the axis of the La Codosera Syncline, which appear to increase towards the west, at Sierra de la Calera. Moderately high $K_{(e)}$ values appear in the northwestern margin of the granite, where the contact aureole widens out to the north in the CEG, suggesting a more shallow dipping contact of the Alburquerque granite in this area.

The $Th_{(e)}$ radiation (Fig. 9.4) shows high values related to the Lower Ordovician units outcropping along the northern limb of the La Codosera Syncline. A maximum is located in the western part of the Central Ridge. The granite and the CEG are associated with low $Th_{(e)}$ values, whilst the Silurian and Lower Devonian sediments show moderate values.

Fig. 9.5 shows a Landsat image, TM5, which has been georeferenced into an UTM grid in order to merge the multispectral classification data to the previous data sets. The red colour represents bare soils derived from hornfels and spotted slates ("contact metamorphic class") which define a variable width band within the CEG along the granite contacts. This band fits well with the contact metamorphic aureole produced by the granite, although it widens out in the northwestern sector of the northern aureole. Other areas located south of the granite, particularly west of La Codosera, show classified contact soils. Medium to high aeroradiometric anomalies have been overlaid on the image: high radiometric $U_{(e)}$ values contour lines (yellow), medium to high $K_{(e)}$ radiation (green) and high $Th_{(e)}$ values (orange).

Fig. 9.6 is the Bouguer gravity anomaly map generated by the gravity survey carried out in this project. This map does not cover the same area as the previous maps, being limited to the north by the parallel of San Vicente de Alcantara, but the southern part covers the whole area with the inclusion of the extension of the gravity survey towards the west of La Codosera.

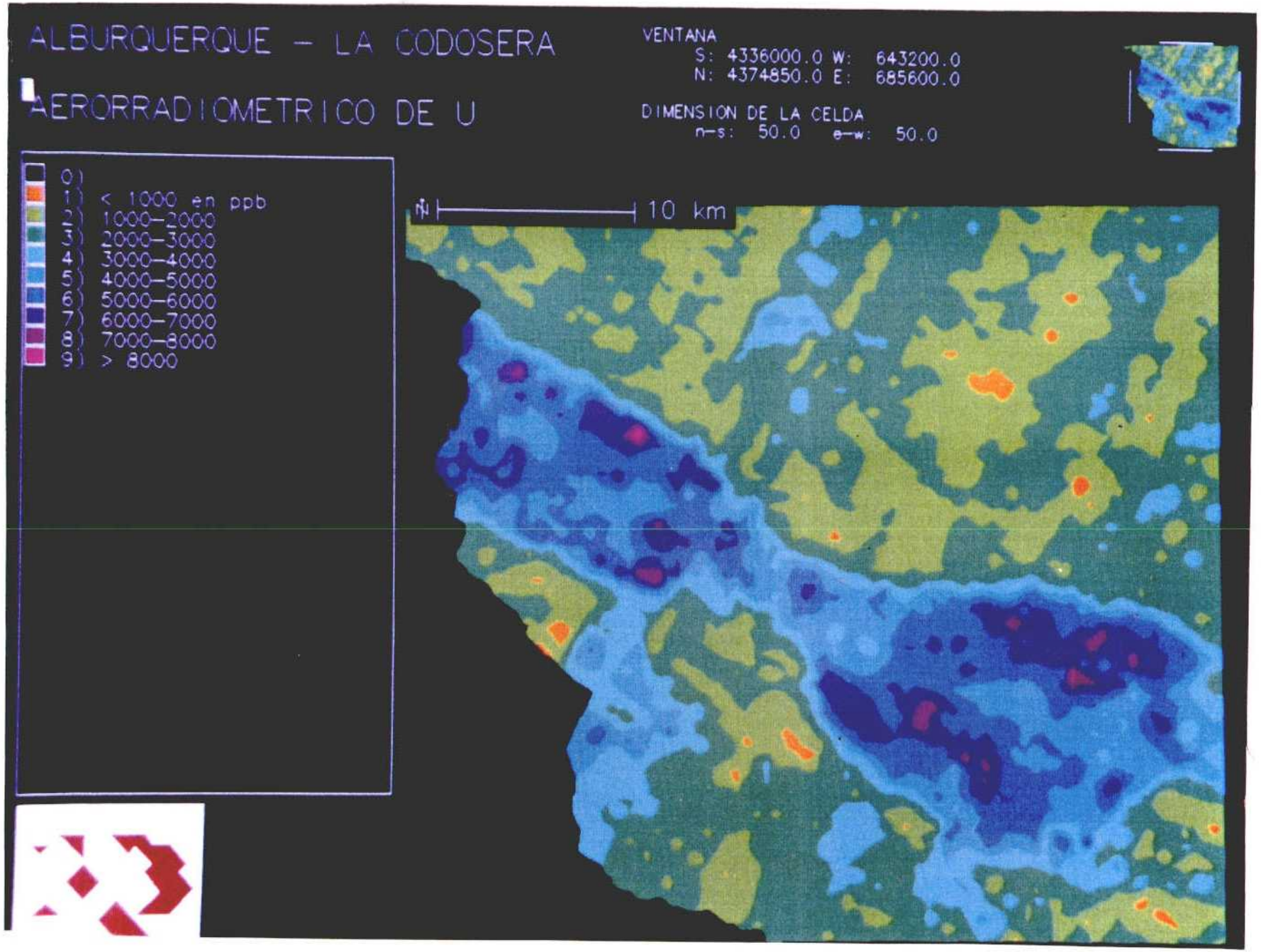

FIG. 9.2 - AERORADIOMETRIC U_e VALUES MAP.

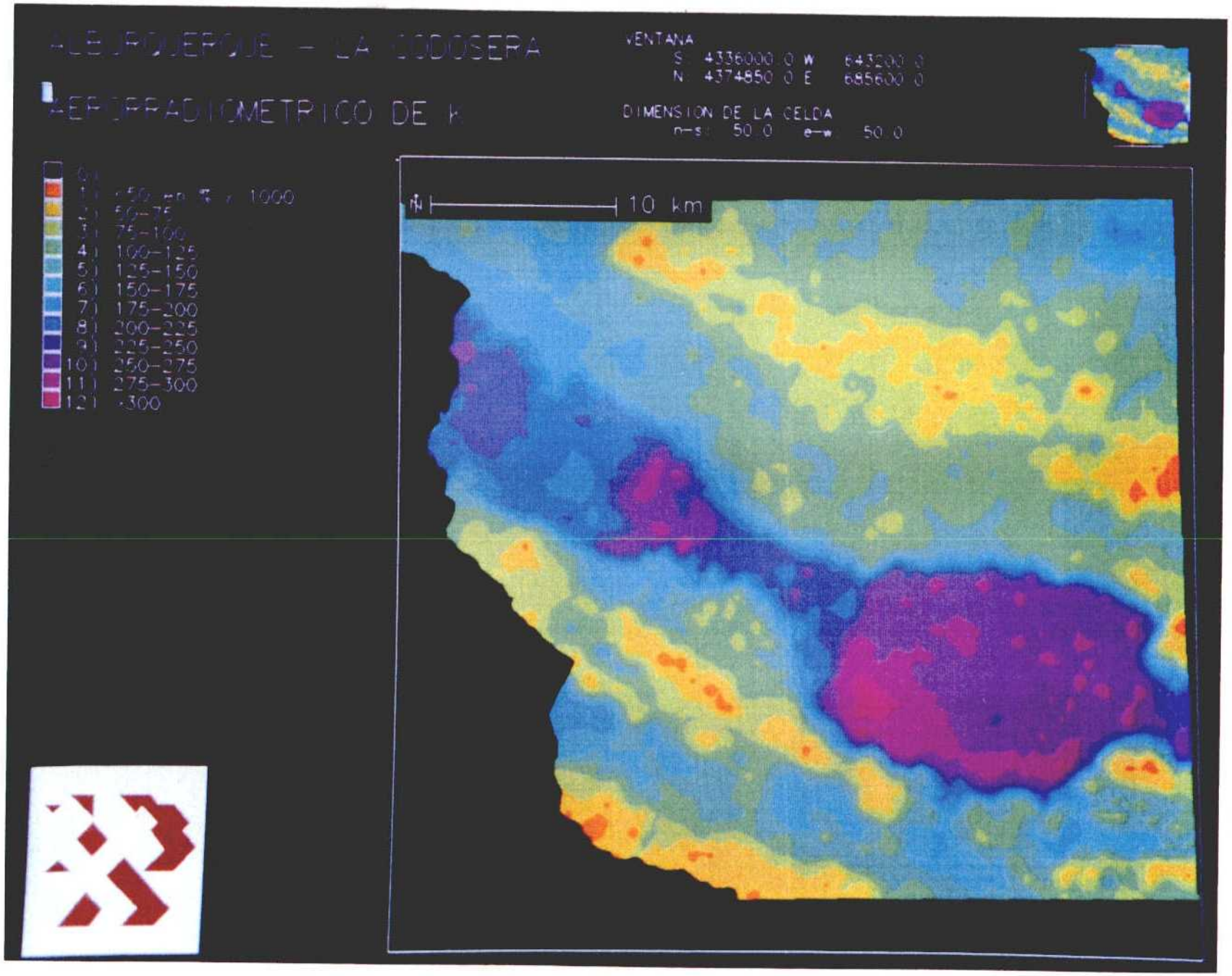

FIG. 9.3 - AERORADIOMETRIC K_e VALUES MAP.

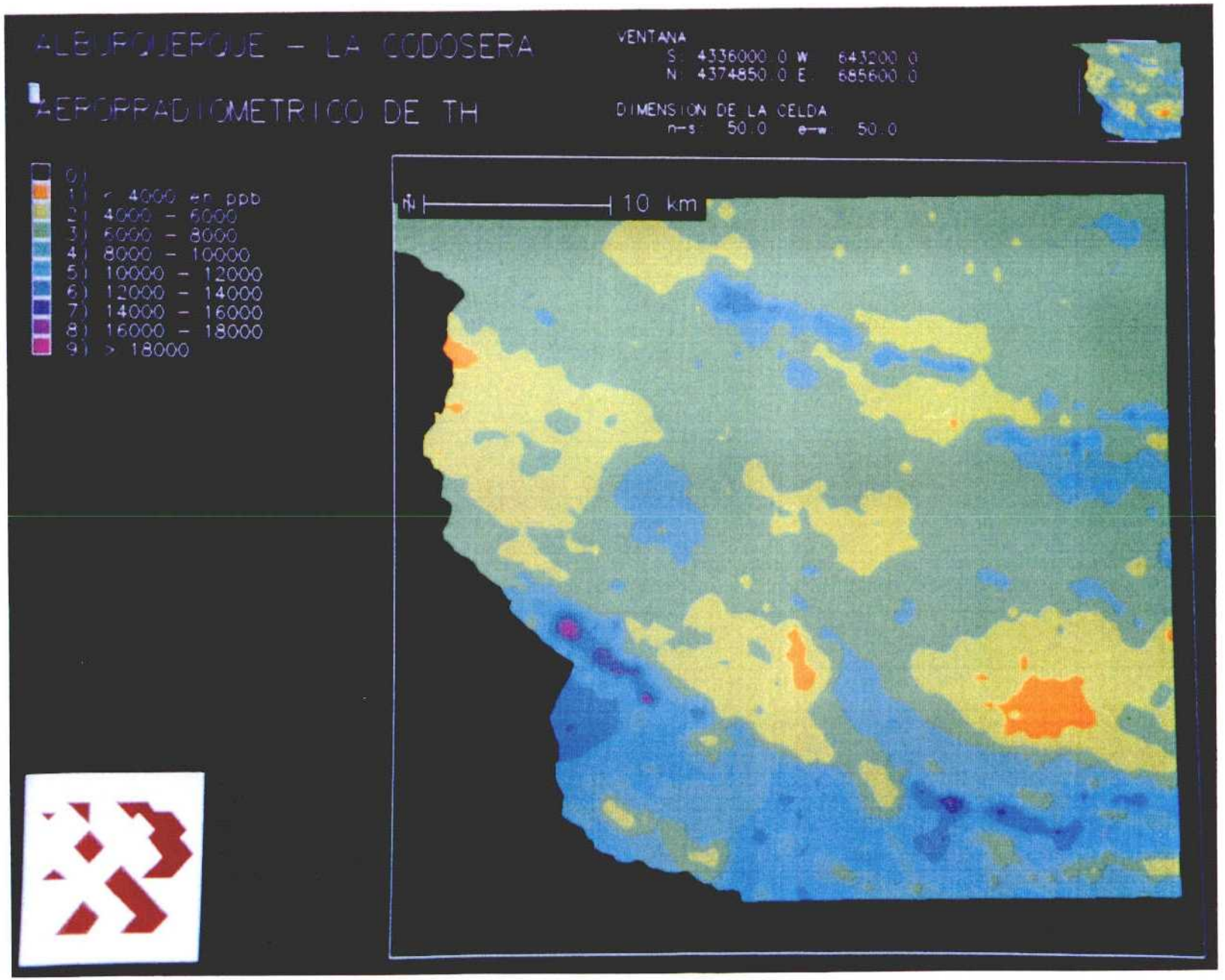

FIG. 9.4 - AERORADIOMETRIC Th_e VALUES MAP.

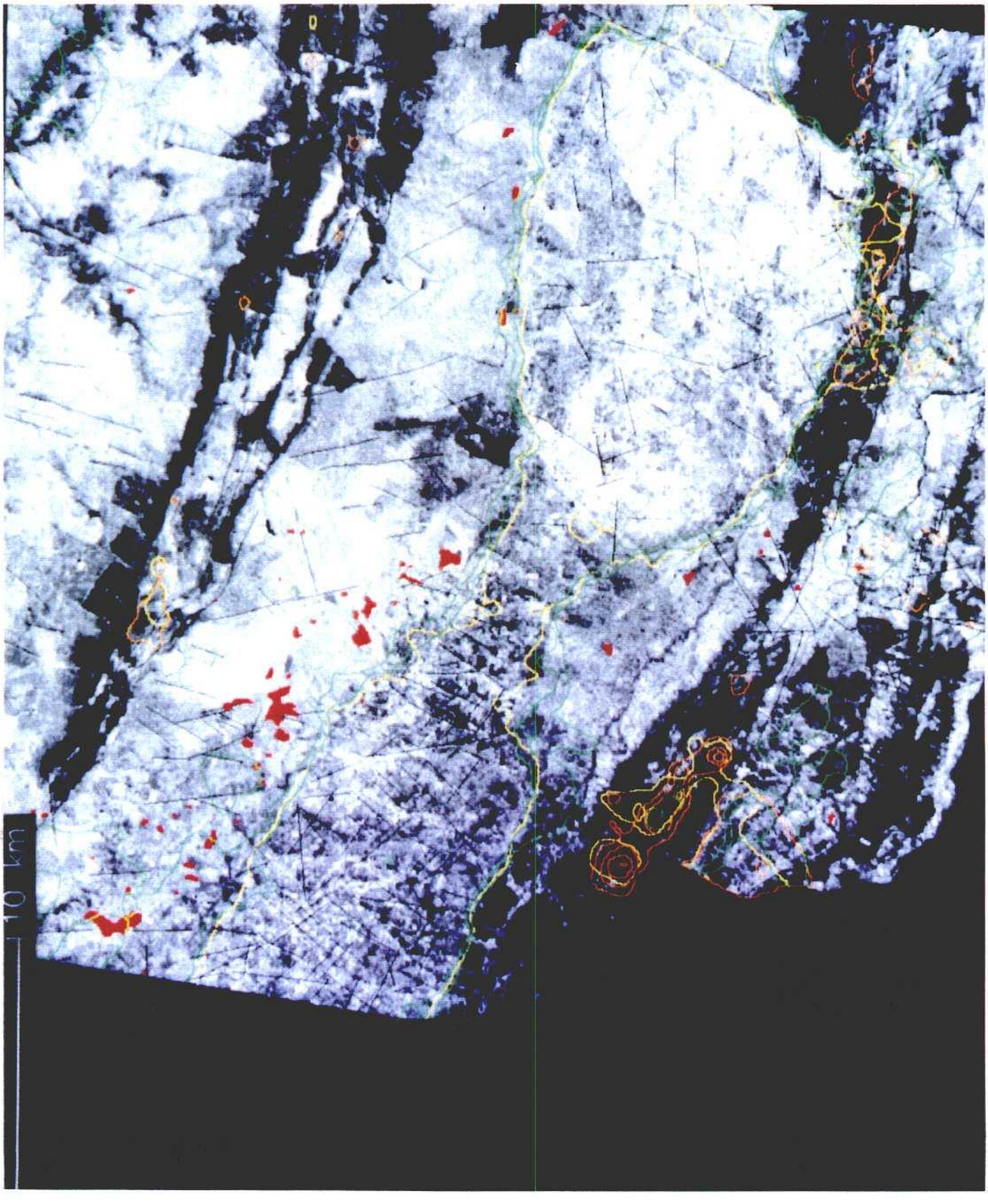

FIG. 9.5 - INTEGRATED ANOMALIES IN LANDSAT TM-5.

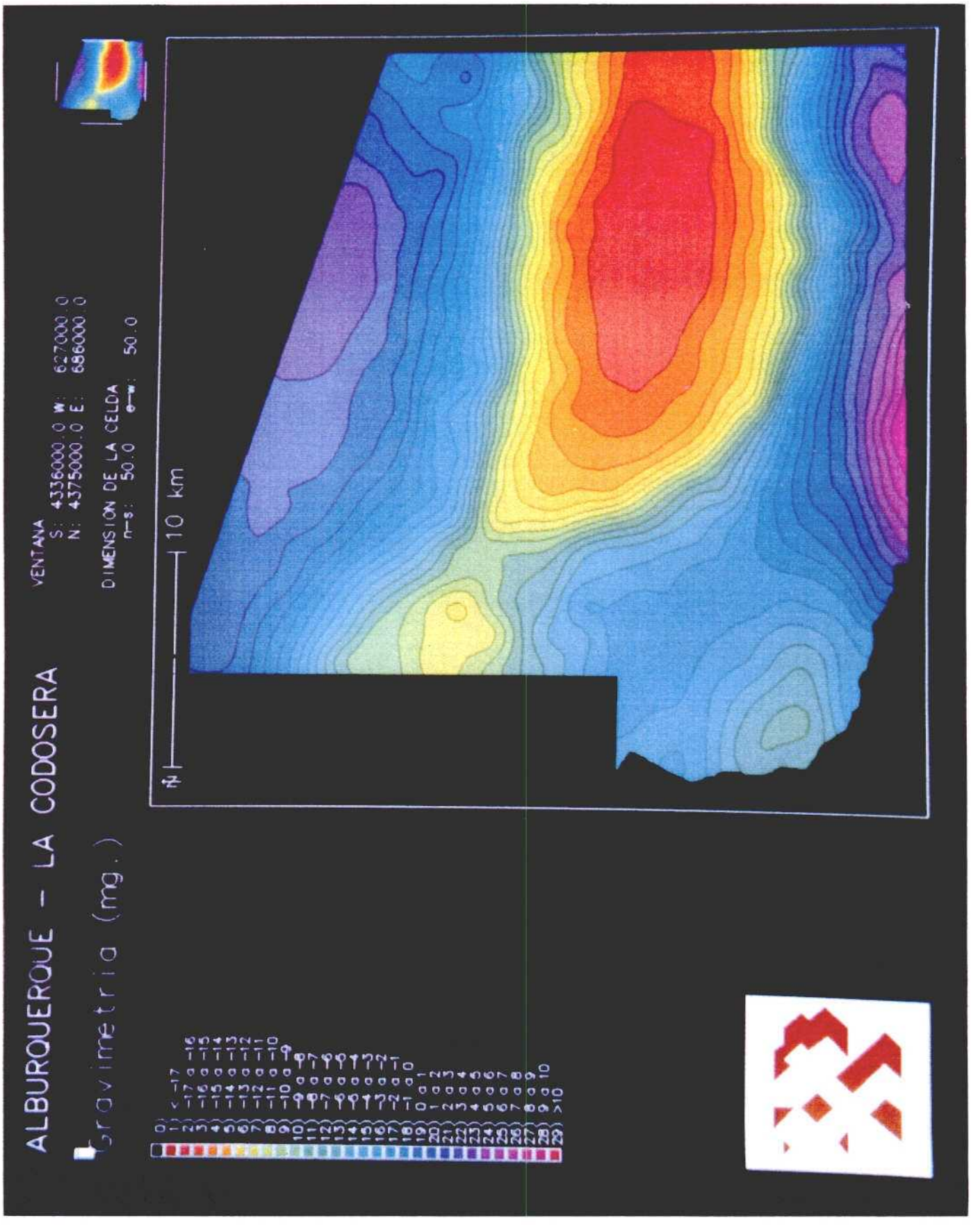

FIG. 9.6 - BOUGUER ANOMALY MAP.

The morphology of the Alburquerque Batholith is well expressed by the prominent negative anomaly. Positive anomalies occur over the Palaeozoic sequences towards north and south of the Alburquerque Batholith. The differences between the gradients of the anomalies generated by the granite can be interpreted as different dips of the contacts of this intrusive body which confirm an asymmetrical shape which is also observed towards east. The extension of the gravity survey shows a prominent gravity minimum located west of La Codosera.

9.3 - INTEGRATION OF DATA.

The previously analyzed data set have been merged in a 1:65.000 synthetical map of the whole Alburquerque-La Codosera area (see Fig. 9.7), which has been obtained from the different G.I.S data base.

Fig. 9.8 is made up by four sets of data: Fig. 9.8.1 shows the multispectral TM classification. In Fig. 9.8.2 the synthetical geological map is displayed as base map in which others data sets have been overlaid: TM contact metamorphic soil class appear in red and $K_{(e)}$ anomaly contour lines in yellow. In this figure it has been outlined the southwestern sector where a $K_{(e)}$ anomaly and a classified contact area coincide. The Fig. 9.8.3 shows the Bouguer Gravity Anomaly map. Fig. 9.8.4 presents an enlargement of La Codosera area with the integration of the former data.

Fig. 9.9 shows a smaller area to the west of La Codosera where the different data sets have been superimposed. This area was selected as it is one in which there has been much focused work in connection with gold exploration and serves to illustrate the potential of GIS in such work. Over the geological base map is displayed the medium-high values of $K_{(e)}$ radiation in blue, the TM contact metamorphic soil in red, the TM limonitic soil in green, the Bouguer gravity contours in white, the numerous gold occurrences in yellow triangles and the drill-holes carried out by ITGE in white spots. The coincidence of the negative gravity anomaly with medium-high K radiation and TM classified contact soil data suggests the existence of an intrusive body in depth. The metallogenic implications of a blind granite in this area could be of major importance to set up a new exploration target (see also Fig. 9.7).

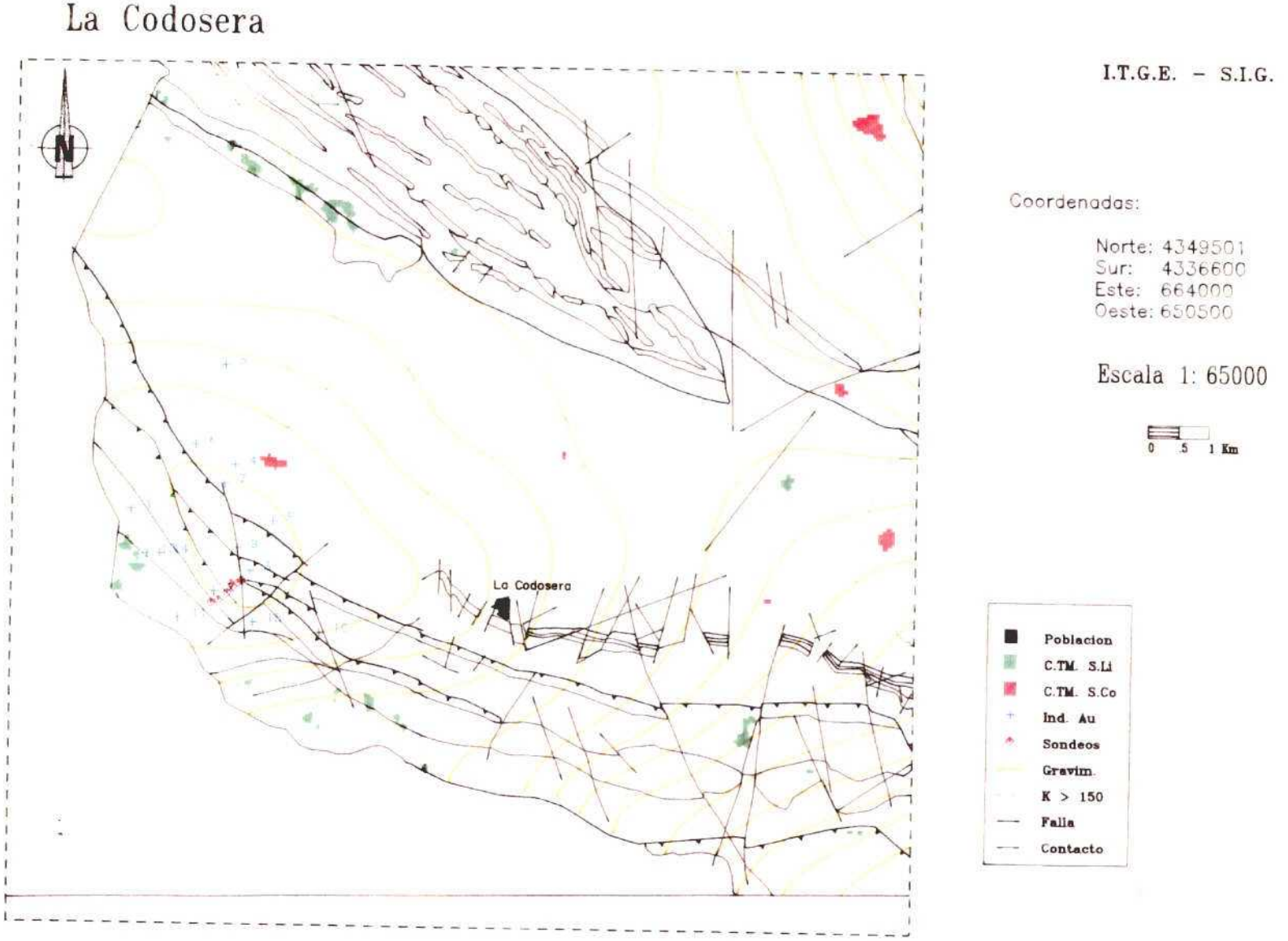

FIG. 9.7 - INTEGRATED DATA MAP OF THE LA CODOSERA AREA

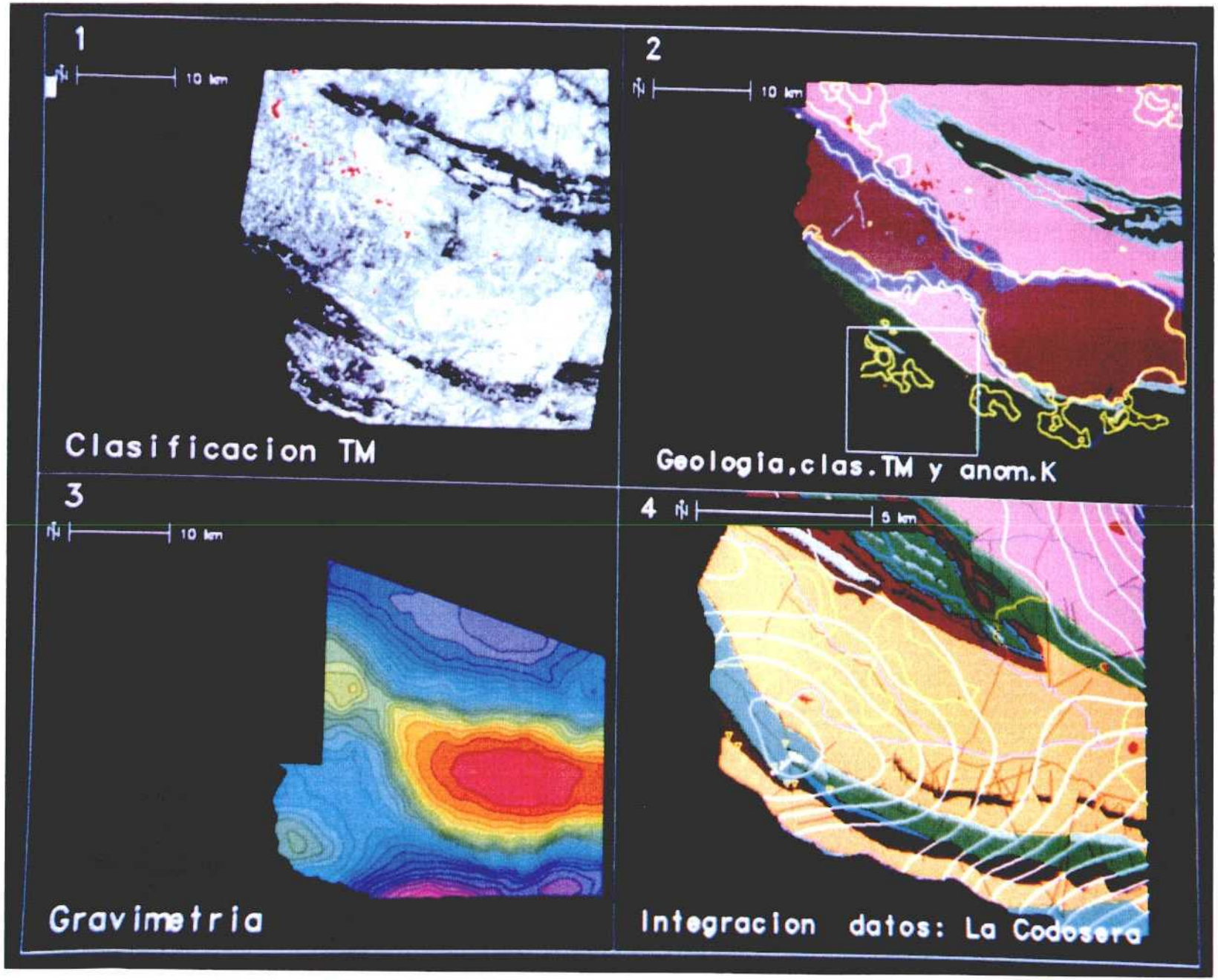

FIG. 9.8 - INTEGRATED DATA SETS OF THE STUDY AREA.

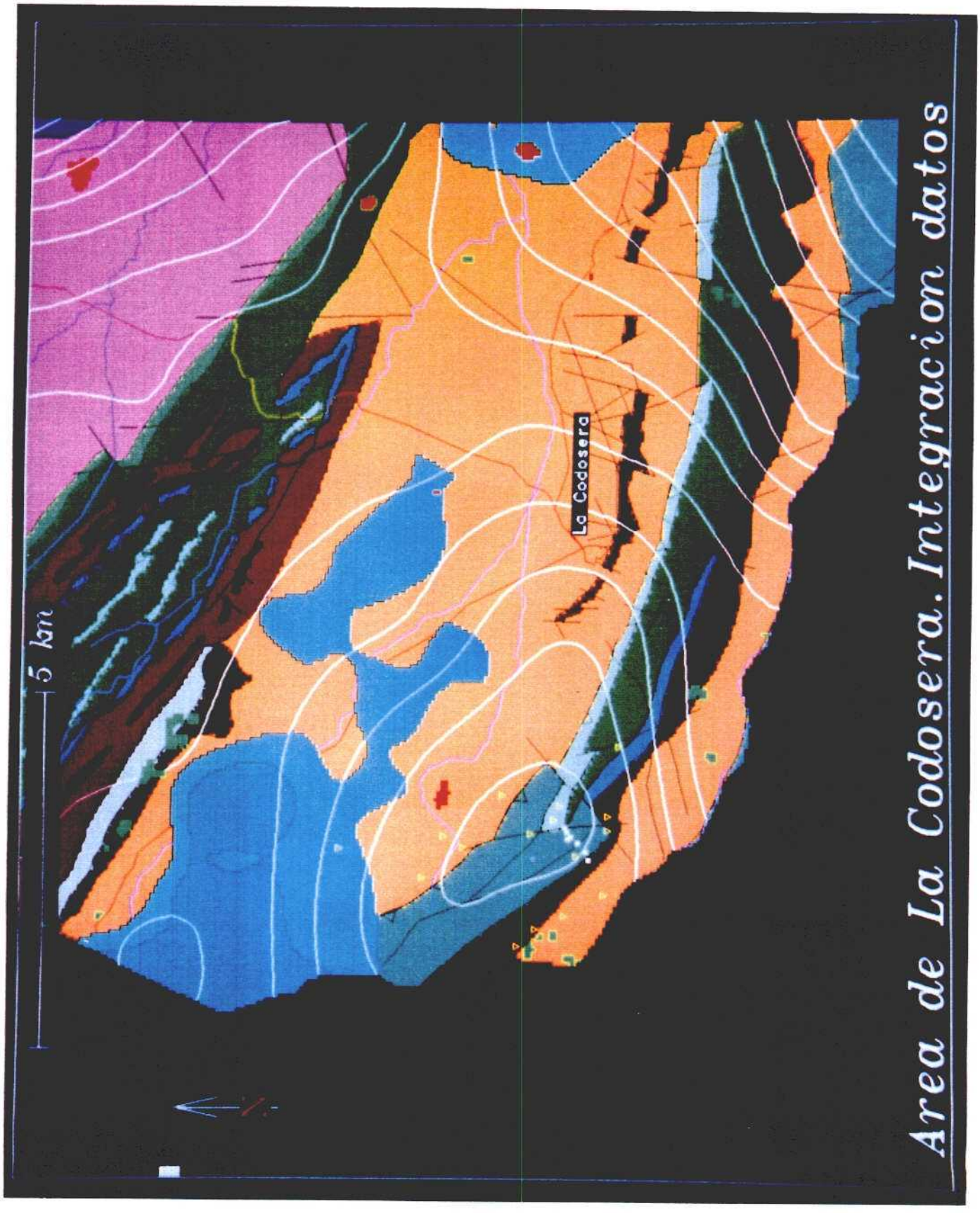

FIG. 9.9 - INTEGRATED DATA SETS OF THE LA CODOSERA AREA.

CHAPTER - 10 - LANDSAT LINEAMENTS AND STRUCTURAL CONTROL OF MINERALIZATION

D.J. Sanderson, C. Chinn, & J. Bentham.

10.1 - INTRODUCTION.

Satellite remote sensing systems, such as Landsat and Spot have provided much useful data for the mapping of tectonic structures and application to mineral exploration. The advent of multi-spectral scanners and radar systems producing digital imagery has led to an explosion of new methods of analysis.

Two main features of remote sensing systems have become widely used in geological exploration:

1) multispectral measurement of surface reflectance (see Chapter 8),

2) spatial reflectance changes produced by sub-surface structure.

In mineral exploration, the multispectral approach involves the detection of an anomalous spectral response from surface rock, soil or vegetation which can be related to an orebody. Thus it is limited to the detection of near-surface targets and has proved most successful in areas with little or no vegetation or where orebodies and the underlying geology produce significant 'alteration' of surface soils and/or vegetation.

The mapping of structures and lineaments is essentially an extension of photogeological interpretation, where surface features are related to subsurface discontinuities, whose detection requires enhancement of gradients and discontinuities in surface reflectance. Traditionally photolineament detection has utilized stereo-images derived from overlapping photographs, but Landsat and most other remote sensing systems produce limited overlap of imagery. The multispectral nature of much remotely sensed imagery and its digital form allow computer enhancement, combination and filtering of the data offering new and challenging opportunities to those engaged in geological exploration.

In many areas, particularly where superficial cover limits spectral resolution of bedrock, lineaments form the most coherent data derivable by remote sensing methods. The main purpose of this chapter is to discuss a structural approach to lineament analysis and to demonstrate some applications of its use in the La Codosera area.

10.2 - IMAGERY AND DIGITAL PROCESSING

10.2.1 - Imagery.

Landsat TM imagery was selected for use in this study, because it combines a moderate spatial resolution (30m) with geologically useful spectral characteristics. The La Codosera area is contained within a single quadrant of Landsat TM data (path 203, row 33, quadrant 2). A cloud-free winter image acquired on the 26th January 1986 was selected for study, the low sun angle at this time of year being useful in enhancing topographically controlled lineaments. CCTs of all seven bands of TM data for this quadrant were obtained, together with quadrant 1 of the same image which covers the Nisa area in Portugal. Thus both images could be easily compared and processes using similar parameters. Additional data for the La Codosera area acquired on 3 August 1985 was available by exchange with ITGE (see chapter 8).

10.2.2 - Spectral image processing.

The data were processed on GEMS image processing systems at the Ordnance Survey Remote Sensing Centre in Belfast and the National Remote Sensing Centre, Farnborough. Later work was carried out using Erdas software on a Sun/4 computer in Southampton University.

The digital data were subject to various enhancement techniques, principally using bands 3, 4, 5 & 7. These were subject to various forms of contrast stretching and band combination, principal components, ratioing and spatial filtering. The resulting images were used to map major lineaments; interpretations of individual image extracts being combined using a band 7 base at a scale of 1:50.000.

10.2.3 - Spatial filtering.

Spatial filtering may be used to transform images and enhance directional features, with recent research into automatic detection of lineaments. Great care is needed in the interpretation of such images, particularly in areas with "cultural" features, which tend to have high amplitude, high frequency characteristics which swamp the subtle gradients and changes in texture which characterise major structural features, and which often change along their length.

Directional or gradient filters are easily applied to digital images by convolution using a n x n operator, such as the Roberts or Sobel operators. In their simplest form these operators can be used to detect gradients in an E-W, N-S, NE-SW or NW-SE direction, but larger operators are easily rotated to other directions if required. The choice of filter size (n) can be adjusted to sample gradients of various wavelength. Application of a single operator gives a measure of the gradient in one direction; two orthogonal filters can be used to estimate the magnitude and direction of the gradient.

Another way of combining two (or more) operators is to simultaneously display different filtered images using different colour guns of the VDU, thus combining aspects of the direction and magnitude of the images (see Sanderson, 1988). The resulting image effectively colour-codes the gradients according to their direction.

Other filters may be used to detect discrete lines; these are essentially a type of high-pass filter set to detect lines of predetermined orientation and width which have a linear arrangement of pixels contrasting with their adjacent values. Whilst roads, railway lines, etc. may have these properties, few geologically significant lineaments have such simple form.

10.3 - LINEAMENT EXTRACTION AND LINEAMENT MAPS.

The drawing of lineaments on images is a traditional skill of the photogeologist, but is inevitably subjective. Various attempts have been made to utilize the digital nature of satellite images in the automatic detection of such linear features. Line and gradient images provide a simple basis for the automatic extraction of lineaments, the data usually being converted to binary form by setting a threshold value and the resulting image interrogated to extract directional information (eg. Haralick, 1983; Conradsen et al., 1988). More complex linear features (circular or elliptical arcs, etc.) can be extracted using more sophisticated filtering algorithms such as the Hough transform (Cross, 1988).

Although automatic extraction of lineaments provide objective data which can be produced rapidly and cheaply, great care is needed in the interpretation of such images. Areas containing "cultural" features such as roads, fields, etc. produce a high amplitude response to the initial directional or line enhancement and often swamp the resulting interpretion. Most geological lineaments, on the other hand, are produced by very subtle gradients and changes in texture, which may be suppressed rather than enhanced by such filters. Larger geological faults are often more obvious as lineaments across which higher-frequency variations, produced by smaller fractures, bedding etc. and even changes in field pattern and landuse, are discontinuous. The detection of such features would require very complex filtering, probably combined with artificial intelligence algorithms. In this study image processing was used to generate a variety of images for interpretation but all lineaments were extracted visually by geologists. The separation of structural features from other geological and cultural lineaments is probably best tackled by the analyst on a subjective basis during image interpretation.

10.3.1 - Lineament maps.

Lineament maps were digitized using a TDS digitizing table linked to an IBM PS/2, using software developed by Sanderson at Queen's University, Belfast and the University of Southampton.

The data are stored on disk ready for input into plotting and processing programs. In this study all data were transformed into UTM coordinates by matching control points on the imagery and maps.

Maps of lineaments often appear as a confused (and confusing?) array of lines. To use such maps for structural analysis we must first ask the question - is the lineament map a reasonable representation of the underlying fracture system? There are several possible ways to investigate this question and these are discussed more fully in later sections.

10.4 - STRUCTURALLY CONTROLLED PROCESSING

Lineament data have scalar (length), directional and spatial information, and these features require different, but interdependent, forms of analysis. Structurally Controlled Processing was developed by Sanderson & Dolan (1986) as part of earlier EEC funded research into the use of remote sensing in the raw materials programme. Basically it consists of a package of computer programmes, which have been re-written for IBM PS/2 microcomputers as part of this project, to facilitate the manipulate and display the directional and spatial attributes of lineament data. These allow plotting, georeferencing, directional filtering, etc. of lineaments and the generation of maps of the following measures:

Rose-diagrams for areas or sub-areas give an effective display of the main sets of lineaments.

Frequency & Density maps calculate the total number (frequency) or length (density) of lineaments in a grid cell. Many authors (eg. Wheeler & Dixon, 1980) have recognised an increase in fracture density in fault zones, but occasional studies claim the inverse relationship. With remotely sensed lineaments, density is not simply related to degree of fracturing and much variation can be attributed to changes in the nature of the land surface (eg. overburden thickness, forestation, etc.).

Directional Filtering involves the separation of lineaments on the basis of their orientation and may involve the inclusion or exclusion of one or more ranges of directions. The display of filtered data and/or the colour coding of various directions can be used to simplify the lineament data and search for patterns of individual directional modes.

Directional Frequency and Density refer to the number or length of lineaments within a pre-defined range of orientations. This measure can be used to filter out certain ranges of lineament orientations and to examine their spatial abundance.

Directional Dominance measures the proportion (percentage) of lineaments within pre-defined orientation limits in relation to the total in a sample cell. Directional dominance maps are useful in delimiting zones of differing fracture pattern. An interesting variant of dominance is Angular Atypicality (Pretorius &

Partridge, 1974) where the anomalous areas with a high proportion of lineaments not belonging to prominent regional trends often correspond to geological targets.

Randomness can be expressed by various measures (eg. Relative Entropy and $\chi^{2/n}$), which are generally very sensitive to the number of directional classes used. Changes in randomness can be related to the development of fracture patterns associated with faults, etc..

Mean Orientation of lineament sets can be calculated by vector addition and anomalous regions found. Rotation in the proximity of major wrench faults and shear zones has been recognised in many studies (eg. Carter & Moore, 1978). Where many sets of lineaments exist mean orientations of individual sets (Group Means) can be obtained after directional filtering.

A common problem with many of these measures is that the small grid cells (1-5km square) used to detect high-frequency anomalies often contain too few lineaments to yield statistically significant results. Various smoothing and filtering techniques may be applied to reduce this problem. 3x3 low-pass filters have been found particularly useful in increasing the effective sample size whilst maintaining a reasonable spatial resolution. Filtering methods must combine the data from adjoining grid cells and not simply operate on derived parameters, since the adjoining cells generally contain differing amounts of data.

The ability of Structurally Controlled Processing to reduce complex lineament patterns to scalar measures of a wide range of attributes can greatly facilitate structural interpretation. The resulting maps allow recognition of structural patterns and domains, can be used to test geological hypotheses and allow detection of faults, shear zones and their terminations, offsets and bends. Zones previously known from ground structural work can be mapped into poorly exposed areas and their margins and terminations delineated more accurately.

10.5 - LINEAMENT ANALYSIS OF TM IMAGERY FROM LA CODOSERA.

The distribution of lineaments mapped from various enhancements of TM data in the La Codosera area is shown in Fig. 10.1, and the orientations of these summarized in Fig. 10.2. The data can be divided into three clearly defined sets trending 045°, 135° and N-S (Table 10.1), with most lineaments being easily assigned to one of these three sets, which contain similar numbers of lineaments.

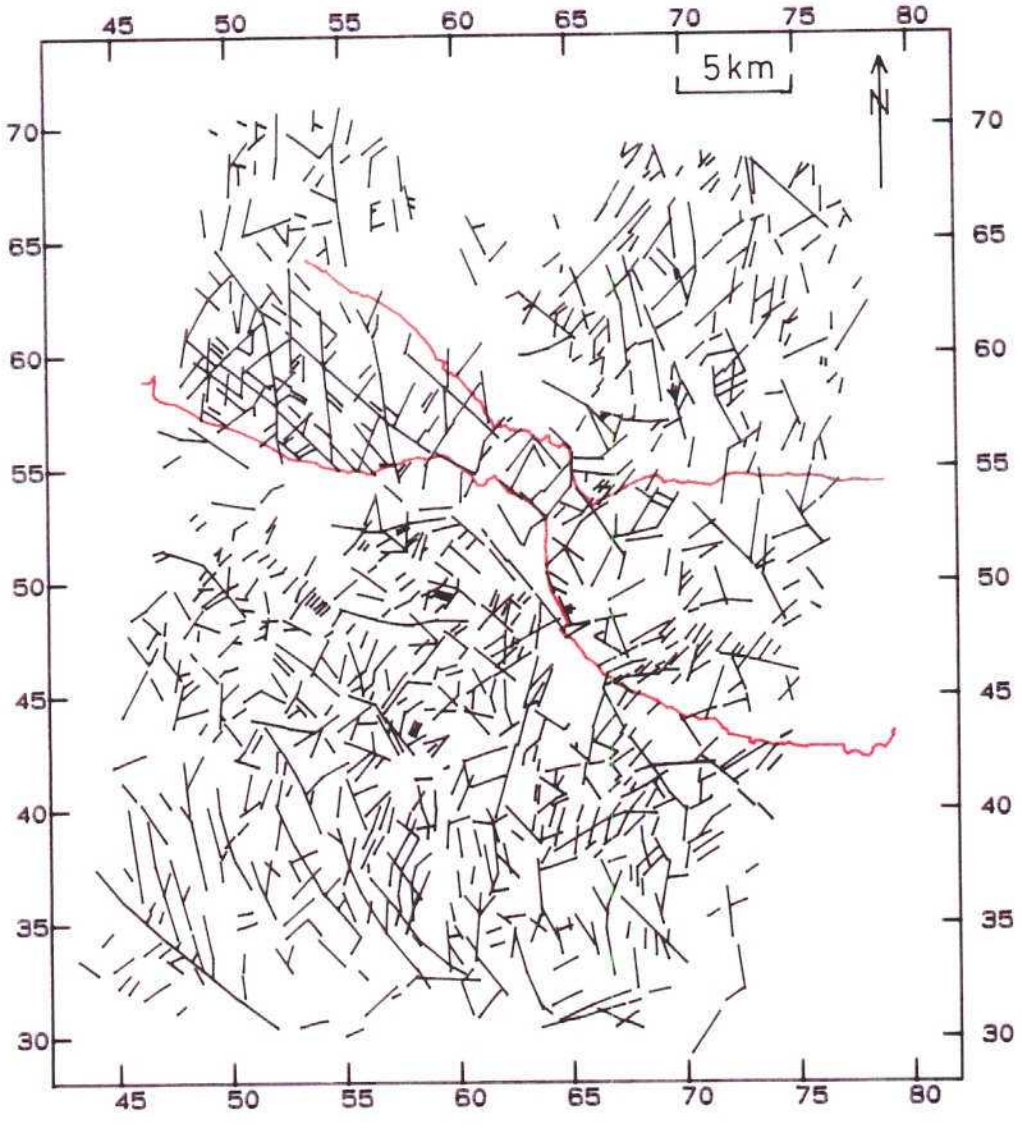

FIG. 10.1 - LINEAMENT MAP OF THE LA CODOSERA AREA BASED ON INTERPRETATION OF LANDSAT TM IMAGERY

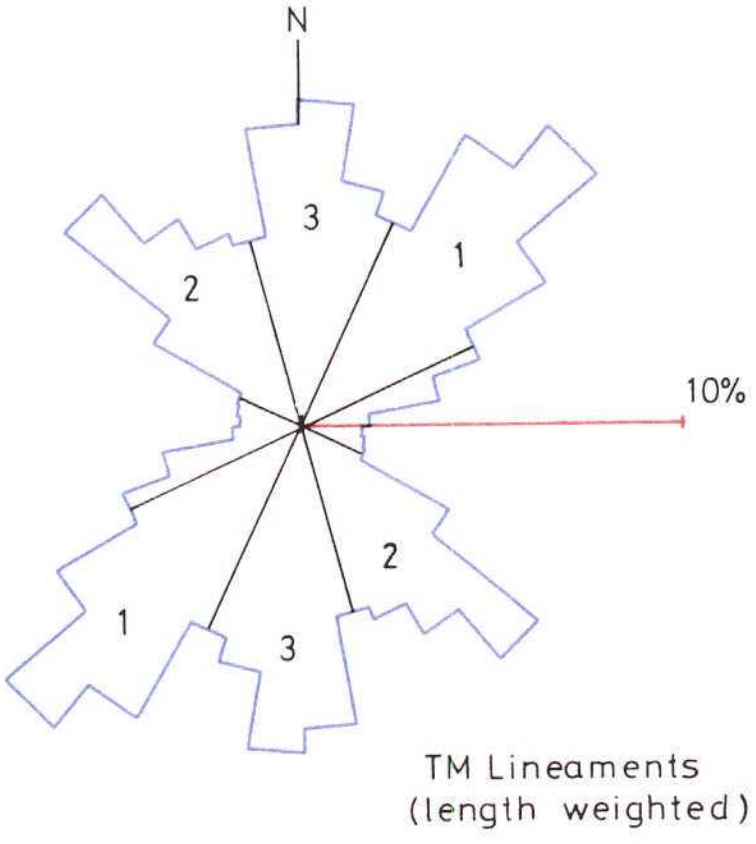

FIG. 10.2 - ROSE DIAGRAM OF LANDSAT TM LINEAMENTS FROM THE LA CODOSERA AREA

Table 10.1 - Summary of TM lineaments, La Codosera area, W. Spain.

Set	Mode	Range	%
1	045°	025-065	31.5
2	135°	115-165	26.6
3	005°	165-025	28.4

The pattern of lineaments is fairly constant throughout the area, but with some local variation in the proportions within each of the three sets. This is fairly clear from the rose diagrams constructed for 5x5 square blocks (Fig. 10.3). This spatial distribution of lineaments will be discussed further in section 10.7.

10.6 - RELATIONSHIP BETWEEN LINEAMENTS AND FRACTURES.

10.6.1 - Regional fracture survey.

Over 1500 fractures were measured at various sites distributed within the three main units, ie. CEG, Palaeozoic metasediments and Alburquerque batholith. Due to the fairly homogeneous nature of the latter unit a more intensive study of granite fracturing has been carried out as part of a more extensive investigation of this unit by Ms C Chinn. Details of this study are summarized separately below, but the data is included in the regional fracture survey.

The fracture system comprises three clearly defined sets (Table 10.2, Fig 10.4). The most dominant set trends approximately NE-SW and detailed studies demonstrate that it is made up of three distinct sub-sets with modal orientations of 020°, 040° and 065°. These fractures generally form barren quartz veins and are widely developed in both the granite and country rocks. A widely developed, although generally less dominant, set of fractures trend 165°. Field studies have demonstrated a progressive rotation through time from 065°, through 040° and 020° sets, to the 345° (165°) set. This changing stress field has produced much reactivation of early formed extension fractures with mixed mode (extension and shear) loading. A less dominant, but clearly developed set of fractures trending 135° is found in all units, but is best developed in the granite.

The good correspondence between the orientations of fractures and lineaments is apparent in Fig. 10.4 and this strongly supports a link between the two features. In studies of this sort one generally finds a good correlation between these data, but differences may arise through inclusion of other features in the lineament data, eg. bedding traces, etc.. In the present study care was taken to exclude bedding, particularly the prominent traces of the quartzite units.

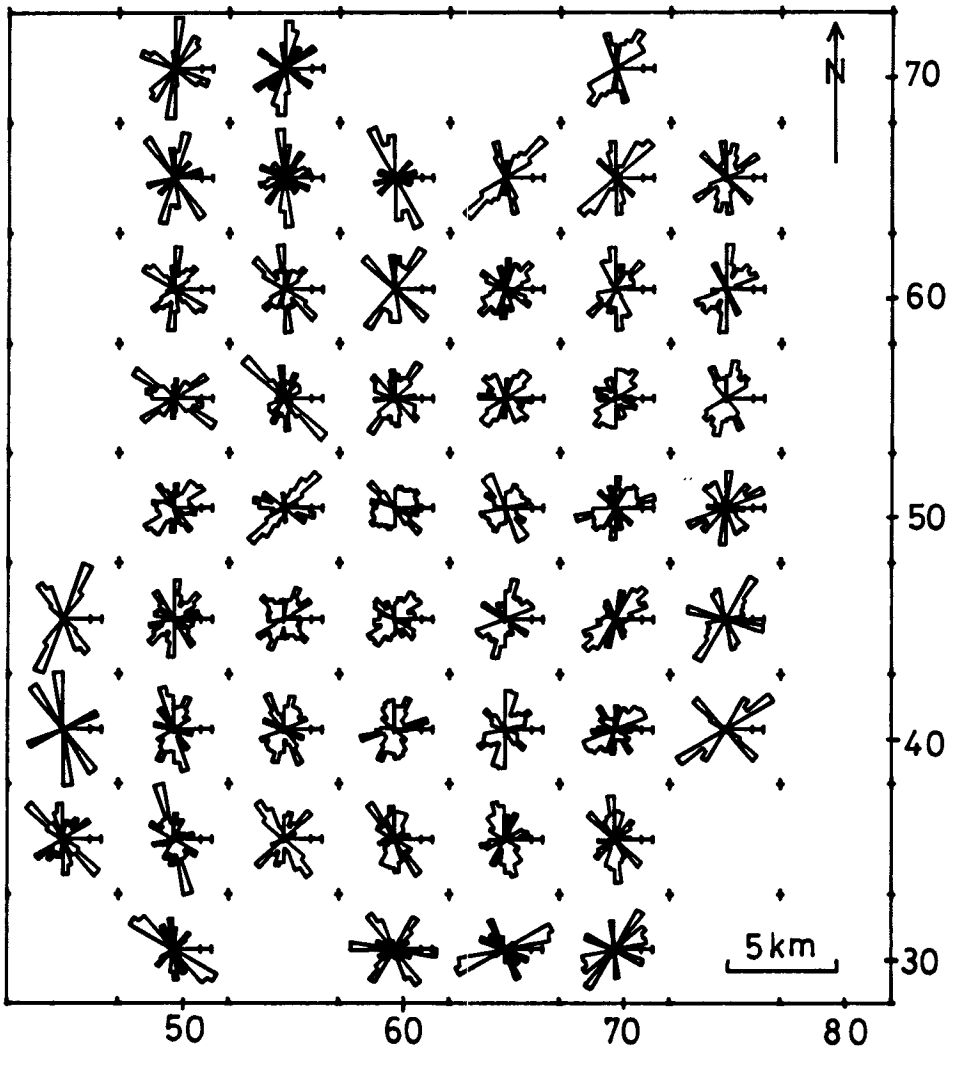

FIG. 10.3 - ROSE DIAGRAMS OF LANDSAT TM LINEAMENTS FOR 5X5 KM SUB-AREAS WITHIN THE LA CODOSERA AREA

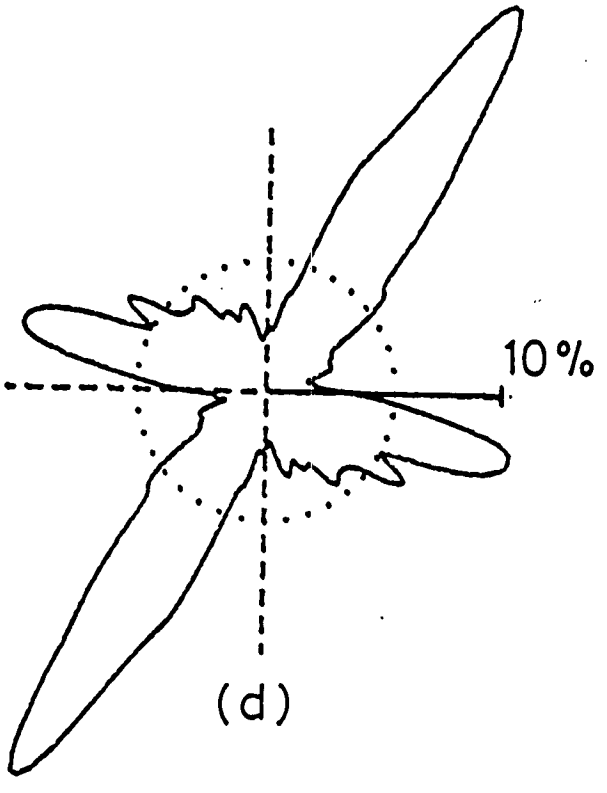

FIG. 10.4 - ROSE DIAGRAM OF FRACTURES MEASURED AT VARIOUS SITES WITHIN THE LA CODOSERA AREA

TABLE 10.2 - Summary of the fracture sets sampled in ground surveys in the La Codosera area.

Set	Mode	Range	Comments
NE-SW	020° 040° 065°	010-075	Dominant sets in both granite and country rocks
N-S	165°	150-000	minor set in granite and country rocks
	105°	090-120	subsidiary set in granite
NW-SE	135°	115-165	well developed in granite but scarce in country rocks

Most of the fractures measured on the ground were extension fractures and veins which need not always correspond to the trends of larger faults, the former usually representing extensional fractures, whilst the latter are zones of shearing often reactivated in several stress systems.

10.6.2 - Fracturing in Alburquerque Batholith.

We have been investigating the ability of different sensing systems to sample fracture patterns in the Alburquerque batholith (Chinn and Sanderson, unpublished work). The sensing systems used were Landsat TM (generally reproduced at scale between 1:50.00 and 1:100.000), air photographs at a scale of 1:18.000 and outcrop mapping and measurement of fractures. The granite was chosen for this study because it represents a fairly homogeneous material within which fracturing has produced lineaments detectable at a wide range of scales. In addition the Alburquerque batholith, particularly to the west of San Vicente, is relatively free from other sources of lineaments, both geological (absence of bedding, etc.) and cultural (few roads, field boundaries, etc..).

For this study a total of 2681 fractures were measured at approximately 70 sites (average 38 fractures per site) arranged fairly evenly across the area (Fig. 10.5). As most of the fractures are steeply inclined they may be represented by rose diagrams, which also facilitate comparison with remotely sensed lineaments. Summary diagrams of the fracture data show a dominance of NW-SE and NE-SW sets, with occasional N-S and WSW-ENE fractures; these correspond to the regionally developed fracture orientations (Table 10.2), a data set which also includes sites within the granite.

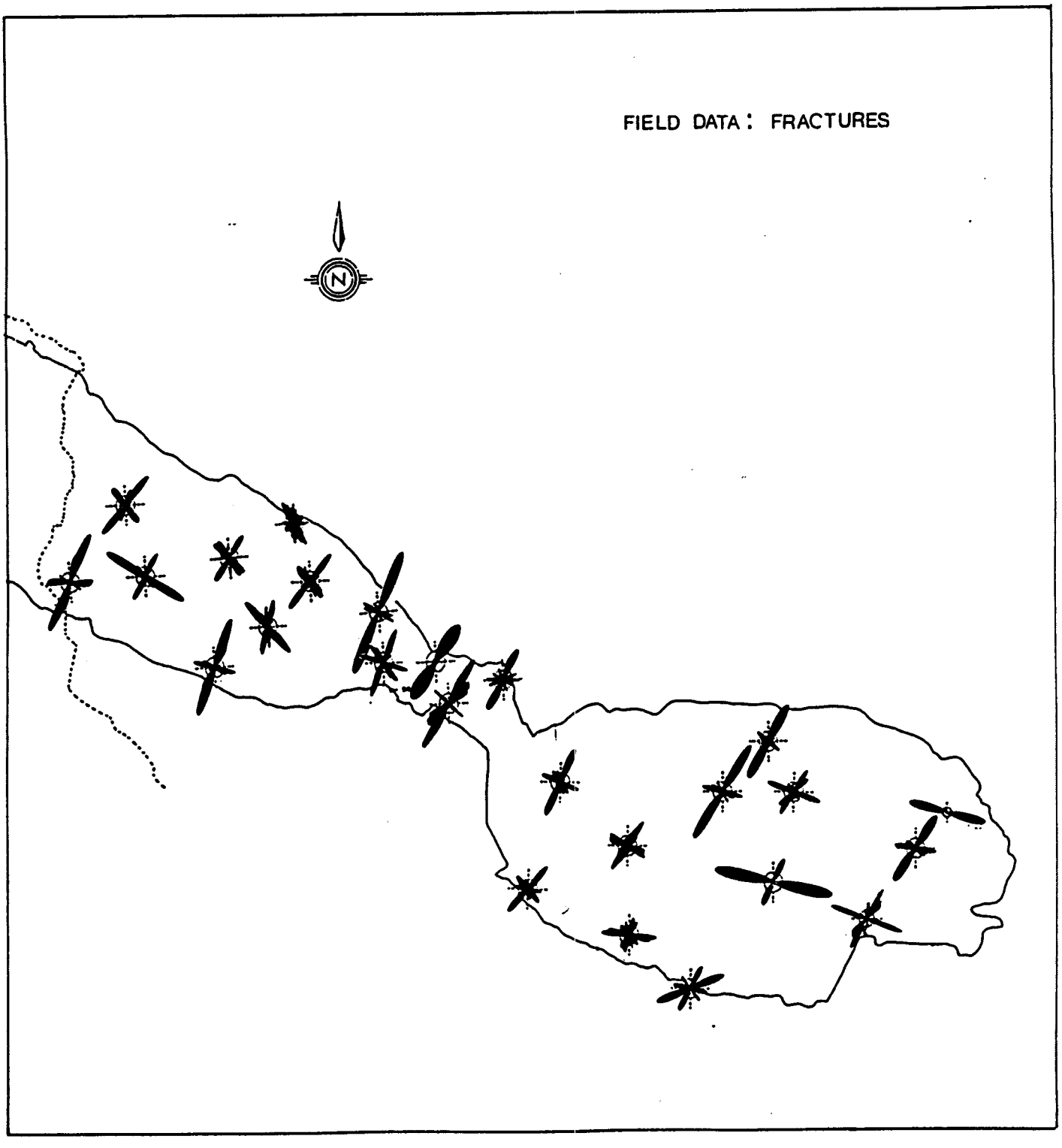

FIG. 10.5 - ROSE DIAGRAMS OF FRACTURED MEASURED AT INDIVIDUAL SITES IN AND AROUND THE ALBURQUERQUE GRANITE

Air photographs covering c.350 km^2 at a scale of 1:18.000 were examined stereoscopically and some 3000 lineaments extracted. These are mostly short (< 1km) and form two prominent sets of fractures trending NE-SW (040°) and NW-SE (135°) (Fig. 10.6). The dominance of each set varies across the batholith, but their orientations remain very constant.

Sub-sets of lineaments interpreted from Landsat TM imagery covering the granite areas between Alburquerque and Valencia de Alcantara show the same modal orientations of 040°, 135° and N-S (Fig. 10.7). These are similar to those obtained in the regional study (Table 10.1), supporting the view that most of the fracturing post-dates granite intrusion.

In addition to these data, the drainage within the granite was digitized, and also the granite margin. These data indicate a close correspondence between TM lineaments and drainage, whereas the granite margin mainly follows E-W to WSW-ENE trends (Fig. 10.8). These observations strongly support an early (pre-granite) origin for E-W and WSW-ENE structures and a late (post-granite) origin for the other fractures. These conclusions are consistent with other geological evidence.

The various data sets allow us to evaluate the different characteristics of the fracture system recorded by the different sampling techniques. The conclusions of this analysis are summarized in Table 10.3.

TABLE 10.3- Summary of characteristics of fractures in the Alburquerque Batholith sampled by different sensing systems.

Character	TM	Air photo	ground
NE-SW set	abundant	abundant	abundant
N-S set	abundant	absent	weak
NW-SEset	abundant	dominant	abundant
Length(m.)	10^2 - 10^4	10^1 - 10^3	10^{-2} - 10^2
Width(m)	10^1 - 10^3	10^0 - 10^2	10^{-3} - 10^1
Within site variability	high	low	high
Between site variability	moderate	low	high

These results confirm the conclusions of Sanderson & Dolan, (1986), that the length of lineaments detected by various sensing systems is broadly related to the resolution of the system, the scale at which the imagery is analyzed, and the experience and objectives of the analyst.

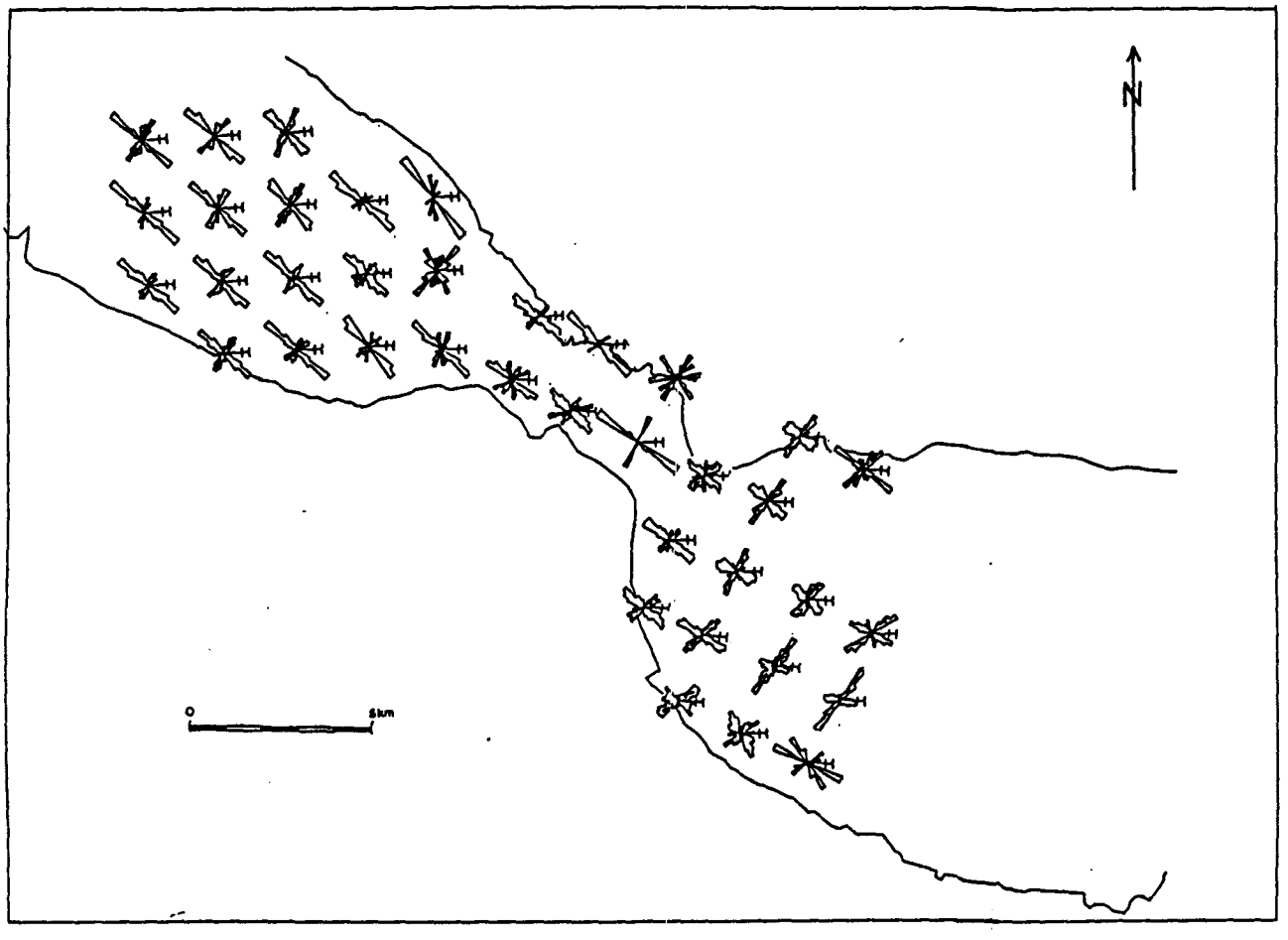

FIG. 10.6 - ROSE DIAGRAMS OF LINEAMENTS INTERPRETED FROM AERIAL PHOTOGRAPHS SUMMARIZED FOR 2X2 KM SUB-AREAS

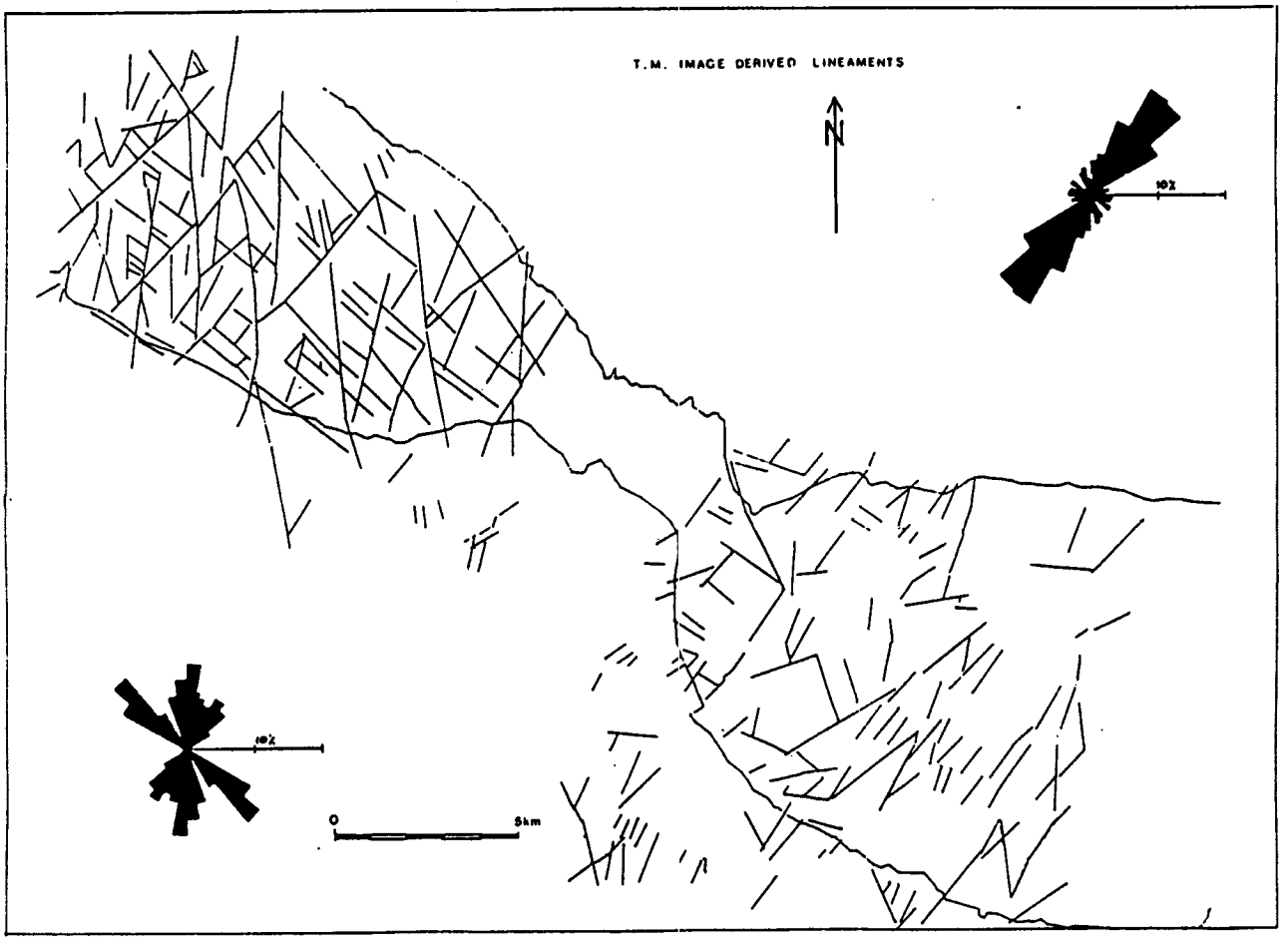

FIG. 10.7 - LANDSAT TM LINEAMENTS WITHIN THE ALBURQUERQUE GRANITE. ROSE DIAGRAMS SUMMARIZE DATA FROM THE VALENCIA DE ALCANTARA (BOTTOM-LEFT) AND ALBURQUERQUE (TOP-RIGHT) SUB-AREAS

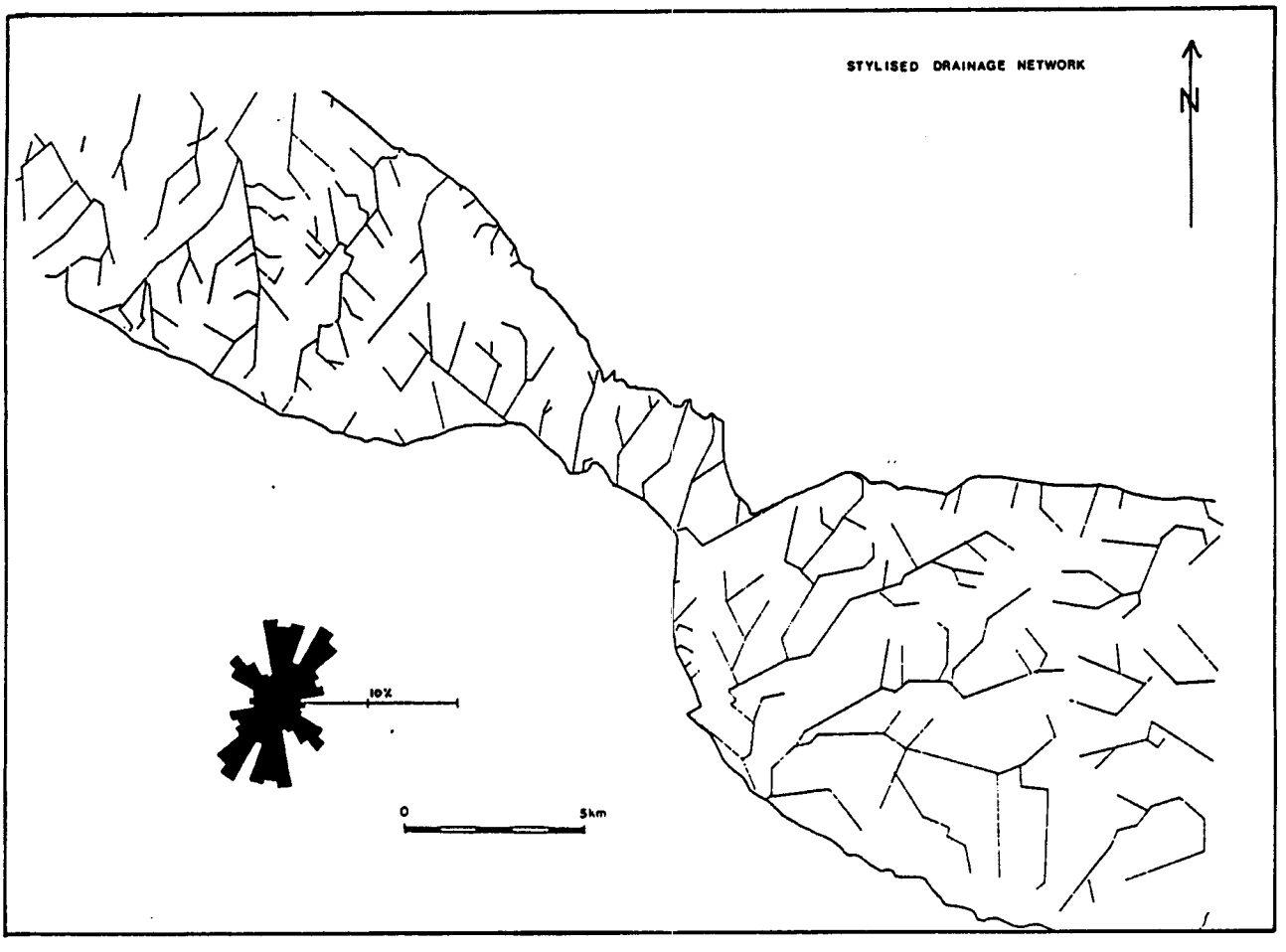

FIG. 10.8 - STYLIZED DRAINAGE WITHIN THE ALBURQUERQUE GRANITE, DERIVED BY LINEARIZATION OF MAPPED STREAMS

Another approach to comparing lineaments and ground fracture patterns is to examine the spatial architecture of these data. Figure 10.9 shows schematically the fracture pattern deduced by different sensing systems. At all levels fracture sets abut and offset one another, with relatively few cross-cutting sets. Additional patterns include branching, offsets and en echelon patterns. Similar architectures are seen in detailed maps of fault patterns especially in areas of extensive mining where faults may be traced in detail. We conclude that the more random, criss-crossing patterns of lineaments seen in some studies may be poor representations of the ground structure.

The Alburquerque experiment has shown that fracture patterns sampled by different sensing systems are not scale invariant (ie. not self-similar), thus, suggesting that it is important to select the appropriate system to locate the required scale of lineament targets. For example, ground mapping might be the most appropriate method to investigate the role of fractures in small- scale engineering projects or in localizing mineralization within a mine, but satellite lineaments might be more significant in the location of major faults and fracture zones for earthquake risk, hydrological studies, waste disposal, etc. and in the location of major mineral prospects within an area.

10.7 - SPATIAL ANALYSIS OF LINEAMENTS

In general individual lineaments are easily assigned to one of the three main sets (Table 10.1). For structurally controlled processing ranges specified in Table 10.1 have been used to sub- divide the data.

10.7.1 - Density.

The density map (Fig. 10.10), calculated for a 3x3 moving window, shows a fairly even spread of lineaments throughout the area, with highest values within the granite to the south of Valencia de Alcantara. Other patches of high density are developed sporadically in the country rocks.

10.7.2 - Directional density and dominance.

By assigning lineaments to one of the three main sets (Table 10.1) it is possible to examine the directional density of each. Since almost all (c.87%) are assigned to one of the three sets, these maps have strong internal correlations. For example, within the fairly uniform densities of the CEG any region of high density of one set is likely to have low density for one or both of the other sets. This internal correlation becomes more acute in the dominance maps, where the closure forces many negative correlations.

The 135° lineament set includes several long lineaments, well developed within the western part of the granite and in the Badajoz Shear zone (Fig 10.11A/B). In the

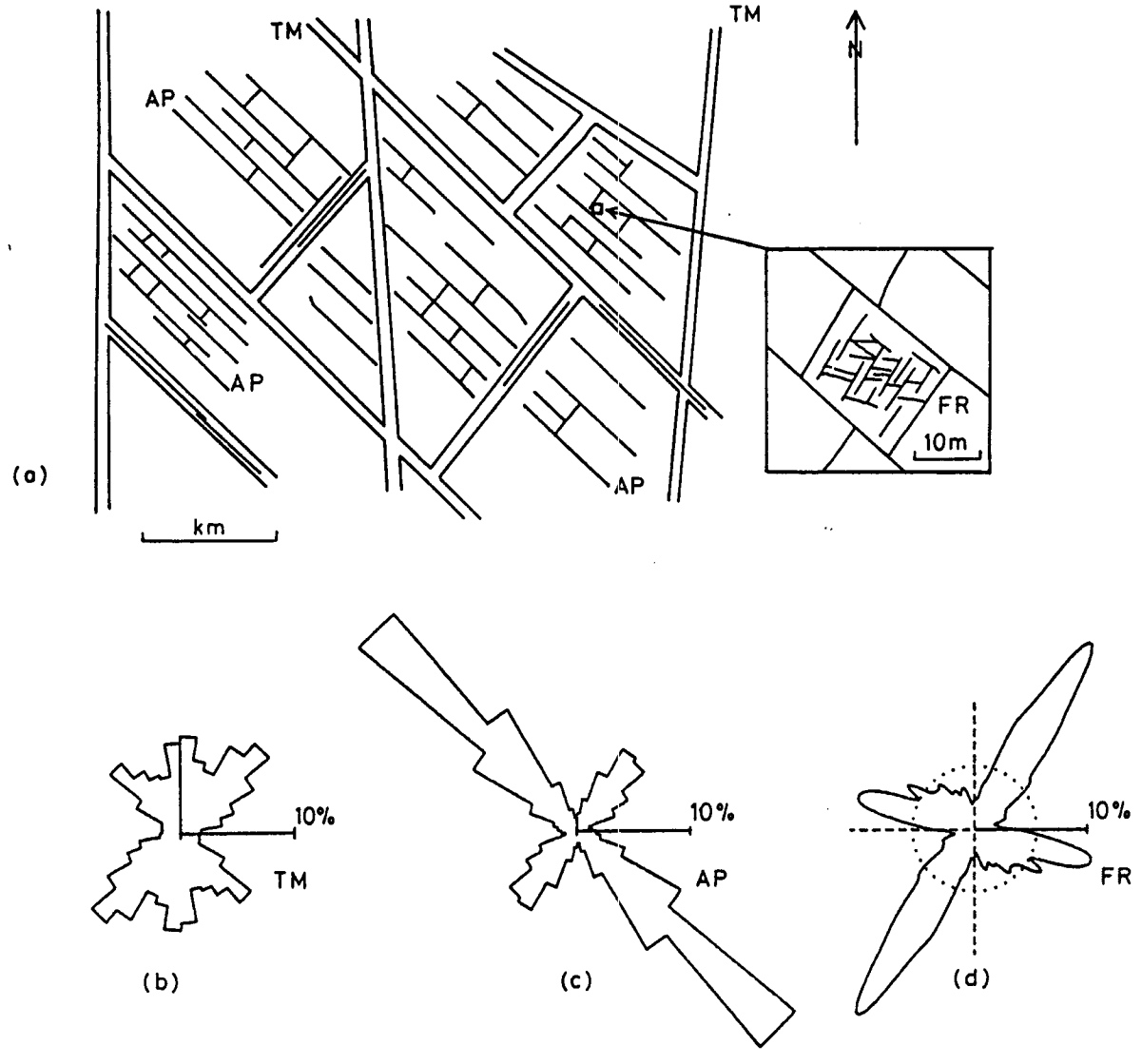

FIG. 10.9 - (A) SCHEMATIC REPRESENTATION OF THE ARCHITECTURE OF LINEAMENTS MAPPED FROM SENSORS OF DIFFERING RESOLUTION. ROSE DIAGRAMS OF (B) LANDSAT TM, (C) AIR PHOTOGRAPH AND (D) GROUND FRACTURE MEASUREMENTS.

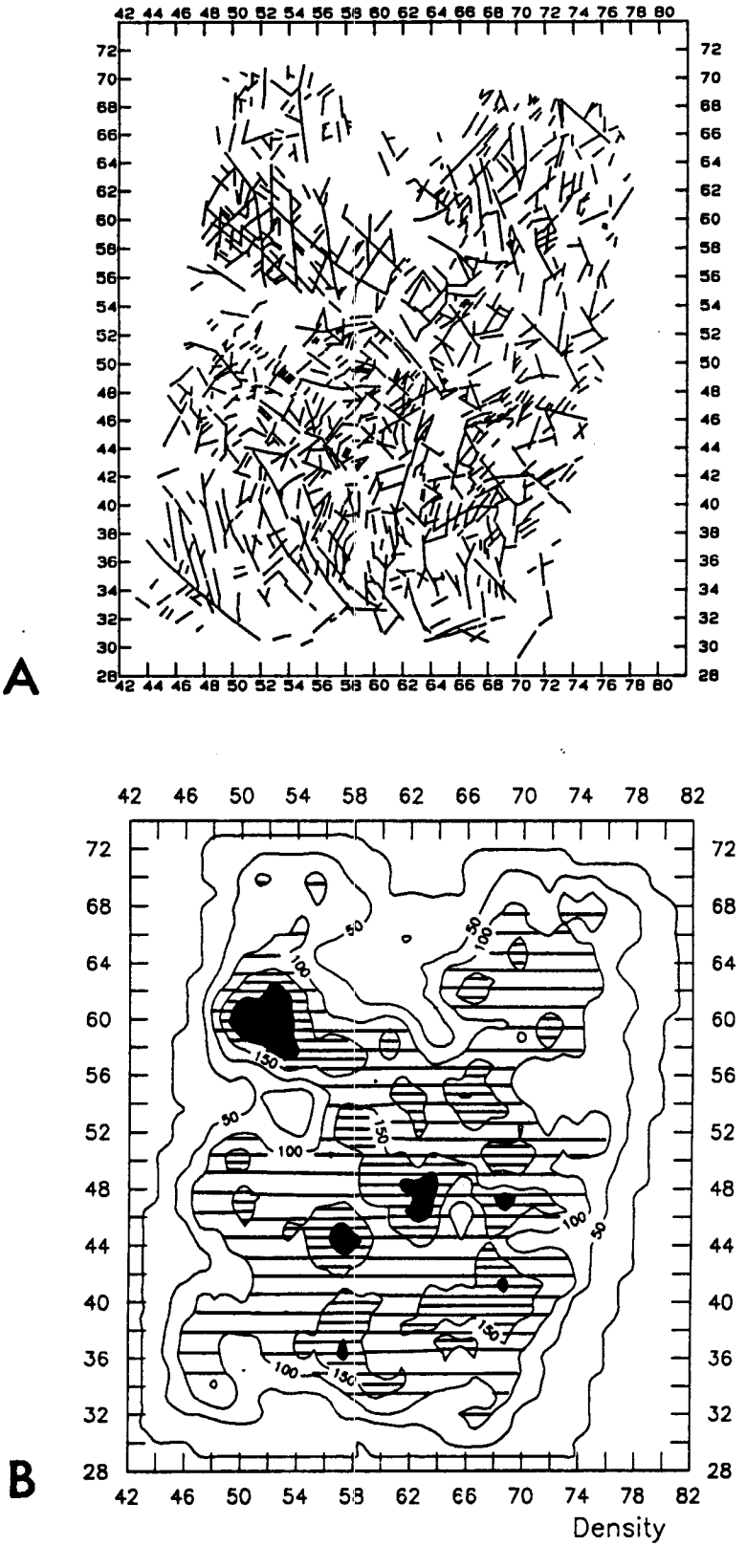

FIG. 10.10 - (A) THE LANDSAT TM LINEAMENT DATA SET, REDUCED FROM FIG.10.1 TO SAME SCALE AS DENSITY AND DOMINANCE MAPS IN FIGS. 10.10 TO 10.13. (B) DENSITY MAP OF THE DATA IN (A).

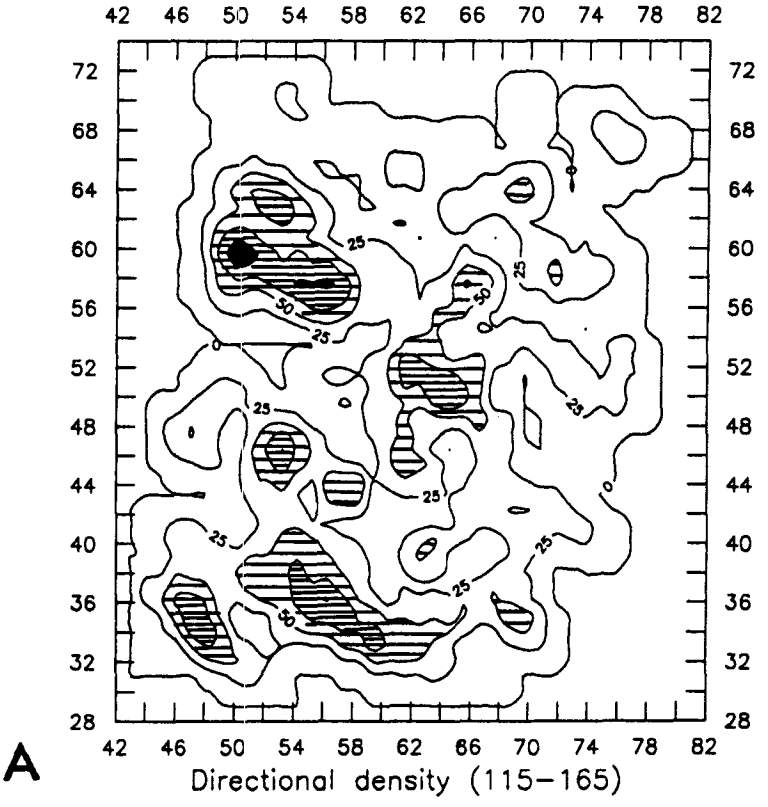

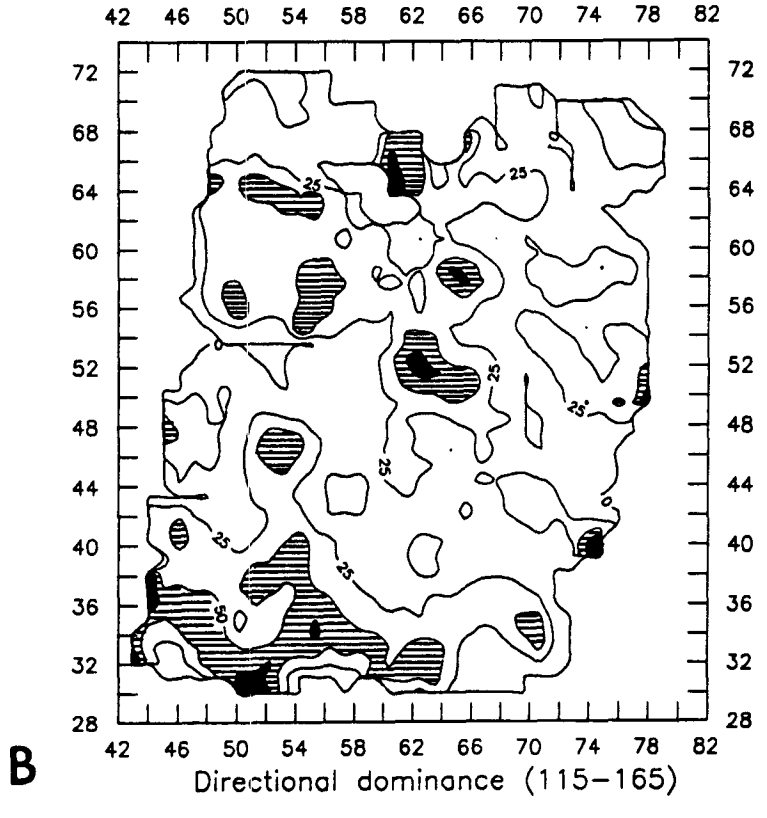

FIG. 10.11 - DIRECTIONAL DENSITY (A) AND DOMINANCE (B) MAPS OF THE 135° (115° - 165°) LINEAMENT SET.

latter area they dominate the lineament pattern and are clearly related to faults which offset the quartzites of the Southern Ridge.

The directional density of the N-S lineaments (Fig. 10.12A) is highest in the western part of the granite, around Valencia de Alcantara, and in the southern part of the area, where this set dominates the lineament pattern in parts of the Southern Ridge and the Badajoz Shear Zone (Fig 10.12B).

The NE-SW lineaments are fairly evenly developed throughout the area, being locally dominant in the Central Ridge and in the granite to the NW of Alburquerque (Fig. 10.13A/B).

A general feature of the La Codosera area is that the three sets of lineaments have a widespread development throughout the different rock units. This is clear from the directional density and dominance maps as well as from the lineament map itself (Fig. 10.1) and the rose diagrams for sub-areas (Fig. 10.3). Thus we can conclude that the lineament pattern has a strong directional anisotropy, with three clearly defined sets, but a poor spatial variability. This in turn supports the view that the pattern was largely developed after the emplacement of the Alburquerque batholith.

10.8 - USE OF LINEAMENT MAPS AS AN AID TO MINERAL EXPLORATION

In this section we will discuss the lineament data in relation to the general structural setting of the La Codosera area its mineralization. The tectonic synthesis (Chapter 2, Sanderson et al., in press) indicates that the area was subject to transpressional Hercynian deformation, followed by granite plutonism and late (domino-style) faulting, with continued Mesozoic and Tertiary fracturing. Detailed work on the relative ages and kinematics of the fracture sets provides important constraints on the tectonics of the area and forms a basis for work on the evolution of mineralizing fluids (see Chapter 11).

Using the Landsat data, combined with the ground structure, air photograph interpretation and gravity data, a clear picture of the fracture system has emerged. Three major sets of lineaments trend 045°, 135° and N-S (Fig. 10.2) and these correlate well with extensional fractures, including those at known mineral prospects. In addition it has been possible to correlate Landsat lineaments with known faults in many parts of the area, particularly in the Southern Ridge. Thus the lineament analysis provides a useful dataset with which to augment the regional structural studies.

In order to convert these data into viable exploration models it is necessary to understand and relate the nature and kinematics of the fracture control to the mineralization. Only then can full use be made of the mapping available from Landsat imagery, through the lineament map its self and the maps of density and dominance, as a basis for the definition of exploration targets.

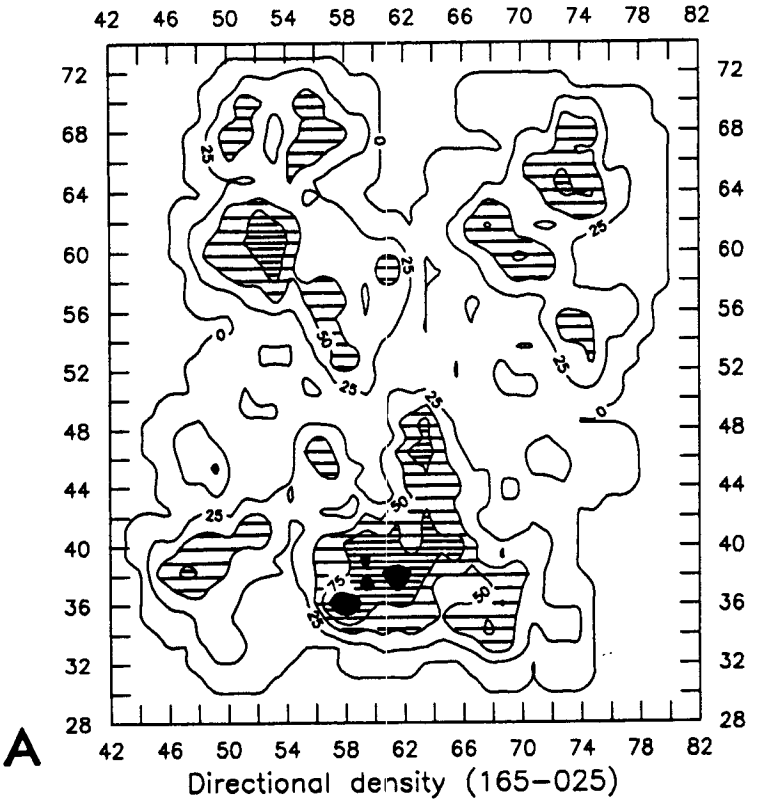

FIG. 10.12 - DIRECTIONAL DENSITY (A) AND DOMINANCE (B) MAPS OF THE N-S (165° -025°) LINEAMENT SET.

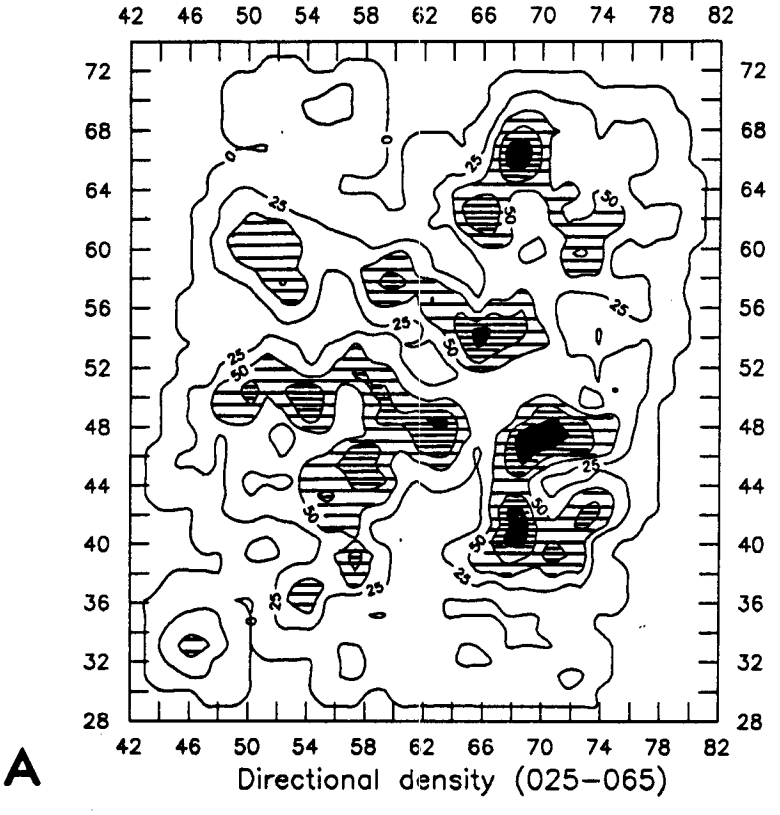

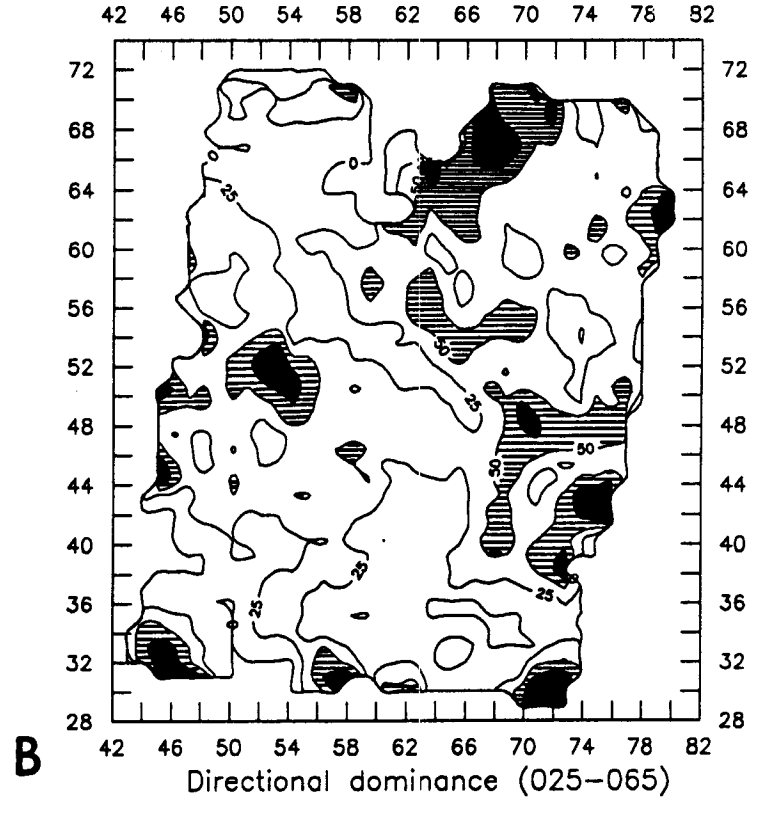

FIG. 10.13 - DIRECTIONAL DENSITY (A) AND DOMINANCE (B) MAPS OF THE NE-SW (025°-065°) LINEAMENT SET.

10.8.1 - U-P mineralization within the granite.

Known U-P mineralization is largely confined to large 045° fractures, with vuggy and brecciated veins containing quartz, chalcedony, apatite, pitchblende, pyrite etc.. (see also chap.6) Evidence from old U workings to the north of Alburquerque suggests that these veins form in arrays along 030° and 065° lineaments, many of which may be identified from Landsat. These lineaments would represent brittle transtensional shear zones with dextral and sinistral movement respectively.

More work is needed to fully define this pattern, using both the ground mapping of fracture zones and air photograph interpretation. Initial results indicate a high dominance of NE- SW lineaments may be a guide to U prospectivity.

10.8.2 - Sn-W and Li prospects.

These mainly occur in the aureole of the Alburquerque granite and are located along both 135° and 045° fractures. There is some correlation between areas of high dominance of 045° + 135° lineaments (and hence low dominance of N-S lineaments - see Fig. 10.12) and the Sn-W mineralization within the granite aureole. The Lithium workings at Tres Arroyos also show the same correlation.

10.8.3 - Gold prospects in the Central Ridge.

The Central Ridge shows a fairly high proportion of 045° lineaments, but on the ground fractures of this trend tend to be barren. Several E-W lineaments cut the Central Ridge and appear to correspond with known mineral prospects of this trend.

10.8.4 - Gold and Antimony prospects in the Southern Ridge.

Old mines (some of them Roman) work quartz veins, mainly in Devonian quartzites and slates. Small workings occur along steep strike-faults with reverse and strike-slip movement, but the main prospects lie on steep N-S to NE-SW veins, which appear to be developed as extensional fractures, with some left-lateral reactivation, sited at the terminations of the larger NE-SW faults. These major fracture zones (lineaments) provide connectivity between the shear zone and the Southern Ridge of Palaeozoic rocks which host the main Au-Sb mineralization. Maximum dilation will occur where the domino faults change orientation or have large displacement (Chapter 2). It is significant that the main area of old Au workings at Los Algarbes occurs at the northwestern end of the main change in orientation of the domino faults and that the San Antonio Antimony mine occurs at the NW extension of a large displacement fault (Fig. 10.14). Using the known structural controls, the lineament map provides a basis from which to identify new target areas which show abundant N-S to NE-SW fracturing in a similar structural setting.

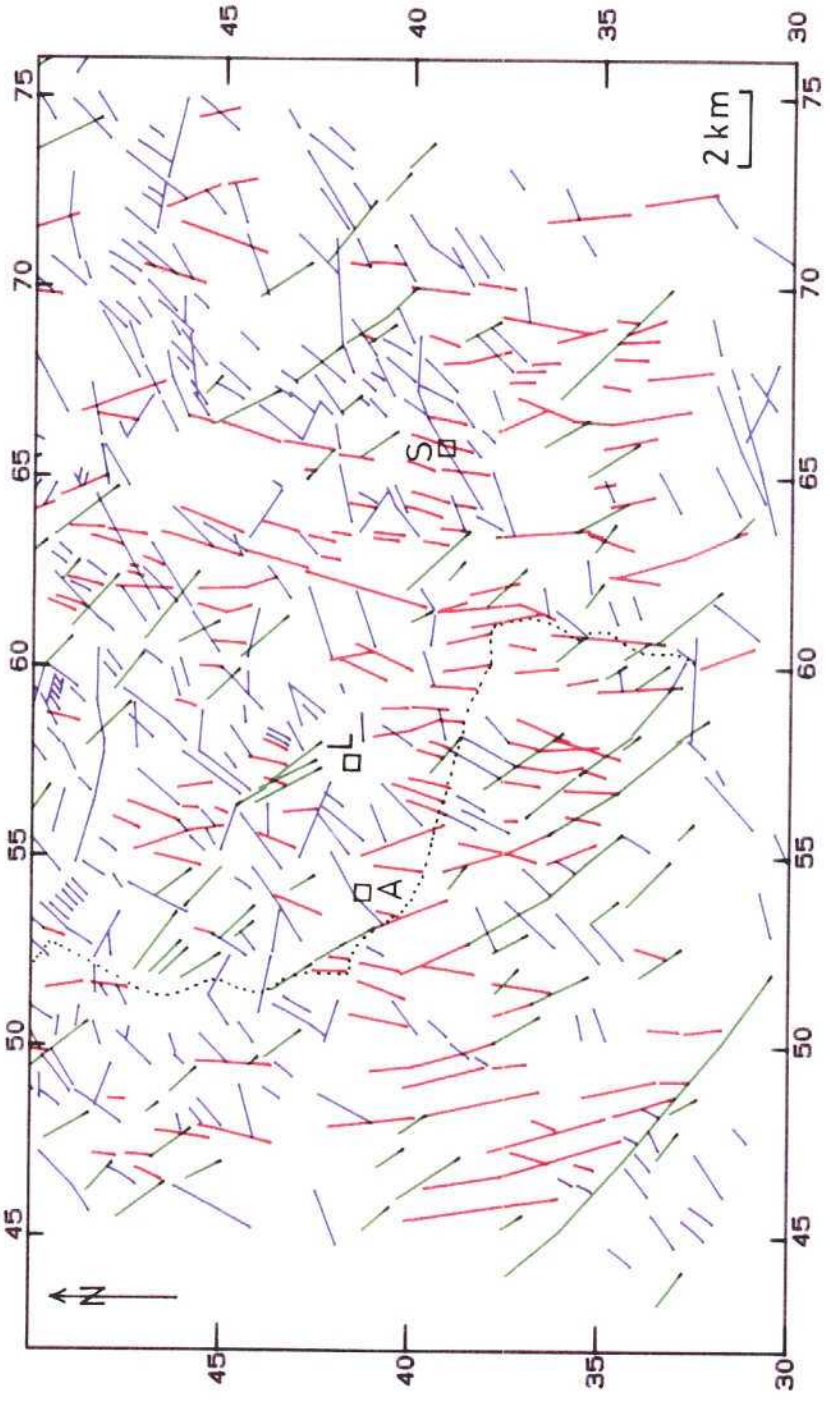

FIG 10.14 - LANDSAT TM LINEAMENT MAP OF SOUTHERN PART OF THE LA CODOSERA AREA. NW-SE LINEAMENTS (GREEN) AND N-S LINEAMENTS (RED) DOMINATE THE SOUTHERN RIDGE. L - LA CODOSERA. A - ALGARBES. S - SAN ANTONIO MINE.

10.9 - CONCLUSIONS

This study has demonstrated that remotely sensed data from Landsat TM and air photography, when combined with a good ground control of the structure, can be used to postulate a strong structural control to the mineralization of the La Codosera area, particularly the gold-antimony and uranium-phosphate deposits. An understanding of the kinematics of these structures when linked to the mapping provided by Landsat imagery allows exploration models to be developed.

These models are built up by the integration of field based and remote sensing work in the following manner. Firstly, it is necessary to establish a clear correlation between sets of lineaments and fractures based on their directional, spatial and temporal relationships. Once this is established the Landsat imagery may be used to map specific lineaments or zones of a particular pattern of lineaments. Only when the kinematics of these structures are understood can models be developed which relate the structural control of the various types of mineralization to specific locations, providing exploration targets.

Thus remote sensing can provide a cheap and efficient way of mapping fracture systems and selecting targets for further exploration. The effort that has gone into the understanding of the controls on mineralization provides the basis for exploration models, which analysis of Landsat imagery may convert into target locations. The results depend heavily on the integration of field studies and correlation with other geological, geophysical and geochemical data.

CHAPTER - 11 - CONCLUSIONS

11.1 - SUMMARY OF MAIN FINDINGS

In this section we present the main conclusions reached in the collaborative investigations of ITGE (Spain) and the University of Southampton (UK) and discuss their relevance to the gold mineralization in the La Codosera area.

Tectonic setting

The La Codosera area is located within the Central Iberian zone immediately north of the Badajoz Shear Zone. The rocks can be correlated with similar sequences elsewhere in Central Spain and comprise a Precambrian (CEG) sequence overlain unconformably by alternations of quartzite and slates ranging from Lower Ordovician to Devonian in age. The latter host most of the gold- antimony mineralization.

The Precambrian rocks were subject to Pre-Ordovician tilting and open folding, accompanied by local faulting and veining, but no cleavage. These, together with overlying Ordovician-Devonian rocks were subsequently affected by Hercynian ductile deformation, which produced steeply inclined folds, cleavage and faulting. Intense left-lateral shearing on the southern limb of the La Codosera Syncline produced augen, shear bands, sub-horizontal stretching lineation, boudinage, variably oriented folds and steep faults, whereas the northern limb of the syncline is characterised by folding and thrusting in a transpressional regime, with limited net northward transport.

The geometry of the structures in the La Codosera area, and their spatial and temporal variations indicate the importance of left-lateral transpression throughout much of the Hercynian deformation. The greatest strike-slip component is localized within the Badajoz-Cordoba Shear Zone. Thus early folding and thrusting within the Central Iberian Zone became increasingly transpressive towards its southern margin, producing a progressive change from thrust to strike-slip tectonics across the La Codosera area. D2 deformation was more localized, but maintained a left- lateral component. Late Hercynian faulting produced N-S and NE-SW faults which overprint the early structures and granites. These rotate to a NW-SE trend and increase in right-lateral displacement as a result of domino or bookshelf faulting which can be attributed to continued left-lateral motion along the Badajoz Shear Zone.

Gold exploration

ITGE's Gold exploration programme has involved geological mapping at various scales, soil and stream sediment geochemical surveys and lithogeochemistry of specific formations. Within the anomalous gold zones, ITGE has re-opened old

workings, trenched and diamond drilled specific targets. Los Algarbes represents one of the most interesting areas, where mapping at a scale of 1:5000, complimented by soil sampling, has indicated three major anomalies (La Portilla, Brena and Matasiete) with Au values higher than 0.3ppm in soils (Figs. 3.5 to 3.8). Furthermore lithogeochemical studies of host lithologies from drill holes suggest that specific horizons where quartz veining is widespread carry significant gold (e.g. Lower Devonian Quartzite 0.49 ppm, iron-rich sandstones 0.013 ppm).

The most significant gold prospects are located on a series of steep quartz veins trending 040°, which show grades of up to 10 gm/t Au, over a maximum thickness of 1.5m, and are generally restricted to the Devonian black slates. These veins are developed on extension faults which post-date the main S1 cleavage. The veins show little visible wall-rock alteration in the field and conform to the commonly described "gold only" veins with a restricted mineralogy of pyrite and arsenopyrite.

Geochemistry

Geochemical analyses indicate that the auriferous veins of the La Codosera area resulted from the passage of dilute, CO_2-rich fluids at temperatures of 350°C and depths of c.10km. The fluid contains appreciable amounts of methane (up to 20 mole %). The common association of mineralized veins within black slates suggests the reaction of fluid with carbonaceous wall-rock plays an important role in gold precipitation. The dilute nature of the fluid and the connectivity of veins to the Badajoz Shear Zone suggests a shear zone origin for the fluid. Beta-autoradiography indicates the gold is most likely lattice bound within the arsenopyrite structure.

Gravity

The gravity survey has demonstrated that the major source of density variation in the upper crust can be attributed to granites such as the Alburquerque Batholith. Some N-S trending profiles (eg. X660R) show additional gravity lows. The interpretation of this particular profile suggests the existence of a lower density body (granite) below the La Codosera syncline, separated from the main body of the Albuquerque batholith by an extension fault. In addition a significant negative anomaly of some -7.5 mgal (anomaly I, Fig 7.3, Fig. 7.8), occurs to the west of La Codosera, extending beneath the Algarbes area.

Landsat TM

Digital classification of Landsat TM data has discriminated two spectrally contrasting soils within the contact aureole of the Alburquerque Batholith. The resulting classification delimits the metamorphic aureole of the granite. Extending this classification over a wider area outlines an area, west of La Codosera, where soils, derived from Devonian slates, show a similar spectral classification as those found within the contact aureole of the granite.

Comparison of the TM classification with aeroradiometric data, using a G.I.S system, showed the coincidence of a moderate $K_{(e)}$ anomaly in the same sector as the anomalous soil classification west of La Codosera. These data in association with the observed gravity low and presence of spotted slates over the same area strongly suggest the presence of a granite cupola at depth.

Lineament Analysis

Using the Landsat data, combined with the ground structure, air photograph interpretation and gravity data, a clear picture of the fracture system has emerged. Three major sets of lineaments trend 045°, 135° and N-S (Fig. 10.2) and these correlate with extensional fractures, including those at known mineral prospects. In addition Landsat lineaments correlate with known faults in many parts of the area, thus providing a useful dataset with which to augment the regional structural studies.

Known U-P mineralization is largely confined to large 045° fractures, with evidence that these veins form in arrays along 030° and 065° lineaments, many of which may be identified from Landsat. Sn, W and Li mineralization mainly occurs along both 135° and 045° fractures in the aureole of the Alburquerque granite, particularly where lineaments of these trends dominate.

Several E-W lineaments cut the Central Ridge and appear to correspond with known Gold prospects of this trend. In the Southern Ridge, where the bulk of the prospects are located on quartz veins within Devonian quartzites and slates, a clear relationship between the mineralization and Landsat lineament pattern has been established (summarized below).

11.2 - USE OF GIS TO INTEGRATE EXPLORATION

The multidisciplinary nature of the project has generated a wide range of different spatial data, which can best be integrated and compared using a geographical information system (GIS). Geological maps, gravity, aeroradiometric data and Landsat TM classification were analyzed using the GRASS software at ITGE. The resulting maps, discussed in Chapter 9, illustrate the great potential of GIS within exploration programmes.

Not only can different data sets be superimposed quickly and accurately, but these data can be readily updated in response to further exploration and drilling. This has been particularly valuable in the intensively investigated area to the west of La Codosera. Fig 11.1 shows the numerous gold occurrences (yellow triangles) and the drill-holes (white spots) carried out by ITGE, superposed on the geological map. In addition selected anomalies are also displayed, these include moderate K(e) values (blue), the TM contact metamorphic soils (red) and the Bouguer gravity contours (white). The resulting coincidence of the negative gravity anomaly, moderate K radiation and TM classified contact soils, suggestive of an intrusive body at depth is clear.

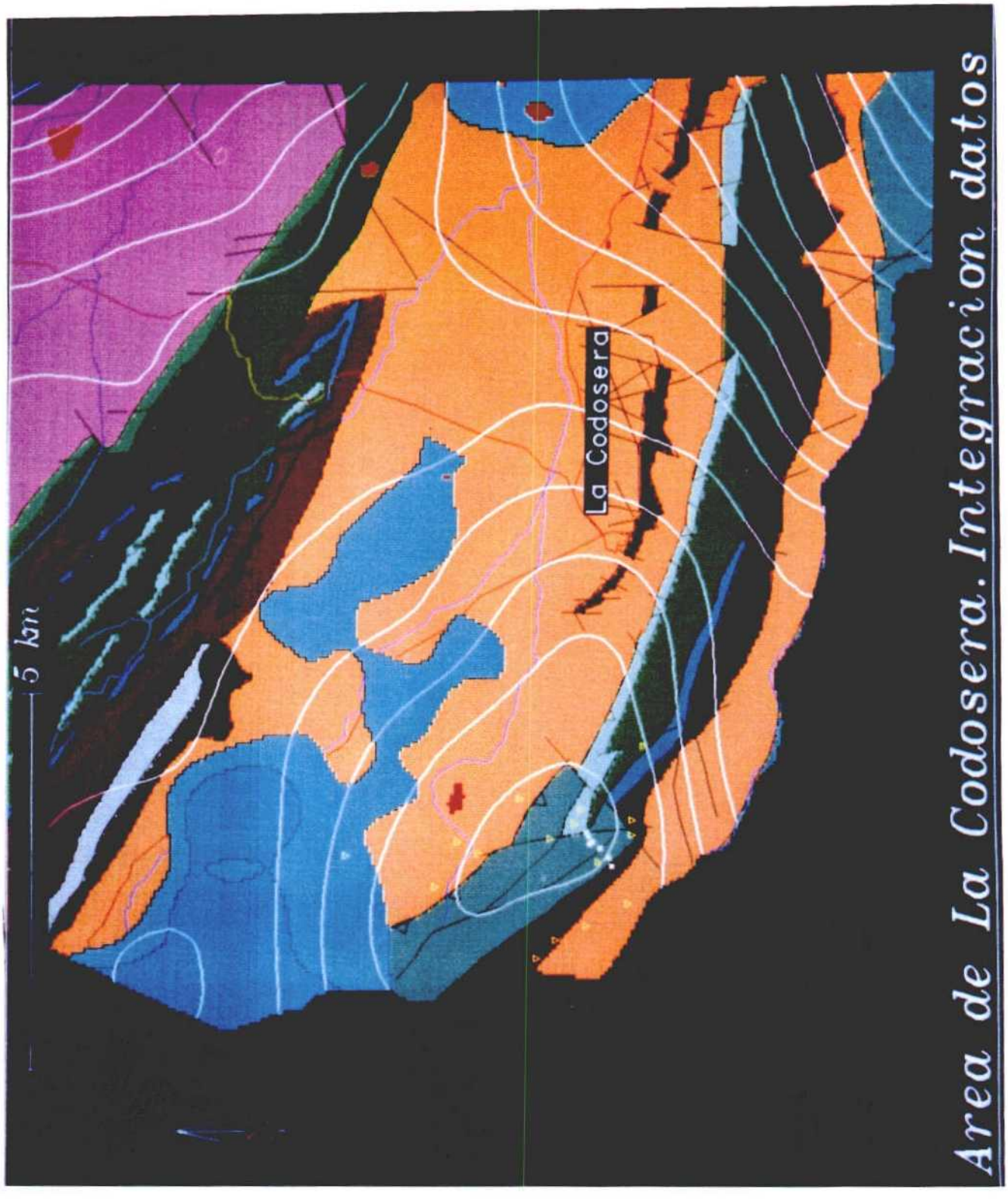

FIG 11.1 - POTENTIAL OF GIS IN CONNECTION WITH MINERAL EXPLORATION. INTEGRATED DATA SETS IN AN AREA TO THE WEST OF LA CODOSERA. GOLD OCCURRENCES (YELLOW TRIANGLES). DRILL-HOLES (WHITE SPOTS) SUPERPOSED ON THE GEOLOGICAL MAP. IN ADDITION SELECTED ANOMALIES ARE ALSO DISPLAYED, THESE INCLUDE MODERATE K VALUES (BLUE), THE TM CONTACT METAMORPHIC SOILS (RED) AND THE BOUGUER GRAVITY CONTOURS (WHITE).

11.3 - STRUCTURAL CONTROL OF GOLD MINERALIZATION IN THE LA CODOSERA AREA

In the Los Algarbes area, the main prospects lie on steep N-S to NE-SW veins developed as extensional fractures with some left- lateral reactivation, sited at the terminations of the larger NE- SW faults. These major fracture zones (lineaments) provide connectivity between the shear zone and the Southern Ridge of Palaeozoic rocks which host the main Au-Sb mineralization.

Based on detailed observation of the structural setting of veins and investigation of their geochemistry and fluid characteristics, we have recognised a number of prospective settings (Fig. 11.2). The gold-bearing veins generally occupy N-S to NE-SW trending extension fractures developed at the terminations (Fig. 11.2A) or offsets (Fig. 11.2B) of major NW-SE trending faults or where dilation was produced at intersections of these with their conjugate (NE-SW) set (Fig. 11.2C).

The NW-SE faults have a right-lateral component of slip and form part of an extensive "bookshelf" of "domino" system linking the Southern Ridge to the Badajoz Shear Zone. Maximum dilation will occur where the domino faults change orientation or have large displacement (Chapter 2). It is significant that the main area of old Au workings at Los Algarbes occurs at the northwestern end of the main change in orientation of the domino faults and that the San Antonio antimony mine occurs at the NW extension of a large displacement fault (Fig 11.3). Using the known structural controls, the lineament map provides a basis from which to identify new target areas which show abundant N-S to NE-SW fracturing in a similar structural setting (Fig. 11.3).

The current drilling programme at Los Algarbes (Section 4.3) is within one of the proposed target areas and confirms that the gold is associated with NNE trending extension veins, possibly developed as pinnates to a NE-SW fault, conjugate to the main NW- SE "feeder" faults.

The spatial association of the Los Algarbes area with a gravity low, anomalous K radiation and TM signatures characteristic of known contact metamorphic soils suggests the presence of a buried pluton. The fluid chemistry of auriferous veins, however, supports a shear zone source; the methane content possibly reflecting interaction with carbonaceous shales. In addition we note the presence of auriferous quartz veins in areas such as the Central Ridge, which are not underlain by granites. Thus, the role of the buried plutons may be to act as stress concentrators, promoting fracturing, or they may control and enhance pore fluid circulation.

This study has demonstrated a strong structural control to the mineralization of the La Codosera area. An understanding of the kinematics of these structures and the nature of the mineralizing fluid then allows exploration models to be developed. Remotely sensed data from Landsat TM, when combined with a good ground control can then be used to systematically define prospective targets.

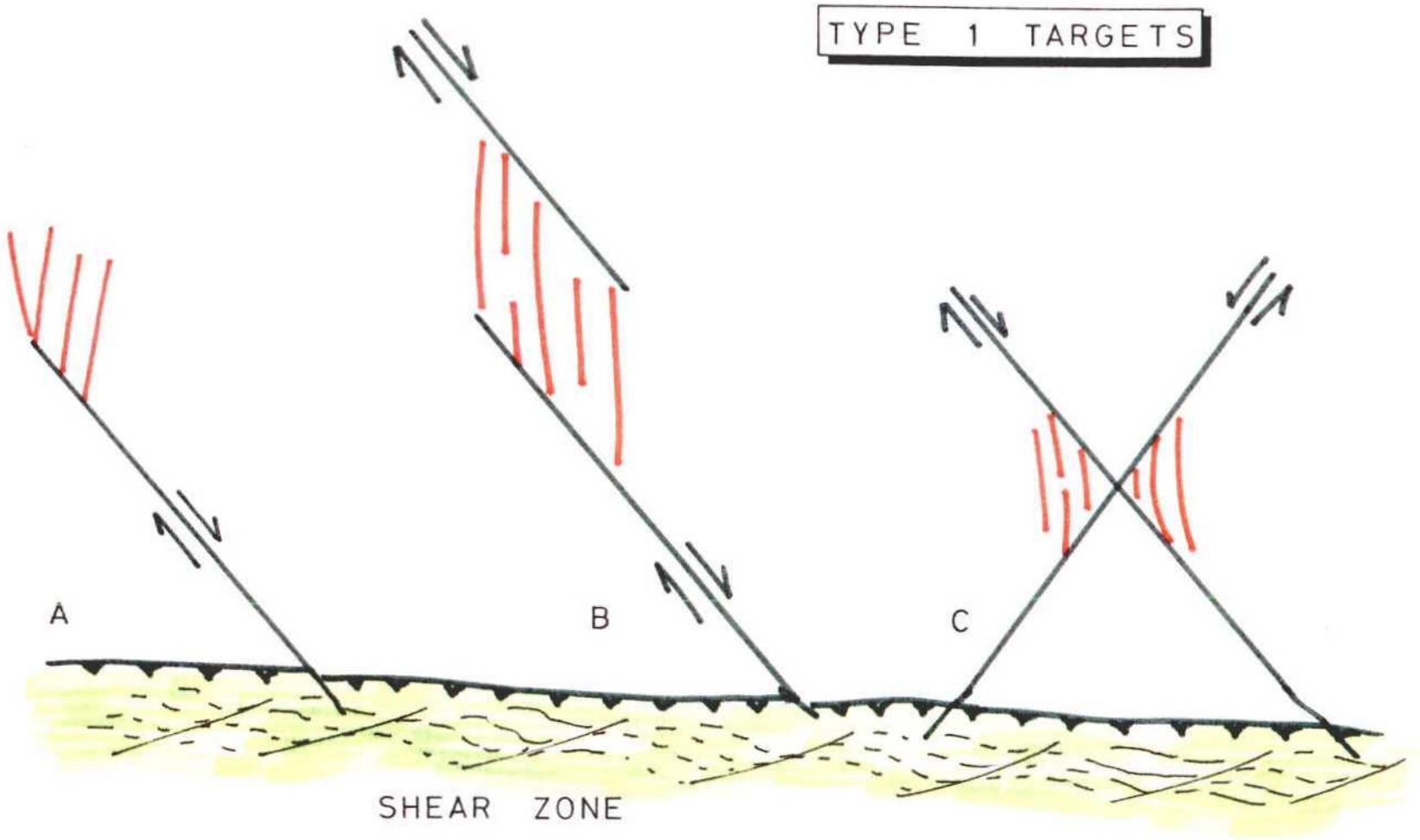

FIG 11.2 - TARGET TYPES RECOGNISED IN THE SOUTHERN RIDGE AT (A) TERMINATIONS AND (B) OFFSETS OF NW-SE FAULTS AND (C) AT DILATIONAL AREAS OF INTERSECTING FAULTS.

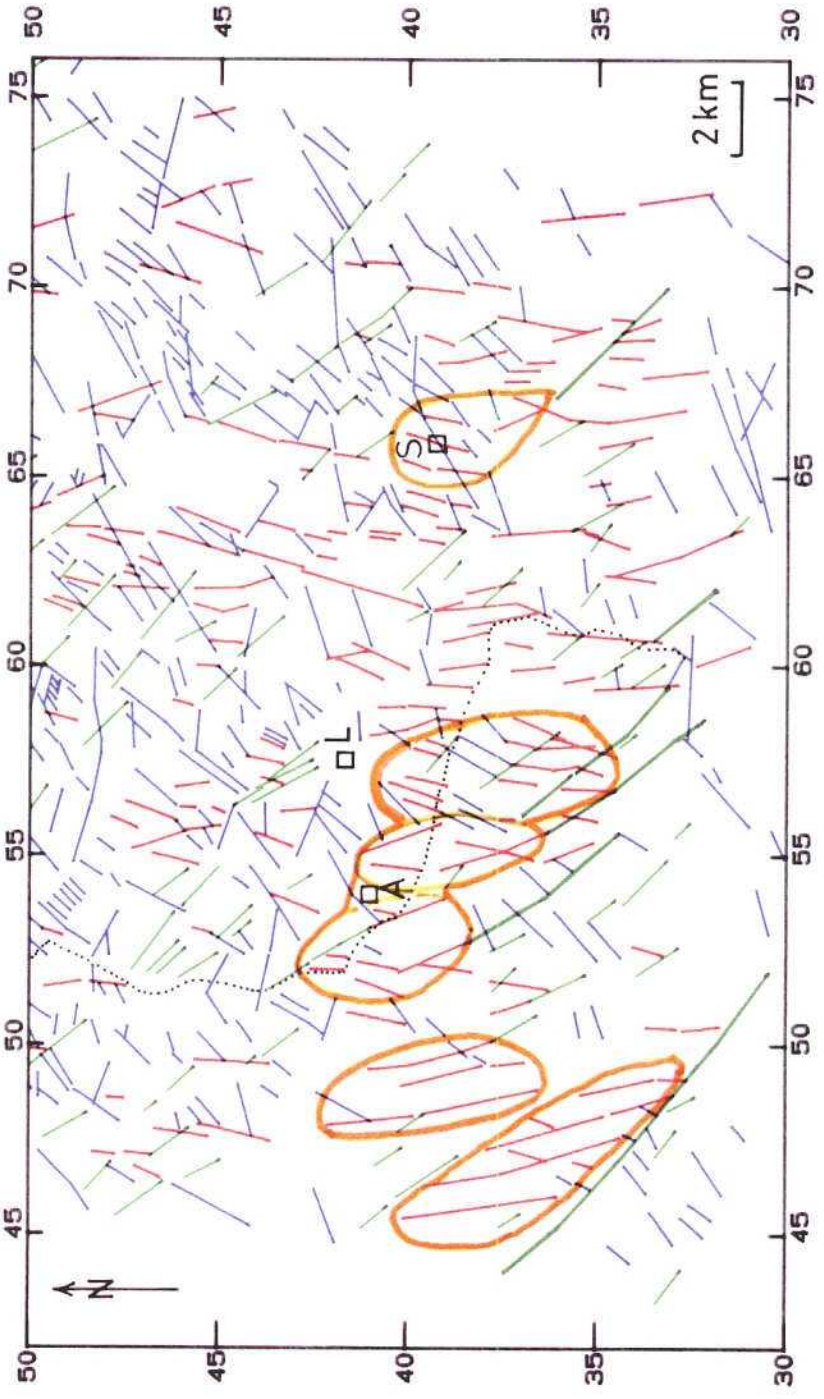

FIG 11.3 - LANDSAT TM LINEAMENT MAP OF THE SOUTHERN PART OF THE LA CODOSERA AREA. LARGE NW-SE LINEAMENTS (GREEN) REPRESENT FAULTS CONNECTING THE SOUTHERN RIDGE TO THE BADAJOZ SHEAR ZONE, WHICH FEED N-S EXTENSION FRACTURES (RED). TARGET AREAS BASED ON THE PATTERNS IN FIG. 11.2 ARE IDENTIFIED IN ORANGE.

The findings of this study have already proven of sufficient interest to warrant a series of presentations and in press publications which are outlined below, the more extensive data upon which these presentations are based is presented in this report.

PRESENTATIONS AT MEETINGS

ROBERTS, S., SANDERSON, D.J., NESBITT, R.W. & ASHWORTH, K. :"Multi-disciplinary techniques for mineral exploration in several areas of the Western Iberian Peninsula". EEC Contact Group Meeting, Padova, September 1988.

GUMIEL. P : "Development of new multidisciplinary techniques for mineral exploration in several areas of the western Iberian Peninsula." First meeting of the contact group: Geochemical methods in exploration. Padova. September 1988.

ROBERTS, S. & ASHWORTH, K. :"Tectonic and fluid evolution of auriferous quartz veins, La Codosera area, southwest Spain". IMM Commodity meeting, London, December 1988.

SANDERSON, D.J., ROBERTS, S. and GUMIEL, P. :"Hercynian thrust/strike-slip tectonics at the southern margin of the Central Iberian Zone, west Spain" Tectonics Studies Group Meeting, Cambridge University, December 1988

ANTON-PACHECO, C. & SANDERSON , D.J. :"Use of Landsat TM data in mineral exploration, Alburquerque-La Codosera area, southwest Spain". Invited contribution, EUG meeting, Strasbourg, March 1989.

ANTON-PACHECO, C.:"Cartografía digital de rocas en el area de Alburquerque-La Codosera, utilizando imagenes Landsat Thematic Mapper." In III Reunion Cientifica del Grupo de Trabajo en Teledeteccion, Madrid, 17-19 Octubre 1989. Ministerio de Industria y Energia.

SANDERSON, D.J. :"Application of Remote Sensing in Tectonics and Mineral Exploration". In III Reunion Cientifica del Grupo de Trabajo en Teledeteccion, Madrid, 17-19 Octubre 1989. Ministerio de Industria y Energia.

PEREZ CERDAN, F.; GARCIA, P.; ANTON-PACHECO, C.; and GUMIEL, J.C.: "Aplicaciones de un Sistema de Informacion Geografico (S.I.G) en Investigación Geologica." In III Reunion Cientifica del Grupo de Trabajo en Teledeteccion, Madrid, 17-19 Octubre 1989. Ministerio de Industria y Energia.

GUMIEL. P, ANTON-PACHECO. C, CAMPOS. R & PEREZ-CERDAN. F.: "Development of new multidisciplinary techniques for mineral exploration in several areas of the western Iberian Peninsula." EEC meeting. Paris 21-23 November 1989.

ANTON-PACHECO, C. :"Digital mapping of rocks in the Alburqueruqe- La Codosera area, Extremadura, Spain, using Landsat TM data." In 2nd Meeting of the WEGS Working Group Remote Sensing. 7-8 March, 1990. BGR. Hannover. FRG.

PUBLICATIONS

ANTON-PACHECO, C. :"Cartografia digital de rocas en el area de Alburquerque-La Codosera, Extremadura, utilizando imagenes Landsat Thematic Mapper." in: III Reunion Cientifica del Grupo de Trabajo en Teledetección. Antón-Pacheco, C, ed. ITGE, 15 pp., in press.

CAMPOS, R. & GUMIEL, P. 1990: "Estudio gravimétrico en Extremadura, (Zonas de La Codosera-Alburquerque y Albalá) y su aplicación a la exploración de yacimientos minerales". (Bol. Geol. Min. vol 101-1 pp 122-134.

PEREZ CERDAN, F.; GARCIA, P.; ANTON-PACHECO, C and GUMIEL, J.C.: "Aplicacion de un Sistema de Informacion Geografico en investigación Geologica." in: III Reunion Cientifica del Grupo de Trabajo en Teledetección. Antón-Pacheco, C., ed., ITGE, 7pp., in press.

ROBERTS S., SANDERSON D.J., GUMIEL P & DEE S. :"Tectonic and fluid evolution of auriferous quartz veins from the La Codosera area, SW Spain." (In prep. Economic Geology).

SANDERSON D.J., ROBERTS S., GUMIEL P. & MCGOWAN J. :" Hercynian thrust/strike-slip tectonics at the southern margin of the Central Iberian Zone, west Spain." (Submitted to J. Geol. Soc. London).

REFERENCES

ABALOS, B., 1989: Structural geology of the Ribera del Fresno window (Badajoz-Cordoba Shear Zone). Reun. Soc. Geol. de España, 2, pp:103-112.

ABRAMS, J.M., BROWN, D., LEPLEY & SADOWSKI. R., 1983: Remote sensing for porphyry copper deposits Southern Arizona. Econ. Geol.,78, pp:591-604.

AGER , C.M., & MILTON, N.M., 1987: Spectral reflectance of lichens and theyr effects on the reflectance of rock substrates. Geophysics, 52,7, pp:898-906.

AIZPURUA, J; GUMIEL, P; PINEDA, A.,1982: Introduccion a los yacimientos de fosfatos del Macizo Ibérico Meridional. Bol.Geol.Min. T. XCIII-V, pp:390-414.

ANDREW, R.L., 1980: Supergene alteration and gossan textures of base metal ores in Southern Africa. Min. Sci. Eng.12, pp:193- 215.

ANTON-PACHECO, C. ROWAN, L.C., PAYAS, A., BEL-LAN, A., KINGSTON, M., RIAZA, A., BIRCKEY, D.W. 1988. The use of supervised Bayesian classification on Landsat digital Thematic Mapper data to map contact metamorphic rocks around the Trujillo and Plasenzuela plutons, Extremadura, Spain. II European Workshop on Remote Sensing in Mineral Exploration, CEE publication, EUR 11317 EN-FR, pp:469-492.

ARRIBAS, A., 1975: Caracteres geológicos de los yacimientos españoles de uranio. Svtudia Geol. Apertura curso Acad. 1974-75. Salamanca.

ARRIBAS, A.,1978: Mineral paragenesis in the Variscan metallogeny of Spain. Stvdia Geol. 14, pp:223-260.

ARRIBAS, A. & GUMIEL, P. 1984. First occurrence of a strata- bound Sb-W-Hg deposit in the Spanish Hercynian massif. In: Syngenesis and epigenesis in the formation of mineral deposits. (edited by A Wauschkuhn et al.) Springer-Verlag, pp:468-481.

ARTHAUD, F. & MATTE, PH. 1975. Les decrochements tardi- Hercynian du sud-ouest de l'Europe. Geometrie et essai de reconstitution des conditions de la deformation. Tectonophysics 25, pp:139-171.

BABCOCK, E.A. 1974. Photolineaments and regional joints: lineament density and terrain parameters, south-central Alberta. Bull. Can. Petrol. Geol. 23, pp:810-826.

BOUYX, E. 1970. Contribution a l'etude des formations Ante- Ordoviciennes de la Meseta Meridionale (Cuidad Real et Badajoz). Memoria del Instituto Geologico y Minero de España 73, 263p.

BOTTRELL, J.H.; SHEPHERD, T.J.; YARDLEY, B.W.D. & DUBESSY, J. 1988: A fluid inclusion model for the genesis of the ores of the Dolgellan Gold Belt, N.Wales. J.Geol. Soc. London. 145, pp:139- 145

BROWN, 1864: Private internal report for the Peninsula Gold Mining and Washing Company. (Ined. Unpub. Report)

BURG, J.P., IGLESIAS; M., LAURENT, PH., MATTE, PH. & RIBEIRO, A. 1981. Variscan intracontinental deformation: the Coimbra- Cordoba shear zone (SW Iberian peninsula). Tectonophysics 78, pp:161-177.

BURRUSS, R.C., 1981: Analysis of fluid inclusions : Phase equilibria at constant volume. Am. J. Sci. 281, pp:1104-1126.

CAMERON, E.N; JAHNS, R.H; MCNAIR, A; PAGE, L.R.,1949: Internal structure of granitic pegmatites. Econ. Geol. Monograph, 2. 115p.

CAMPOS, R. & GUMIEL, P. 1990: "Estudio gravimétrico en Extremadura, (Zonas de La Codosera-Alburquerque y Albalá) y su aplicación a la exploración de yacimientos minerales". (Bol. Geol. Min. vol 101-1 pp:122-134.

CARRINGTON DA COSTA, J., 1952: Os movimentos Caledonicos e preliminares hercinicos na Peninsula Iberica. Bol. Soc. Geol. Portugal. V-10 (1-3), pp:1-12.

CARTER, J.S. & MOORE, J.McM. 1978. Some major lineaments in the northern Pennine orefield. Trans. Inst. Min. Metal. 87B, pp:90- 93.

CLARKE, A. 1960: The Fe-As-S system. Phase relations and applications. Econ. Geol. 55, pp:1345-1381.

CASTRO, A., 1984: Los granitoides y la estructura hercínica en Extremadura Central. Tesis Doc. Univ. Salamanca. 202p.

COLLINS, P.L.F. 1979: Gas Hydrates in CO_2-bearing fluid inclusions and the use of freezing data for the estimation of salynity. Econ. Geol. 74, pp:1435-1444.

CONRANDSEN, K.; NIELSEN, B.J.; PEDERSEN, J.H. 1988: Automated analysis of linear feautures based on satelite imagery compared with geological setting. in: II European Workshop on Remote Sensing in Mineral Exploration, CEE publication, EUR 11317 EN- FR, pp:273-292.

COLVINE, A.C.; FYON, J.A.; HEATHER, K.B.; MARMONT, S.; SMITH, P.M. & TROOP, D.G. 1988: Archaean lode gold deposits in Ontario. Mines & minerals division. Ontario Geol. Surv. Misc. Paper. 139, 136p.

CORREIA PERDIGAO & PEINADOR FERNANDES, 1976:Carta geologica de Portugal. Noticia explicativa da folha 29-C (Marvao). Serv. Geol. Portugal (Lisboa).

CROSS, A.M. 1988. Detection of circular geological features using the Hough transform. Int. J. Remote Sensing 9, pp:1519- 1528.

CROWELL, J.C. 1974. Origin of late Cenozoic basins in Southern California. In: Tectonics and Sedimentation (edited by W.R. Dickinson). Society of Economic Palaeontologist and Mineralogist Special Paper 22, pp:190-204.

DALY, M.A. 1933: Igneous rocks and the depths of the earth. New York. McGraw Hill Book Co. 598p.

DIBBLEE, T.W. 1977. Strike-slip tectonics of the San Andreas fault and its role in Cenozoic basin evolvement. In: Late Mesozoic and Cenozoic sedimentation and tectonics in California (edited by T.H. Nilsen). San Joaquin Geological Society, pp:26- 38.

GARFUNKEL, Z & RON, H. 1986. Block rotation and deformation by strike-slip faults 2. the properties of a type of macroscopic discontinuous deformation. Journal of Geophysical Research 90, pp:589-602.

GUMIEL, P; ARRIBAS, A y SAAVEDRA, H.,1976: Geologia y metalogenia del yacimiento de estibina - scheelita de San Antonio. Alburquerque (Badajoz). Stvdia Geol. V-10, pp:61-93.

GUMIEL, P. 1982: Metalogenia de los yacimientos de antimonio de la Península Ibérica. Tecniterrae 54, 120p.

GUMIEL, P., & ARRIBAS, A., 1987.: "Antimony Deposits in the Iberian Peninsula". Economic Geology, Vol.82, pp:1453-1463.

HAMMER, S. 1939: Terrain corrections for gravimeter stations. Geophysics.IV-3, pp:184-209.

HANCOCK , P.L. & BARKA, A.A. 1987: Kinematic indicators on active faults in western Turkey. J. Struct. Geol. 9, pp:573-584.

HARALICK, R.M. 1983. Ridges and valleys on digital images. Computer Vision Graphics and Image Processing 22, pp:28-38.

HEWARD, A.P. & READING, H.G. 1980: Deposits associated with an Hercynian to late Hercynian continental strike-slip system. Cantabrian Mountains. N. Spain. Spec. Publ. Int. Ass. Sediment. 4.pp:105-125.

HOLLISTER H.S. & BURRUSS R.C. 1976: Phase equilibria in fluid inclusions from the Khtada Lake metamorphic complex. Geochem. Cosm. Acta. 40, pp:163-175.

HUNT, G.R.; SALLISBURY, J.W. & LENHOFF, C.J. 1971: Visible and near-infrared spectra of minerals and rocks: III Oxydes and hidroxydes. Mod. Geol. 2, pp:195-205.

HUNT , G.R., SALISBURY, J.W.,1976: Visible and near infrared spectra of minerals and rocks: XII metamorphic rocks , Mod. Geol, 5, pp:219-228.

HEYEN, S.; RAMBOZ, C. & DUBESSY, J. 1982: Modelling of phase equilibria in the system CO_2-CH_4 below 50°C and 100 bar. Applications to inclusion fluids. Compt. Rend. Accad. Sci. Paris. 294 - II, pp:203-206.

ITGE: 1987 Exploración en el área de La Codosera (Badajoz) Sustancias Au, Sb, Sn, W. Unpub. Report.

ITGE 1989: Proyecto para investigación de Au, W, Sn y Sb en las reservas de La Codosera y apliación al subsector X - Badajoz - Cáceres. Unpub. Report. Junta de Extremadura.

ITGE. 1989: Gravimetría en Extremadura - Apoyo geofísico a investigaciones mineras. Unpub. report. Documentación ITGE.

KRETSCHMAR, U. & SCOTT, S.D. 1976: Phase relations involving arsenopyrite in the system Fe-As-S and their application. Can. Min. 14, pp:364-386.

LE FORT, J.P. & RIBEIRO, A. 1980. La faille Porto-Badajoz- Cordoue a-t-elle controle l'evolution de l'ocean palaeozoique sud-armorican? Bulletin de la Societé Geologique de France, 7th Series, 22, pp:455-62.

MANDL, G. 1987. Tectonic deformation by rotating parallel faults: the "bookshelf" mechanism. Tectonophysics 141, pp:277- 316.

MCKENZIE, D & JACKSON, J. 1983. The relationship between strain rates, crustal thickening, palaeomagnetism, finite strain and fault movements within a deforming zone. Earth and Planetary Science Letters 65, pp:182-202.

McKENZIE, D. & JACKSON, J. 1986. A block model of distributed deformation by faulting. Journal of the Geological Society, London 143, pp:349-53.

MAUCHER, A.,1965: Die Antimon - wolfram - quecksilber - formation und ihre Beziehungen zu Magmatismus und geotektonik. Freiberg Forsch. C186. pp:173-187

NADEN, J. & SHEPHERD, T.J. 1989: Role of methane and carbon dioxide in gold deposition. Nature 342. pp: 793-795.

NEUMAN, R. 1963: Contribution au calcul simplifie des corrections de relief a grande distance a gravimetrie. Geoph. Prosp. XII-4 pp523-534.

ORTEGA, E. 1988. Geology and metallogeny of the Almaden area, centro-Iberian zone, Spain. In: Second European Workshop on Remote Sensing in Mineral Exploration. CEC Report EUR 11317, 145-173.

PLATA, J.L. 1983: Nuevo método de cálculo de la densidad de reducción en gravimetría. Bol. Geol. Min. XCIV-VI. pp510-520.

POTTS, P.J. 1984: Neutron activation induced beta- autoradiography as a technique for locating minor phases in thin sections: Application to rare earth element and platinum-group element mineral analysis. Econ. Geol. 79. pp: 738-747.

POTTER, R.W.; CLYNNE, M.A. & BROWN D.L. 1978: Freezing point depression of aqueous sodium chloride solutions. Econ. Geol. 73. pp: 284-285.

PRETORIUS, J.P.G & PARTRIDGE, T.C. 1974. The analysis of angular atypicality of lineaments as an aid to mineral exploration. J. S. Afr. Inst. Min. Metall. 74, 367-369.

RAMDOHR, P. 1969: The ore minerals and their intergrowths Pergamon. New York.

RODA QUEROL, J. 1986. Nuevos datos sobre la fase de deformación sárdica. Geometría de los pliegues pre-hercínicos del Rio Salor (Cáceres). Geogaceta 1, 13-15.

ROEDDER, E. & BODNAR, R.J. 1980: Geologic pressure determinations from fluid inclusion studies. Ann. Rev. Earth Planet Sci. 8. pp:263-301.

ROWAN. L.C.; WETLAUTER, P.M.; GOETZ, A.F.; BILLINGSLEY, E.C. & STEWARD, J.H. 1974: Discrimination of rock types and detection of hydrothermally altered areas in South-Central Nevada by use of computer- enhanced ERTS images. U.S. Geol. Surv. Prof. Paper 883, 35p.

ROWAN, L.C., ANTON-PACHECO, C.; BRICKEY, D.; KINGSTON, M.J.; PAYAS, A.; VERGO, N. & CROWLEY, J.K., 1987,:" Digital classification of Contact metamorphic rocks in Extremadura, Spain, using Landsat Thematic Mapper data, Geophysics 52, 7. pp- 885-897.

ROWAN, L.C.; SALISBURY, J.W.; KINGSTON, M.J. & VERGO, N. in press, "Evaluation of visible, near-infrared and thermal- infrared reflectance spectra for studying thermal maturity of Pierre Shale, Wolcott, Colorado".

RON, H.; FREUND, R.; GARFUNKEL, Z. & NUR, A. 1984. Block rotation by strike-slip faulting: structural and paleomagnetic evidence. Journal of Geophysical Research 89, 6256-70.

SANDERSON, D.J.; ANDREWS, J.R.; PHILLIPS, W.E.A. & HUTTON, D.H.W. 1980: Deformation studies in the Irish Caledonides. J. Geol. Soc. London 137. pp 289-302.

SANDERSON, D.J. & DOLAN, J.M. 1986. Structural and statistical analysis of lineament patterns as a guide to exploration. In: First European Workshop on Remote Sensing and Mineral Exploration. EEC Publication EUR 10511 EN-FR, 9-33.

SANDERSON, D.J. & MARCHINI, W.R.D. 1984. Transpression. J. Struct. Geol. 6, 449-58.

SANDERSON, D.J. 1988. Remote sensing and the structural control of mineralization in the Rhodope Massif, northern Greece. In First European Workshop on Remote Sensing and Mineral Exploration. EEC Publication EUR 11317 EN-FR, 347-67.

SANDERSON, D.J.; ROBERTS, S.R.; McGOWAN, J. & GUMIEL, P. 1990. Hercynian transpressive tectonics at the southern margin of the Central Iberian Zone, West Spain. submitted to J. Geol. Soc. Lond.

SANTOS, J.A. & CASAS, J., 1979: Geologia del sinclinorio de Sao Mamede - La Codosera. Zona española (provincias de Cáceres y Badajoz). Bol. Geol. Min. 95. pp:420-431.

SHARP, Z.D.; ESSERE, E.J. & KELLY, W.C. 1987: A re-examination of the arsenopyrite geothermometer, pressure considerations and applications to natural assemblages. Can. Min. 23, pp: 517-534.

SHEPHERD, T.J. 1981: Temperature-programmable heating-freezing stage for microthermometric analysis of fluid inclusions. Econ. Geol. 76. pp: 1244-1247.

SOPER, N.J.; WEDB,B.C. & WOODCOCK, N.H. 1987: Late Caledonian (Acadian) transpression in Northwest England: timnig, geometry and geotectonic significance. Proc. Yorks. Geol. Soc. 46. pp: 175-192.

SMITH, T.J.; CHOKE, P.H. & KESLER, S.E. 1984: Geochemistry of fluid inclusions from the McIntyre-Hollinger gold deposit. Timmins, Ontario. Canada. Econ. Geol. 79. pp: 1265-1285.

TALWANI, M; WORZEL, J.L & LANDISMAN, M. 1959: Rapid gravity computations for two-dimensional bodies with application to the Mendocino Submarine Fracture Zone. J. Geophys. Res. V-64, pp49- 59.

TAMAIN, G., 1972: Recherches geologiques et minieres en Sierra Morena Orientales (Spagne). These Univ. Paris Sud (Centre d'Orsay). 3T.

TAMAIN, G; OUTRACHT, A; CARRE, J; HELOIR, JP; PERAN, M; POUPON, G.,1971: L'Ordovicien de la Sierra Morena Orientale (Espagne). C.R. 94. Cong. Nat. des Soc. Savantes Pan. 1969. Sciences. T - II. pp: 275-292.

WERNICKE, B. & BURCHFIEL, B.C. 1982. Modes of extensional tectonics. Jour. of Struct. Geol. 4, 105-15.

WHEELER, R.L. & DIXON, J.M. 1980. Intensity of systematic joints: methods and applications. Geology 8, 230-233.

WILLIAMS, P.L; SYKES, L.R; NICHOLSON, C. & SEEBER, L. 1990: Seismotectonics of the Easternmost Transverse Ranges, California: relevance for seismic potential of the southern San Andreas Fault. Tectonics, 9, pp:185-204.

LIST OF FIGURES

LIST OF TABLES

ACKNOWLEDGMENTS

The authors would like to acknowledge the support and funding of the **EC Comission** and the **participant Institutions**, and to **Fernando Perez Moras** for assistance with the preparation of illustrations and **Maria Eugenia Lozano** for her assistance during the edition of this final report.

Alburquerque - La Codosera

Norte: 4374714.85
Este: 685494.85

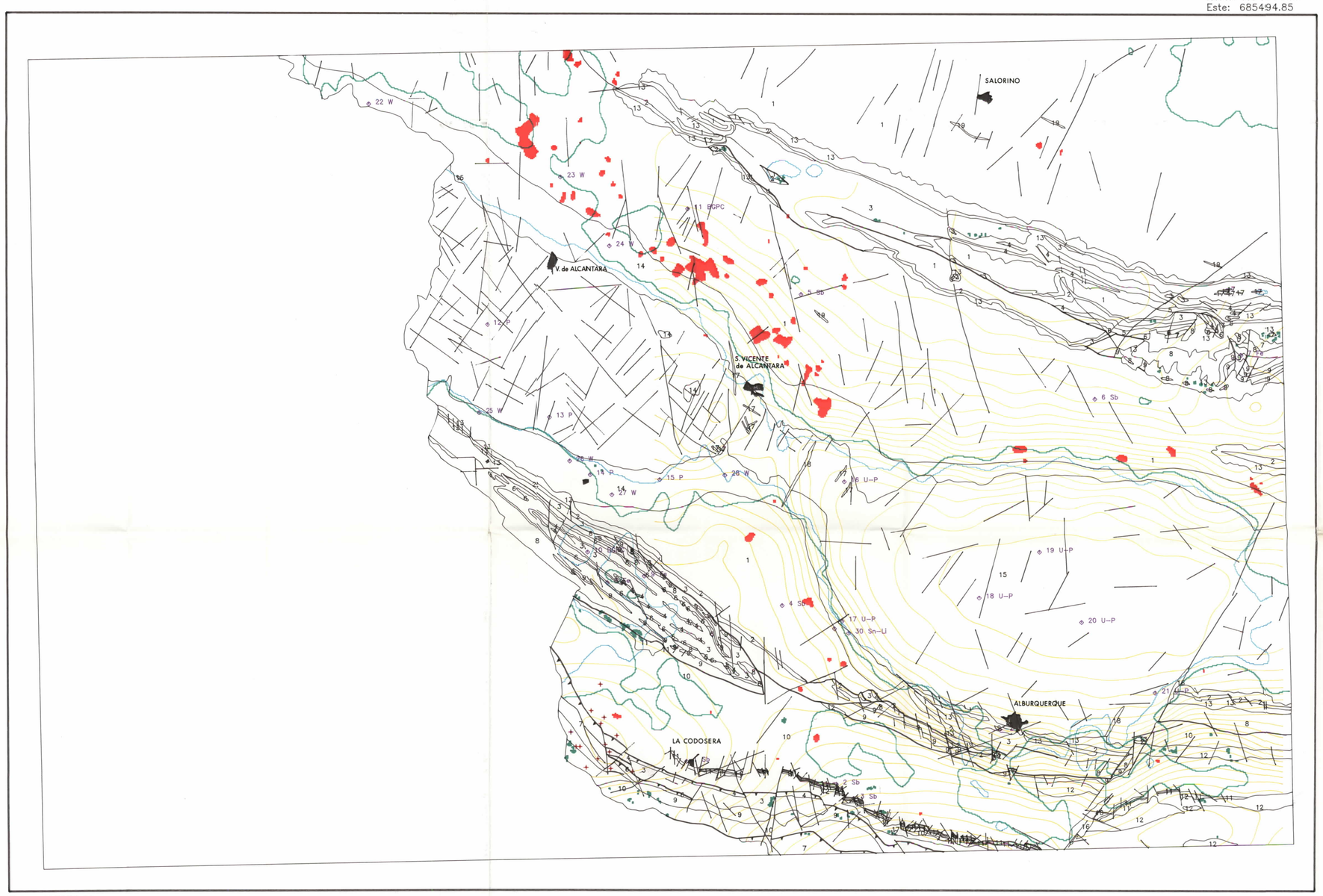

Este: 627279.42
Norte: 4336549.75

LEYENDA

1:Complejo Esquisto Grauwaquico
2:Cuarcita Armoricana. Ord. Inf.
3:Capas Pochico
4:Cuarcita de Cantera
5:Serie Intermedia Ord.Superior
6:Cuarcita de Criadero
7:Pizarras con Graptolites. Silurico
8:Cuarcitas y Areniscas. Dev. Inf.
9:Cuarcitas y Pizarras
10:Filitas. Devonico Medio
11:Calizas
12:Rocas Volcanicas. Dev. Medio
13:Derrubios de ladera. Cuaternario

ROCAS METAMORFICAS
14:Corneanas y piz. mosqueadas

ROCAS INTRUSIVAS
15:Granito de Alburqerque
16:Ofitas y diabasas
17:Aplitas
18:Diques de Cuarzo
19:Porfiroides y Queratofidos

- Poblacion
- C.TM. S.Lim.
- C.TM. S.Cont.
- Ind. Au
- Ind. Mineros
- Gravimetria
- Anom. U
- Anom. K
- Falla
- Contacto

I.T.G.E. - S.I.G.

Escala 1: 100000

0 1 2 3 4 5 Km

FIG. 1.3 - GEOLOGICAL MAP OF THE ALBURQUERQUE - LA CODOSERA AREA.